SCUOLA DI DOTTORATO
UNIVERSITÀ DEGLI STUDI DI MILANO-BICOCCA

Department of Biotechnologies and Biosciences
PhD program on Converging Technologies for Biomolecular Systems (TeCSBi)
XXXIV cycle

Osteoarthritis theranostics: extracellular vesicles and drug microfluidic screening platforms as innovative tools

Surname: D'Arrigo

Name: Daniele

Registration n. 848845

Tutor: Prof. Marco Vanoni

Supervisor: Prof. Matteo Moretti

Coordinator: Prof.ssa Paola Branduardi

ACADEMIC YEAR 2020/2021

Contents

Abstract

Knee osteoarthritis (OA) is the most common form of arthritis, and it represents a world-leading cause of disability, especially in the elderly population. Despite its increasing incidence, the early diagnosis of OA is still unattainable. In fact, the diagnostic process is based on the physical examination of the patient, usually associated with the joint imaging, mainly with radiography. However, this approach has several limitations, especially because indications for physical and clinical investigations are usually prescribed after the onset of symptoms, when OA is already in an advanced and probably irreversible stage. In addition, the biological processes activated during the OA progression, such as inflammation and cell phenotype drift, are not considered. In this scenario, the research is now focusing on biological markers that can reflect the early biological alterations that successively cause the structural changes in the articular tissues visible with radiography. Several candidates have been proposed, including markers of cartilage synthesis and degradation, synovitis and subchondral bone remodelling. Although promising, all the biomarkers failed during their validation toward the clinical use. More recently, the extracellular vesicles (EVs) are gaining importance as biomarkers of different pathophysiological conditions, including OA. Contrarily to the classical view, the EVs that are isolated from biofluids consist in many subpopulations with different physicochemical features

and biological roles. For instance, focusing on the dimension, the large size EVs have a more noticeable role than the small ones in the inflammation process, a key process in OA. However, most of the studies in literature were focused on small size EVs. Thus, the first aim of this PhD project was the finding of the most effective technique that allow the isolation and the separation of different size EV subpopulations. With this view, I evaluated the effectiveness of different experimental approaches, namely differential centrifugation, size exclusion chromatography, high performance liquid chromatography (HPLC) and asymmetrical flow field-flow fractionation (AF4). Among them, the AF4 proved to be the most suitable as it allowed the isolation and the separation of EV subpopulations from the synovial fluid (SF) within a broad size range. This part of the project was performed at the Italian Institute of Technology in Genoa, Italy. We collected SF from the shoulder of 3 donors after biceps tenotomy and from the knee of 3 donors underwent total knee replacement. By comparing the EV subpopulations from a load-bearing joint with those isolated from a not bearing one, we could understand the impact of different microenvironments in the EV profile. Firstly, the flow rates in the AF4 were optimized until being able to isolate particles with a radius ranging from 20 up to more than 700 nm, that were gathered in 4 different subpopulations. The EV profile and the relative percentage of each subpopulation

resulted different in each biofluid and the larger EVs showed a decreasing trend of Z potential and protein concentration, but not of nucleic acid content. To confirm the morphology of the EVs, transmission electron microscopy imaging was performed. Finally, the luminal and surface EV proteins were assessed, and the presence of EV-specific markers was demonstrated also by immune EM. The last part of the project was performed at the University of Gothenburg, in Sweden. The isolation and the characterization of the different size EV subpopulations in biofluids would give intriguing new opportunities to find diagnostic biomarkers, an approach applicable not only in the OA. In fact, this protocol proved to be effective in the separation of EV subpopulations also from other biofluids.

In addition to the impossibility of an early diagnosis, the OA is also characterized by the lack of therapeutic approaches able to halt and revert the degeneration processes in the articular tissues. In fact, the currently therapeutic options aim at reducing the symptoms and increasing the quality of life of the patients. More recently, different biological approaches, that are still under investigation, showed promising results in the reversion of the OA degenerative pathways. Unfortunately, the clinical translation of these preparations is still hampered especially by their intrinsic variability in the preparation. In this scenario, the generation of drug screening platforms can accelerate their

development by limiting the clinical trial only to the most effective candidates. Among the other available approaches, microfluidics is promising as it can more closely reproduce the 3D microenvironment of the arthritic joint. However, the OA drug screening platforms already developed lack in providing the articular cells with a relevant support matrix, a crucial factor especially for the chondrocytes. In this perspective, the second aim of the project was focused on the development of a relevant patient-specific microfluidic model to be used as drug screening platform for the evaluation and the comparison of OA innovative treatments. To resemble the arthritic joint environment, the device consisted in a multi-compartment microfluidic chip that allowed the separated culture of primary patient-matched synovial fibroblasts and chondrocytes in 3D relevant hydrogel with synovial fluid interposed. In addition, the device was designed to allow the injection of biological treatments, mimicking an intra-articular injection. To recreate a more relevant cartilaginous compartment for the chondrocyte culture, I optimized commercially available hydrogels based on hyaluronic acid and/or type I collagen that were crosslinked enzymatically or via UV light. Their biomechanical properties and their biocompatibility were tested, as well as the phenotype of the cells cultured within them. The expression of chondrocyte-specific markers was significantly higher when cells were

cultured in relevant hydrogels. Then, I optimized the OA microenvironment by evaluating the effect of the synovial fluid in the device microenvironment. The results showed that its addition was beneficial for the articular cells, that behaved differently when cultured with healthy or arthritic synovial fluid. This demonstrated that within the model a relevant arthritic microenvironment was effectively reproduced. Finally, the anti-inflammatory capabilities of adipose and bone-marrow mesenchymal stromal cells (MSCs) were assessed. The model effectively supported the injection of MSCs and the evaluation of their biological effects on articular cells. In the future, this platform could also be used to evaluate and compare the effectiveness of other biological treatments, such as secretome and EVs. In fact, these MSC-derived biological products showed promising anti-inflammatory and regenerative capabilities in the treatment of OA, as I systematically reviewed.

Chapter 1

Introduction: course, diagnosis, and treatment of osteoarthritis

1. Osteoarthritis: onset and progression

Osteoarthritis (OA) is a highly disabling and degenerative disease that can affect all the diarthrodial joints. It is the most common form of arthritis and it represents a relevant and increasing health burden characterized also by huge socio-economic costs and notable implications for the national health systems [1]. In fact, globally it is estimated that more than 500 millions of people suffer from OA, with a prevalence higher than 7% [2]. This value is even higher in countries with a well-established market economy, and it is still increasing due to the ageing population. For instance, in the US the prevalence of this disease reaches 14% [2]. The estimated medical cost related to the OA can reach 1-2,5% of the gross domestic product in various high-income countries [3]. Due to its increasing prevalence and the high disability, in 2019 OA was ranked 15th on the list of leading causes of years lived with disability (YLDs) in the world, with an increasing of 48% since 1990 [4,5]. In this scenario, the knee is the most commonly joint affected by OA (Figure 1). In fact, when compared with the other joints, the knee OA accounts for approximately 85% of the cases of osteoarthritis, and the 2,2% of the total YLDs were ascribed to knee OA [6,7].

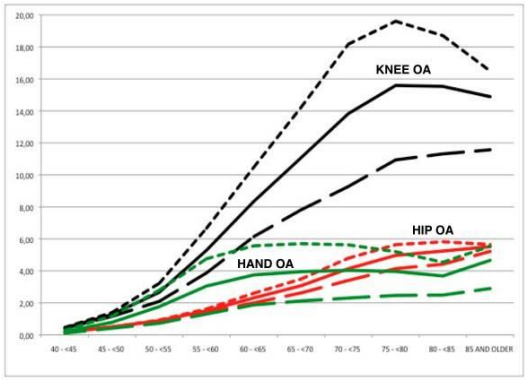

Figure 1. The prevalence of OA in knee, hip and OA in different age groups. Adapted from [8].

Knee OA is a very complex chronic degenerative disease, often worsened by the presence of multimorbidity, especially atherosclerosis-related diseases [9,10].

1.1. New insights on OA pathogenesis

The knee osteoarthritis is characterized by a complex and multifactorial pathogenesis. Classically, OA was first described as a degenerative "wear and tear" disease that affect primarily and almost exclusively the cartilage compartment [11]. However, this paradigm has been notably changed in the last decades. In fact, it is currently well demonstrated that the pathogenetic process is complex and multifactorial. Moreover, in this process the inflammatory response plays a crucial role. Over the years since the 1990s, many pro-inflammatory mediators released by cartilage, synovial membrane and subchondral bone have been discovered [11]. It is currently well documented that there are

many risk factors that can increase the susceptibility to develop OA by triggering or sustaining the inflammatory response. The predisposing factors are divided in non-modifiable (age, gender, genetic and ethnicity) and modifiable systemic factors, such as obesity and bone metabolism. In addition, there are also susceptibility factors that can be local (physical activity, wrong movements, joint injuries and muscle strength) or systemic, such as diet and metabolism [12]. In a weight-bearing joint like the knee, both biomechanical and biochemical factors, that are strictly related, can trigger and sustain local inflammatory and degenerative processes [13]. Different cellular signalling pathways that can initiate and sustain the inflammation can be activated in the cells of all the tissues in the knee. Therefore, OA is currently considered a pathology that affects the whole organ, i.e. the diarthrodial joint. In fact, it causes structural and functional alterations in the cartilage, synovial membrane, subchondral bone, ligaments, capsule, menisci and periarticular muscles [14]. For all these reasons, this disease is now considered more similar to a syndrome rather than a simple disease [15].

1.1.1 The role of cartilage, synovitis and synovial fluid in inflammation

The inflammation in the OA is usually a low-grade and chronic process and it is the result of the local damages in the articular

tissues, the dysfunction in the cell metabolism and the recruitment of immune cells [11,16]. The mild inflammation in the OA is clearly different from the high-grade inflammation that characterizes rheumatoid arthritis, that is considered as the prototypical inflammatory arthritis [17]. In a weight-bearing joint as the knee, the mechanical cues play a crucial role in the pathologic processes. In fact, excessive or prolonged mechanical forces can directly cause structural damages in the articular tissues, especially in those made more susceptible by the several risk factors previously described. On a cellular level, the mechanical stress can trigger the inflammatory response, that is responsible, especially in the cartilaginous compartment, for the activation of several catabolic and degenerative processes. To exemplify, mechanical alterations with a harmful potential may occur in two opposite settings. In the first one, an excessive mechanical stress (in intensity and/or in duration) is applied on physiologic articular tissues that ensure the stability and the mechanical protection of the joint, such as cartilage, menisci, ligaments and the peri-articular muscles, that act both as joint stabilising and shock adsorber [14,18]. Otherwise, the mechanical stress applied is within the normal range but it acts in a non-stable joint environment, in which the articular components are already damaged or compromised [14]. Obviously, the general *in vivo* clinical setting is not so demarcated. In fact, due also to the

numerous risk factors that can increase the OA susceptibility, there is often a contribution of both the factors in the onset of this pathology. Despite the specific mechanism behind, the altered joint biomechanical environment can elicit several biochemical signalling pathways in the articular cells, causing an imbalance of the dynamic equilibrium between the anabolic and catabolic processes [19]. Especially in the chondrocytes, this imbalance stimulates the expression of catabolic and degradative mediators, such as cytokines, matrix proteases and oxygen radicals [14]. These mediators are responsible for the primary breakdown of the cartilage, and fragments of the tissue are released in the synovial fluid [20]. The pro-inflammatory molecules and these fragments diffuse through the synovial fluid and act on the near portion of the synovial membrane. The synoviocytes in the synovial membrane consider the matrix fragments as foreign bodies and react synthetising pro-inflammatory cytokines. This represents the most accredited hypothesis explaining the triggering of the inflammatory response in the synovial membrane, called as synovitis [11,21]. During this process the synoviocytes are activated and the immune cells are recruited (primarily macrophages and lymphocytes) from the blood stream. These cells in turn secrete additional pro-inflammatory mediators such as cytokines, chemokines, proteases, oxygen reactive species and lipidic mediators in the synovial fluid. This

plethora of pro-inflammatory and degenerative effectors can directly degrade the cartilaginous matrix but also sustain the dysregulation of the chondrocyte metabolism towards the catabolic phenotype. This process further amplify the inflammation in the cartilage and in the synovial membrane, establishing a positive pro-inflammatory feedback (Figure 2) [20]. Another important player in the setting of this pro-inflammatory environment during the OA is the synovial fluid. Physiologically, it serves as a lubricant and, thanks to its peculiar viscoelastic properties, it helps the cartilage to respond to different mechanical stresses [22]. In addition, it also allows the intercommunication between different articular tissues, and this role is even more important during the OA. In fact, the articular cells released the pro-inflammatory mediators in the synovial fluid where they can diffuse and reach the other articular tissues [23].

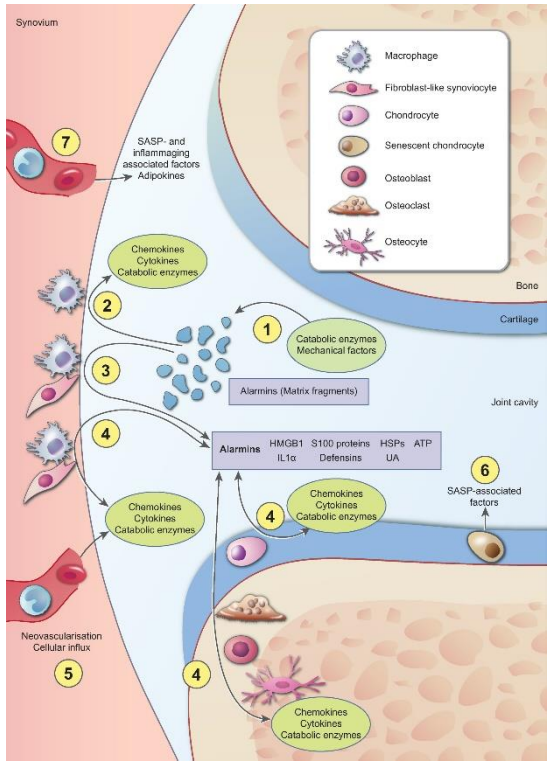

Figure 2. Overview of the pro-inflammatory feedback activated in the articular tissue during the progression of knee OA. Picture taken from [24].

1.1.2 The inflammatory mediators

There are different classes of biomolecules that are involved in the low-grade inflammation process of OA. The most studied class of pro-inflammatory mediators is undoubtedly the cytokines. Example of the most studied cytokines are interleukin-1 beta (IL-1β), tumour necrosis factor (TNF) alpha, IL-6, IL-15, IL-17 and IL-18. IL-1β and TNF-α have been found in high level in arthritic cartilage, synovial membrane, synovial fluid, and subchondral bone [25]. In two independent follow-up studies the

concentration of IL-6 in the blood resulted higher in patients suffering from knee OA and they also correlated with the loss of cartilage [26,27]. Similarly, increasing levels of IL-8 in the knee synovial fluid of arthritic patients were associated with the clinical progression of the disorder [28]. Pro-angiogenic factors, responsible for the calcification of the cartilage, are produced upon the stimulation of IL-17, synthetized by both synovial fibroblasts and chondrocytes [29]. Another class of crucial players are the proteases, responsible for the direct degradation of the extracellular matrix. Several enzyme classes are active in the degradation of different constituent of the cartilage. The aggrecan-degrading enzymes have the ability to degrade the aggrecan, a large proteoglycan enriched in the cartilage. It's difficult to elucidate which target is firstly degraded in the course of OA, but there are experimental evidences that the aggrecan degradation is a very early event in the developing of OA [30,31]. Different isotypes of metalloproteinases (MMPs) have been shown to be able to digest the aggrecan [32]. Another well-known family is the A Disintegrin And Metalloproteinase with Thrombospondin motifs (ADAMTS), also called as aggrecanases [32]. Similarly to MMPs, several isoforms of proteases belonging to this family are activated in the OA in response to the pro-inflammatory cues. A second important target of proteases in the cartilage is collagen type II, the major constituent of the

cartilaginous matrix. This fibrillar isoform of collagen can be digested by few enzymes: collagenolytic MMPs and cathepsin K [32]. MMP-1, -8, -13 and -14 belong to this group, and among them the MMP-13 is considered to be the most active enzyme in OA [33]. The expression of most of these proteolytic enzymes is positively regulated by different factors: pro-inflammatory cytokines, mechanical stimuli, hypoxia, miRNA and heparan sulfate and sulfatases expression following articular tissue damages [32]. The chemokines are another family of pro-inflammatory mediators highly expressed by the inflamed articular cells. The main function of these molecules is to stimulate the cellular motility, especially in the immune cells that express sets of chemokine receptors [34]. In addition, they can also participate in the matrix degradation: CCL2, expressed by chondrocyte, increased the production of MMP-3 and the loss of proteoglycan in *in vitro* human cartilage [35]. Also adipokines and neuropeptides have a direct or indirect role in the inflammation response and the subsequent matrix degradation. For instance, the adipokine level in the serum correlated with the severity of OA [36], while the neuropeptides can stimulate the proliferation of synoviocytes and the synthesis of prostaglandin E2 and collagenase [20].

1.2. The course of osteoarthritis

Depending on the individual risk factors, OA is usually characterized by a slow progression over decades or it can occur in an intermediate form in which periods of slow evolution alternate with period in which the OA gets worse very quickly [37]. During its progression, different symptoms and signs characterize the knee OA. The most common are pain, joint stiffness, reduced motion and muscle weakness [38]. The long-term effects of this symptomatology are various and include both physical, such as decreased physical activity, fatigue and disability, and psychological consequences, like depression and impaired sleep [38]. In OA evolution, the low-grade inflammation is associated with two main features: the progressive mechanical and structural deterioration of the cartilage and the structural changes in the subchondral bone (osteophyte formation and sclerosis) [39]. The structural changes that occur in the arthritic joint are summarized in Figure 3. The inflammation and the degradative processes have their effects in all the articular tissues, however the cartilage, the synovial membrane, the synovial fluid, and the subchondral bone are the key players.

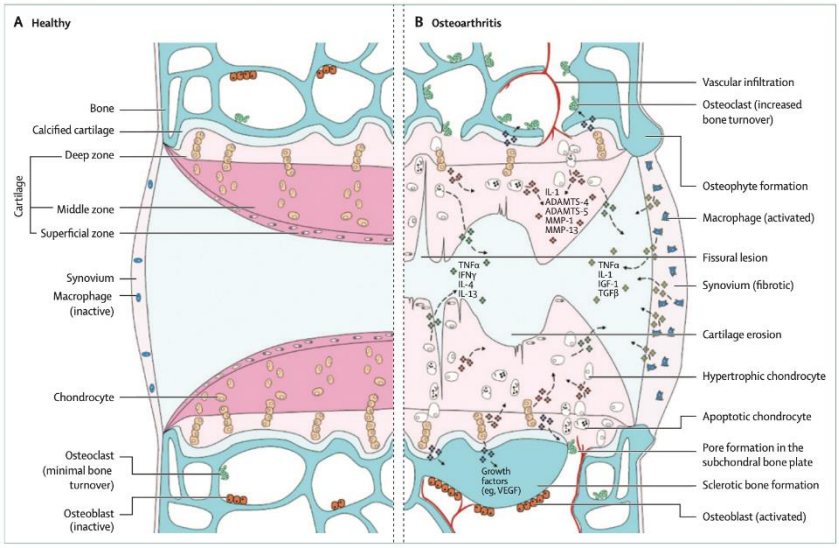

Figure 3. Structural and anatomical modifications and the signaling pathways activated during the osteoarthritis progression. IFN: interferon. IGF: insulin-like growth factor. TGF: transforming growth factor. VEGF: vascular endothelial growth factor. Picture taken from [40].

Clinically, it is possible to subdivide the OA progression process in 5 different stages according to the severity of the symptoms and the structural and functional changes in the knee.

1.2.1 Grade 0 (pre-osteoarthritis)

This stage describes a physiologic and healthy joint, and usually the disease is not yet manifested. However, the very early stage of OA can be also included, when the damage is still on a cellular level, such as the initial alteration of the cell metabolism in cartilage and synovial membrane. No clinical signs or symptoms are detected [41].

1.2.2 Grade 1 (early or doubtful)

In grade 1 two processes are potentially initiated: the narrowing of the joint space, even if in a non-evident manner, and the formation of osteophytes [42]. In fact, in the subchondral bone the pro-inflammatory mediators can stimulate the expression of angiogenic factors and new vessels penetrate within the bone tissue reactivating the process of endochondral ossification [40]. This process can explain the formation of osteophytes and cysts, that usually are formed in the periphery of the joint, at the junction site with the synovial membrane [37]. A similar angiogenetic process occurs also in the synovial membrane. In fact, the inflammatory cells release pro-angiogenic factor, promoting further vascular invasion and facilitating an additional recruitment of immune cells. Therefore, this process facilitates the persistence of the inflammatory state [43]. Regarding the cartilage, only the superficial layer begins to structurally change, resulting softer, while the deeper area is preserved. This is due to the secretion of degrading enzymes by chondrocytes that lead to the loss of glycosaminoglycan, with the subsequent increase retention of water [44]. Over the time, local focal discontinuities are formed in this zone, while in the mid zone of the tissue some harmful changes can start to occur, such as chondrocyte proliferation and death. In this stage some people

can start to experience mild pain in the knee, while others don't show any sign or symptom yet [42].

1.2.3 Grade 2 (mild or minimal)

During the stage 2 of OA progression the number and the dimension of osteophytes increase, and they can cause pain determining an initial reduced joint mobility [37]. In addition, the joint space between the bony heads may begin to narrow, especially if evaluated in weight-bearing conditions [42]. The cartilage can show initial sign of erosion. The first clear manifestations in the cartilaginous matrix consist in vertical fissures that reach the middle zone. These fissures are the hallmarks of abnormal stress in the deeper cartilage layer [37]. At this point, the symptoms can vary from person to person. Some people may start to feel pain during or after physical activity. In addition, someone can also start to have problems in bending or straightening the affected joint, leading to the impairment of some movements [42].

1.2.4 Grade 3 (moderate)

The grade 3 is characterized by the formation of multiple osteophytes, the narrowing of the joint space is now clearly visible and the subchondral bone presents sclerosis and possible deformity [45]. The loss of the cartilage is now important, characterized by the appearance of local eroded zones. These

modifications lead to the worsening of the symptoms. In fact, most people have frequent pain when doing daily activity like moving or walking. Joint stiffness is higher, and usually is worse in the morning or after prolonged sitting. At this point, the swelling of the knee can also be noticeable [42].

1.2.5 Grade 4 (severe)

In the end-stage arthritic knee the structure of the joint is widely rearranged. It is possible to see microfractures, zone of repair, and subchondral bone sclerosis and remodelling that result in an advanced joint deformity [37]. The osteophytes are numerous and large and the joint space narrowing is marked [42]. The hyaline cartilage is significantly thinner and locally can also be completely eroded. In these area, the mineralized cartilage, or even the subchondral bone, is exposed and act as articular surface [37]. At this stage also the synovial fluid present visible alterations. Its peculiar viscoelastic properties, especially viscosity and elasticity, are compromised, due to the fluid exudation from the more permeable synovial vessels that dilute the hyaluronan in the fluid, that also presents a lower molecular weight [46]. This can increase the friction between the articular facets, leading to pain, joint stiffness and reduced mobility [37]. In addition, the minor viscosity of the synovial fluid allows the pro-inflammatory mediators to reach the sensory nerve cells in

the knee, increasing the pain sensation in the patients [23]. In fact, most of the end-stage arthritic patients suffer from huge pain when doing low intensity and daily activities. Joint stiffness, swelling, and inflammation result further aggravated, causing disability and undermining the everyday life [42].

2. The diagnosis of OA

2.1 The current diagnostic process

The diagnosis of OA is still primarily based on the thorough examination of the clinical history and of the symptoms of the patient. The process can be also supported by radiographic evidence, while laboratory testing for biomarkers is usually not foreseen [47].

2.1.1 Clinical examination

The clinical features usually found in patients affected by knee OA are the consequence of the alterations previously described that are mainly related to the inflammation process, cartilage erosion and bone deformity. The diagnostic process is mainly based on a physical exam by the physician [47]. The personal medical history together with the classical signs and symptoms that affect the knee joint are examined. The latter include pain and crepitus during different range of motion, effusion within the joint cavity, presence of popliteal cyst, lateral joint instability and

valgus or varus deformity [48]. Other signs, that are common of OA process in other joints are joint tenderness, reduced movement range and bone swelling [49]. The pain is the most relevant sign, and it is described as intense, deep, and "achy" [50]. The pain in the knee leads to a decrease of the mobility range, of the joint function and in general of the physical activity. Over the time, the patient will be less active, increasing the probability of developing co-morbidity. For instance, the decreased physical activity could lead to the augment of the body mass and consequently of the load acting on the knee, worsening the already precarious conditions of the arthritic articular tissues [50]. Another factor that limits the mobility of arthritic patients is joint stiffness, the feeling that the motion of a joint is limited or difficult. This perception may occur also at rest or in the morning [50].

Usually, laboratory testing is not prescribed for the diagnosis of OA. In fact, common systemic inflammatory markers, such as C-reactive protein and erythrocyte sedimentation rate, typically result within the physiological ranges [51]. Similarly, immunological tests are useful only in those, relatively rare, cases in which a strong inflammation response is present, making an autoimmune response more probable [47]. As a matter of fact, the clinical guidelines provided by the American College of

Rheumatology did not recommend routinely laboratory analyses in patients with knee OA [52].

2.1.2 Radiography imaging of the joint

The plain radiography of the knee is commonly used to support and confirm the diagnosis of OA, also because this exam is widely and readily available, and relatively cost-effective [48,53]. X-ray imaging can evaluate the alterations in the bone tissue, such as the bone sclerosis, osteophyte and cyst formation and the joint space narrowing. The first classification scheme based on x-ray imaging was developed by Kellgren and Lawrence in the late 1950s, to overcome the disagreement on the evaluation of the joint conditions among different observers [54]. They proposed their classification based on a set of standardized radiographs of eight different joints. This scale has proved to be effective for the evaluation of the clinical signs especially in the knee joint. In fact, the interobserver correlation coefficient was the highest compared with the other joints and the intraobserver correlation resulted the second highest [54]. This is the reason why the Kellgren and Lawrence classification is still among the most used diagnostic tool for the diagnosis and the evaluation of the severity of knee OA [55]. This scale provides the five different stages of the progression of knee OA described in the paragraph 1.2, with score ranging from 0 to 4 according to the increasing severity of

the disease, where grade 0 indicates no presence of OA while grade 4 signifies severe OA [54]. Over the years, five other classification scales have been developed that are now widely used in addition to the Kellgren and Lawrence one. They are International Knee Documentation Committee (IKDC) radiographic scale, Fairbank, Brandt, Ahlbäck and Jäger-Wirth [56]. The interobserver reliability of this six widely used radiographic classification systems resulted good, while the arthroscopic findings correlated with a medium degree with the arthroscopic evaluations [57]. In addition, the IKDC classification resulted the most effective in terms of combination between reliability and interobserver correlation [56].

2.1.3 Magnetic Resonance Imaging (MRI)

The MRI is less widely used, even if it allows to get more information, such as early alterations in the cartilage and subchondral bone features (e.g. chondral thinning, structural changes, osteophytes and bone marrow oedema-like lesions (BMLs)) [55]. In fact, with MRI it is possible to obtain a precise morphological evaluation of the cartilaginous surface, thus providing crucial information about the thickness, the structural integrity, the presence of fissuring and loss of cartilage [55]. Moreover, recent evolvements of this technique also allow the detection of very early changes of the cartilage, providing a

precise evaluation of the degenerative process. These innovative approaches can highlight the initial softening of the tissue, an early modification that is due to the increase in the water content that reduces the concentration of collagen and glycosaminoglycans [44]. MRI can also detect early changes in the subchondral bone, such as BMLs. They are related to the progressive degeneration of the cartilaginous matrix and can include oedema, bone marrow necrosis, fibrosis and modifications in the trabecular structure [58,59]. These early changes in the cartilage and in the subchondral bone are usually not visible with radiographs. In fact, conventional radiographic imaging can only indirectly assess the cartilage thickness by the joint space narrowing, that became evident only in the late stage of OA. In addition, the BMLs are usually not visible [55]. MRI can be also useful in the detection of comorbidities that have to be treated differently or more urgently than the OA, such as subchondral insufficiency fracture, tumours, or infection [48].

2.1.4 Computed Tomography (CT)

While the MRI can detect the alterations that mainly affect the superficial layer of the cartilage, the CT can reveal and quantify structural alterations and evaluate the pathophysiological state of the whole cartilage tissue [60]. This technique, even if not widely used in the diagnosis of OA, is performed during arthroscopy,

when the instrument is incorporated into the arthroscope and is able to generate a high-resolution reconstruction of the tissue [61]. The CT imaging is also used to detect other abnormalities that occur in the joint, such as disorders of patellofemoral joint, such as its misalignment [50].

2.1.5 Ultrasonography

Ultrasonography can be used to investigate pathological processes in the articular tissues, including cartilage degeneration, and to assist physicians during intra-articular injections [50]. Several harmful processes can be visualized with this technique: joint effusion, osteophytes formation, synovitis and others [62]. The ultrasonography is more sensible and specific in detecting osteophytes than MRI, but it results less effective in the evaluation of the joint space narrowing [63]. Furthermore, ultrasonography can also help to identify and differentiate other joint pathologies such as osteomyelitis and bone metastasis [50]. Overall, given the lower costs of this examination and the higher handling, its use is increasing in the diagnosis of OA [48].

2.2 Limitations of the current diagnostic process

Despite the numerous techniques and approaches currently available, the diagnostic process of the knee OA still fails to detect the pathology at an early stage. In fact, the clinical examination

and the indication for the instrumental investigations are prescribed only after the onset of the symptoms. However, at this stage the OA is most likely at an advanced stage and probably already irreversible because it is the result of a relatively long period of subclinical modifications [40]. For this reason, the diagnosis of early OA can't be based on the symptom evaluation, as this has limited diagnostic value [40]. Moreover, the symptoms vary a lot from patient to patient, can fluctuate over the time, and can also be influenced by other factors, pathologies or modulating pathways [64]. Imaging approaches have several and important limitations too, which are summarized in Figure 4. Generally, structural changes can take up to 1 or 2 years to be clearly detectable by common imaging techniques such as radiographs [65]. X-ray imaging is also associated with high-energy radiation exposure, lack in sensitivity and cannot detect cartilage degradative cues [66]. For instance, Amin et al., reported that in a huge number of patients with symptoms, no evident harmful cues were found by radiographs, even if they suffered from cartilage loss, as shown by MRI [67]. In addition, the measurements on radiographic images lack also in specificity: the joint space narrowing, one of the crucial parameters, can be affected by the structural integrity of the meniscus and by the positioning of the joint during the examination [68,69]. The MRI is more sensitive in detecting early structural alterations and for

this reason the Osteoarthritis Research Society International suggests the use of this technique to assess the cartilage morphology [70]. However, this approach has also some important drawbacks, mainly due to the diversity of the symptoms and the individual response. Firstly, the early cartilaginous modifications cannot be symptomatic in all the arthritic patients and the morphological examination doesn't take in consideration the inflammation process and its consequences, such as oedema [71,72]. In addition, the clinical applicability is limited by higher scanning times and, especially for the more recent approaches, the need of nephrotoxic contrast agents, ultra-high magnetic fields and specific software [40,73]. Similarly to x-ray imaging, the CT has the disadvantage of high radiation exposure, even higher of the radiographs, but it allows the 3D visualization of the bone and the cartilage [62]. In addition, it is characterized by a lower capability in the assessment of the soft articular tissues compared to MRI. Moreover, when used in combination with arthroscopy, its widely applicability is greatly limited by the invasiveness that characterize this approach [74]. With the ultrasound imaging it is possible to image the soft tissues, including the synovial tissue without the use of contrast agents. However, the results strongly depend on the competence of the operator and the depth that the signal can reach within the articular tissues [62]. This could represent an important issue in

the load-bearing joints as the knee because the ultrasounds are affected by acoustic shadowing due to the physical properties of the ultrasonography [75]. Even if the MRI is gaining importance, the radiography still remains the standard for the diagnosis and the evaluation of OA progression [76]. Therefore, in most of the arthritic patients the structural alterations and the clinical progresses are not detectable in the very early phases of the pathology.

	Primary use	Analyses	Advantages	Disadvantages
Plain radiograph*	Cartilage thickness	(Semi)quantitative	Low cost, easy applicable	Indirect, two-dimensional image of a three-dimensional problem
CT				
Standard*	Bone characteristics	Semiquantitative	Three dimensional	Radiation exposure, only bone
CECT	As standard plus cartilage volume	Semiquantitative	Three dimensional, information on cartilage	As standard plus contrast agent needed
Ultrasound				
Standard*	Inflammation	Impression	Cheap	User dependent
Power doppler	Vascularisation	Semiquantitative	Direct measure	Relative importance for osteoarthritis
MRI				
Standard SPGR*	Cartilage morphology	Quantitative	Three dimensional, quantitative	Time-consuming analyses
T2 MRI relaxation	Collagen distribution	Semiquantitative	Information on cartilage quality	Complex interpretation
$T1\rho$	Proteoglycan distribution	Semiquantitative	Information on cartilage quality	Complex interpretation
^{23}Na MRI	FCD/proteoglycan content	Semiquantitative	Information on cartilage quality	Field strength ≥3T
dGEMRIC	FCD/proteoglycan content	Semiquantitative	Information on cartilage quality, early changes	Contrast agent needed
MRI whole-organ scoring				
KOSS	..	Semiquantitative	Whole-organ score	Time consuming, observer variance
WORMS	..	Semiquantitative	Whole-organ score	Time consuming, observer variance
BLOKS	..	Semiquantitative	Whole-organ score	Time consuming, observer variance

CECT=contrast-enhanced CT. SPGR=spoiled gradient echo. FCD=fixed charge density. dGEMRIC=delayed gadolinium-enhanced MRI of cartilage. KOSS=knee osteoarthritis scoring system. WORMS=whole-organ magnetic resonance imaging score. BLOKS=Boston Leeds osteoarthritis knee score. *Techniques that have a more common clinical and research applications for the assessment of cartilage (and bone), bone, and synovial inflammation, as well as quantitative cartilage morphology (at present the most used MRI modality in clinical trials).

Figure 4. Features, advantages and disadvantages of the imaging techniques used for the OA diagnosis. Picture from [62].

2.3 Biomarkers

Due to the limitations of current diagnostic approaches described above, the development of sensitive ad predictive OA biomarkers is of paramount importance. These biomarkers could serve not only as diagnostic tools for the early assessment of OA, but also for the evaluation of the clinical OA stage, the prognosis, the patient stratification for personalized treatment and the

prediction and monitoring of the clinical response to a therapy [77,78]. Biomarkers for the knee OA that have been proposed in the last years are represented by molecules or molecular fragments that are released into biological fluids, in particular synovial fluid, blood or urine. These molecules are usually generated in the articular cartilage, subchondral bone and synovial membrane and reflect extracellular matrix turnover (e.g. collagen and proteoglycans, highlighting both the synthesis and the degradation) and altered cell metabolism, such as cytokines, chemokines, proteases and others [79]. The aim of using soluble biomarkers for the diagnosis of knee OA is to reflect the pathological processes acting on the articular tissues earlier and in a more relevant way before they induce the structural alterations visible with the imaging approaches. In fact, while the latter provide information and quantification only on the structure of the joint, the formers are produced within the pathological processes that cause visible structural alterations in the long term [80]. In 2001 the Biomarkers Definitions Working Group defined the biomarkers as: "a characteristic that is objectively measured and evaluated as an indicator of normal biological processes, pathogenic processes, or pharmacologic responses to a therapeutic intervention" [81]. Therefore, these biomarkers could ultimately represent a relevant alternative for the current imaging diagnostic approaches to guarantee an

earlier, more targeted and personalized treatment for the OA. As previously described, the articular tissues that are mostly involved in the OA are the cartilage, the synovial membrane, the subchondral bone, and the synovial fluid that allows the intercommunication between them. Within these tissues, the important pathological pathways activated are cartilage degradation, reduced cartilage synthesis, inflammation, and bone remodelling. Therefore, the research of potential innovative biomarkers is focused on molecular players in these pathways.

2.3.1 Biomarkers of altered cartilage homeostasis

Resembling the metabolic alterations that occur in the articular cells, increases in the catabolic markers and decreases in the anabolic ones have been associated with the progression of OA [79]. Being the major and more specific component of the cartilaginous matrix, type II collagen has been extensively studied. In fact, several potential biomarkers reflecting its turnover has been proposed [82]. In particular, the C- terminal telopeptides, which are the product of the collagen degradation, and the N-terminal propeptides, which indicate the synthesis of the molecule (Figure 5) [79].

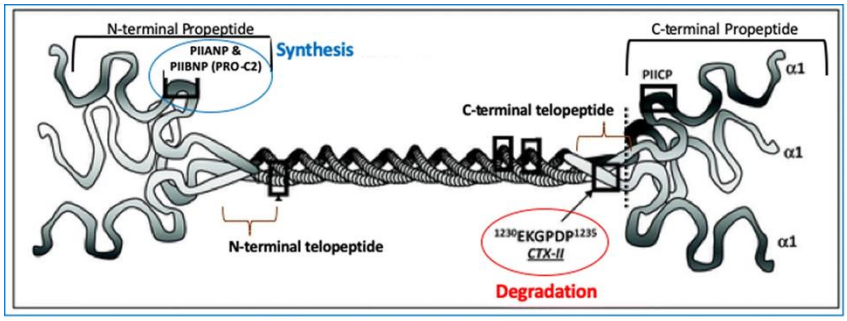

Figure 5. Key biomarkers derived from the type II collagen indicating both its degradation and synthesis processes. Picture from [79].

C-telopeptide fragments of type II collagen (CTX-II) is one of most studied degradation products as OA biomarkers. It is generated following the digestion by MMP-9 and -13 and its presence was detected in proteoglycan-depleted areas of *ex vivo* cartilage explants stimulated with pro-inflammatory mediators [83]. This digestion fragment was also found in the bone-cartilage interface and in the damaged cartilage, whereby it was correlated with the bone turnover, the formation of osteophytes and the joint space narrowing process [84]. CTX-II was also detected in urine, where its level positively correlated with the probability to develop a relevant clinical OA and total knee replacement [85,86]. In addition to the CTX-II fragment, the concentration in the serum of hyaluronic acid and cartilage oligomeric matrix protein (COMP) resulted higher in early stage and established arthritic patients, as recently reviewed [76]. Conversely, the systemic concentration of the N-terminal propeptides, hallmark of the

cartilage synthesis, inversely correlated with the probability to develop a clinical relevant OA, resulting lower in patients with established OA [85,87].

2.3.2 Biomarkers of the inflammatory response

Despite the inflammation process in the OA is usually a low-grade response, increasing evidences demonstrated a correlation between radiographic-diagnosed OA and inflammatory hallmarks, such as effusion, synovial thickening, popliteal cysts and activated immune cells [88,89]. Recently, six potential inflammatory biomarkers (MMP-3, sVCAM-1, sICAM-1, VEGF, TIMP-1, and MCP-1) found in the synovial fluid correlated with the synovitis, the radiographs and the severity of the symptoms [90]. Interestingly, these mediators were positively linked to the activation of macrophages and neutrophils and two products of these cells, TGF-β1 and elastase, resulted correlated with synovitis and the OA worsening [91]. Deveza et al., reported a modest association but a high specificity of hyaluronic acid and MMP-3 with the effusion in synovitis [92]. Similar outcomes demonstrated that increased blood levels of IL-1b, TNF-a and cyclooxygenase-2 (COX-2), indicated a higher risk for knee OA worsening [93]. In addition, other previously proposed inflammatory-related biomarkers for OA were adipokines [94].

2.3.3 *Biomarkers of the subchondral bone remodelling*

One of the structural alterations that affect the subchondral bone during the OA is the so-called stress shielding, that leads to the initial thickening of the horizontal trabeculae while the vertical ones result thicker only in later stage of the OA [95]. Therefore, it's not surprising that bone remodelling biomarkers have been proposed for the OA diagnosis. In fact, many different peptides resulting from the digestion of collagen type I showed correlation with OA progression [79]. In particular, a serum form of collagen I-derived peptide correlate with higher risk of undergoing total knee replacement [86], while two different peptides found in the urine are associated with the progression of knee arthrosis [96]. The digestion of Collagen type I and type IV by MMPs can be predictive not only for joint and cartilage erosion but also for the responsiveness of specific anti-inflammatory treatments [97,98]. Moreover, genomic studies revealed pathways associated with Periostin and Leptin that are involved in the higher turnover of the subchondral bone [99], and several genes whose expression resulted coordinated in the cartilage and in the underlying bone [100].

2.3.4 *Limitations of the available OA biomarkers*

Although promising, several of the potential biomarkers proposed failed the validation process toward their clinical use.

For instance, the correlation between urinary concentration of C-telopeptide of the type II collagen, pain and radiographic findings wasn't significant [101]. Similarly, the biomarkers of the subchondral bone remodelling showed even less effectiveness, most likely because the portion of the tissue involved in the knee OA is relatively small and the turnover is rapid [62]. The markers of synovitis have been the least studied, but they showed promising results, even if different aspects have to be addressed [62]. For instance, being the inflammation a general response to harmful stimuli, it is more difficult to find systemic biomarker candidates that reflect specifically the inflammation in the knee joint. Other issues include the sample collection needs to be standardized, the relation with the imaging outcomes should be improved and the effect of circadian rhythm and the exercise on the biomarker concentration has to be evaluated [102–104]. Figure 6 summarizes the most reported biomarkers and their clinical significance until few years ago. Unfortunately, the most important issues remained currently undressed [76].

	Diagnostic value	Relation to burden of disease	Prognostic value	Relation to efficacy of treatment	Overall positive proportion
Cartilage degradation					
CTXII in urine*	12/13	16/25	17/23	4/5	74%
COMP in serum*	9/12	15/26	6/17	1/2	54%
Coll 2-1 (NO_2)† in urine and serum	7/8	2/6	2/4	..	61%
KS in serum	1/2	3/8	3/5	1/2	47%
YKL-40 in serum	1/3	5/12	0/4	1/1	35%
C2C in urine and serum	1/1	3/9	0/4	1/3	29%
C1,2C in urine and serum	..	1/6	0/4	0/2	8%
Cartilage synthesis					
PIIANP in serum*	2/2	1/4	2/3	0/1	50%
PIICP in serum	..	3/7	0/4	..	27%
CS846 in serum	0/1	1/7	0/3	..	9%
Bone degradation					
NTX-I in urine and serum*	1/2	1/1	2/5	2/2	60%
(D)PYR† in urine	2/3	6/15	0/10	2/2	33%
CTXI in urine and serum	2/4	1/16	1/6	0/1	15%
Bone synthesis					
OC in serum*	1/5	2/12	2/6	1/2	24%
BSP in serum	2/2	1/3	0/2	..	43%
PINP in serum	0/1	1/4	0/4	..	11%
Synovium degradation					
HA in serum*	7/9	7/22	8/11	1/3	51%
Glc-Gal-PYR in urine	2/2	3/4	..	0/1	71%
Synovial synthesis					
PIIINP in serum	1/1	2/4	0/2	..	43%

Data are n/N unless otherwise stated. Biomarkers with less than five reports are not included. Data from van Spil and colleagues.[68] *The most relevant and best performing commercial biomarkers. †Combined biomarkers: Coll 2-1 with Coll 2-1 NO_2 and PYR with D-PYR.

Figure 6. The most reported works on different knee and hip OA biomarkers. The reported studied were published until 2011, data from [62].

In addition, for many of the proposed biomarkers we still don't know their kinetics, metabolism, and the exact molecular and systemic validity [105,106]. For instance, the concentration of different markers can fluctuate in accordance to the progression of the pathology and, given the numerous risk factors and the pathogenetic processes, they cannot show the same trend in all the patients [62]. In fact, until few years ago the knowledge about the correlation between biomarkers and structural alteration of

the joint tissue was higher than their association with the clinical signs [107]. For all these reasons, despite the relatively high number of potential biomarkers that have been proposed in the last decades, none of them is sufficiently sensible and specific to be used in the diagnosis and in the prognosis of OA in a clinical setting [79]. New potential or better set of markers are still under investigation. In fact, it's unlikely that a single biomarker would fulfil all the requirements needed for its clinical employment, such as early OA discrimination, prediction of the pathology progression and responsiveness to treatments. It's more probable that different biomarkers candidates need to be used in combination [79]. In this scenario, new potential biomarkers could be represented by the extracellular vesicles (EVs). In fact, the EVs could act as OA markers as itself or in combination with the plethora of bioactive molecules carried within them.

2.4 Extracellular vesicles

The EVs have recently gained increasing interest as they could serve both as early diagnostic and as prognostic biomarkers of OA [108]. EVs are lipid vesicles secreted by virtually all the cell types and they represent key mediators in the process of intercellular communication. They are released by the donor cell into the extracellular space or body fluids like blood and synovial fluid and can transfer to the acceptor cells a wide range of

different bioactive molecules, such as nucleic acids, proteins, enzymes and lipids [109]. The advantages of EVs as biomarkers are mainly associated to their stability, their ubiquitous presence in biofluids and to their capacity to reflect the metabolic state of the origin cell. Thanks to these features, they have been proposed as potential powerful diagnostic tools to monitor the state and the progression of specific diseases [110].

2.4.1 EV classification

Classically, EVs were classified in exosomes, microvesicles and apoptotic bodies according to their origin and their specific release pathway [111]. Exosomes are the vesicles that originate from the endosomal pathway. Specifically, the invagination of the plasma membrane during the endocytosis or the trafficking of the cells' material produces the early endosome [112]. A further inward invagination of the lipid membrane of these structures originates the exosomal vesicles. The early endosomes then mature in the multivesicular bodies (MVBs) that can fuse with lysosome to be degraded or with the plasma membrane, thus releasing their content, including the exosomes, into the extracellular space [113]. The microvesicles, also referred as ectosomes, are formed by the direct budding of the plasma membrane of the cells, a process called pinching [114]. The biogenetic pathway of these vesicles is not yet fully elucidated,

but evidences reported that is a calcium-dependent process during which different cytoplasmatic machineries are needed: components of the cytoskeleton (actin and microtubules), motor proteins (kinesins ad myosin) and fusion machinery complexes (SNAREs and tethering factors) [115,116]. The apoptotic bodies are the largest vesicles and their biogenesis is well known for a long time. They represent the converging step of different molecular pathways that can lead to the programmed cell death and the disassembly of the cell [117]. The cell membrane form blebs and protrusions and finally apoptotic bodies are released after the fragmentation, during which different size vesicles are formed [117]. Conversely to the traditional view, increasing experimental evidences support the hypothesis that the cell material enclosed within the apoptotic bodies can be transferred to phagocytic cells and even recycled [118].

Currently it is still not possible to separately collect the EVs according to their biogenesis. In fact, nobody has yet identified markers able to specifically reflect the different biogenetic pathways of the three subtypes of EVs [119]. For this reason, over the years this subdivision was modified, becoming based on the dimension of the EVs. In this way, the vesicles with a diameter below 150 nm were defined as exosomes, the microvesicles are those with dimensions ranging from 100 up to 800 nm while the apoptotic bodies were classified as the largest EVs, with a

diameter that can range between 200 nm and few micrometres [119]. Despite this classification has been used in a multitude of studies for years, it proved to be limited. In fact, as it can be seen from the size limits set, there is an overlap in the dimensions of the three different categories. It has also been reported that EVs originated in the endosomal pathway can be larger than 100 nm as well as vesicles smaller than 100 nm can bud off from the plasma membrane [120,121]. A similar overlap was observed also in the protein profiles of the three different EV subtypes [122]. In addition, increasing experimental evidence have demonstrated that the EVs are a heterogeneous population of lipid particles with different chemical-physical features. In fact, according to the specific characteristic considered and the isolation technique employed, it is possible to obtain several subpopulations of EVs. The EVs can differ based on their size, density, morphology, content, biological effect and others parameters, as shown in Figure 7, making even more limited the classic subdivision of the EVs in exosome, microvesicles and apoptotic bodies [119].

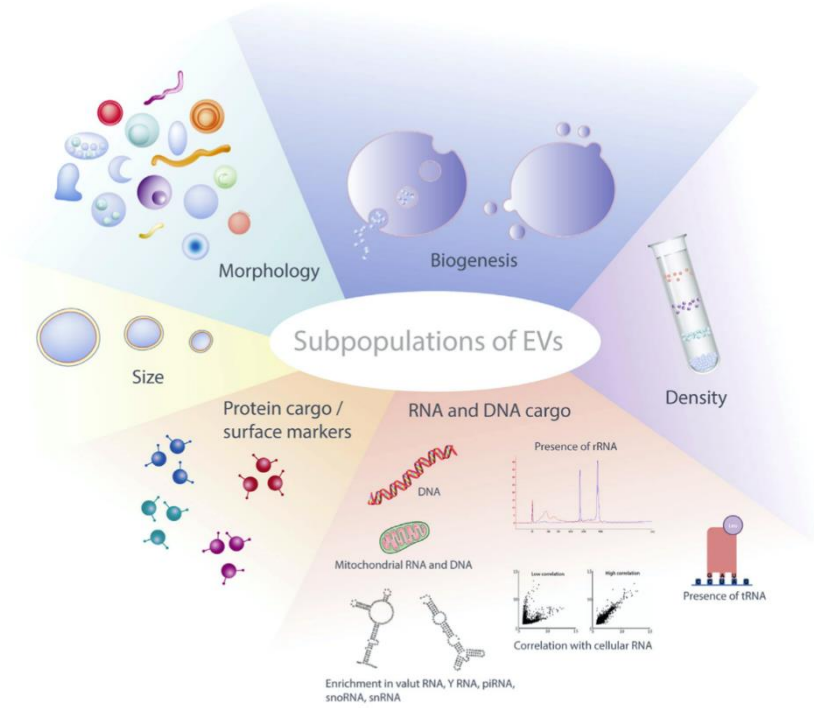

Figure 7. Overview of the chemical-physical features of the EVs that can be used to recognize different subpopulations. Image taken from [119].

For this reason, the International Society for Extracellular Vesicles recommended to use the term "extracellular vesicles" in association with operational terms that can be referred to physical properties (e.g. small or large size EVs, low or high density EVs), biochemical composition (e.g. CD81+ EVs) or description of condition or origin cells (e.g. chondrocyte EVs, hypoxic EVs) [123].

2.4.2 EVs in the OA diagnosis

All the articular cell types can secrete EVs in the synovial joint environment. Even if not numerous as in other disease, evidence of the potential use of EVs for the OA diagnosis have been reported. The rationale of their use in the diagnostic process is based on the fact that the content of the EVs secreted from a specific cell reflects the metabolic state of the origin cell. Therefore, harmful signals can be enclosed within EVs and sent to the other articular cells, thus affecting the catabolic/anabolic balance in other articular cell types participating in the onset and development of OA [124]. For instance, EVs secreted by activated macrophages promoted the expression of inflammatory mediators (IL-8, IL6, and MMPs) in chondrocytes [125]. Similarly, the EVs isolated from the synovial fluid of arthritic patients had higher content of cytokines and chemokines and significantly activated macrophages that in turn secreted inflammatory cytokines, chemokines and MMPs [126,127]. Therefore, the content of the EVs is not predetermined but reflects the metabolic conditions of the origin articular cell and for this reason the EVs attracted attention as potential innovative biomarkers for OA. Since the synovial fluid is in direct contact with virtually all the articular tissues, it represents a valuable source of EVs that can be used to monitor the pathophysiological alterations in the joint environment. Two different studies reported that the size and the

concentration of EVs in arthritic patients and in healthy donors was similar [128,129]. However, Gao et al. reported that in more severe OA stages small size EVs were increased when compared to lower grade OA [127]. In addition, the expression of a long non-coding RNA contained in the small-size EVs isolated from the synovial fluid of arthritic patients correlated with the clinical stage of OA [130]. Other similar studies found that another long non-coding RNA was significantly upregulated in serum-derived EVs of arthritic patients [131], while a miRNA was lower in plasma-EVs of arthritic patients when compared with healthy people [132]. The relatively low number of evidences and some contradictory findings reflect the relative youth of this research field. But it also denote a lack of standardized experimental procedures for the EV isolation and the characterization of their content [124]. In fact, most of these studies were focused on small-size vesicles or, according to the classic nomenclature, exosomes. However, different subpopulations of EVs do exist and might have relevant pathophysiological implications [119,133].

2.4.3 EV subpopulations

As mentioned in the paragraph 2.4.1, EVs present a huge variability om their features, originating different subtypes. This observation led to the hypothesis that the diagnostic potential as well as the therapeutic activity of EVs can be mediated by only

one or few of these subpopulations, as previously reported [119]. For this reason, increasing efforts are currently being made in isolating and characterizing the different EV subpopulations [134–136]. The aim of this research line is to isolate, separate and possibly purify the different EV subpopulations to be able to understand if and which of them could have the optimal diagnostic value. This hypothesis could have huge implications on the potential use of the EVs also in the diagnosis of knee OA. For instance, it has been demonstrated that the medium and large size EVs play an important role in the inflammation process. These subpopulations of EVs can be secreted by several cell types involved in the inflammation process, including platelets, endothelial and immune cells, and they can have anticoagulant, pro and anti-inflammatory capabilities [137]. In fact, they can carry proteases and matrix-remodelling enzymes [138,139], anti- and pro-inflammatory miRNA [140] and can also regulate the oxidative stress [141]. Given the importance of the inflammatory process in the OA, the large size EVs subpopulations in the synovial fluid, more than other subtypes, could reflect the physio-pathological conditions of the articular tissues, thus representing a promising approach in the research of innovative OA biomarkers.

2.4.4 *Size-based EV isolation and separation techniques*

The spectrum of the EV subpopulations that it is possible to isolate strictly depends on the technique used. Several isolation methods, based on physicochemical or molecular features of the EVs, have been developed [142]. The most widely used approaches are summarized in Figure 8.

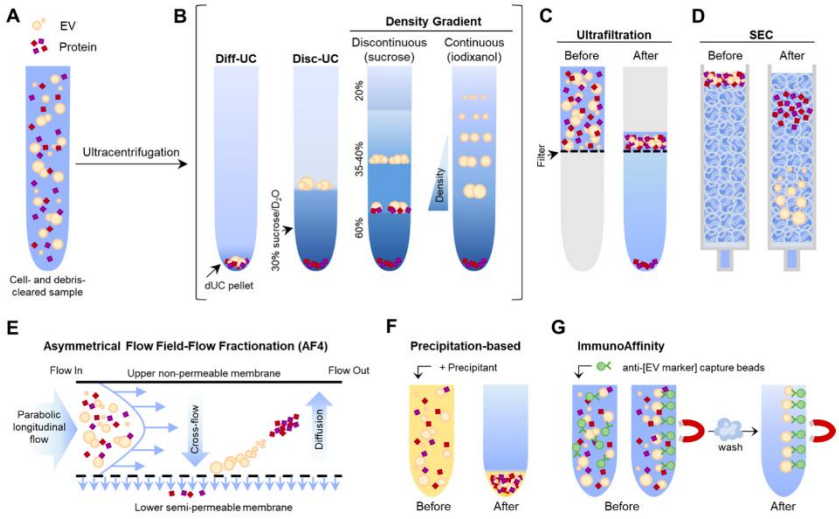

Figure 8. Graphical summary of the most used techniques to isolate EVs. Scheme taken from [142].

However, EVs isolation can be difficult, especially from biofluids. In fact, in addition to the intrinsic complexity of the sample, there is not a gold-standard technique that allow the separation of EV subpopulation with defined features. In fact, several approaches, often with different experimental protocols, are generally used to isolate and separate EV subpopulations based on their size.

The first and still most used method is the differential centrifugation, that is based on the sedimentation properties of the solutes with different size present in a solution, including the EVs (Figure 8B) [143]. Despite its practical facility, this technique is characterized by low purity, in terms of contaminants isolated together with EVs, and high operator-dependency [142]. In the attempt to better remove the contaminants, the size-exclusion chromatography (SEC, Figure 8D) approach has been adapted for the isolation of EVs several years ago [144]. Despite the higher purity, recovery and the availability of commercial chromatography columns, SEC is characterized by sample dilution and low resolution, defined as the inability to separate EVs with a low size difference [145]. This is also due to the fact that the commercially available stationary phases, including HPLC columns, are optimized for the isolation of only the small-sized EVs. Recently, another technique called asymmetrical flow field-flow fractionation (AF4), has been used for EVs isolation and the separation of subpopulations, following its development in the chemistry field several years ago [146].

2.4.5 Asymmetric flow field-flow fractionation

As depicted in Figure 8E, the operating principle of the AF4 requires an external flow that is applied perpendicularly to a parabolic longitudinal flow carrying the sample, leading to the

accumulation of the analytes on the bottom of the isolation chamber. Following their Brownian motion, the particles then diffuse and the smaller are the vesicles, the faster they diffuse and elute from the separating chamber following the parabolic flow [147]. In this way, the difference in the diffusion coefficients, that is related to the size of the EVs, allows to fractionate them. Moreover, the perpendicular flow can be modulated, making AF4 able to separate analytes with a broad size range, from few nanometres up to few micrometres, while maintaining a high resolution [147,148]. Therefore, with this instrument is possible to collect EV with a small difference in their elution time, separately collecting EVs with a similar size [147]. The AF4 was already used for the isolation of EV subpopulations from the culture medium. In fact, Zhang et al. used this approach, combined with ultracentrifugation, to isolate and separate a new subtype of EVs with a very small size. In particular, taking advantage of the high resolution that characterize the AF4, they were able to separate 3 different subpopulations of EVs with a very narrow size. The larger one was called large exosome vesicles, with a diameter of 90-120 nm, they isolated also the small exosome vesicles, with a size of 60-80 nm and a new and relatively abundant population of non-membranous particles called 'exomeres', with an average dimension of about 35 nm [149]. This approach was also used, in combination with an immunoaffinity chromatography, to

remove lipoproteins from the EV population and the to isolate and separate the three subpopulations found by Zhang et al. The combination of these two techniques allowed also to increase the yield of the EV isolation compared to SEC and ultracentrifugation [150,151]. Lipoproteins are in fact common contaminants found after using other size-based techniques as SEC and differential ultracentrifugation [142]. This system was successively on-line combined with the AF4, automatizing the entire isolation process [152]. Other studies used the AF4 to isolate the EVs from different starting specimens, such as culture medium, serum, plasma or urine or to characterize them, as recently reviewed [153]. However, the AF4 also presents some drawbacks that explain why it is not widely used in the EV field as other isolation techniques. First of all, it is based on a relatively expensive instrumentation that need purposely trained personnel, preventing its widespread diffusion in the research labs. From an experimental point of view, only small volume of the starting material can be loaded, usually a maximum of 100 μL. For this reason AF4 is not suited for large-scale preparations of EVs [147]. Moreover, the eluted samples are characterized by a very high dilution that, together with the low loading capacity, usually requires a concentration step before or after the fractionation [147]. This could determine a loss, especially if working with the

larger ones that are more fragile, or a contamination of the EVs [154].

Up to date, this approach has never been used in the isolation and characterization of the EVs in the musculoskeletal system. Also, despite the capability of this technique to separate analytes within a broad size range, most of the studies used AF4 to isolate and separate small size EVs [153]. Nevertheless, considering instead the advantages and the features of the AF4, it can represent a promising approach to isolate and characterize all the different sized EV subpopulations from the synovial fluid, increasing the probability and accelerating the research of new biomarkers for the OA. For this reason, in this PhD project I developed a protocol based on this technique to isolate all the EV subpopulations from the synovial fluid.

3. The clinical treatment of OA

Unfortunately, up to date there is no effective clinical treatment that can revert the tissues' degeneration and cure OA disorder. In fact, currently available approaches mainly aim at to managing the pain and at improving the life quality of the patients [155]. The treatments can be categorized in four different classes. The first one includes the nonpharmacologic approaches, including the reduction of modifiable risk factors, the physical activity, and the alternative therapies. The other categories are focused on the

management of the symptoms and consist of pharmacologic, surgical treatments and innovative therapies. Figure 9 schematically reports the currently available nonpharmacological and pharmacological clinical approaches for the OA.

	Treatment	OARSI Guidelines Recommendation
Reduction in modifiable risk factor	Weight loss	Appropriate
	Exercise	Appropriate: both land and water based, including strengthening
Bracing and physical modalities	Cane	Appropriate for knee-only OA
	Crutches	Uncertain
	Biomechanical interventions	Appropriate
Alternative therapies	T'ai Chi	No recommendation
	Acupuncture	Uncertain
	Balneotherapy/spa	Appropriate with individuals with multiple joint OA
		Uncertain with knee-only OA
	NMES	Not appropriate
	Self-management and education	Appropriate
	Cognitive behavioral therapy	No recommendation
	TENS	Uncertain in knee-only OA, otherwise inappropriate
	Ultrasound	Uncertain in knee-only OA, otherwise inappropriate
	Laser therapy	No recommendation
	Electromagnetic field therapy	No recommendation
Pharmacologic (oral)	Acetaminophen	Appropriate depending on comorbidities
	Avocado soybean unsaponfiables	Uncertain
	Chondroitin/glucosamine	Uncertain for symptom relief, not appropriate for disease modification
	Diacerein	Uncertain
	Duloxetine	Appropriate with multijoint OA, uncertain in knee-only OA
	NSAIDs	Appropriate in those without significant comorbidities
	Opioids	Uncertain
	Risedronate	Not appropriate
	Rosehip	Uncertain
Pharmacologic (topical)	Capsaicin	Appropriate in knee-only OA
	NSAIDs	Appropriate in knee-only OA, uncertain in multijoint OA
	Tramadol	No recommendation
	Opioids	Uncertain
	Topical NSAIDs	No recommendation
Pharmacologic (intraarticular)	Corticosteroids	Appropriate
	Hyaluronic acid	Uncertain in knee-only OA, not appropriate in multijoint OA

Figure 9. The currently available pharmacologic and nonpharmacologic treatment options for OA, including guidelines and recommendations given by the OARSI. Table taken from [49].

Generally, in the treatment of OA, these different approaches are combined and personalized according to the individual symptoms and risk factors [62]. As shown in Figure 10, the specific treatment chosen is also based on the stage of the OA progression. For instance, in the early stages the therapy is mainly focused on the management of the pain and the joint stiffness and to prevent as much as possible the cartilage degradation. On the contrary, in the late stages it is more focused on supporting the functionality of the knee to allow the conduct of the daily activities [62].

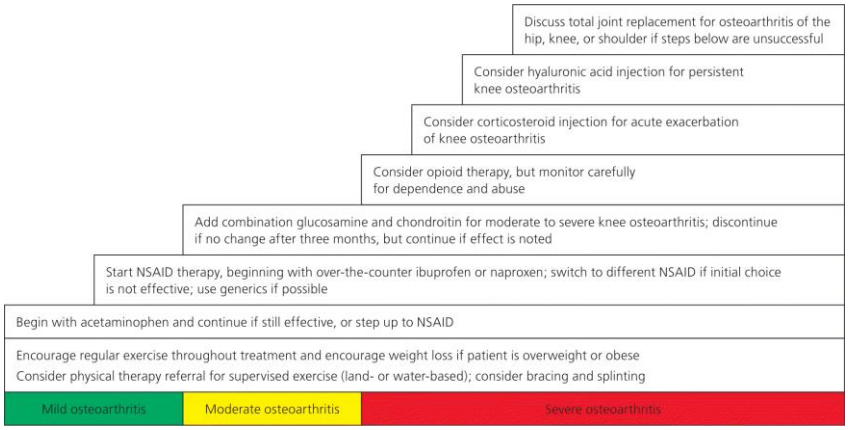

Figure 10. Recommended treatments based on the progression of osteoarthritis. NSAID = nonsteroidal anti-inflammatory drug. Data from [47].

3.1 Nonpharmacological treatments

Many aetiological factors or symptoms in the early stages of OA can be ameliorated by lifestyle changes, even if there is not a general approach to be followed. In fact, these approaches are prescribed according to the personal physical conditions.

Moreover, they are effective in the very early stages of OA, and they can slower its progression, preventing the cartilaginous degeneration. Different nonpharmacologic options are currently available.

3.1.1 Reduction of modifiable risk factors

One of the most influential risk factors are overweight or obesity. A randomized trial demonstrated that the decrease of the body weight significantly decreased the load that act on the knee [156]. This diminished load was correlated to a lower probability of developing symptomatic OA in future [157]. This approach is also effective in patients with established arthrosis, in which the loss of weight can ameliorate the structure of the cartilage and reduce the symptoms, especially the pain [40,158]. These structural improvements were detectable with both morphological and physiological MRI and were also detectable with cartilage biomarkers (increased synthesis and decreased degradation of the cartilaginous ECM). However, these changes were not always visible with the radiographic imaging [158,159]. These interventions are patient-centred and are organized to promote the active participation of the patient and to inform them about the pathology, the symptoms, the aims and the importance of the improvement in the general health condition [160]. The changes in the lifestyle of the patients are not intended to cure the

OA (their effect size is only <0,20 [161]) but they are meant to increase the general life quality and to delay the onset or manage the symptoms, especially the pain. In fact, several components can define and control the sensation of pain, that can be worsened by psychological factors, like loneliness, sleeping and mood disorders and depression [162]. Therefore, in some patients the improvement of the general wellbeing can have a considerable impact in the first stages of the OA to alleviate the pain and mitigate the degradative process.

3.1.2 Physical modalities

The effect of the physical activity on the symptoms management of OA has been evaluated for years. Generally, the exercise has a beneficial effect as it can decrease the pain while improving the joint functionality, cardiovascular health and decreasing mortality in arthritic patients, with an effect size >0,8 [163]. In particular, the aerobic and aquatic activities are usually suggested because they can improve the muscular strength and the flexibility of the knee [164,165]. This intervention was able to decrease the pain and to improve the physical function, thus ameliorating the life quality of the patients. Interestingly, the improvements were similar to those given by the administration of nonsteroidal anti-inflammatory drugs [166]. There is a plethora of different physical exercises that can be prescribed. However,

the specific types and amount of exercise that should be performed are not yet standardized. Usually stretching, muscle reinforcement, tissue mobilization and active range motion are recommended [49], as well as some specific approaches expressly designed for knee OA [167]. Anyway, the physical activity of each patient should be personalized and set considering individual factors [62]. Other less used physical measures include braces, cranes, taping and other approaches that aim to protect the knee. They can give some relief of symptoms effect and, given their affordability, can represent adjuvant measures [49].

3.1.3 Alternative therapies

The clinical evidence of the effectiveness of the commonly used alternative treatments such as lasers, acupuncture, transcutaneous electrical stimulation of nerves, ultrasound, and electromagnetic therapy is generally limited [168]. For instance, the low effect of acupuncture emerged from high quality studies. However, there is no significant risks in performing this procedure in the knee, and it can result useful for some arthritic patients [169].

3.2 Pharmacological treatments

Currently, the purposes of the pharmacological clinical treatments aim merely focused on the managing of the symptoms, especially the pain. Unfortunately, there is no disease-

modifying drug that is able to stop the OA progression and the structural degradation of the articular tissues [170]. Different classes of drugs are currently employed in the management of the OA symptoms.

3.2.1 Nonsteroidal anti-inflammatory drugs (NSAIDs) and paracetamol

The NSAIDs and paracetamol usually represent the first pharmacological choice for the OA when the nonpharmacological procedures fail to manage pain and other symptoms [49]. The NSAIDs display not only an analgesic but also an anti-inflammatory function, therefore they represent a relevant option for the managements of inflammatory-induced OA [171]. For instance, the orally-administered NSAIDs resulted to be effective in OA pain reduction, as demonstrated in several studies [172,173]. In addition, no strong evidence have suggested the preferential use of one specific drug over the others [49]. However, they have gastrointestinal side effects, so it has been suggested to use them in combination with COX-2 inhibitors or gastroprotective agents in chronic patients or in those with comorbidity in the gastrointestinal tract [174]. Another way to overcome the gastrointestinal side effects consists in the topical administration of the NSAIDs, that resulted effective in limiting

the side effects but not in the pain reduction when compared to the orally-administered NSAIDs [171].

Paracetamol, that has generally fewer side effects than NSAIDs, showed only a modest effectiveness for the management of the OA symptoms [174] and it is not recommended in the current clinical guidelines for the treatment of knee OA [171].

3.2.2 Serotonin and norepinephrine reuptake inhibitors

It has been suggested that when the pain is chronic in the advanced OA stage, it can origin in the central nervous system and, as a consequence, the NSAIDs and paracetamol are on longer effective [49]. Therefore, according to this theory the efficacy of these drugs can be reduced over time. Being the noradrenergic and serotonergic neurons involved in this process, Chappell et al., evaluated the effectiveness of duloxetine in the first randomized trial for this drug category. The results demonstrated that this approach significantly decreased the pain in arthritic patients [175]. In addition, the association of a NSAID with duloxetine showed more effectiveness in pain reduction than the anti-inflammatory alone. Following these evidence, the duloxetine is now approved from Food and Drug Administration (FDA) for the treatment of knee OA [176]. Therefore, similarly to the other clinical approaches, the inhibitors of the serotonin-

norepinephrine reuptake can play an important role only in controlling the pain in OA, but they cannot cure the disease.

3.2.3 Opioids and narcotic analgesics

Opioids and narcotic analgesic represent much stronger approaches and are usually employed only when the other pain-killer treatments failed or are contraindicated for other reasons [177]. Generally, it occurs in the most severe cases of OA, when the pain is chronic and limit the daily activities of the patients. However, even in these cases the use of these pharmaceuticals is as limited as possible because of their high addiction potential. For this reason, they are subjected to a very restrictive regulations and usually the clinical guidelines recommend them only in case of tumour-related pain [171]. In the treatment of OA symptoms the use of opioids or strong analgesics is suggested only for short period of administration, usually for 1-3 months, and only in the patients in which the pain does not allow to perform the normal daily activities [171].

3.2.4 Intra-articular therapy

Being invasive treatments, the intra-articular delivery of medicinal products always needs critical considerations. In fact, the risk of iatrogenic infection is relatively high even if all the hygiene recommendations are strictly followed [171]. The glucocorticoids and the hyaluronic acid are the most used drugs

for the intra-articular therapy. The use of glucocorticoids is controversial, as it showed pain reduction [178] but this effect could be also due to other factors, including functional, psychologic or social aspects [179]. On the other hand, the rationale behind the use of hyaluronic acid is to increase its concentration in the synovial fluid, since during OA both the molecular size and the quantity of hyaluronic acid decrease, as previously described. Similarly to glucocorticoids, the efficacy of the intra-articular administration of hyaluronic acid is still under debate, despite the high number of studies that have been performed [171].

3.3 Surgical treatment

When the conservative and the pharmacological approaches fail to halt the progression of OA, the surgical treatments, such as total knee arthroplasty, represents the last choice for end-stage arthritic patients. It is the gold-standard treatment when pain and loss of functionality heavily affect the life quality of patients. In fact, clinical evidence reported that functional recovery and life quality were higher in patients with severe OA after 12 months from the surgery when compared to conservative approaches [180]. Another advantage of the modern surgical techniques, is that they allow the patients to load the affected knee immediately after the surgery, improving and accelerating the recovery [181].

This approach have also some complications, including infections, failure of the prosthesis, dehiscence of the surgical wound, thrombosis, joint swelling and pain that can last for 1 year after the surgery [49]. To assure the best functional recovery of the knee, the physical activity after the surgery represents a crucial point. However, there are no clinical guidelines and consensus regarding the rehabilitation, in terms of frequency, duration and intensity [49]. The physical therapy should principally guarantee the muscle strengthening and the recovery of the joint mobility, to assure the return to the normal daily activities in a short time [182].

3.4 Biological therapies and regenerative approaches

As previously described, the current therapeutic options are predominately palliative and does not allow articular cartilage regeneration, but only, in the best scenario, a delay in OA progression. Therefore, there are no possibilities to restore the physiological joint environment. For this reason, the research is focusing on the development of new treatments that are able both to modulate the inflammatory response and to support the regeneration of the joint tissues [62]. In this context, regenerative medicine aims to re-establish the joint homeostasis, through different strategies based on biologically active components. The approaches that are currently available are based on the injection

of cocktails of growth factors or cells, i.e. infusion of platelet rich plasma (PRP) or cell-derived products [183].

3.4.1 Platelet Rich Plasma (PRP)

PRP represents one of the most used regenerative treatments for musculoskeletal disorders. Its use spans from OA to cartilage lesions up to tendon injuries [184]. This biological product is an autologous preparation obtained from the peripheral venous blood of the patient and consists of a volume of plasma containing a concentration of platelets higher than the physiological one [185]. Different methodologies can be used to obtain PRP, and the centrifugation steps of the peripheral blood determine the differences among the protocols. PRP has proven to be effective in the treatment of OA thanks to the combined anti-inflammatory and regenerative properties. Its tissue healing capability is due to the high content in growth factors, anti-inflammatory chemokines and cytokines, that are involved in numerous tissue repair and regeneration processes [186]. A major limitation of PRP consists in a low reproducibility of its preparation, and consequently of its composition and efficacy, which renders it difficult to achieve homogeneous outcomes in clinical studies [187]. In addition to the availability of different preparation protocols, another source of variability that affect the PRP preparation is related to its autologous origin and thus to

inter-individual differences between patients. This high variability also made it impossible to establish rigid quality criteria for this product so far [188]. Thus, although showing some positive preliminary clinical findings, PRP products remain under active investigation to understand mechanism of action and real potential in the OA clinical setting.

3.4.2 Cell therapies

Different cell therapies have been developed for the treatment of knee OA. The great potential of this approach was demonstrated by the autologous chondrocyte implantation, one of the first cell therapy approaches in knee OA. This treatment in fact showed greater results when compared with the other techniques that were available at the time, as microfracture and cartilage debridement [189,190]. More recently, mesenchymal stromal cells (MSCs) are increasingly being considered as a promising alternative as injective approach to target OA. Indeed, MSCs isolated from different sources have been shown to secrete many bioactive trophic factors that exert both immunomodulatory and regenerative actions [191,192]. In particular, the two most used MSC types are those isolated from the bone marrow and from the adipose tissue. Especially the adipose tissue-derived MSCs (ASCs), have shown in various clinical studies an improvement of the OA joint functionality and a reduction of the cartilage

degradation rate, thanks to their immunomodulatory and chondro-protective action [193,194].

A further evolution in this field is coming by the use of tissue-derived biological products containing several cell types instead of *in vitro* expanded cells. For instance, one of the most promising approaches involves the mechanical micro-fragmentation of the adipose tissue, followed by a centrifugation to concentrate the nucleated cells. At the end of the procedure a heterogeneous mix of cells and growth factors is obtained, namely the stromal vascular fraction (SVF) [195]. Other procedures allow to obtain different biological products, such as bone marrow concentrate (BMC). The common limiting feature between the different processed tissues (SVF and BMC) is the relative low content of MSCs (2-10% in the SVF; 0,01-0,0001% in the BMC) and the presence of further cellular and extracellular components, making their composition less standardizable as in the case of PRP [196]. Despite this limitation, numerous clinical and experimental evidence indicated how these approaches in the treatment of knee OA are safe, minimally invasive and relatively simple to prepare, especially the SVF [197,198]. The main advantage of these methods compared to the PRP and traditional cell therapy lies in the minimal manipulation required by the operator, thus allowing to perform a one-step procedure in the surgical room, without expensive and risky passages in

laboratory. However, despite the promising results shown by cell therapies and these innovative approaches, their widespread use in the treatment of OA is still hampered by the high heterogeneity of the preparations. This is mainly due to inter-donor variability and it leads to a scarcely predictable efficacy in different patients [199]. Thus, the results are still controversial, as well as the choice of the most suitable and effective approach.

3.4.3 MSC-derived biologics: secretome and EVs

To overcome the standardization issues posed by the cell and the biological therapies, in recent years the research is focusing on the study of the MSCs secretome. The aim of this approach is to achieve the same beneficial effects as the cellular therapies, while avoiding the experimental and ethical limits related to the use of live or expanded cells [200]. The hypothesis underlying the use of MSC secretome is based on the recent assumption that the therapeutic effect of MSCs seems to be more attributable to their trophic and immune-modulatory activity, exerted by secreted biological mediators, rather than their presence itself [201]. Recently, among the various factors secreted by MSCs, the extracellular vesicles (EVs) have gained increasing importance also for their therapeutic potential. In fact, the MSC-EVs retain the immunomodulatory and regenerative potential of the parent cells, thanks to the transported bioactive molecules such as

growth factors, cytokines and chemokines, enzymes, lipids and nucleic acids [202]. Therapeutic EVs have a general anabolic effect on articular cells and can stimulate the expression of chondrogenic markers or proteins of the cartilaginous ECM. They can also inhibit the harmful processes such as inflammatory response, cell hypertrophy, or chondrocyte apoptosis [203]. Recently, it has been demonstrated that MSC-derived EVs present a higher therapeutic potential than EVs from other sources, as they are richer in factors with marked anti-inflammatory, immunomodulatory, and regenerative activity [204,205]. In addition, numerous experimental evidence currently support the potential use of MSC-EVs for the treatment of OA, as recently reviewed [202]. Despite the good potential in these preliminary studies, there are still aspects that have to be addressed to allow the effective use of EVs as clinical approach for OA. For instance, the interaction between MSC-derived EVs and the articular or inflammatory cells involved in OA need to be elucidated, as well as the comprehensive understanding of their role in immunoregulation [202]. In addition, nobody evaluated the effect of specific subpopulations, in fact, as in the diagnosis process, most of the study were focused only on the effect of the small size EVs.

All these biological therapies showed promising results for the treatment of OA, but no evidence demonstrated if there is and

which is the best performing therapy, or which is the category of patients that would mostly benefit for each specific treatment. The evaluation and the comparison of different treatments for the OA is not easily implementable in a single clinical study, mainly because of the limited availability of quantitative, objective and non-invasive analytical tools [206]. In this perspective, drug screening platforms represent key tools in the assessment of innovative treatments.

3.5 Drug screening platforms for OA treatments

The Food and Drug Administration approves on average less than one out of ten new drug candidates that underwent clinical trial, with a huge economic impact for pharmaceutical companies [207]. In the attempt to overcome this important issue, several drug screening platforms have been developed for improving the pre-clinical research. These tools can help in the choice of which drug candidates are most suitable before entering the clinical examination and which have the higher probability to fail, allowing the saving of time and money [208]. Another important advantage is that the screening platforms are in compliance with the 3R principle, allowing the "reduction, replacement, and refinement" of the use of animals in the drug development process. Classically, two approaches can provide the screening of different new potential drugs without the use of live animals. The

first one involves software to design and test thousands different candidates to select the most promising molecules for the *in vivo* tests. This approach, called "in silico test", can predict the safety, toxicity, and interactions of these drugs [209]. In the second process, the candidate molecules are tested in *in vitro* systems and most promising are then selected for the *in vivo* experimentations [210]. Focusing on the latter, different *in vitro* models have been developed. They can be broadly subdivided in two-dimensional (2D) and three-dimensional (3D) models. In the 2D models the cells are grown on normal supports for cell cultures and they are characterized by an easy handling and quick development. Conversely, cells grow in an environment markedly different from the physiological ones. In fact, with this approach the physiologic cell-cell and cell-ECM interactions are not reproduced. On the contrary, with the 3D models it is possible to grow different cell types in a more relevant 3D microenvironment that can include physiologic ECM polymers, better recapitulating the *in vivo* tissues [211]. These models have also some limitations, as their development and handling is more difficult and they cannot provide the entire complexity of a whole organ [212]. Overall, presently 3D models represent the most promising screening platforms to select the new drug candidates for the successive developmental phases. Especially in the OA, where all the articular tissues play a role in its progression, 3D models are

the best choice as they support the co-culture of different cell types in a 3D microenvironment that can provide more physiological cues. In this scenario, microfluidics is one of the most favourable approaches to develop OA joint models resembling the articular microenvironment with high fidelity and precise control.

3.5.1 Microfluidics

With microfluidic approaches it is possible to generate 3D microenvironments that reflect the *in vivo* counterparts with highly controlled physicochemical conditions, providing the cells with relevant ECM and other cell types normally present in the tissue. It is also possible to precisely and constantly monitor the microenvironment by employing sets of accurate and real time analytical tools [213]. When compared with other screening platforms, the microfluidic ones are characterized by an easier manipulation, a more reliable resembling of the *in vivo* processes, a high potential for the scaling up and a greater possibility to perform high-throughput analyses [214,215]. Hence, the microfluidic models can reduce the number of the drug candidates for the *in vivo* experimentation, allowing the saving of both money and time, thus accelerating the development of new therapeutic approaches [211]. For all these reasons, in my PhD project I used a microfluidic approach to develop a drug

screening platform for the evaluation of innovative treatments for the OA.

Several microfluidic devices have been developed for the study of joint disorders, as recently comprehensively reviewed by Piluso et al. [216], and some of these were developed to reproduce an arthritic environment. Among the arthritic joint on chip models, some of these devices were designed to specifically model and study pathogenetic processes activated during the progression of the OA. For instance, models resembling the osteochondral interface [217,218], the excessive mechanical loading [219,220], and inflammation [220] have been developed. Together with these models, other microfluidic devices were designed to specifically serve as drug screening platforms for OA.

3.5.2 OA joint on chip models as drug screening platform

The model developed by Occhetta et al., in addition to evaluate the effect of the excessive load, assessed also the effect of different drugs for the treatment of OA. In particular, they tested molecules that are currently under evaluation in preclinical or clinical trials, such as dexamethasone, rapamycin, and celecoxib, as well as two new drugs [219]. As illustrated in Figure 11, this model included only the articular compartment in which the authors cultured healthy chondrocytes in a Polyethylene glycol (PEG)-based hydrogel. The underlying compartment was

designed to cyclically compress the cartilaginous one and thanks to the repeated compressions and the addition of IL-1β they induced an OA phenotype in the chondrocytes.

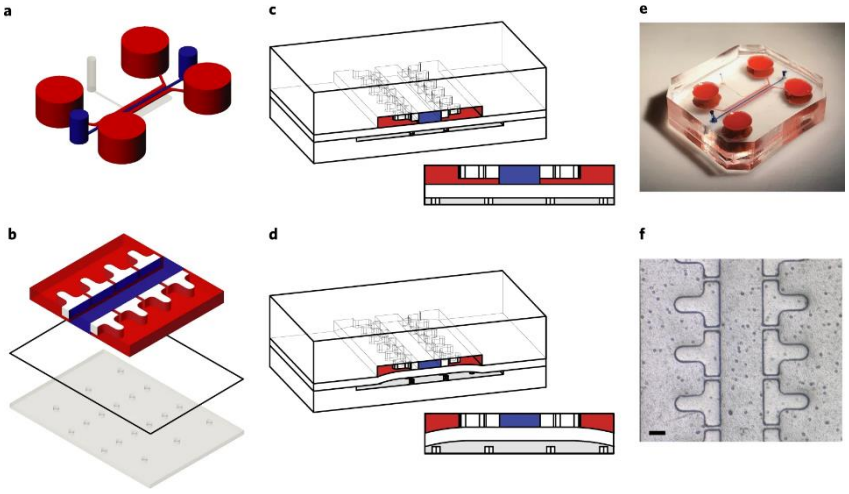

Figure 11. a, The design of the model. b, Two rows of T-shaped hanging posts (white), created in the top compartment a central channel hosting the 3D hydrogel with chondrocytes (blue) and two side channels for the culture medium (red). c, During rest position, the bottom membrane is flat. d, To furnish the cell with mechanical stimulation, the membrane deforms and compress the chondrocyte 3D microconstruct e, Photograph of the assembled device. f, Stereomicroscope image of a section on the central channel. Scale bar, 100 μm. Image taken from [219].

The effects of the drugs used in this device were in good accordance with those found in the clinical trial, in terms of reduced expression of MMP-13 and, even if in a lesser extent, IL-8. In addition, they reported that one of the two new tested drugs was more effective that the other in reducing the expression of MMP-13 [219]. In another study, the drug celecoxib was tested in a three-layers osteochondral device in which human induced pluripotent stem cells were embedded in gelatine hydrogel and

cultured within a microdual-flow bioreactor [221]. In this system, in the top channel the authors injected chondrogenic medium, while in the bottom they used osteogenic medium. This allowed the cells to respectively differentiate toward the cartilaginous or bone phenotype (Figure 12).

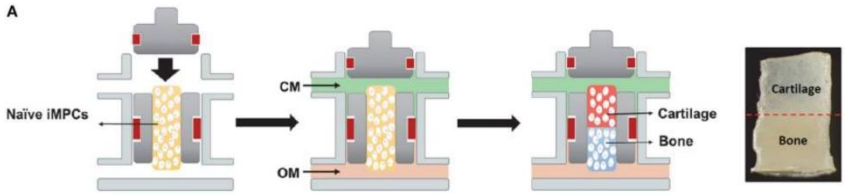

Figure 12. Fabrication of osteochondral model in the dual-flow bioreactor. The naïve iMCs were encapsulated into the gelatine hydrogel and placed into bioreactor. Chondrogenic and osteogenic media were injected in two different channels to recreate two different microenvironments. Image from [221].

The authors were also able to simulate an intra-articular or systemic administration of the drug by injecting it respectively only in the top or in both the channels, as shown in Figure 13.

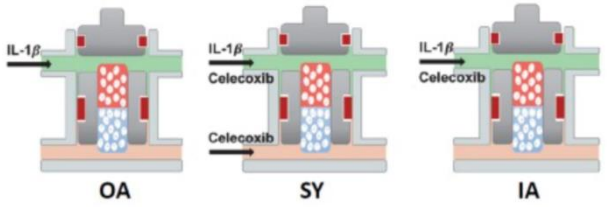

Figure 13. In the system IL-1β was used to generate the arthritic model (OA group). The injection of Celecoxib to both cartilage and bone channels simulated the systemic administration (SY group), while injection to only cartilaginous compartment resembled the intraarticular treatment (IA group) [221].

The results showed that the systemic injection of the drug had higher effects in counteracting the OA phenotype of the cells.

Mondadori et al. developed a microfluidic model to resemble the synovitis and to study the extravasation process of the macrophages. In their model, represented in Figure 14, two compartments with synovial fibroblasts embedded in a fibrin hydrogel were separated by a smaller channel in which they recreated a monolayer of endothelial cells, mimicking a blood vessel. Arthritic synovial fluid was injected in another small channel that separated one synovial compartment from the cartilaginous one, that was in turn composed of primary chondrocyte cultured in a fibrin hydrogel [222]. The monocytes were injected in the vessel-resembling channel and the effect of chemokines, arthritic synovial fluid and chemokine receptor antagonists on the extravasation process of macrophages was assessed.

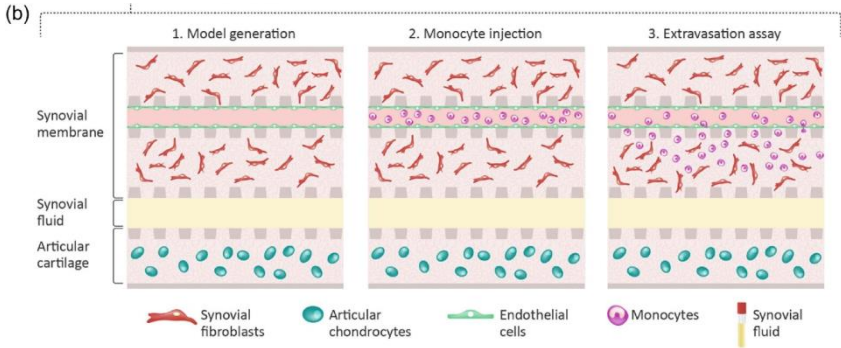

Figure 14. Representation of the configuration of the device, resembling the synovial membrane with the vasculature, the cartilage and the synovial compartment and the assessment of the monocyte extravasation process and assessment [222].

The authors reported that chemokines and arthritic synovial fluid stimulated the extravasation of the macrophages, while the

chemokine receptor antagonists inhibited this process also in presence of OA synovial fluid [222].

3.5.3 OA drug screening platforms: future perspectives

One of the most important aspects in the development of 3D microfluidic drug screening platforms is the microenvironment reproduced within the model. In fact, the support matrix in which the cells are embedded plays a fundamental role in providing them with relevant interaction with the ECM, that is not possible to obtain in the conventional 2D cultures. This is especially true for the chondrocytes, as they are a terminally differentiated cells with very limited metabolic activity *in vivo* in which the microenvironment is fundamental to maintain the physiologic differentiation [223]. In fact, it has been demonstrated that chondrocytes cultured in conventional 2D cultures rapidly lose their phenotype. The expression of chondrocyte-specific markers, such as type II collagen and aggrecan, progressively decreased with the increasing cell passage, while the expression of de-differentiation markers such as type I collagen increased [224,225]. In addition, also the support on which the chondrocytes are cultured can affect their phenotype and the differentiation capability [226].

On the contrary, culturing the chondrocytes in a 3D culture system, such as relevant scaffolds made of agarose gels, collagen

gels and hyaluronic acid, better maintained their correct phenotype and their differentiation state [227]. The importance of providing cells with a relevant microenvironment is highlighted also by the fact that some signs of differentiation have been reported also in chondrocytes cultured in 3D alginate beads [224]. This represents a crucial aspect that still need to be addressed in the development of drug screening platforms for the OA. In fact, within the previously produced models, the chondrocytes were embedded in hydrogels made of PEG [219], gelatin [221] and fibrin [222], that are not physiologically present in the cartilage tissue. For this reason, the use of more physiologic hydrogels would be of great importance in this field. Another missing point of the devices previously described is that the tested only chemical drugs. In fact, no platforms assessed the innovative biological therapies, even if they showed promising results on the OA treatment. In this scenario, new and more relevant microfluidic approaches can be implemented to improve and accelerate the development of innovative biological therapies for the OA.

4. Scope of the thesis and experimental design

During this PhD project I aim at tackling the OA disorder with a theranostic approach: my first objective is to investigate innovative OA biomarkers based on the synovial fluid EVs, through the development of a new experimental protocol for their obtainment. The second one is the setup of a drug screening platform to evaluate new biological treatments for OA. A schematic representation of the project is depicted in Figure 14.

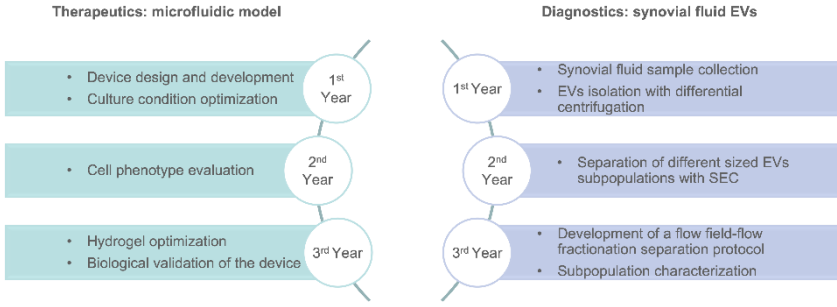

Figure 15. The experimental work performed in each year of the PhD.

OA Diagnosis

Regarding the diagnosis, the project focuses on the evaluation of the subpopulations of EVs isolated from the synovial fluid as potential new biomarkers for OA. In particular, since the large EVs have an important role in the inflammation process, I will develop an experimental protocol based on the AF4 with the aim to isolate and separate all the EVs present in the synovial fluid according to their size. Firstly, I will optimize the pre-treatment of the synovial fluid to reduce its viscosity thus facilitating the

isolation and separation process of EVs. Then, the AF4 protocol will be optimized. I will use this technique since its effectiveness has been demonstrated also in other biofluids, namely plasma, serum, urine and culture medium. Finally, the EVs belonging to each subpopulation will be characterized, by evaluating the EV average size, the subpopulation relative abundance, the Z potential and the nucleic acid concentration. The protein concentration and the luminal content will be assessed, as well as the presence of vesicle markers. In addition, both transmission and immune electron microscopy will be performed. This protocol would expand the spectrum of the EVs that can be isolated from different biological sources, increasing the probability to find innovative potential biomarkers.

OA Treatment

The aim of this part of the project will be the development of a patient-specific microfluidic drug screening platform able to assess and compare the biological effect of new biological therapies for the treatment of OA. First of all, I will optimize the culture conditions of the chondrocytes by culturing them in a more physiologically relevant hydrogel, as compared to the most used ones. For this purpose, the literature will be previously reviewed to identify already used polymers in the microfluidic models of musculoskeletal tissues. Then, commercially available hydrogels will be optimized for the chondrocyte culture and

tested outside the device, assessing the chondrogenic and biomechanical properties as well as the cell viability. Based on these results, the best performing hydrogel will be chosen and its chondrogenic properties will be evaluated also within a microfluidic device. The patient-matched chip which will be designed to culture chondrocytes and synovial fibroblasts in a 3D microenvironment in presence of native synovial fluid, all collected from the same end-stage arthritic patient. The arthritic microenvironment within the chip will be then assessed and optimized by culturing the device in presence of healthy or arthritic synovial fluid. Finally, resembling an intra-articular injection of allogenic MSCs, the biological effect of two different MSC types on the arthritic articular cells will be evaluated. In particular, two different pools obtained from 4 donors will be used to mimic an allogeneic injection of MSCs. This model could be used in future to assess other biological products for OA, such as MSCs secretome and EVs. For this reason, the literature was systematically reviewed to assess and compare the anti-inflammatory and regenerative potential of the biological products secreted by MSCs: secretome, small EVs and large EVs.

Beside the main projects that I carried out, during my PhD, I was also involved in different side research projects:

1- Development of a bioreactor that allow the multiple and independent culture of tendon matrices to be used in tendon regenerative medicine. This bioreactor provided the tendinous scaffold with an intermittent, uniaxial strain and bidirectional oscillatory perfusion. (See section "Other publications", Independent, Controllable Stretch-Perfusion Bioreactor Chambers to Functionalize Cell-Seeded Decellularized Tendons. Ann Biomed Eng 48, 1112–1126 (2020))

2- *In vivo* study in which decellularized tendon matrices repopulated with MSCs and cultured in the bioreactor previously developed were used as xenografts in a rabbit model of Achilles tendon full transection. (See section "Other publications", Achilles Tendon Repair by Decellularized and Engineered Xenografts in a Rabbit Model, Stem Cells International, vol. 2019, Article ID 5267479, 14 pages, 2019)

3- The capabilities of pulsed electromagnetic magnetic field to improve the tendon regenerative process in a rat model of collagenase-induced Achilles tendinopathy. (See section "Other publications", Pulsed electromagnetic fields improve the healing process of Achilles tendinopathy: a pilot study in a rat model, Bone Joint Res. 2020 Oct 5;9(9):613-622. eCollection 2020 Sep)

5. References

1. Marshall, D.A.; Vanderby, S.; Barnabe, C.; MacDonald, K. V; Maxwell, C.; Mosher, D.; Wasylak, T.; Lix, L.; Enns, E.; Frank, C.; et al. Estimating the Burden of Osteoarthritis to Plan for the Future. *Arthritis Care Res. (Hoboken).* **2015**, *67*, 1379–1386.
2. Leifer, V.P.; Katz, J.N.; Losina, E. The burden of OA-health services and economics. *Osteoarthr. Cartil.* **2021**.
3. Hunter, D.J.; Schofield, D.; Callander, E. The individual and socioeconomic impact of osteoarthritis. *Nat. Rev. Rheumatol.* 2014, *10*, 437–441.
4. Hunter, D.J.; March, L.; Chew, M. Osteoarthritis in 2020 and beyond: a Lancet Commission. *Lancet* **2020**, *396*, 1711–1712.
5. Network, G.B.D.C. Global burden of disease study 2017 (GBD 2017) results. *Seattle, United States* **2018**.
6. Abicalaf, C.A.R.P.; Nakada, L.N.; Dos Santos, F.R.A.; Akiho, I.; Dos Santos, A.C.A.; Imamura, M.; Battistella, L.R. Ultrasonography findings in knee osteoarthritis: a prospective observational cross-sectional study of 100 patients. *Sci. Rep.* **2021**, *11*, 16589.
7. Vos, T.; Allen, C.; Arora, M.; Barber, R.M.; Bhutta, Z.A.; Brown, A.; Carter, A.; Casey, D.C.; Charlson, F.J.; Chen, A.Z.; et al. Global, regional, and national incidence, prevalence, and years lived with disability for 310 diseases and injuries, 1990–2015: a systematic analysis for the Global Burden of Disease Study 2015. *Lancet* **2016**, *388*, 1545–1602.
8. Prieto-Alhambra, D.; Judge, A.; Javaid, M.K.; Cooper, C.; Diez-Perez, A.; Arden, N.K. Incidence and risk factors for clinically diagnosed knee, hip and hand osteoarthritis: influences of age, gender and osteoarthritis affecting other joints. *Ann. Rheum. Dis.* **2014**, *73*, 1659–1664.
9. Muckelt, P.E.; Roos, E.M.; Stokes, M.; McDonough, S.; Grønne, D.T.; Ewings, S.; Skou, S.T. Comorbidities and their link with individual health status: A cross-sectional analysis of 23,892 people with knee and hip osteoarthritis from primary care. *J. Comorbidity* **2020**, *10*, 2235042X20920456.
10. Bierma-Zeinstra, S.M.A.; Waarsing, J.H. The role of atherosclerosis in osteoarthritis. *Best Pract. Res. Clin. Rheumatol.* **2017**, *31*, 613–633.
11. Berenbaum, F. Osteoarthritis as an inflammatory disease (osteoarthritis is not osteoarthrosis!). *Osteoarthr. Cartil.* **2013**, *21*, 16–21.
12. Jafarzadeh, S.R.; Felson, D.T. Updated Estimates Suggest a Much Higher Prevalence of Arthritis in United States Adults Than Previous Ones. *Arthritis Rheumatol.* **2018**.
13. Lambova, S.N.; Müller-Ladner, U. Osteoarthritis - Current Insights in Pathogenesis, Diagnosis and Treatment. *Curr. Rheumatol. Rev.* 2018, *14*, 91–97.

14. Brandt, K.D.; Radin, E.L.; Dieppe, P.A.; van de Putte, L. Yet more evidence that osteoarthritis is not a cartilage disease. *Ann. Rheum. Dis.* 2006, *65*, 1261–1264.
15. Deveza, L.A.; Loeser, R.F. Is osteoarthritis one disease or a collection of many? *Rheumatology (Oxford).* **2018**, *57*, iv34–iv42.
16. Haseeb, A.; Haqqi, T.M. Immunopathogenesis of osteoarthritis. *Clin. Immunol.* **2013**, *146*, 185–196.
17. Robinson, W.H.; Lepus, C.M.; Wang, Q.; Raghu, H.; Mao, R.; Lindstrom, T.M.; Sokolove, J. Low-grade inflammation as a key mediator of the pathogenesis of osteoarthritis. *Nat. Rev. Rheumatol.* **2016**, *12*, 580–592.
18. Jones, G.M.; Watt, D.G. Muscular control of landing from unexpected falls in man. *J. Physiol.* **1971**, *219*, 729–737.
19. Fu, K.; Robbins, S.R.; McDougall, J.J. Osteoarthritis: the genesis of pain. *Rheumatology (Oxford).* **2018**, *57*, iv43–iv50.
20. Henrotin, Y.; Pesesse, L.; Lambert, C. Targeting the synovial angiogenesis as a novel treatment approach to osteoarthritis. *Ther. Adv. Musculoskelet. Dis.* **2014**, *6*, 20–34.
21. Mathiessen, A.; Conaghan, P.G. Synovitis in osteoarthritis: current understanding with therapeutic implications. *Arthritis Res. Ther.* **2017**, *19*, 18.
22. More, S.; Kotiya, A.; Kotia, A.; Ghosh, S.K.; Spyrou, L.A.; Sarris, I.E. Rheological properties of synovial fluid due to viscosupplements: A review for osteoarthritis remedy. *Comput. Methods Programs Biomed.* **2020**, *196*, 105644.
23. Chakrabarti, S.; Jadon, D.R.; Bulmer, D.C.; Smith, E.S.J. Human osteoarthritic synovial fluid increases excitability of mouse dorsal root ganglion sensory neurons: an in-vitro translational model to study arthritic pain. *Rheumatology (Oxford).* **2020**, *59*, 662–667.
24. van den Bosch, M.H.J. Inflammation in osteoarthritis: is it time to dampen the alarm(in) in this debilitating disease? *Clin. Exp. Immunol.* **2019**, *195*, 153–166.
25. Wojdasiewicz, P.; Poniatowski, Ł.A.; Szukiewicz, D. The role of inflammatory and anti-inflammatory cytokines in the pathogenesis of osteoarthritis. *Mediators Inflamm.* **2014**, *2014*, 561459.
26. Livshits, G.; Zhai, G.; Hart, D.J.; Kato, B.S.; Wang, H.; Williams, F.M.K.; Spector, T.D. Interleukin-6 is a significant predictor of radiographic knee osteoarthritis: the Chingford study. *Arthritis Rheum. Off. J. Am. Coll. Rheumatol.* **2009**, *60*, 2037–2045.
27. Stannus, O.; Jones, G.; Cicuttini, F.; Parameswaran, V.; Quinn, S.; Burgess, J.; Ding, C. Circulating levels of IL-6 and TNF-α are associated with knee radiographic osteoarthritis and knee cartilage loss in older adults. *Osteoarthr. Cartil.* **2010**, *18*, 1441–1447.
28. García-Manrique, M.; Calvet, J.; Orellana, C.; Berenguer-Llergo, A.; Garcia-Cirera, S.; Llop, M.; Albiñana-Giménez, N.; Galisteo-Lencastre,

C.; Gratacós, J. Synovial fluid but not plasma interleukin-8 is associated with clinical severity and inflammatory markers in knee osteoarthritis women with joint effusion. *Sci. Rep.* **2021**, *11*, 5258.

29. Honorati, M.C.; Bovara, M.; Cattini, L.; Piacentini, A.; Facchini, A. Contribution of interleukin 17 to human cartilage degradation and synovial inflammation in osteoarthritis. *Osteoarthr. Cartil.* **2002**, *10*, 799–807.
30. Fell, H.B.; Barratt, M.E.; Welland, H.; Green, R. The capacity of pig articular cartilage in organ culture to regenerate after breakdown induced by complement-sufficient antiserum to pig erythrocytes. *Calcif. Tissue Res.* **1976**, *20*, 3–21.
31. Lim, N.H.; Kashiwagi, M.; Visse, R.; Jones, J.; Enghild, J.J.; Brew, K.; Nagase, H. Reactive-site mutants of N-TIMP-3 that selectively inhibit ADAMTS-4 and ADAMTS-5: biological and structural implications. *Biochem. J.* **2010**, *431*, 113–122.
32. Troeberg, L.; Nagase, H. Proteases involved in cartilage matrix degradation in osteoarthritis. *Biochim. Biophys. Acta* **2012**, *1824*, 133–145.
33. Little, C.B.; Barai, A.; Burkhardt, D.; Smith, S.M.; Fosang, A.J.; Werb, Z.; Shah, M.; Thompson, E.W. Matrix metalloproteinase 13-deficient mice are resistant to osteoarthritic cartilage erosion but not chondrocyte hypertrophy or osteophyte development. *Arthritis Rheum.* **2009**, *60*, 3723–3733.
34. Scanzello, C.R. Chemokines and inflammation in osteoarthritis: Insights from patients and animal models. *J. Orthop. Res. Off. Publ. Orthop. Res. Soc.* **2017**, *35*, 735–739.
35. Borzì, R.M.; Mazzetti, I.; Cattini, L.; Uguccioni, M.; Baggiolini, M.; Facchini, A. Human chondrocytes express functional chemokine receptors and release matrix-degrading enzymes in response to C-X-C and C-C chemokines. *Arthritis Rheum.* **2000**, *43*, 1734–1741.
36. de Boer, T.N.; van Spil, W.E.; Huisman, A.M.; Polak, A.A.; Bijlsma, J.W.J.; Lafeber, F.P.J.G.; Mastbergen, S.C. Serum adipokines in osteoarthritis; comparison with controls and relationship with local parameters of synovial inflammation and cartilage damage. *Osteoarthr. Cartil.* **2012**, *20*, 846–853.
37. Johnston, S.A. Osteoarthritis: Joint Anatomy, Physiology, and Pathobiology. *Vet. Clin. North Am. Small Anim. Pract.* **1997**, *27*, 699–723.
38. Sharma, L. Osteoarthritis of the Knee. *N. Engl. J. Med.* **2021**, *384*, 51–59.
39. Pulsatelli, L.; Addimanda, O.; Brusi, V.; Pavloska, B.; Meliconi, R. New findings in osteoarthritis pathogenesis: therapeutic implications. *Ther. Adv. Chronic Dis.* **2013**, *4*, 23–43.
40. Glyn-Jones, S.; Palmer, A.J.R.; Agricola, R.; Price, A.J.; Vincent, T.L.; Weinans, H.; Carr, A.J. Osteoarthritis. *Lancet* **2015**, *386*, 376–387.
41. Ryd, L.; Brittberg, M.; Eriksson, K.; Jurvelin, J.S.; Lindahl, A.; Marlovits, S.; Möller, P.; Richardson, J.B.; Steinwachs, M.; Zenobi-Wong, M. Pre-

Osteoarthritis: Definition and Diagnosis of an Elusive Clinical Entity. *Cartilage* **2015**, *6*, 156–165.
42. Lespasio, M.J.; Piuzzi, N.S.; Husni, M.E.; Muschler, G.F.; Guarino, A.; Mont, M.A. Knee Osteoarthritis: A Primer. *Perm. J.* **2017**, *21*, 16–183.
43. Bonnet, C.S.; Walsh, D.A. Osteoarthritis, angiogenesis and inflammation. *Rheumatology (Oxford).* **2005**, *44*, 7–16.
44. Favero, M.; Ramonda, R.; Goldring, M.B.; Goldring, S.R.; Punzi, L. Early knee osteoarthritis. *RMD Open* **2015**, *1*, e000062.
45. Kolasinski, S.L.; Neogi, T.; Hochberg, M.C.; Oatis, C.; Guyatt, G.; Block, J.; Callahan, L.; Copenhaver, C.; Dodge, C.; Felson, D.; et al. 2019 American College of Rheumatology/Arthritis Foundation Guideline for the Management of Osteoarthritis of the Hand, Hip, and Knee. *Arthritis Care Res.* **2020**, *72*, 149–162.
46. Myers, S.L.; Brandt, K.D. Effects of synovial fluid hyaluronan concentration and molecular size on clearance of protein from the canine knee. *J. Rheumatol.* **1995**, *22*, 1732–1739.
47. Sinusas, K. Osteoarthritis: diagnosis and treatment. *Am. Fam. Physician* **2012**, *85*, 49–56.
48. Katz, J.N.; Arant, K.R.; Loeser, R.F. Diagnosis and Treatment of Hip and Knee Osteoarthritis: A Review. *JAMA* **2021**, *325*, 568–578.
49. Abramoff, B.; Caldera, F.E. Osteoarthritis: Pathology, Diagnosis, and Treatment Options. *Med. Clin. North Am.* **2020**, *104*, 293–311.
50. Taruc-Uy, R.L.; Lynch, S.A. Diagnosis and treatment of osteoarthritis. *Prim. Care* **2013**, *40*, 821–36, vii.
51. Lichtenstein, M.J.; Pincus, T. How useful are combinations of blood tests in "rheumatic panels" in diagnosis of rheumatic diseases? *J. Gen. Intern. Med.* **1988**, *3*, 435–442.
52. Guidelines for the initial evaluation of the adult patient with acute musculoskeletal symptoms. American College of Rheumatology Ad Hoc Committee on Clinical Guidelines. *Arthritis Rheum.* **1996**, *39*, 1–8.
53. Hinton, R.; Moody, R.L.; Davis, A.W.; Thomas, S.F. Osteoarthritis: diagnosis and therapeutic considerations. *Am. Fam. Physician* **2002**, *65*, 841–848.
54. Kellgren, J.H.; Lawrence, J.S. Radiological assessment of osteo-arthrosis. *Ann. Rheum. Dis.* **1957**, *16*, 494–502.
55. Braun, H.J.; Gold, G.E. Diagnosis of osteoarthritis: imaging. *Bone* **2012**, *51*, 278–288.
56. Kohn, M.D.; Sassoon, A.A.; Fernando, N.D. Classifications in Brief: Kellgren-Lawrence Classification of Osteoarthritis. *Clin. Orthop. Relat. Res.* **2016**, *474*, 1886–1893.
57. Wright, R.W.; Group, M. Osteoarthritis Classification Scales: Interobserver Reliability and Arthroscopic Correlation. *J. Bone Joint Surg. Am.* **2014**, *96*, 1145–1151.
58. Roemer, F.W.; Guermazi, A.; Javaid, M.K.; Lynch, J.A.; Niu, J.; Zhang,

Y.; Felson, D.T.; Lewis, C.E.; Torner, J.; Nevitt, M.C. Change in MRI-detected subchondral bone marrow lesions is associated with cartilage loss: the MOST Study. A longitudinal multicentre study of knee osteoarthritis. *Ann. Rheum. Dis.* **2009**, *68*, 1461–1465.

59. Felson, D.T.; McLaughlin, S.; Goggins, J.; LaValley, M.P.; Gale, M.E.; Totterman, S.; Li, W.; Hill, C.; Gale, D. Bone marrow edema and its relation to progression of knee osteoarthritis. *Ann. Intern. Med.* **2003**, *139*, 330–336.
60. Chu, C.R.; Williams, A.; Tolliver, D.; Kwoh, C.K.; Bruno, S. 3rd; Irrgang, J.J. Clinical optical coherence tomography of early articular cartilage degeneration in patients with degenerative meniscal tears. *Arthritis Rheum.* **2010**, *62*, 1412–1420.
61. Herrmann, J.M.; Pitris, C.; Bouma, B.E.; Boppart, S.A.; Jesser, C.A.; Stamper, D.L.; Fujimoto, J.G.; Brezinski, M.E. High resolution imaging of normal and osteoarthritic cartilage with optical coherence tomography. *J. Rheumatol.* **1999**, *26*, 627–635.
62. Bijlsma, J.W.J.; Berenbaum, F.; Lafeber, F.P.J.G. Osteoarthritis: An update with relevance for clinical practice. *Lancet* 2011.
63. Podlipská, J.; Guermazi, A.; Lehenkari, P.; Niinimäki, J.; Roemer, F.W.; Arokoski, J.P.; Kaukinen, P.; Liukkonen, E.; Lammentausta, E.; Nieminen, M.T.; et al. Comparison of Diagnostic Performance of Semi-Quantitative Knee Ultrasound and Knee Radiography with MRI: Oulu Knee Osteoarthritis Study. *Sci. Rep.* **2016**, *6*, 22365.
64. Dieppe, P.A.; Lohmander, L.S. Pathogenesis and management of pain in osteoarthritis. *Lancet (London, England)* **2005**, *365*, 965–973.
65. Vignon, E.; Conrozier, T.; Hellio Le Graverand, M.-P. Advances in radiographic imaging of progression of hip and knee osteoarthritis. *J. Rheumatol.* **2005**, *32*, 1143–1145.
66. Guermazi, A.; Niu, J.; Hayashi, D.; Roemer, F.W.; Englund, M.; Neogi, T.; Aliabadi, P.; McLennan, C.E.; Felson, D.T. Prevalence of abnormalities in knees detected by MRI in adults without knee osteoarthritis: population based observational study (Framingham Osteoarthritis Study). *BMJ* **2012**, *345*, e5339.
67. Amin, S.; LaValley, M.P.; Guermazi, A.; Grigoryan, M.; Hunter, D.J.; Clancy, M.; Niu, J.; Gale, D.R.; Felson, D.T. The relationship between cartilage loss on magnetic resonance imaging and radiographic progression in men and women with knee osteoarthritis. *Arthritis Rheum.* **2005**, *52*, 3152–3159.
68. Hunter, D.J.; Zhang, Y.Q.; Tu, X.; Lavalley, M.; Niu, J.B.; Amin, S.; Guermazi, A.; Genant, H.; Gale, D.; Felson, D.T. Change in joint space width: hyaline articular cartilage loss or alteration in meniscus? *Arthritis Rheum.* **2006**, *54*, 2488–2495.
69. Kinds, M.B.; Vincken, K.L.; Hoppinga, T.N.; Bleys, R.L.A.W.; Viergever, M.A.; Marijnissen, A.C.A.; Welsing, P.M.J.; Lafeber, F.P.J.G. Influence of

variation in semiflexed knee positioning during image acquisition on separate quantitative radiographic parameters of osteoarthritis, measured by Knee Images Digital Analysis. *Osteoarthr. Cartil.* **2012**, *20*, 997–1003.

70. Conaghan, P.G.; Hunter, D.J.; Maillefert, J.F.; Reichmann, W.M.; Losina, E. Summary and recommendations of the OARSI FDA osteoarthritis Assessment of Structural Change Working Group. *Osteoarthr. Cartil.* **2011**, *19*, 606–610.
71. Eckstein, F.; Mc Culloch, C.E.; Lynch, J.A.; Nevitt, M.; Kwoh, C.K.; Maschek, S.; Hudelmaier, M.; Sharma, L.; Wirth, W. How do short-term rates of femorotibial cartilage change compare to long-term changes? Four year follow-up data from the osteoarthritis initiative. *Osteoarthr. Cartil.* **2012**, *20*, 1250–1257.
72. Cotofana, S.; Buck, R.; Wirth, W.; Roemer, F.; Duryea, J.; Nevitt, M.; Eckstein, F. Cartilage thickening in early radiographic knee osteoarthritis: a within-person, between-knee comparison. *Arthritis Care Res. (Hoboken).* **2012**, *64*, 1681–1690.
73. Zilkens, C.; Miese, F.; Kim, Y.-J.; Jäger, M.; Mamisch, T.C.; Hosalkar, H.; Antoch, G.; Krauspe, R.; Bittersohl, B. Direct comparison of intra-articular versus intravenous delayed gadolinium-enhanced MRI of hip joint cartilage. *J. Magn. Reson. Imaging* **2014**, *39*, 94–102.
74. Hayashi, D.; Guermazi, A.; Roemer, F.W. Radiography and computed tomography imaging of osteoarthritis. In; Oxford University Press: Oxford, UK, 2016 ISBN 9780191807176.
75. Keen, H.I.; Wakefield, R.J.; Conaghan, P.G. A systematic review of ultrasonography in osteoarthritis. *Ann. Rheum. Dis.* **2009**, *68*, 611 LP – 619.
76. Mobasheri, A.; Bay-Jensen, A.-C.; van Spil, W.E.; Larkin, J.; Levesque, M.C. Osteoarthritis Year in Review 2016: biomarkers (biochemical markers). *Osteoarthr. Cartil.* **2017**, *25*, 199–208.
77. Mobasheri, A.; Henrotin, Y. Biomarkers of (osteo)arthritis. *Biomarkers* **2015**, *20*, 513–518.
78. Mobasheri, A. Osteoarthritis year 2012 in review: biomarkers. *Osteoarthr. Cartil.* **2012**, *20*, 1451–1464.
79. Kraus, V.B.; Karsdal, M.A. Osteoarthritis: Current Molecular Biomarkers and the Way Forward. *Calcif. Tissue Int.* **2021**, *109*, 329–338.
80. Sand, J.M.B.; Knox, A.J.; Lange, P.; Sun, S.; Kristensen, J.H.; Leeming, D.J.; Karsdal, M.A.; Bolton, C.E.; Johnson, S.R. Accelerated extracellular matrix turnover during exacerbations of COPD. *Respir. Res.* **2015**, *16*, 69.
81. Biomarkers and surrogate endpoints: preferred definitions and conceptual framework. *Clin. Pharmacol. Ther.* **2001**, *69*, 89–95.
82. Karsdal, M.A.; Woodworth, T.; Henriksen, K.; Maksymowych, W.P.; Genant, H.; Vergnaud, P.; Christiansen, C.; Schubert, T.; Qvist, P.; Schett, G.; et al. Biochemical markers of ongoing joint damage in

rheumatoid arthritis - current and future applications, limitations and opportunities. *Arthritis Res. Ther.* **2011**, *13*, 215.

83. Sondergaard, B.C.; Henriksen, K.; Wulf, H.; Oestergaard, S.; Schurigt, U.; Bräuer, R.; Danielsen, I.; Christiansen, C.; Qvist, P.; Karsdal, M.A. Relative contribution of matrix metalloprotease and cysteine protease activities to cytokine-stimulated articular cartilage degradation. *Osteoarthr. Cartil.* **2006**, *14*, 738–748.
84. Huebner, J.L.; Bay-Jensen, A.C.; Huffman, K.M.; He, Y.; Leeming, D.J.; McDaniel, G.E.; Karsdal, M.A.; Kraus, V.B. Alpha C-telopeptide of type I collagen is associated with subchondral bone turnover and predicts progression of joint space narrowing and osteophytes in osteoarthritis. *Arthritis Rheumatol. (Hoboken, N.J.)* **2014**, *66*, 2440–2449.
85. Kraus, V.B.; Collins, J.E.; Hargrove, D.; Losina, E.; Nevitt, M.; Katz, J.N.; Wang, S.X.; Sandell, L.J.; Hoffmann, S.C.; Hunter, D.J. Predictive validity of biochemical biomarkers in knee osteoarthritis: data from the FNIH OA Biomarkers Consortium. *Ann. Rheum. Dis.* **2017**, *76*, 186–195.
86. Bjerre-Bastos, J.J.; Bay-Jensen, A.-C.; Karsdal, M.A.; Byrjalsen, I.; Andersen, J.R.; Riis, B.J.; Christiansen, C.; Bihlet, A.R. Biomarkers of bone and cartilage turnover CTX-I and CTX-II predict total joint replacements in osteoarthritis. *Osteoarthr. Cartil.* **2019**, *27*, S31–S32.
87. Luo, Y.; He, Y.; Reker, D.; Gudmann, N.S.; Henriksen, K.; Simonsen, O.; Ladel, C.; Michaelis, M.; Mobasheri, A.; Karsdal, M.; et al. A Novel High Sensitivity Type II Collagen Blood-Based Biomarker, PRO-C2, for Assessment of Cartilage Formation. *Int. J. Mol. Sci.* **2018**, *19*.
88. Tarhan, S.; Unlu, Z. Magnetic resonance imaging and ultrasonographic evaluation of the patients with knee osteoarthritis: a comparative study. *Clin. Rheumatol.* **2003**, *22*, 181–188.
89. Hsueh, M.-F.; Lu, Y.; Wellman, S.S.; Bolognesi, M.P.; Kraus, V.B. Functional folate receptor cell-associated inflammatory cytokines predict the progression of knee osteoarthritis. *Osteoarthr. Cartil.* **2018**, *26*, S121–S122.
90. Haraden, C.A.; Huebner, J.L.; Hsueh, M.-F.; Li, Y.-J.; Kraus, V.B. Synovial fluid biomarkers associated with osteoarthritis severity reflect macrophage and neutrophil related inflammation. *Arthritis Res. Ther.* **2019**, *21*, 146.
91. Hsueh, M.-F.; Zhang, X.; Wellman, S.S.; Bolognesi, M.P.; Kraus, V.B. Synergistic Roles of Macrophages and Neutrophils in Osteoarthritis Progression. *Arthritis Rheumatol. (Hoboken, N.J.)* **2021**, *73*, 89–99.
92. Deveza, L.A.; Kraus, V.B.; Collins, J.E.; Guermazi, A.; Roemer, F.W.; Nevitt, M.C.; Hunter, D.J. Is synovitis detected on non-contrast-enhanced magnetic resonance imaging associated with serum biomarkers and clinical signs of effusion? Data from the Osteoarthritis Initiative. *Scand. J. Rheumatol.* **2018**, *47*, 235–242.
93. Attur, M.; Belitskaya-Lévy, I.; Oh, C.; Krasnokutsky, S.; Greenberg, J.;

Samuels, J.; Smiles, S.; Lee, S.; Patel, J.; Al-Mussawir, H.; et al. Increased interleukin-1β gene expression in peripheral blood leukocytes is associated with increased pain and predicts risk for progression of symptomatic knee osteoarthritis. *Arthritis Rheum.* **2011**, *63*, 1908–1917.

94. Koskinen-Kolasa, A.; Vuolteenaho, K.; Moilanen, T.; Moilanen, E. Adipokines leptin, adiponectin and resistin and their associations to MMPS, IL-6, COMP and radiographic severity of OA. *Osteoarthr. Cartil.* **2016**, *24*, S78.
95. Kraus, V.B.; Collins, J.E.; Charles, H.C.; Pieper, C.F.; Whitley, L.; Losina, E.; Nevitt, M.; Hoffmann, S.; Roemer, F.; Guermazi, A. Predictive validity of radiographic trabecular bone texture in knee osteoarthritis: the Osteoarthritis Research Society International/Foundation for the National Institutes of Health Osteoarthritis Biomarkers Consortium. *Arthritis Rheumatol.* **2018**, *70*, 80–87.
96. Bettica, P.; Cline, G.; Hart, D.J.; Meyer, J.; Spector, T.D. Evidence for increased bone resorption in patients with progressive knee osteoarthritis: longitudinal results from the Chingford study. *Arthritis Rheum.* **2002**, *46*, 3178–3184.
97. Gudmann, N.S.; Junker, P.; Juhl, P.; Thudium, C.S.; Siebuhr, A.S.; Byrjalsen, I.; Karsdal, M.A.; Bay-Jensen, A.C. Type IV collagen metabolism is associated with disease activity, radiographic progression and response to tocilizumab in rheumatoid arthritis. *Clin Exp Rheumatol* **2018**, *36*, 829–835.
98. Siebuhr, A.S.; Bay-Jensen, A.C.; Leeming, D.J.; Plat, A.; Byrjalsen, I.; Christiansen, C.; van de Heijde, D.; Karsdal, M.A. Serological identification of fast progressors of structural damage with rheumatoid arthritis. *Arthritis Res. Ther.* **2013**, *15*, 1–9.
99. Chou, C.-H.; Wu, C.-C.; Song, I.-W.; Chuang, H.-P.; Lu, L.-S.; Chang, J.-H.; Kuo, S.-Y.; Lee, C.-H.; Wu, J.-Y.; Chen, Y.-T. Genome-wide expression profiles of subchondral bone in osteoarthritis. *Arthritis Res. Ther.* **2013**, *15*, 1–12.
100. Chou, C.-H.; Lee, C.-H.; Lu, L.-S.; Song, I.-W.; Chuang, H.-P.; Kuo, S.-Y.; Wu, J.-Y.; Chen, Y.-T.; Kraus, V.B.; Wu, C.-C. Direct assessment of articular cartilage and underlying subchondral bone reveals a progressive gene expression change in human osteoarthritic knees. *Osteoarthr. Cartil.* **2013**, *21*, 450–461.
101. Karsdal, M.A.; Byrjalsen, I.; Alexandersen, P.; Bihlet, A.; Andersen, J.R.; Riis, B.J.; Bay-Jensen, A.C.; Christiansen, C. Treatment of symptomatic knee osteoarthritis with oral salmon calcitonin: results from two phase 3 trials. *Osteoarthr. Cartil.* **2015**, *23*, 532–543.
102. Andersson, M.L.E.; Petersson, I.F.; Karlsson, K.E.; Jonsson, E.N.; Månsson, B.; Heinegård, D.; Saxne, T. Diurnal variation in serum levels of cartilage oligomeric matrix protein in patients with knee osteoarthritis or rheumatoid arthritis. *Ann. Rheum. Dis.* **2006**, *65*, 1490–

1494.
103. Gordon, C.D.; Stabler, T. V; Kraus, V.B. Variation in osteoarthritis biomarkers from activity not food consumption. *Clin. Chim. Acta.* **2008**, *398*, 21–26.
104. Kong, S.Y.; Stabler, T. V; Criscione, L.G.; Elliott, A.L.; Jordan, J.M.; Kraus, V.B. Diurnal variation of serum and urine biomarkers in patients with radiographic knee osteoarthritis. *Arthritis Rheum.* **2006**, *54*, 2496–2504.
105. Otterness, I.G.; Brandt, K.D.; Le Graverand, M.-P.H.; Mazzuca, S.A. Urinary TIINE concentrations in a randomized controlled trial of doxycycline in knee osteoarthritis: implications of the lack of association between TIINE levels and joint space narrowing. *Arthritis Rheum.* **2007**, *56*, 3644–3649.
106. Eyre, D.R.; Weis, M.A. The Helix-II epitope: a cautionary tale from a cartilage biomarker based on an invalid collagen sequence. *Osteoarthr. Cartil.* **2009**, *17*, 423–426.
107. van Spil, W.E.; DeGroot, J.; Lems, W.F.; Oostveen, J.C.M.; Lafeber, F.P.J.G. Serum and urinary biochemical markers for knee and hip-osteoarthritis: a systematic review applying the consensus BIPED criteria. *Osteoarthr. Cartil.* **2010**, *18*, 605–612.
108. Withrow, J.; Murphy, C.; Liu, Y.; Hunter, M.; Fulzele, S.; Hamrick, M.W. Extracellular vesicles in the pathogenesis of rheumatoid arthritis and osteoarthritis. *Arthritis Res. Ther.* **2016**, *18*, 286.
109. Cosenza, S.; Ruiz, M.; Maumus, M.; Jorgensen, C.; Noël, D. Pathogenic or therapeutic extracellular vesicles in rheumatic diseases: Role of mesenchymal stem cell-derived vesicles. *Int. J. Mol. Sci.* 2017.
110. La Marca, V.; Fierabracci, A. Insights into the diagnostic potential of extracellular vesicles and their miRNA signature from liquid biopsy as early biomarkers of diabetic micro/macrovascular complications. *Int. J. Mol. Sci.* 2017.
111. Yáñez-Mó, M.; Siljander, P.R.-M.; Andreu, Z.; Zavec, A.B.; Borràs, F.E.; Buzas, E.I.; Buzas, K.; Casal, E.; Cappello, F.; Carvalho, J.; et al. Biological properties of extracellular vesicles and their physiological functions. *J. Extracell. vesicles* **2015**.
112. Borges, F.T.; Reis, L.A.; Schor, N. Extracellular vesicles: structure, function, and potential clinical uses in renal diseases. *Brazilian J. Med. Biol. Res. = Rev. Bras. Pesqui. medicas e Biol.* **2013**, *46*, 824–830.
113. Bebelman, M.P.; Smit, M.J.; Pegtel, D.M.; Baglio, S.R. Biogenesis and function of extracellular vesicles in cancer. *Pharmacol. Ther.* **2018**, *188*, 1–11.
114. Doyle, L.; Wang, M. Overview of Extracellular Vesicles, Their Origin, Composition, Purpose, and Methods for Exosome Isolation and Analysis. *Cells* **2019**, *8*, 727.
115. Thakur, A.; Ke, X.; Chen, Y.-W.; Motallebnejad, P.; Zhang, K.; Lian, Q.;

Chen, H.J. The mini player with diverse functions: extracellular vesicles in cell biology, disease, and therapeutics. *Protein Cell* **2021**.
116. Cai, H.; Reinisch, K.; Ferro-Novick, S. Coats, tethers, Rabs, and SNAREs work together to mediate the intracellular destination of a transport vesicle. *Dev. Cell* **2007**, *12*, 671–682.
117. Levine, A.J. p53, the cellular gatekeeper for growth and division. *Cell* **1997**, *88*, 323–331.
118. Xu, X.; Lai, Y.; Hua, Z.-C. Apoptosis and apoptotic body: disease message and therapeutic target potentials. *Biosci. Rep.* **2019**, *39*.
119. Lässer, C.; Jang, S.C.; Lötvall, J. Subpopulations of extracellular vesicles and their therapeutic potential. *Mol. Aspects Med.* **2018**, *60*, 1–14.
120. Ronquist, G.; Brody, I. The prostasome: its secretion and function in man. *Biochim. Biophys. Acta* **1985**, *822*, 203–218.
121. Booth, A.M.; Fang, Y.; Fallon, J.K.; Yang, J.-M.; Hildreth, J.E.K.; Gould, S.J. Exosomes and HIV Gag bud from endosome-like domains of the T cell plasma membrane. *J. Cell Biol.* **2006**, *172*, 923–935.
122. Palmisano, G.; Jensen, S.S.; Le Bihan, M.-C.; Lainé, J.; McGuire, J.N.; Pociot, F.; Larsen, M.R. Characterization of membrane-shed microvesicles from cytokine-stimulated β-cells using proteomics strategies. *Mol. Cell. Proteomics* **2012**, *11*, 230–243.
123. Théry, C.; Witwer, K.W.; Aikawa, E.; Alcaraz, M.J.; Anderson, J.D.; Andriantsitohaina, R.; Antoniou, A.; Arab, T.; Archer, F.; Atkin-Smith, G.K.; et al. Minimal information for studies of extracellular vesicles 2018 (MISEV2018): a position statement of the International Society for Extracellular Vesicles and update of the MISEV2014 guidelines. *J. Extracell. Vesicles* **2018**, *7*, 1535750.
124. Lin, J.; Wang, L.; Lin, J.; Liu, Q. The Role of Extracellular Vesicles in the Pathogenesis, Diagnosis, and Treatment of Osteoarthritis. *Molecules* **2021**, *26*.
125. Peng, S.; Yan, Y.; Li, R.; Dai, H.; Xu, J. Extracellular vesicles from M1-polarized macrophages promote inflammation in the temporomandibular joint via miR-1246 activation of the Wnt/β-catenin pathway. *Ann. N. Y. Acad. Sci.* **2021**, *1503*, 48–59.
126. Domenis, R.; Zanutel, R.; Caponnetto, F.; Toffoletto, B.; Cifù, A.; Pistis, C.; Di Benedetto, P.; Causero, A.; Pozzi, M.; Bassini, F.; et al. Characterization of the Proinflammatory Profile of Synovial Fluid-Derived Exosomes of Patients with Osteoarthritis. *Mediators Inflamm.* **2017**, *2017*, 4814987.
127. Gao, K.; Zhu, W.; Li, H.; Ma, D.; Liu, W.; Yu, W.; Wang, L.; Cao, Y.; Jiang, Y. Association between cytokines and exosomes in synovial fluid of individuals with knee osteoarthritis. *Mod. Rheumatol.* **2020**, *30*, 758–764.
128. Jeon, O.H.; Wilson, D.R.; Clement, C.C.; Rathod, S.; Cherry, C.; Powell, B.; Lee, Z.; Khalil, A.M.; Green, J.J.; Campisi, J.; et al. Senescence cell-associated extracellular vesicles serve as osteoarthritis disease and

therapeutic markers. *JCI insight* **2019**, *4*.

129. Kolhe, R.; Hunter, M.; Liu, S.; Jadeja, R.N.; Pundkar, C.; Mondal, A.K.; Mendhe, B.; Drewry, M.; Rojiani, M. V; Liu, Y.; et al. Gender-specific differential expression of exosomal miRNA in synovial fluid of patients with osteoarthritis. *Sci. Rep.* **2017**, *7*, 2029.
130. Zhao, Y.; Xu, J. Synovial fluid-derived exosomal lncRNA PCGEM1 as biomarker for the different stages of osteoarthritis. *Int. Orthop.* **2018**, *42*, 2865–2872.
131. Meng, Y.; Qiu, S.; Sun, L.; Zuo, J. Knockdown of exosome-mediated lnc-PVT1 alleviates lipopolysaccharide-induced osteoarthritis progression by mediating the HMGB1/TLR4/NF-κB pathway via miR-93-5p. *Mol. Med. Rep.* **2020**, *22*, 5313–5325.
132. Meng, F.; Li, Z.; Zhang, Z.; Yang, Z.; Kang, Y.; Zhao, X.; Long, D.; Hu, S.; Gu, M.; He, S.; et al. MicroRNA-193b-3p regulates chondrogenesis and chondrocyte metabolism by targeting HDAC3. *Theranostics* **2018**, *8*, 2862–2883.
133. Crescitelli, R.; Lässer, C.; Jang, S.C.; Cvjetkovic, A.; Malmhäll, C.; Karimi, N.; Höög, J.L.; Johansson, I.; Fuchs, J.; Thorsell, A.; et al. Subpopulations of extracellular vesicles from human metastatic melanoma tissue identified by quantitative proteomics after optimized isolation. *J. Extracell. Vesicles* **2020**, *9*, 1722433.
134. Willms, E.; Cabañas, C.; Mäger, I.; Wood, M.J.A.; Vader, P. Extracellular Vesicle Heterogeneity: Subpopulations, Isolation Techniques, and Diverse Functions in Cancer Progression. *Front. Immunol.* **2018**, *9*, 738.
135. Lundström, A.; Mobarrez, F.; Rooth, E.; Thålin, C.; von Arbin, M.; Henriksson, P.; Gigante, B.; Laska, A.C.; Wallén, H. Prognostic Value of Circulating Microvesicle Subpopulations in Ischemic Stroke and TIA. *Transl. Stroke Res.* **2020**.
136. Lázaro-Ibáñez, E.; Lässer, C.; Shelke, G.V.; Crescitelli, R.; Jang, S.C.; Cvjetkovic, A.; García-Rodríguez, A.; Lötvall, J. DNA analysis of low- and high-density fractions defines heterogeneous subpopulations of small extracellular vesicles based on their DNA cargo and topology. *J. Extracell. Vesicles* **2019**.
137. Słomka, A.; Urban, S.K.; Lukacs-Kornek, V.; Żekanowska, E.; Kornek, M. Large Extracellular Vesicles: Have We Found the Holy Grail of Inflammation? *Front. Immunol.* **2018**, *9*, 2723.
138. Dolo, V.; D'Ascenzo, S.; Violini, S.; Pompucci, L.; Festuccia, C.; Ginestra, A.; Vittorelli, M.L.; Canevari, S.; Pavan, A. Matrix-degrading proteinases are shed in membrane vesicles by ovarian cancer cells in vivo and in vitro. *Clin. Exp. Metastasis* **1999**, *17*, 131–140.
139. Nawaz, M.; Shah, N.; Zanetti, B.R.; Maugeri, M.; Silvestre, R.N.; Fatima, F.; Neder, L.; Valadi, H. Extracellular Vesicles and Matrix Remodeling Enzymes: The Emerging Roles in Extracellular Matrix Remodeling, Progression of Diseases and Tissue Repair. *Cells* **2018**, *7*, 167.

140. Youn, Y.-J.; Shrestha, S.; Lee, Y.-B.; Kim, J.-K.; Lee, J.H.; Hur, K.; Mali, N.M.; Nam, S.-W.; Kim, S.-H.; Lee, S.; et al. Neutrophil-derived trail is a proinflammatory subtype of neutrophil-derived extracellular vesicles. *Theranostics* **2021**, *11*, 2770–2787.
141. Bodega, G.; Alique, M.; Puebla, L.; Carracedo, J.; Ramírez, R.M. Microvesicles: ROS scavengers and ROS producers. *J. Extracell. vesicles* **2019**, *8*, 1626654.
142. Monguió-Tortajada, M.; Gálvez-Montón, C.; Bayes-Genis, A.; Roura, S.; Borràs, F.E. Extracellular vesicle isolation methods: rising impact of size-exclusion chromatography. *Cell. Mol. Life Sci.* 2019.
143. Théry, C.; Amigorena, S.; Raposo, G.; Clayton, A. Isolation and Characterization of Exosomes from Cell Culture Supernatants and Biological Fluids. *Curr. Protoc. Cell Biol.* **2006**.
144. Pan, B.T.; Johnstone, R.M. Fate of the transferrin receptor during maturation of sheep reticulocytes in vitro: Selective externalization of the receptor. *Cell* **1983**.
145. Baranyai, T.; Herczeg, K.; Onódi, Z.; Voszka, I.; Módos, K.; Marton, N.; Nagy, G.; Mäger, I.; Wood, M.J.; El Andaloussi, S.; et al. Isolation of Exosomes from Blood Plasma: Qualitative and Quantitative Comparison of Ultracentrifugation and Size Exclusion Chromatography Methods. *PLoS One* **2015**, *10*, e0145686.
146. Giddings, J.C. A New Separation Concept Based on a Coupling of Concentration and Flow Nonuniformities. *Sep. Sci.* **1966**.
147. Zhang, H.; Lyden, D. Asymmetric-flow field-flow fractionation technology for exomere and small extracellular vesicle separation and characterization. *Nat. Protoc.* **2019**.
148. Fraunhofer, W.; Winter, G. The use of asymmetrical flow field-flow fractionation in pharmaceutics and biopharmaceutics. *Eur. J. Pharm. Biopharm.* 2004.
149. Zhang, H.; Freitas, D.; Kim, H.S.; Fabijanic, K.; Li, Z.; Chen, H.; Mark, M.T.; Molina, H.; Martin, A.B.; Bojmar, L.; et al. Identification of distinct nanoparticles and subsets of extracellular vesicles by asymmetric flow field-flow fractionation. *Nat. Cell Biol.* **2018**, *20*, 332–343.
150. Multia, E.; Tear, C.J.Y.; Palviainen, M.; Siljander, P.; Riekkola, M.-L. Fast isolation of highly specific population of platelet-derived extracellular vesicles from blood plasma by affinity monolithic column, immobilized with anti-human CD61 antibody. *Anal. Chim. Acta* **2019**, *1091*, 160–168.
151. Morani, M.; Mai, T.D.; Krupova, Z.; Defrenaix, P.; Multia, E.; Riekkola, M.-L.; Taverna, M. Electrokinetic characterization of extracellular vesicles with capillary electrophoresis: A new tool for their identification and quantification. *Anal. Chim. Acta* **2020**, *1128*, 42–51.
152. Multia, E.; Liangsupree, T.; Jussila, M.; Ruiz-Jimenez, J.; Kemell, M.; Riekkola, M.-L. Automated on-line isolation and fractionation system for nanosized biomacromolecules from human plasma. *Anal. Chem.*

2020, *92*, 13058–13065.
153. Liangsupree, T.; Multia, E.; Riekkola, M.-L. Modern isolation and separation techniques for extracellular vesicles. *J. Chromatogr. A* **2021**, *1636*, 461773.
154. Linares, R.; Tan, S.; Gounou, C.; Arraud, N.; Brisson, A.R. High-speed centrifugation induces aggregation of extracellular vesicles. *J. Extracell. vesicles* **2015**, *4*, 29509.
155. Felson, D.T.; Lawrence, R.C.; Hochberg, M.C.; McAlindon, T.; Dieppe, P.A.; Minor, M.A.; Blair, S.N.; Berman, B.M.; Fries, J.F.; Weinberger, M.; et al. Osteoarthritis: New Insights. Part 2: Treatment Approaches. *Ann. Intern. Med.* **2000**, *133*, 726–737.
156. Messier, S.P.; Legault, C.; Loeser, R.F.; Van Arsdale, S.J.; Davis, C.; Ettinger, W.H.; DeVita, P. Does high weight loss in older adults with knee osteoarthritis affect bone-on-bone joint loads and muscle forces during walking? *Osteoarthr. Cartil.* **2011**, *19*, 272–280.
157. Pai, Y.C.; Rymer, W.Z.; Chang, R.W.; Sharma, L. Effect of age and osteoarthritis on knee proprioception. *Arthritis Rheum.* **1997**, *40*, 2260–2265.
158. Anandacoomarasamy, A.; Leibman, S.; Smith, G.; Caterson, I.; Giuffre, B.; Fransen, M.; Sambrook, P.N.; March, L. Weight loss in obese people has structure-modifying effects on medial but not on lateral knee articular cartilage. *Ann. Rheum. Dis.* **2012**, *71*, 26 LP – 32.
159. Richette, P.; Poitou, C.; Garnero, P.; Vicaut, E.; Bouillot, J.-L.; Lacorte, J.-M.; Basdevant, A.; Clément, K.; Bardin, T.; Chevalier, X. Benefits of massive weight loss on symptoms, systemic inflammation and cartilage turnover in obese patients with knee osteoarthritis. *Ann. Rheum. Dis.* **2011**, *70*, 139–144.
160. Iversen, M.D.; Hammond, A.; Betteridge, N. Self-management of rheumatic diseases: state of the art and future perspectives. *Ann. Rheum. Dis.* **2010**, *69*, 955–963.
161. Zhang, W.; Nuki, G.; Moskowitz, R.W.; Abramson, S.; Altman, R.D.; Arden, N.K.; Bierma-Zeinstra, S.; Brandt, K.D.; Croft, P.; Doherty, M.; et al. OARSI recommendations for the management of hip and knee osteoarthritis: part III: Changes in evidence following systematic cumulative update of research published through January 2009. *Osteoarthr. Cartil.* **2010**, *18*, 476–499.
162. Geenen, R.; Bijlsma, J.W.J. Psychological management of osteoarthritic pain. *Osteoarthr. Cartil.* 2010, *18*, 873–875.
163. Uthman, O.A.; van der Windt, D.A.; Jordan, J.L.; Dziedzic, K.S.; Healey, E.L.; Peat, G.M.; Foster, N.E. Exercise for lower limb osteoarthritis: systematic review incorporating trial sequential analysis and network meta-analysis. *Br. J. Sports Med.* **2014**, *48*, 1579.
164. Uthman, O.A.; van der Windt, D.A.; Jordan, J.L.; Dziedzic, K.S.; Healey, E.L.; Peat, G.M.; Foster, N.E. Exercise for lower limb osteoarthritis:

systematic review incorporating trial sequential analysis and network meta-analysis. *BMJ Br. Med. J.* **2013**, *347*, f5555.

165. Hinman, R.S.; Heywood, S.E.; Day, A.R. Aquatic physical therapy for hip and knee osteoarthritis: results of a single-blind randomized controlled trial. *Phys. Ther.* **2007**, *87*, 32–43.
166. Fransen, M.; McConnell, S.; Harmer, A.R.; Esch, M. Van der; Simic, M.; Bennell, K.L. Exercise for osteoarthritis of the knee. *Cochrane Database Syst. Rev.* **2015**.
167. Deyle, G.D.; Allison, S.C.; Matekel, R.L.; Ryder, M.G.; Stang, J.M.; Gohdes, D.D.; Hutton, J.P.; Henderson, N.E.; Garber, M.B. Physical therapy treatment effectiveness for osteoarthritis of the knee: a randomized comparison of supervised clinical exercise and manual therapy procedures versus a home exercise program. *Phys. Ther.* **2005**, *85*, 1301–1317.
168. Rutjes, A.W.S.; Nüesch, E.; Sterchi, R.; Jüni, P. Therapeutic ultrasound for osteoarthritis of the knee or hip. *Cochrane Database Syst. Rev.* **2010**.
169. Zhang, Q.; Yue, J.; Golianu, B.; Sun, Z.; Lu, Y. Updated Systematic Review and Meta-Analysis of Acupuncture for Chronic Knee Pain. *Acupunct. Med.* **2017**, *35*, 392–403.
170. Yusuf, E. Pharmacologic and Non-Pharmacologic Treatment of Osteoarthritis. *Curr. Treat. Options Rheumatol.* **2016**, *2*, 111–125.
171. Steinmeyer, J.; Bock, F.; Stöve, J.; Jerosch, J.; Flechtenmacher, J. Pharmacological treatment of knee osteoarthritis: Special considerations of the new German guideline. *Orthop. Rev. (Pavia).* **2018**, *10*, 7782.
172. Bannuru, R.R.; Schmid, C.H.; Kent, D.M.; Vaysbrot, E.E.; Wong, J.B.; McAlindon, T.E. Comparative effectiveness of pharmacologic interventions for knee osteoarthritis: a systematic review and network meta-analysis. *Ann. Intern. Med.* **2015**, *162*, 46–54.
173. Steinmeyer, J.; Konttinen, Y.T. Oral treatment options for degenerative joint disease--presence and future. *Adv. Drug Deliv. Rev.* **2006**, *58*, 168–211.
174. Towheed, T.; Maxwell, L.; Judd, M.; Catton, M.; Hochberg, M.C.; Wells, G.A. Acetaminophen for osteoarthritis. *Cochrane database Syst. Rev.* **2006**.
175. Chappell, A.S.; Desaiah, D.; Liu-Seifert, H.; Zhang, S.; Skljarevski, V.; Belenkov, Y.; Brown, J.P. A double-blind, randomized, placebo-controlled study of the efficacy and safety of duloxetine for the treatment of chronic pain due to osteoarthritis of the knee. *Pain Pract.* **2011**, *11*, 33–41.
176. Brown, J.P.; Boulay, L.J. Clinical experience with duloxetine in the management of chronic musculoskeletal pain. A focus on osteoarthritis of the knee. *Ther. Adv. Musculoskelet. Dis.* **2013**, *5*, 291–304.
177. Zhang, W.; Moskowitz, R.W.; Nuki, G.; Abramson, S.; Altman, R.D.; Arden, N.; Bierma-Zeinstra, S.; Brandt, K.D.; Croft, P.; Doherty, M.; et

al. OARSI recommendations for the management of hip and knee osteoarthritis, Part II: OARSI evidence-based, expert consensus guidelines. *Osteoarthr. Cartil.* **2008**, *16*, 137–162.
178. Hepper, C.T.; Halvorson, J.J.; Duncan, S.T.; Gregory, A.J.M.; Dunn, W.R.; Spindler, K.P. The efficacy and duration of intra-articular corticosteroid injection for knee osteoarthritis: a systematic review of level I studies. *J. Am. Acad. Orthop. Surg.* **2009**, *17*, 638–646.
179. Hirsch, G.; Kitas, G.; Klocke, R. Intra-articular corticosteroid injection in osteoarthritis of the knee and hip: factors predicting pain relief--a systematic review. *Semin. Arthritis Rheum.* **2013**, *42*, 451–473.
180. Skou, S.T.; Roos, E.M.; Laursen, M.B.; Rathleff, M.S.; Arendt-Nielsen, L.; Simonsen, O.; Rasmussen, S. A randomized, controlled trial of total knee replacement. *N. Engl. J. Med.* **2015**, *373*, 1597–1606.
181. Chen, A.F.; Stewart, M.K.; Heyl, A.E.; Klatt, B.A. Effect of immediate postoperative physical therapy on length of stay for total joint arthroplasty patients. *J. Arthroplasty* **2012**, *27*, 851–856.
182. Bade, M.J.; Stevens-Lapsley, J.E. Restoration of physical function in patients following total knee arthroplasty: an update on rehabilitation practices. *Curr. Opin. Rheumatol.* **2012**, *24*.
183. Moatshe, G.; Morris, E.R.; Cinque, M.E.; Pascual-Garrido, C.; Chahla, J.; Engebretsen, L.; Laprade, R.F. Biological treatment of the knee with platelet-rich plasma or bone marrow aspirate concentrates. *Acta Orthop.* **2017**, *88*, 670–674.
184. McCarrel, T.M.; Mall, N.A.; Lee, A.S.; Cole, B.J.; Butty, D.C.; Fortier, L.A. Considerations for the use of platelet-rich plasma in orthopedics. *Sport. Med.* 2014.
185. Wu, P.I.-K.; Diaz, R.; Borg-Stein, J. Platelet-Rich Plasma. *Phys. Med. Rehabil. Clin. N. Am.* **2016**, *27*, 825–853.
186. Andia, I.; Maffulli, N. Platelet-rich plasma for managing pain and inflammation in osteoarthritis. *Nat. Rev. Rheumatol.* 2013.
187. Filardo, G.; Kon, E. PRP: Product Rich in Placebo? *Knee Surg. Sports Traumatol. Arthrosc.* 2016, *24*, 3702–3703.
188. Dohan Ehrenfest, D.M.; Andia, I.; Zumstein, M.A.; Zhang, C.-Q.; Pinto, N.R.; Bielecki, T. Classification of platelet concentrates (Platelet-Rich Plasma-PRP, Platelet-Rich Fibrin-PRF) for topical and infiltrative use in orthopedic and sports medicine: current consensus, clinical implications and perspectives. *Muscles. Ligaments Tendons J.* **2014**, *4*, 3–9.
189. Fu, F.H.; Zurakowski, D.; Browne, J.E.; Mandelbaum, B.; Erggelet, C.; Moseley, J.B.J.; Anderson, A.F.; Micheli, L.J. Autologous chondrocyte implantation versus debridement for treatment of full-thickness chondral defects of the knee: an observational cohort study with 3-year follow-up. *Am. J. Sports Med.* **2005**, *33*, 1658–1666.
190. Kon, E.; Filardo, G.; Berruto, M.; Benazzo, F.; Zanon, G.; Della Villa, S.;

Marcacci, M. Articular cartilage treatment in high-level male soccer players: a prospective comparative study of arthroscopic second-generation autologous chondrocyte implantation versus microfracture. *Am. J. Sports Med.* **2011**, *39*, 2549–2557.

191. Prockop, D.J.; Youn Oh, J. Mesenchymal stem/stromal cells (MSCs): Role as guardians of inflammation. *Mol. Ther.* 2012.
192. Caplan, A.I.; Correa, D. The MSC: An injury drugstore. *Cell Stem Cell* 2011.
193. Jo, C.H.; Lee, Y.G.; Shin, W.H.; Kim, H.; Chai, J.W.; Jeong, E.C.; Kim, J.E.; Shim, H.; Shin, J.S.; Shin, I.S.; et al. Intra-articular injection of mesenchymal stem cells for the treatment of osteoarthritis of the knee: a proof-of-concept clinical trial. *Stem Cells* **2014**, *32*, 1254–1266.
194. Lopa, S.; Colombini, A.; Moretti, M.; de Girolamo, L. Injective mesenchymal stem cell-based treatments for knee osteoarthritis: from mechanisms of action to current clinical evidences. *Knee Surg. Sports Traumatol. Arthrosc.* **2019**, *27*, 2003–2020.
195. Bora, P.; Majumdar, A.S. Adipose tissue-derived stromal vascular fraction in regenerative medicine: a brief review on biology and translation. *Stem Cell Res. Ther.* **2017**, *8*, 145.
196. Andia, I.; Maffulli, N. Biological Therapies in Regenerative Sports Medicine. *Sports Med.* **2017**, *47*, 807–828.
197. Nguyen, P.D.; Tran, T.D.-X.; Nguyen, H.T.-N.; Vu, H.T.; Le, P.T.-B.; Phan, N.L.-C.; Vu, N.B.; Phan, N.K.; Van Pham, P. Comparative Clinical Observation of Arthroscopic Microfracture in the Presence and Absence of a Stromal Vascular Fraction Injection for Osteoarthritis. *Stem Cells Transl. Med.* **2017**, *6*, 187–195.
198. Russo, A.; Condello, V.; Madonna, V.; Guerriero, M.; Zorzi, C. Autologous and micro-fragmented adipose tissue for the treatment of diffuse degenerative knee osteoarthritis. *J. Exp. Orthop.* **2017**, *4*, 33.
199. Habib, N.A.; Gordon, M.Y. Clinical applications of stem cell therapy--the pros and cons of stem cell sources. *Regen. Med.* 2006, *1*, 301–302.
200. Ni, Z.; Zhou, S.; Li, S.; Kuang, L.; Chen, H.; Luo, X.; Ouyang, J.; He, M.; Du, X.; Chen, L. Exosomes: roles and therapeutic potential in osteoarthritis. *Bone Res.* **2020**, *8*, 25.
201. Lai, R.C.; Chen, T.S.; Lim, S.K. Mesenchymal stem cell exosome: a novel stem cell-based therapy for cardiovascular disease. *Regen. Med.* **2011**, *6*, 481–492.
202. Zhao, X.; Zhao, Y.; Sun, X.; Xing, Y.; Wang, X.; Yang, Q. Immunomodulation of MSCs and MSC-Derived Extracellular Vesicles in Osteoarthritis. *Front. Bioeng. Biotechnol.* **2020**, *8*, 575057.
203. Zhou, Q.-F.; Cai, Y.-Z.; Lin, X.-J. The dual character of exosomes in osteoarthritis: Antagonists and therapeutic agents. *Acta Biomater.* **2020**, *105*, 15–25.
204. Zhang, Y.; Yu, M.; Tian, W. Physiological and pathological impact of

exosomes of adipose tissue. *Cell Prolif.* **2016**, *49*, 3–13.
205. Cho, B.S.; Kim, J.O.; Ha, D.H.; Yi, Y.W. Exosomes derived from human adipose tissue-derived mesenchymal stem cells alleviate atopic dermatitis. *Stem Cell Res. Ther.* 2018, *9*, 187.
206. Binks, D.A.; Hodgson, R.J.; Ries, M.E.; Foster, R.J.; Smye, S.W.; McGonagle, D.; Radjenovic, A. Quantitative parametric MRI of articular cartilage: a review of progress and open challenges. *Br. J. Radiol.* **2013**, *86*, 20120163.
207. Zhang, H.; Whalley, R.D.; Ferreira, A.M.; Dalgarno, K. High throughput physiological micro-models for in vitro pre-clinical drug testing: a review of engineering systems approaches. *Prog. Biomed. Eng.* **2020**, *2*, 22001.
208. Sun, J.; Warden, A.R.; Ding, X. Recent advances in microfluidics for drug screening. *Biomicrofluidics* **2019**, *13*, 61503.
209. Rodriguez, B.; Carusi, A.; Abi-Gerges, N.; Ariga, R.; Britton, O.; Bub, G.; Bueno-Orovio, A.; Burton, R.A.B.; Carapella, V.; Cardone-Noott, L. Human-based approaches to pharmacology and cardiology: an interdisciplinary and intersectorial workshop. *Ep Eur.* **2015**, *18*, 1287–1298.
210. Couto, G.K.; Segatto, N.V.; Oliveira, T.L.; Seixas, F.K.; Schachtschneider, K.M.; Collares, T. The Melding of Drug Screening Platforms for Melanoma . *Front. Oncol.* 2019, *9*, 512.
211. Zou, Z.; Luo, X.; Chen, Z.; Zhang, Y.S.; Wen, C. Emerging microfluidics-enabled platforms for osteoarthritis management: from benchtop to bedside. *Theranostics* **2022**, *12*, 891–909.
212. Samvelyan, H.J.; Hughes, D.; Stevens, C.; Staines, K.A. Models of Osteoarthritis: Relevance and New Insights. *Calcif. Tissue Int.* **2021**, *109*, 243–256.
213. Aleman, J.; Kilic, T.; Mille, L.S.; Shin, S.R.; Zhang, Y.S. Microfluidic integration of regeneratable electrochemical affinity-based biosensors for continual monitoring of organ-on-a-chip devices. *Nat. Protoc.* **2021**, *16*, 2564–2593.
214. Bhise, N.S.; Ribas, J.; Manoharan, V.; Zhang, Y.S.; Polini, A.; Massa, S.; Dokmeci, M.R.; Khademhosseini, A. Organ-on-a-chip platforms for studying drug delivery systems. *J. Control. Release* **2014**, *190*, 82–93.
215. Kimura, H.; Sakai, Y.; Fujii, T. Organ/body-on-a-chip based on microfluidic technology for drug discovery. *Drug Metab. Pharmacokinet.* **2018**, *33*, 43–48.
216. Piluso, S.; Li, Y.; Abinzano, F.; Levato, R.; Moreira Teixeira, L.; Karperien, M.; Leijten, J.; van Weeren, R.; Malda, J. Mimicking the Articular Joint with In Vitro Models. *Trends Biotechnol.* **2019**, *37*, 1063–1077.
217. Shi, X.; Zhou, J.; Zhao, Y.; Li, L.; Wu, H. Gradient-regulated hydrogel for interface tissue engineering: steering simultaneous

osteo/chondrogenesis of stem cells on a chip. *Adv. Healthc. Mater.* **2013**, *2*, 846–853.

218. Bao, X.; Li, Z.; Liu, H.; Feng, K.; Yin, F.; Li, H.; Qin, J. Stimulation of chondrocytes and chondroinduced mesenchymal stem cells by osteoinduced mesenchymal stem cells under a fluid flow stimulus on an integrated microfluidic device. *Mol. Med. Rep.* **2018**, *17*, 2277–2288.
219. Occhetta, P.; Mainardi, A.; Votta, E.; Vallmajo-Martin, Q.; Ehrbar, M.; Martin, I.; Barbero, A.; Rasponi, M. Hyperphysiological compression of articular cartilage induces an osteoarthritic phenotype in a cartilage-on-a-chip model. *Nat. Biomed. Eng.* **2019**, *3*, 545–557.
220. Paggi, C.A.; Venzac, B.; Karperien, M.; Leijten, J.C.H.; Le Gac, S. Monolithic microfluidic platform for exerting gradients of compression on cell-laden hydrogels, and application to a model of the articular cartilage. *Sensors Actuators B Chem.* **2020**, *315*, 127917.
221. Lin, Z.; Li, Z.; Li, E.N.; Li, X.; Del Duke, C.J.; Shen, H.; Hao, T.; O'Donnell, B.; Bunnell, B.A.; Goodman, S.B.; et al. Osteochondral Tissue Chip Derived From iPSCs: Modeling OA Pathologies and Testing Drugs. *Front. Bioeng. Biotechnol.* **2019**, *7*, 411.
222. Mondadori, C.; Palombella, S.; Salehi, S.; Talò, G.; Visone, R.; Rasponi, M.; Redaelli, A.; Sansone, V.; Moretti, M.; Lopa, S. Recapitulating monocyte extravasation to the synovium in an organotypic microfluidic model of the articular joint. *Biofabrication* **2021**, *13*.
223. Goldring, M.B.; Goldring, M.B.; Harris, E.D.; Budd, R.C.; Genovese, M.C. Kelley's Textbook of Rheumatology. *Harris, ED* **2008**, 203–234.
224. Darling, E.M.; Athanasiou, K.A. Rapid phenotypic changes in passaged articular chondrocyte subpopulations. *J. Orthop. Res.* **2005**, *23*, 425–432.
225. Otero, M.; Favero, M.; Dragomir, C.; El Hachem, K.; Hashimoto, K.; Plumb, D.A.; Goldring, M.B. Human chondrocyte cultures as models of cartilage-specific gene regulation. *Methods Mol. Med.* **2005**, *107*, 69–95.
226. Barbero, A.; Grogan, S.P.; Mainil-Varlet, P.; Martin, I. Expansion on specific substrates regulates the phenotype and differentiation capacity of human articular chondrocytes. *J. Cell. Biochem.* **2006**, *98*, 1140–1149.
227. Okubo, R.; Asawa, Y.; Watanabe, M.; Nagata, S.; Nio, M.; Takato, T.; Hikita, A.; Hoshi, K. Proliferation medium in three-dimensional culture of auricular chondrocytes promotes effective cartilage regeneration in vivo. *Regen. Ther.* **2019**, *11*, 306–315.

Chapter 2

Comparison of conventional techniques to isolate different size EV subpopulations from the synovial fluid in view of a clinical translation

Comparison of conventional techniques to isolate different size EV subpopulations from the synovial fluid in view of a clinical translation

D'Arrigo D.[1,2], Arrigoni C.[1], Delcogliano M.[3], Vanoni M.[2,3], Candrian C.[4,5], Moretti M.[1,5,6]

1 - Regenerative Medicine Technologies Lab, Service of Orthopaedics and Traumatology, Department of Surgery, EOC, via Federico Chiesa 5, 6500 Bellinzona, Switzerland (CH)

2 - Department of Biotechnology and Bioscience, Università degli studi di Milano-Bicocca, 20126 Milan (IT)

3 - ISBE/SYSBIO Centre of Systems Biology, Milan, Italy (IT)

4 - Service of Orthopaedics and Traumatology, Department of Surgery, EOC, Via Tesserete 46, 6900 Lugano, Switzerland (CH)

5 - Euler Institute, Biomedical Sciences Faculty, Università della Svizzera Italiana (USI), via Buffi 13, 6900 Lugano, Switzerland (CH)

6 - Cell and Tissue Engineering Laboratory, IRCCS Istituto Ortopedico Galeazzi, Via Riccardo Galeazzi 4, 20161 Milan, Italy (IT)

Status: finalizing experimental section and preparation of the manuscript for submission

Abstract

Introduction

Extracellular vesicles (EVs) isolated with liquid biopsies from biofluids, emerged as a promising diagnostic tool for several diseases, including osteoarthritis (OA). Contrarily to the classical view, it has been demonstrated that EVs consist in different subpopulations, but the development of effective isolation and separation methods to obtain them is not always straightforward. The process of EV separation is made even more difficult due to the complexity of biofluids like the synovial fluid (SF). For this reason, most of the studies in literature were focused on small size EVs, despite evidence demonstrating that large size EVs also have a pathophysiological role. Aiming at developing a protocol to isolate and separate EV subpopulations with different size from SF, we optimized its pre-treatment and compared different separation techniques.

Methods

We collected SF from the shoulder of donors underwent biceps long head tenotomy and from the knee of end-stage arthritic patients underwent joint replacement. We optimized the SF pretreatment, evaluating the effect of the viscosity, centrifugation time and regimen on the yield and on the removal of large EVs. Then, we tested and compared the effectiveness of ultracentrifugation, size-exclusion chromatography (SEC) and

HPLC by nanoparticle tracking analysis, western blot and quantification of the protein concentration.

Results

We found the best centrifugation parameters, in terms of decreasing SF viscosity, time and speed, that allowed the pelleting of large contaminants without affecting the EV yield and avoiding the removal of large EVs. The ultracentrifugation allowed the isolation of two different subpopulations with different mean size. However, the yield of the process is low, and the isolation time is relatively long. The SEC and the HPLC did not allow an effective separation of different size EV subpopulations, as demonstrated by light scattering analysis, western blot (e.g. CD63, TSG101, Mitofilin and Albumin) and protein quantification.

Conclusions

We demonstrated that conventional size-based separation methods have a different effectiveness in isolating EV subpopulations with different size, resulting adequate only for the separation of small sized EVs from SF.

Keywords: Extracellular vesicles, EV subpopulations, asymmetrical flow-field flow fractionation, synovial fluid, liquid biopsies, diagnosis

Introduction

Extracellular vesicles (EVs) consist in heterogeneous populations of lipid bilayers-enclosed vesicles released by virtually all the cell types with a size ranging from 20-30 nanometres to few micrometers[1]. Seventy years ago, one of the first indications about EVs was reported[2] and since then, they increasingly gained importance as key actors in the cell communication processes. Due to their cargo, that comprises proteins, enzymes, nucleic acids and lipids, the EVs are currently considered as promising diagnostic tools in several pathological conditions affecting different tissues[3,4], including the joints and the related diseases, such as osteoarthritis (OA)[5]. In fact, the EVs resemble the metabolic state of their parent cell, therefore those isolated from liquid biopsies, including from the synovial fluid (SF), are considered as innovative diagnostic tools for many different diseases[6]. In the arthritic joints, the SF represents the source of EVs that could be used to monitor the pathophysiological conditions of the joints[5,7]. In literature, some groups have already evaluated the potential use of EVs as OA biomarkers, however most of the studies in this field focused on the small size EVs, classically termed as exosomes[8–10].

However, an increasing number of experimental evidences demonstrated that beyond the small size EVs, larger EV subpopulations do exist and that might have important

physiological, pathological, therapeutic and diagnostic implications in many different tissues and diseases[11,12]. For this reason, increasing efforts are made to characterize and understand the pathophysiological role of larger EVs. However, the development of effective isolation and separation methods to obtain different-sized EV subpopulations from biofluids is not straightforward. In fact, the biofluids such as SF are generally rich in soluble proteins and aggregates and EVs are present in lower concentration than these other components[13]. Thus, the classic isolation methods, such as differential ultracentrifugation, size exclusion chromatography and ultrafiltration, can have difficulties to achieve an effective separation of the different-sized EVs subpopulation[14,15].

With this study we aim to compare these size-based isolation techniques in the isolation and the separation of different-sized EV subpopulations from the SF. This work, giving useful information about the potential translation of these techniques towards a clinical setting, could be important for future studies of the different-size EV subpopulations from the biofluids.

Material and methods

Biological sample donors

All the human-derived biological specimens used in this study and the sampling techniques were performed in accordance with

the respective guidelines and the regulations of the Ente Ospedaliero Cantonale and were approved by the Cantonal ethical committee (approval n. 2020-00029) (Switzerland). Human synovial fluid was collected from the shoulders of donors underwent tenotomy of the long head of the biceps. Knee synovial fluid derived from the knee of end-stage arthritic patients after total knee arthroplasty. All these surgical procedures were performed at the Traumatology and Orthopedic Unit of the Regional Hospital of Lugano. All the biological material was collected upon the acceptance of the informed consent by the donors. The information of the donors are summarized in Table 1.

Group	**Source**	**Pathological conditions**	**Pre-treatment**
Shoulder	Synovial fluid	Biceps long head tenotomy	Hyaluronidase digestion + centrifugation
Knee	Synovial fluid	Osteoarthritis	Hyaluronidase digestion + centrifugation

Table 1. Information about the donors from which we collected the biofluids for our work.

Optimization of the synovial fluid pre-treatment

The synovial fluid from three donors (one from the shoulder and two from arthritic knee) was collected from the operating room and transported to the laboratory in sterile containers, and aliquoted in 1 mL aliquots. To evaluate the effect of different centrifugation regimens in pelleting the cell and large cell-

derived contaminants without removing the large size EVs, three aliquots from each donor were differentially centrifuged at 1000, 3000 or 5000g for 5 minutes at 10°C. Then the supernatant was aliquoted and stored at -80°C. The SF was successively thawed at RT, added with 5 μL of Hyaluronidase I type-S (2000 U/mL, in PBS; Sigma-Aldrich, St. Louis, USA) and digested for 30 minutes in a thermomixer at 37°C and 300 rpm, to facilitate and increase the isolation of EVs[16]. After the digestion, the samples were centrifuged at 1.000g for 5 min at 10°C to remove large protein aggregates and stored at -80°C until used for the EV isolation. To isolate the EVs, the differentially centrifuged SF samples were thawed and ultracentrifuged overnight at 100000g at 4°C (Optima XPN equipped with rotor 90 Ti, all from Beckman Coulter). The isolated EVs were successively characterized.

EV isolation – Differential ultracentrifugation

First of all, we optimized the ultracentrifugation step by evaluating the effect of the SF viscosity and centrifugation time on the yield of the isolation protocol. Briefly, digested SF, undiluted or diluted 3:1 in PBS, was ultracentrifuged overnight at 100000g at 4°C. Then we evaluated the yield of EVs after ultracentrifuging the samples for 3 hours, overnight or for two overnight at 100000g at 4°C. Based on the results of this optimization step, we selected the optimized pre-treatment parameters for all the subsequent samples. The optimized

procedure was as follows: the digested SF samples from the knee and the shoulder (1 mL) were transferred to polycarbonate ultracentrifugation tubes (Beckman Coulter, Brea, USA) and diluted with 2 mL of PBS and centrifuged twice at 10000g for 30 minutes at 4°C. The two pellets were resuspended in PBS and put together constituting the so called "10K pellet". The supernatant was further ultracentrifuged overnight twice at 100000g at 4°C. As for the 10K pellet, the two pellets were resuspended and put together in a final volume of 100 μL of PBS.

EV isolation – Size exclusion chromatography (SEC)

As SEC is currently one of the most used approaches to isolate EVs according to their size, we used a commercial pre-packed SEC column and two different columns for the High-Performance Liquid Chromatography (HPLC). For the commercial SEC columns (qEVoriginal from IZON Burnside, Christchurch, New Zealand), 1 mL of digested knee and shoulder synovial fluid was loaded on the top. 30 fractions of 500 μL each were collected and gathered to obtain 4 different potential subpopulations, grouping together fractions 1-3; 4-6; 7-11 and 12-16. Due to the higher dilution of these samples, we concentrated the eluate of each potential subpopulation by means of centrifugal filter unit (Amicon Ultra-4, Merck, Darmstadt, Germany).

For the HPLC approach, 120 μL of digested knee-SF were injected in the HPLC instrument (Agilent Infinity, Agilent, Santa Clara,

USA), using PBS as mobile phase and setting the flow at 0,5 mL/min to maintain the pressure below 30 bar. We compared two different SEC columns, OHpak SB-806M HQ (Plate Number: > 12.000; Particle size: 13 μm; Pore size: 15.000 Å) and OHpak SB-807 HQ (Plate Number: > 1.500; Particle size: 35 μm; Pore size: 30.000 Å) (both from Shodex, New York, USA). We recorded the signals from multiple wavelength detectors at wavelengths of 204, 220, 254 and 280 nm. Based on the peaks observed during the elution, we separated the eluate in 8 different subgroups, as specified in Table 2.

Fraction	Elution time
1	13-15
2	15-17
3	17-19
4	19-22
5	22-23
6	23-25
7	26-28
8	29-33

Table 2. Timing details of the fractions collected from the HPLC.

Nanoparticle tracking analysis (NTA)

To evaluate the size and the concentration of the nanoparticles isolated with the differential centrifugation and the SEC, 1 μL of the EV preparation was diluted in 999 μL of PBS. The concentration and the size of the nanoparticle were assessed by NTA, using NanoSight LM10 equipped with 405 nm laser (Malvern Instruments, United Kingdom). For each sample, five

videos of 60 seconds were recorded and analysed with NTA 2.3 analytic software.

Protein content quantification

The ultracentrifuged specimens were diluted 50 times in PBS to a final volume of 100 μL and then sonicated at the maximum power for 5 seconds (Bandelin, Berlin, Germany). The total protein content was quantified with the Pierce BCA Protein Assay Kit (Thermo Fisher Scientific, Waltham, USA) following the specifications of the manufacturer. The standard curve was obtained with serial dilution in PBS of Human Serum Albumin included in the kit and the r^2 for each assay was > 0.99. After the incubation, the absorbance at 562 nm was read with plate reader (Biotek, Winooski, USA). Finally, the protein concentration of each sample was extrapolated from the standard curve using a linear equation.

Western blot analyses

For western blot analyses we used a number of EVs corresponding to 30 μg of proteins, based on the BCA quantification. The total proteins were obtained from the samples by lysing the EVs with ice-cold RIPA buffer with the addition of SIGMAFAST™ Protease Inhibitors and Phosphatase Inhibitor Cocktail 3 and 2 (all from Sigma, St. Louis, MI, USA). Then, the proteins were boiled with 6x Laemmli SDS sample buffer (VWR International, Dietikon, Switzerland), and separated using 4-20%

Mini-PROTEAN®TGX™ Precast Gel, and successively they were transferred onto a membrane made of PVDF using a semi-dry transfer system (all from Bio-Rad Europe, Basel, Switzerland). Membranes were incubated with the following antibodies: anti-CD63 (1:100, SantaCruz Biotechnology, Dallas, USA), anti-TSG101 (1:1000, Abcam, Cambridge, United Kingdom), anti-Mitofillin (1:1000, Abcam) and anti-albumin (1:1000 Abcam). We then incubated samples with IRDye® 680RD or 800CW goat anti-mouse or goat anti-rabbit secondary antibody (LI-COR Biosciences, Lincoln, Nebraska, USA). Finally, the infrared or fluorescent signals were detected with the Odyssey CLx Detection System (LI-COR Biosciences).

Statistical analysis

The results presented in this work are shown as mean ± SD (standard deviation). Statistical analyses were performed using the software Prism GraphPad Software Version 9. The statistical difference between the experimental groups was assessed by one-way ANOVA followed by post-hoc Tukey's multiple tests. Statistical significance was defined as $p<0,05$.

Results

Synovial fluid pre-treatment

To compare the effectiveness of different size-based isolation techniques, we first evaluated the effect of the pre-treatment of

the synovial fluid on the size distribution of the EVs. This procedure consisted in a centrifugation step to remove contaminant cells, including erythrocytes, and cell debris that would result in the clotting of SF. Then a digestion step with hyaluronidase, important for decreasing the viscosity of the SF thus facilitating the EV isolation[16], was performed. To maximize the removal of the contaminants while avoiding the depletion of larger EVs, we evaluated the effect of different centrifugation regimens on the total isolated EV. As shown in Figure 1A, we found a decreasing trend in the particle mean diameter (172,7 nm ± 17,5 nm for 1000g; 164,7 nm ± 19,7 nm for 3000g and 144 nm ± 12,3 nm for 5000g) and in the D90 (289,3 nm ± 30,1 nm; 270,3 nm ± 29,1 nm and 241,7 nm ± 18,2 nm, respectively) (Fig. 1B) with higher centrifugal forces, even if not significant (Table S1 and S2). The same trend was observed in the average concentration of EVs (Fig. 1C) and proteins (Fig. 1D), even if in this case the variability resulted higher. In addition, with centrifugation at 1000g we were not able to visually remove all the red blood cells present in the SF (data not shown). Considering these outcomes, we chose the centrifugation at 3000 g for the pre-treatment of SF, since probably the largest EVs started to be pelleted with a centrifugation step at 5000g.

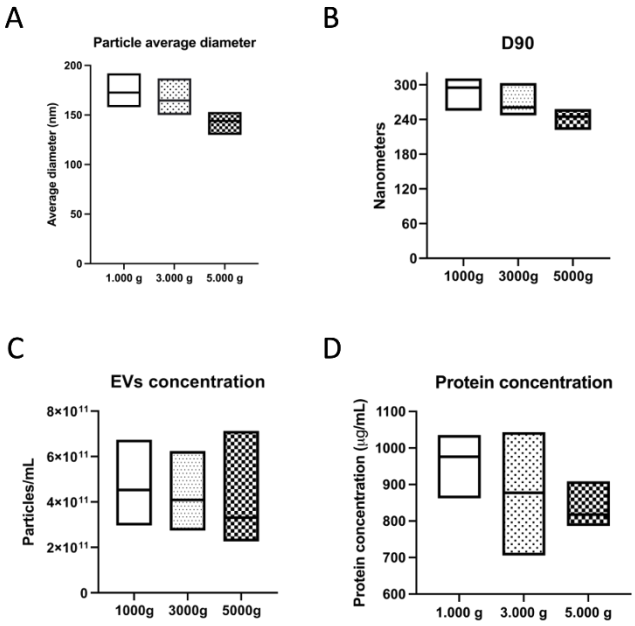

Figure 1. Results of the different centrifugation regimen on (A) average diameter of the particles; (B) particle size distribution; (C) EVs and (D) protein concentration.

Differential centrifugation

To optimize the ultracentrifugation step, we first checked the effect of centrifugation time and the SF sample viscosity on the EV yield. As shown in Table 3 and 4, the dilution of the SF samples allowed to recover an amount more than double of EVs, without affecting the average size of the isolated particles. In addition, the pelleted EVs were more easily resuspended in the diluted samples, probably indicating a minor concentration of contaminants that could determine formation of EV aggregates. In fact, NTA analysis showed less variability and lower signal from larger particles in the diluted samples (Fig. 2A). The increase

of the centrifugation time had an even more evident effect on the yield of EVs. In fact, 3 hours of centrifugation led to the recovery of much less EVs (3,4 x 10^9 ± 0,8 x 10^9) compared to one (5,2 x 10^10± 0,24 x 10^10) or two (8,42 x 10^10 ± 0,19 x 10^10) overnight centrifugations (Table 3). In addition, the EVs isolated with a 3-hour centrifugation had also a slightly different size distribution assessed with the NTA, showing an intensity peak for particles with a size of 250 nm (Fig 2B; Table 4). Based on these results, we decided to dilute samples in PBS before performing two overnight ultracentrifugation.

	3 hours	**Overnight**	**Overnight -twice**
Not diluted	n.a.	$2{,}1 \times 10^{10} \pm 0{,}5 \times 10^{10}$	n.a.
Diluted	$3{,}4 \times 10^{9} \pm 0{,}8 \times 10^{9}$	$5{,}2 \times 10^{10} \pm 0{,}24 \times 10^{10}$	$8{,}42 \times 10^{10} \pm 0{,}19 \times 10^{10}$

Table 3. Total number of isolated EVs during the optimization phase of the ultracentrifugation protocol.

	3 hours	**Overnight**	**Overnight -twice**
Not diluted	n.a.	211,5 ± 10,1 nm	n.a.
Diluted	192 ± 3,1 nm	191 ± 14,1 nm	178 ± 5,1 nm

Table 4. Average diameter of the isolated EVs during the optimization phase of the ultracentrifugation protocol. The size has been quantified by NTA. n.a. = not available.

After this optimization step, we started the isolation of different size EV subpopulations by using differential centrifugation. With this approach we were able to isolate two EV subpopulations with different size. In fact, as depicted in Figure 2C, the average diameter of the EVs in the 10K pellet was higher both in the knee

and in the shoulder (215 nm ± 10,8 and 244 nm ± 19,4 nm, respectively) than that of the EVs in the 100K pellet (168 nm ± 7,4 nm and 192 nm ± 15,3 nm, respectively), as expected. In addition, a higher peak at around 400 nm was visible in the 10K pellet, together with signal from particles with diameter up to 700 nm, especially in the shoulder SF-EVs (Fig 2C). No difference was found in the particle concentration in the two pellets from the same sample. However, a slightly higher particle number was found in the knee SF. Generally, the EVs isolated from the shoulder resulted always slightly bigger than those from the knee. In fact, the graph obtained from the NTA showed higher signal and variability for larger particles in in both the pellets. Although we were able to isolate two different EV subpopulations, from the supernatant after the two overnight ultracentrifugations we still found a high number of particles with an average size compatible with small-sized EVs (142 ± 13,3 nm). These data are summarized in Table 5.

Parameter	10K pellet		100K pellet		Supernatant	
	Knee	Shoulder	Knee	Shoulder	Knee	Shoulder
Total EVs number	3,29 ± 0,18 x 10^{10}	1,2 ± 0,1 x 10^{10}	3,4 ± 0,24 x 10^{10}	1,68 ± 0,21 x 10^{10}	3,08 ± 0,1x 10^{10}	2,31 ± 0,13 x 10^{10}
Mean size	215 ± 10,8	244 ± 19,4	168 ± 7,4	192 ± 15,3	142 ± 1,5	154 ± 15,6
Mode size	166 ± 6,8	169 ± 10,9	134 ± 5,2	132 ± 9,7	101 ± 1,9	134 ± 6,2

Table 5. The total number and the size of the EVs contained in the 10K and 100K pellet and in the supernatant from knee and shoulder SF.

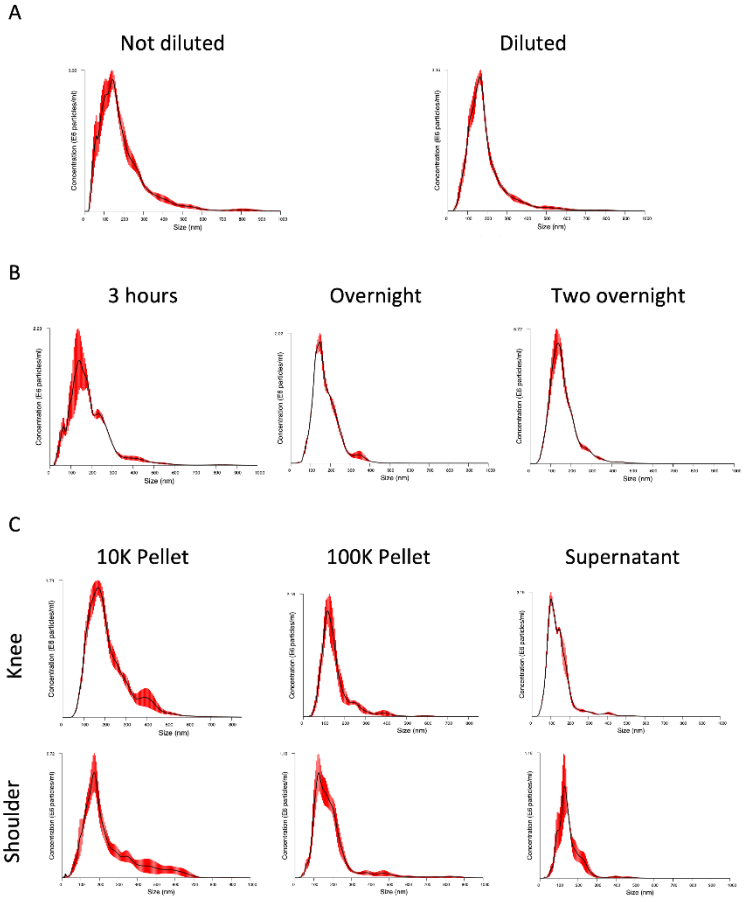

Figure 2. Effect of the (A) decrease of viscosity of the synovial fluid by dilution and of the (B) centrifugation time on the size distribution assessed by NTA of EVs isolated with ultracentrifugation. (C) Size distribution of the particles contained in the 10K pellet, the 100K pellet and in the supernatant after the two ultracentrifugations.

Size exclusion chromatography

The SEC performed with the commercial column allowed the effective removal of synovial proteins from the EVs preparation obtained from the knee and the shoulder synovial fluid, as highlighted by the dotted lines in Figure 3A. By quantifying the

particle concentration in each of the 30 fractions collected, we put together different fractions, as described in materials and methods section, to obtain four potential subpopulations that were successively characterized. From the analysis of the average size of these particle subsets we found a specular trend in knee and shoulder synovial fluid, with very similar values. In fact, the NTA detected the larger particles in the fractions 1-3 with value higher than 200 nm (237,3 nm ± 63,9 nm in the knee and 225,7 nm ± 27nm in the shoulder). The average diameter of the objects in fractions 4-6 was still over 200 nm from the knee SF (209,2 nm ± 8,8 nm), while from the shoulder samples it decreased to 186 nm ± 21,4 nm. The smallest particles were detected in fractions 7-11, around 180 nm in both the samples. In the fractions 12-16 the average size of the particles tended to increase, probably because of the increasing protein concentration that can cover the EVs and cause aggregation (Fig. 3A). However, from the western blot analysis it emerged that the objects detected by NTA in the first six fractions were not ascribed to EVs, but more likely to large aggregates. In fact, we found positivity for the classical markers of the small-size EVs such as CD63 (Fig. 3C) and TSG101 (Fig. 3D) in the fractions 7 to 11, as expected. However, we did not find signal from Mitofilin, a marker of larger EVs[17], in the fractions from 1 to 6 (Fig. 3E).

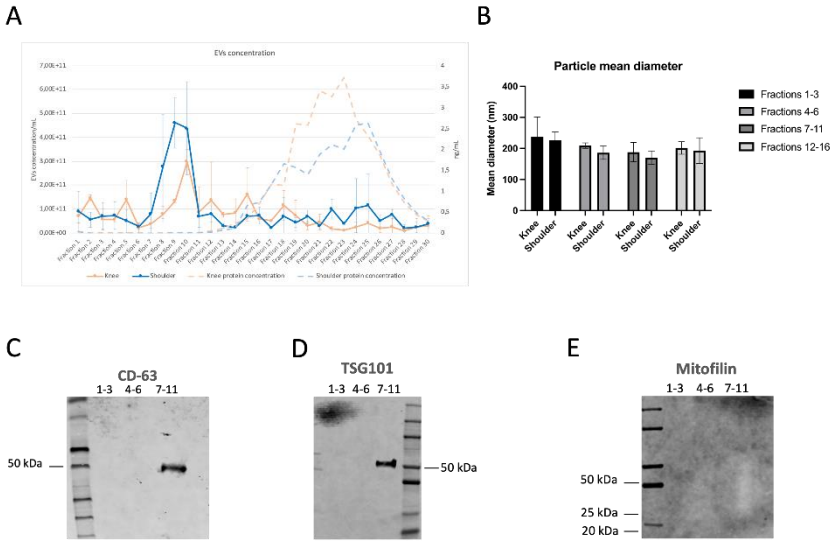

Figure 3. (A) Particle and protein concentration (dotted line) in all the fractions collected from the commercial SEC column after the separation of shoulder (blue) and knee (orange) synovial fluid. In the four potential subpopulations, we quantified the mean particle diameter (B) and the presence of classic small EV markers (C,D) and a marker of large EVs (E). Data are reported as mean ± standard deviation.

HPLC

In the chromatogram obtained from the column with smaller pore size in the HPLC we detected 5 different peaks (Fig. 4A) and we analysed 8 different fractions eluted from the instrument. As reported in Figure 4B, the NTA revealed a higher total particle concentration in fraction 1 that decreased in later fractions, reaching values under 10^10 particles/mL from fraction 5 to 8. NTA analysis performed on fraction 1, showed two intensity peaks for particles with a diameter of 150-200 nm and one at 250 nm. In addition, when compared to other NTA graphs, the values

are shifted towards larger particle size (Fig. 4C for convenience reports only the NTA graph of fraction 1). These evidences could demonstrate the effective presence of large EVs in our sample. Following the western blot analyses, we found enrichment for small EVs, indicated by the positivity for TSG101, only in fraction 1, while no signal was detected in the later fractions (Fig. 4D). This fraction contained the material eluted just after the column void volume, that did not diffuse within the pore of the stationary phase being not retarded. We also detected signal from albumin in all the fractions (Fig. 4E). The results of these investigations seemed to demonstrate that probably large EVs were present in the eluate, however this column was not able to effectively separate vesicles with different size. The second column, having larger pore size, resulted even less effective than the first for our goal (data not shown).

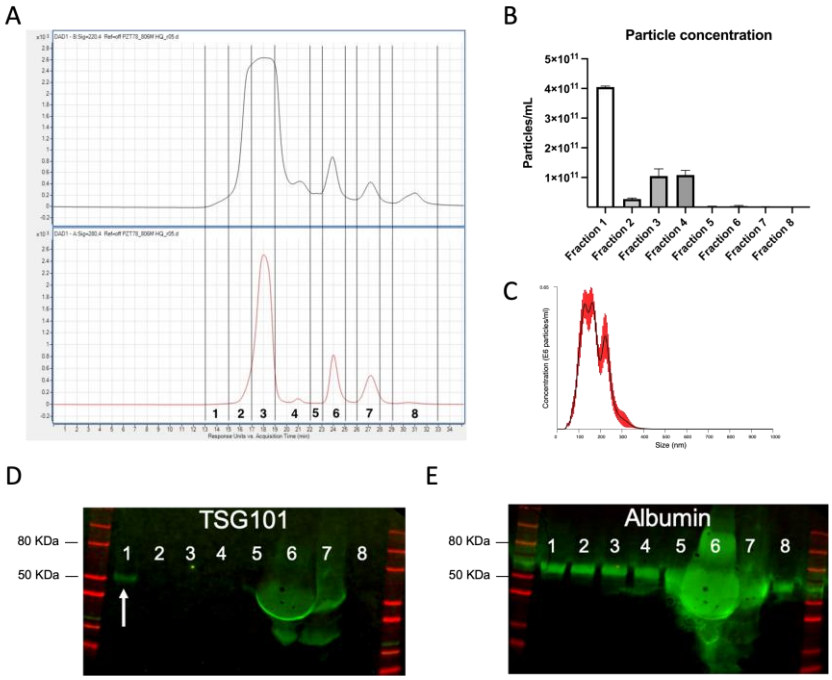

Figure 4. (A) Example of chromatograms obtained from the separation of knee synovial fluid. Signals detected at 220 (top) and 280 (bottom) nm were reported. The vertical lines indicate the fractions collected and characterized. (B) The concentration of the particles in the 8 fractions. Data are reported as mean ± standard deviation.

Discussion

Due to the dimension of EVs, their isolation process is not straightforward, and this process is made even more difficult by the fact that we used synovial fluid as starting material. In fact, Boere and colleagues previously addressed the problem of high concentration of hyaluronic acid in the EV isolation process. The authors, after a comprehensive review of the previous literature, demonstrated that the treatment of the SF with hyaluronidase

increases the efficiency of small size EVs isolation, especially after centrifugation at 100000g, probably due to the lower amount of hyaluronan bound to the EVs[16]. In our work we evaluated the effect of a further decrease of SF viscosity by diluting it with PBS. The aim of this dilution is to impede as much as possible the formation of complexes between the large chains of hyaluronic acid or other extracellular proteins with the EVs, liberating the vesicles and increasing the yield. The outcomes of our optimization analyses supported the hypothesis that the decrease of SF viscosity and a longer centrifugation time are associated with a higher yield of the isolation process. However, the high number of particles in the supernatant after two overnight ultracentrifugations demonstrated that decreasing the viscosity of the sample is not sufficient. In fact, the high protein concentration, together with the presence of large protein aggregates and other contaminants, makes the EV isolation process challenging. First of all, these contaminants can be present in higher concentration than the EVs[13], decreasing the probability of isolating specific EV subpopulations, especially those more rare. In addition, in many biofluids there are also lipoproteins that have a comparable size with the EVs[18]. In a healthy joint the concentration of lipoproteins in the synovial fluid is usually much lower than that in the blood[19]. However, during chronic inflammatory joint diseases, including OA, the

permeability of the synovial membrane is compromised, and proteins and lipids can pass the endothelial barrier entering into the synovial cavity[20]. Therefore, the EVs isolated from SF by means of size-based techniques can be contaminated with lipoproteins. For this reason, an increasing number of experimental approaches are now using complementary techniques that can isolate the EVs according to their density. This approach is based on the fact that the lipoproteins have a different density than EVs and they float differently in a density gradient, so by coupling a size-based technique with a density-based one the samples could result cleaner[21,22]. However, an intriguing discussion recently started in the scientific community. It is focused on the question whether the presence of lipoproteins or proteins on the surface of EVs (the so-called protein corona) should be really considered as a contaminant or not. In fact, physiologically the EVs coexist in the biofluids with proteins and lipoproteins and recent evidence demonstrated that a protein corona is spontaneously formed around EVs in biofluids, and that lipoproteins can associate with the EVs upon in vitro mixing[23,24]. The answer to this question is not simple and probably, as suggested by the International Society for Extracellular Vesicles (ISEV), the grade of "purity" should depend on the aims of the specific project[25]. In our study we didn't aim to perform functional studies, rather our long-term objective consists in the

evaluation of different size EV subpopulations from the SF as potential biomarkers for arthritic diseases. In this case, our opinion is that we could even miss some potential diagnostic hint if we try to get the purest EV preparation, by removing every molecule considered as a contaminant, which can cause also the depletion of the rarest EV subtypes. In fact, the difference between the healthy and the pathologic condition could be not exclusively related to the "pure" EVs but to the concomitant presence of co-eluted proteins or lipoproteins. This is the reason why we chose to compare the conventional techniques without associating other methodologies.

Our results demonstrated that the conventional size-based isolation techniques present different effectiveness when it comes to separate large EVs and to obtain different size subpopulations. Our aim was focused on the isolation of different size EV subpopulations that include also large vesicles as they have been associated, among the other pathophysiological processes, with the inflammatory response[26]. In fact, this subtype of EVs can carry metalloproteinases and can also act as ROS scavengers or can increase the production of ROS by the acceptor cells[27,28]. With differential centrifugation we were effectively able to isolate two subpopulations of EVs with different mean diameter. However, the NTA showed a relatively high percentage of vesicles with a diameter smaller than 200 nm also in the 10K pellet. So, to have a

preparation more enriched in large EVs we should probably add another centrifugation step at lower rate. For example, Kowal and colleagues performed a further centrifugation step at 2000g to isolate and characterize larger EVs, finding some potential new markers of large EVs[17]. However, adding a step means further lengthen the experimental time, increasing the samples that need to be processed and probably, in the case of SF, also the incomplete removal of cellular debris or other larger structures due to the high viscosity. These issues could limit the potential future clinical employment of this approach in a clinical setting for OA diagnosis. Another concern is the high number of particles that were still present in the supernatant after the collection of the second 100K pellet. This is probably due to the high viscosity of the SF that could limit the EV sedimentation process. We speculate that a possible reason is related to the presence, in addition of hyaluronic acid, of other glycosaminoglycans and other very large structural proteins that can create a sort of lattice, preventing the EVs to be pelleted. Mustonen et al. reported that the EVs isolated from the synovial fluid were coated with a layer of hyaluronic acid[29]. This interaction can be facilitated by the presence of CD44, the receptor for the hyaluronic acid, on the surface of the vesicles. The same situation can happen for other extracellular proteins, explaining the relatively low yield of this process. In addition, this approach can lead to the sedimentation

of proteins that may be not usually associated with the EVs inducing the formation of aggregates[22,30]. For these reasons, together with the fact that elevated centrifugation rates can damage the EVs, differential centrifugation cannot be considered as the most promising approach for the systematic isolation of different size EV subpopulations.

The commercial SEC column proved to be very effective in removing the soluble proteins from the EV preparation. This is one of the most important strengths of this technique, especially if compared with differential centrifugation. Different studies in fact reported that SEC allows a better removal of soluble proteins not associated with EVs[31,32]. In addition, the yield of this approach was higher by an order of magnitude if compared with ultracentrifugation. This result was in accordance with the outcomes of Takov et al., that reported a higher number of particles, protein content and EV-specific markers in EVs isolated with SEC than those isolated with ultracentrifugation[33]. In this work the authors isolated EVs from plasma, a complex biofluid characterized by minor viscosity but higher protein concentration than synovial fluid. Despite the total number of the eluted EVs was higher, they were much more diluted than those isolated with centrifugation. In fact, we performed a concentration step using centrifugal filters, that are the most widely used. This step can be deleterious as the impact with the plastic can damage the

EVs, especially the larger ones that can be more fragile than the smaller, that can also clot to the filter[34]. This can be of course relevant if the target are rare EV subpopulations as may be the large ones, determining their further reduction in the number, ultimately making more difficult and less probable their potential detection and the successive characterization. But the most important results for the purpose of our study was the finding that EVs eluted only in fractions 7 to 11. In the previous fractions in fact, we didn't find any EV-specific marker, both for small and for large EVs. We used Mitofilin as marker of large EVs as suggested by Kowal and coworkers[17]. In this work the authors used EVs isolated from culture medium, however another study that evaluated EVs isolated directly from solid tumoral tissue also reported the presence of Mitofilin exclusively in the larger EVs[35]. The lack of this specific marker, together with the presence of classic small-EV markers in the fractions 7 to 11 demonstrated that the commercial SEC column were effective in the isolation of small vesicles with a great removal of soluble proteins non associated with EVs. However, they were not able to separate EVs with diameter larger than 200 nm. We'd like to stress out the term "separation" to highlight that we are not claiming that they were ineffective to isolate those vesicles, but that if they were present, they were not separated from the smaller ones and if so, they were in much lower number, since we didn't detect Mitofilin

signal neither in the fractions 7-11. In our study we used only commercially available columns with the view of a translation towards the clinic. In fact, there are several handmade SEC columns that used principally Sepharose as stationary phase[22], but they are optimized for the isolation of small EVs, and the potential high variability in their preparation could be an obstacle for their transfer to the clinical setting.

The HPLC chromatogram obtained with the column with the smaller pores showed 5 different peaks and, in the attempt to characterize them, we subdivided the eluate in eight different fractions. The NTA showed a higher concentration of particle in fraction 1 that progressively decrease in the later fractions. However, the western blot analysis showed the presence of small size EV marker, TSG101, already in the first fraction, that included the void column of the column, while no signal was detected in other fractions. From the NTA two peaks, one between 150-200 nm and one at around 250 nm were observed. In addition, the size distribution was shifted toward larger particle size, meaning that probably large EVs were present in the eluate but that this column was not able to separate them from the small ones. In addition, being eluted in the void volume of the column, it implied a poor or null interaction between the stationary phase and the EVs, and the second column, with larger pores, was even less suited. The potential of this approach strongly depended on

the choice of the column. In fact, several studies previously employed HPLC for the isolation of EVs, but they were focused mainly on the isolation of the small ones. In particular, Foers and colleagues used this approach on SF sample after the centrifugation at 10000g, so after the depletion of the larger EVs[36]. The column that they used was specifically produced for the separation of large biomolecules and viruses, that generally have dimensions comparable to those of the sEVs[37]. As expected, the authors found EVs with a maximum diameter of about 200 nm. This result was in accordance with the NTA of the fraction 1 in our samples, even if in our case we detected signal from particles up to 300 nm, probably because we didn't centrifuge the sample before the separation. From the comparison of the two works, we can speculate that a separation of different size EV subpopulations from the SF with HPLC could be possible, but it would probably need more than one column connected in series and a huge amount of time and work for the development and the optimization of the protocol. Our western blot analysis indicated that albumin co-eluted with EVs in the fractions. However, as previously stated, this could be an intrinsic feature when the EVs are isolated from biofluids. In fact, it has been reported that the majority of small size EVs isolated with different SEC columns from the blood plasma co-eluted with albumin[32]. Taken together these outcomes demonstrated that, even if the

authors of this study performed gravity chromatography, we cannot easily get rid of all the soluble proteins, as suggested elsewhere[23]. Especially in presence of proteins with high binding capabilities or those for which EVs have binding receptors. Of course, the concept that some proteins are naturally associated and that can co-elute with EVs should not always be applied, but it strongly depends on the specific aim of the study and should be considered case by case.

Conclusions

In conclusion, this work demonstrated that three conventional techniques that can separate EVs based on their different size are characterized by a different effectiveness. Differential centrifugation showed the potentiality to obtain different size subpopulations. In addition, the EV preparations have an adequate concentration, facilitating the successive analyses. However, this technique is also characterized by low yield and purity and with high processing time, especially if the aim is the isolation of more subpopulations, that could limit the potential translation of this technique to the clinical setting. The gravity-SEC in our opinion showed the lowest capability of separate the EVs in different size subpopulation. Despite the higher yield and removal of proteins non associated with the EVs, the commercial columns seemed to be optimized for the isolation of small size

EVs. In addition, it's unlikely to obtain an improvement of these results as it is not possible to control the flow rate and the low number of different resins available for their stationary phase. Finally, the HPLC can theoretically be considered a potential approach, as it is already largely used in the diagnostic field. However, due to the very broad size range characterizing the EVs, it still needs an accurate and long optimization process, during which several SEC columns should be compared and, most likely, more of them should be connected in series to reach satisfactory results. To conclude, there are currently no methodologies available that allow the separation of different size EV subpopulations, so further optimization of the conventional techniques or the development of new approaches are still needed in this field.

Supplementary materials

Group compared	P value
1000g vs 3000g	0,6589
1000g vs 5000g	0,1108
3000g vs 5000g	0,3111

Table S1. P-values obtained with ANOVA statistic test for the particle mean diameter.

Group compared	P value
1000g vs 3000g	0,8182

1000g vs 5000g	0,2234
3000g vs 5000g	0,4949

Table S2. P-values obtained with ANOVA statistic test for the d90.

References

1. Willms, E., Cabañas, C., Mäger, I., Wood, M. J. A. & Vader, P. Extracellular Vesicle Heterogeneity: Subpopulations, Isolation Techniques, and Diverse Functions in Cancer Progression. Front. Immunol. 9, 738 (2018).
2. CHARGAFF, E. & WEST, R. The biological significance of the thromboplastic protein of blood. J. Biol. Chem. (1946). doi:10.1016/s0021-9258(17)34997-9
3. Raposo, G. G. & Stoorvogel, W. Extracellular vesicles: Exosomes, microvesicles, and friends. J. Cell Biol. 200, 373–383 (2013).
4. Barile, L. & Vassalli, G. Exosomes: Therapy delivery tools and biomarkers of diseases. Pharmacol. Ther. 174, 63–78 (2017).
5. Murphy, C. et al. Emerging role of extracellular vesicles in musculoskeletal diseases. Mol. Aspects Med. 60, 123–128 (2018).
6. Armstrong, D. & Wildman, D. E. Extracellular Vesicles and the Promise of Continuous Liquid Biopsies. J. Pathol. Transl. Med. 52, 1–8 (2018).
7. Foers, A. D., Cheng, L., Hill, A. F., Wicks, I. P. & Pang, K. C. Review: Extracellular Vesicles in Joint Inflammation. Arthritis Rheumatol. (Hoboken, N.J.) 69, 1350–1362 (2017).
8. Gao, K. et al. Association between cytokines and exosomes in synovial fluid of individuals with knee osteoarthritis. Mod. Rheumatol. 30, 758–764 (2020).
9. Jeon, O. H. et al. Senescence cell-associated extracellular vesicles serve as osteoarthritis disease and therapeutic markers. JCI insight 4, (2019).
10. Kolhe, R. et al. Gender-specific differential expression of exosomal miRNA in synovial fluid of patients with osteoarthritis. Sci. Rep. 7, 1–14 (2017).
11. György, B. et al. Membrane vesicles, current state-of-the-art: emerging role of extracellular vesicles. Cell. Mol. Life Sci. 68, 2667–2688 (2011).
12. Lässer, C., Jang, S. C. & Lötvall, J. Subpopulations of extracellular vesicles and their therapeutic potential. Mol. Aspects Med. 60, 1–14 (2018).
13. Li, J., He, X., Deng, Y. & Yang, C. An Update on Isolation Methods for Proteomic Studies of Extracellular Vesicles in Biofluids. Molecules 24, (2019).
14. Liangsupree, T., Multia, E. & Riekkola, M.-L. Modern isolation and separation techniques for extracellular vesicles. J. Chromatogr. A 1636, 461773 (2021).

15. Doyle, L. & Wang, M. Overview of Extracellular Vesicles, Their Origin, Composition, Purpose, and Methods for Exosome Isolation and Analysis. Cells 8, 727 (2019).
16. Boere, J. et al. Synovial fluid pretreatment with hyaluronidase facilitates isolation of CD44+ extracellular vesicles. J. Extracell. Vesicles (2016). doi:10.3402/jev.v5.31751
17. Kowal, J. et al. Proteomic comparison defines novel markers to characterize heterogeneous populations of extracellular vesicle subtypes. Proc. Natl. Acad. Sci. U. S. A. (2016). doi:10.1073/pnas.1521230113
18. Johnstone, B. et al. Tissue engineering for articular cartilage repair - The state of the art. Eur. Cells Mater. (2012).
19. Makkar, R., Behl, T., Kumar, A., Uddin, M. S. & Bungau, S. Untying the correlation between apolipoproteins and rheumatoid arthritis. Inflamm. Res. Off. J. Eur. Histamine Res. Soc. ... [et al.] 70, 19–28 (2021).
20. Oliviero, F. et al. A comparative study of serum and synovial fluid lipoprotein levels in patients with various arthritides. Clin. Chim. Acta. 413, 303–307 (2012).
21. Karimi, N. et al. Detailed analysis of the plasma extracellular vesicle proteome after separation from lipoproteins. Cell. Mol. Life Sci. (2018). doi:10.1007/s00018-018-2773-4
22. Monguió-Tortajada, M., Gálvez-Montón, C., Bayes-Genis, A., Roura, S. & Borràs, F. E. Extracellular vesicle isolation methods: rising impact of size-exclusion chromatography. Cellular and Molecular Life Sciences (2019). doi:10.1007/s00018-019-03071-y
23. Tóth, E. Á. et al. Formation of a protein corona on the surface of extracellular vesicles in blood plasma. J. Extracell. vesicles 10, e12140 (2021).
24. Sódar, B. W. et al. Low-density lipoprotein mimics blood plasma-derived exosomes and microvesicles during isolation and detection. Sci. Rep. 6, 24316 (2016).
25. Théry, C. et al. Minimal information for studies of extracellular vesicles 2018 (MISEV2018): a position statement of the International Society for Extracellular Vesicles and update of the MISEV2014 guidelines. J. Extracell. Vesicles 7, 1535750 (2018).

26. Słomka, A., Urban, S. K., Lukacs-Kornek, V., Żekanowska, E. & Kornek, M. Large Extracellular Vesicles: Have We Found the Holy Grail of Inflammation? Front. Immunol. 9, 2723 (2018).
27. Dolo, V. et al. Matrix-degrading proteinases are shed in membrane vesicles by ovarian cancer cells in vivo and in vitro. Clin. Exp. Metastasis 17, 131–140 (1999).
28. Bodega, G., Alique, M., Puebla, L., Carracedo, J. & Ramírez, R. M. Microvesicles: ROS scavengers and ROS producers. J. Extracell. vesicles 8, 1626654 (2019).

29. Mustonen, A.-M. et al. Characterization of hyaluronan-coated extracellular vesicles in synovial fluid of patients with osteoarthritis and rheumatoid arthritis. BMC Musculoskelet. Disord. 22, 247 (2021).
30. Linares, R., Tan, S., Gounou, C., Arraud, N. & Brisson, A. R. High-speed centrifugation induces aggregation of extracellular vesicles. J. Extracell. vesicles 4, 29509 (2015).
31. An, M., Wu, J., Zhu, J. & Lubman, D. M. Comparison of an Optimized Ultracentrifugation Method versus Size-Exclusion Chromatography for Isolation of Exosomes from Human Serum. J. Proteome Res. 17, 3599–3605 (2018).
32. Baranyai, T. et al. Isolation of Exosomes from Blood Plasma: Qualitative and Quantitative Comparison of Ultracentrifugation and Size Exclusion Chromatography Methods. PLoS One 10, e0145686 (2015).
33. Takov, K., Yellon, D. M. & Davidson, S. M. Comparison of small extracellular vesicles isolated from plasma by ultracentrifugation or size-exclusion chromatography: yield, purity and functional potential. J. Extracell. Vesicles (2019). doi:10.1080/20013078.2018.1560809
34. Wallace, S. J., Li, J., Nation, R. L. & Boyd, B. J. Drug release from nanomedicines: Selection of appropriate encapsulation and release methodology. Drug Deliv. Transl. Res. 2, 284–292 (2012).
35. Crescitelli, R. et al. Subpopulations of extracellular vesicles from human metastatic melanoma tissue identified by quantitative proteomics after optimized isolation. J. Extracell. Vesicles 9, 1722433 (2020).
36. Foers, A. D. et al. Enrichment of extracellular vesicles from human synovial fluid using size exclusion chromatography. J. Extracell. vesicles 7, 1490145 (2018).
37. Nolte-'t Hoen, E., Cremer, T., Gallo, R. C. & Margolis, L. B. Extracellular vesicles and viruses: Are they close relatives? Proc. Natl. Acad. Sci. 113, 9155 LP – 9161 (2016).

Chapter 3

Development of a protocol based on asymmetrical flow field-flow fractionation to isolate EV subpopulations from the nanoscale to the microscale

Development of a protocol based on asymmetrical flow field-flow fractionation to isolate EV subpopulations from the nanoscale to the microscale

D'Arrigo D.[1,2], Gennari A.[3], Arrigoni C.[1], Delcogliano M.[4], Vanoni M.[2,5], Candrian C.[4,6], Tirelli N.[3], Moretti M.[1,6,7]

1 - Regenerative Medicine Technologies Lab, Service of Orthopaedics and Traumatology, Department of Surgery, EOC, via Federico Chiesa 5, 6500 Bellinzona, Switzerland (CH)

2 - Department of Biotechnology and Bioscience, Università degli studi di Milano-Bicocca, 20126 Milan (IT)

3 - Laboratory of Polymers Biomaterials, Istituto Italiano di Tecnologia, Via Morego 30, 16163 Genoa, Italy (IT)

4 - Service of Orthopaedics and Traumatology, Department of Surgery, EOC, Via Tesserete 46, 6900 Lugano, Switzerland (CH)

5 - ISBE/SYSBIO Centre of Systems Biology, Milan, Italy (IT)

6 - Euler Institute, Biomedical Sciences Faculty, Università della Svizzera Italiana (USI), via Buffi 13, 6900 Lugano, Switzerland (CH)

7 - Cell and Tissue Engineering Laboratory, IRCCS Istituto Ortopedico Galeazzi, Via Riccardo Galeazzi 4, 20161 Milan, Italy (IT)

Status: manuscript in preparation for publication on Journal of Extracellular Vesicles (I.F. 25.8)

Abstract

Introduction

As we previously showed, conventional methods employed and optimized for the isolation of small size extracellular vesicles (EVs) are not applicable to the isolation of the whole spectrum of EVs sizes from synovial fluid (SF). Aiming at developing a new protocol to isolate and separate the entire range of EV subpopulations with different size from SF, we evaluated the use of asymmetrical flow field flow fractionation (AF4), an innovative technique based on microfluidics.

Methods

We collected SF from the shoulder of donors underwent biceps long head tenotomy and from the knee of end-stage arthritic patients underwent joint replacement. We setup and optimized a separation protocol based on asymmetrical flow field flow fractionation (AF4), testing its effectiveness in isolating and separating different-sized EV subpopulations. After EVs isolation and separation, we thoroughly characterized the EVs belonging to each subpopulation. We assessed different features related to each subpopulation (EV profile, relative abundance and average

size) and to EVs belonging to them (Z potential, protein and nucleic acid concentration, morphology, and protein content). We also evaluate the effectiveness of this approach in other biofluids, such as plasma and culture medium.

Results

With AF4 we were able to isolate EVs from the nanoscale to the microscale, with radius ranging from 30 up to 700 nm and with the classic morphology. We found difference in the Z potential and the protein concentration between the four subpopulations, but not in the nucleic acid content. This protocol also proved to be consistent in separating EVs from different biofluids and it allowed the obtainment the whole EV profile and the relative subpopulation abundance, that differed based on the starting material.

Conclusions

The AF4 based protocol proved to be able to separate EVs within a broad size range, even effective in different biofluids. This could be useful for future studies aiming to isolate different-sized EV subpopulations from complex biofluids like SF.

Keywords: Extracellular vesicles, EV subpopulations, asymmetrical flow-field flow fractionation, synovial fluid, liquid biopsies, diagnosis

Introduction

In the last years, the potential use of extracellular vesicles (EVs) in the diagnostic field has been supported by an increasing number of experimental evidence [1]. This hypothesis lays on the fact that the biological content of the EVs reflects the metabolic state of the origin cell and that EVs are almost ubiquitously present, and stable, in all the tissues and the biofluids of the body [2]. The biofluids represent an intriguing source of EVs in the diagnostic field as they can be collected by liquid biopsies, simple and minimally invasive procedures. The goal of this research field is the isolation of the EVs from specific biofluids to diagnose, classify and monitor the progression of the disease [3]. However, the isolation of the EVs from the biofluids is not a straightforward process for at least two reasons. The first one is the general complexity of the sample, in terms of protein concentration, viscosity and the presence of other biological structures such as lipoproteins. The second reason is related to the heterogeneity that characterizes the EV preparations. Contrarily to the classical view, it is now evident that EVs consist in heterogeneous subpopulations and that their diagnostic potential, as well as the therapeutic potential, could be ascribed to specific subtypes [4]. Focusing on the different size EV subpopulations, most of the studies in literature were focused on small size EVs, classically called as exosomes. However, an increasing number of

experimental evidences have demonstrated that larger EV, with dimension up to more than 1 μm, do exist and that have important biological roles [5]. Most of the evidence in this regard came from the EVs involved in tumoral diseases, but recent studies demonstrated that large EVs play an important role also in the inflammatory response, a key process also in the progression of osteoarthritis (OA) [6], [7]. In the joint diseases as OA, the synovial fluid (SF) represents the biofluid from which it is possible to isolate these different size EVs that could allow the diagnosis of OA and other articular diseases [8]. However, as we previously showed, the conventional methods (ultracentrifugation and size exclusion chromatography) that allow the separation of the EVs according to their size, are optimized for the isolation of the small ones and they are still not applicable for the separation of the whole spectrum of EVs sizes from the SF. In this scenario, the asymmetrical flow field-flow fractionation (AF4) gained importance in the EV isolation process, as it is characterized by an efficient removal of soluble proteins and a high resolution in a very broad size range [9], [10]. In this technique, the particles are fractionated according to their diffusion coefficient, that is related to their size [11]. For instance, in two recent studies the authors fractionated subpopulations of small size EVs with a difference in their diameter of few dozen nanometers [12], [13]. However, the perpendicular flow that

characterizes this technique can be finely modulated, making AF4 able to separate analytes with a broad size range maintaining a high resolution. It has been reported that this technique is capable to separate analytes from 1 nm up to dozens of μm [14], making it attractive for the separation of the whole spectrum of EVs sizes from biofluids including the synovial fluid. But despite this fractionation potential, as far as we know this techniques has been employed only to separate EVs with a maximum diameter of about few hundreds nanometers [9], [15]–[22].

With this work we aim to develop a new protocol based on the AF4 to isolate and separate different-sized EV subpopulations from the SF and other biofluids. Once separated, we will characterize the EVs belonging to different subpopulations to look for potential differences between them. This separation protocol could be important for future studies of the different-size EV subpopulations from the biofluids. In addition, eventual differences between the EV subpopulations could shed light on their pathophysiological role in OA, providing useful indication about their potential role as innovative biomarkers for the OA.

Material and methods

Biological sample donors

All the human-derived biological specimens used in this study and the sampling techniques were performed in accordance with

the respective guidelines and the regulations of the Ente Ospedaliero Cantonale and were approved by the ethical committee (approval n. 2020-00029) of the Regional Hospital of Lugano (Switzerland). Human synovial fluid used for the development of the separation protocol was collected from the shoulders of 3 donors (males; average age: 57 ± 4.4 years) underwent tenotomy of the long head of the biceps. Knee synovial fluid derived from the knee of three end-stage arthritic patients (2 males, 1 female; average age: 65.7 ± 19.6 years) after total knee arthroplasty. During the optimization phase, aliquots of SF from shoulders and from knees of other donors underwent same clinical procedures were used. Primary synovial fibroblasts were isolated from the synovial membranes of 4 arthritic patients (2 males, 2 females; average age: 61,8 ± 7,6 years) underwent the total knee replacement. All these surgical procedures were performed at the Traumatology and Orthopedic Unit of the Regional Hospital of Lugano. The plasma was obtained at the blood transfusion service of the Regional Hospital of Lugano from a 67-year-old male donor. All the biological material was collected upon the acceptance of the informed consent by the donors. The detailed information of the donors are summarized in Table 1.

Group	Source	Donors	Age (years)	Pathological conditions	Pre-treatment
Shoulder	Synovial fluid	3 males	57 ± 4,4	Biceps long head tenotomy	Hyaluronidase digestion + centrifugation
Knee	Synovial fluid	2 males, 1 female	65,7 ± 19,6	Osteoarthritis	Hyaluronidase digestion + centrifugation
Plasma	Peripheric blood	1 male	67	Healthy	CPD anticoagulant + centrifugation
Culture medium	Supernatant of pooled primary synovial fibroblasts	2 males, 2 female	61,8 ± 7,6	Arthritic synovial membrane	Centrifugation

Table 1. Information about the donors from which we collected the biofluids for our work. CPD = Citrate phosphate dextrose.

Plasma obtainment

Peripheral blood of was collected from the cubital vein of a healthy donor using CompoFlow kit with CPD (Citrate phosphate dextrose) anticoagulant (Fresenius Kabi, Sweden). Blood was kept at room temperature and was processed within 3h after collection by a double centrifugation at 2500g at RT for 15 minutes avoiding the activation of the centrifuge brake, following the recommendation of the International Society on Thrombosis and Haemostasis for the obtainment of platelet-free plasma (PFP) [23]. The plasma was then aliquoted and stored at -80°C until used for EV isolation.

Primary cell isolation and supernatant collection

The synovial membranes collected from the knee of four arthritic donors were first mechanically cut into small pieces (~ 2 x 2 x 1 mm) and then digested with Collagenase type I (Worthington Biochemical Corporation, Lakewood, USA) at a concentration of

2.5 mg/mL in complete culture medium (CM). The CM consisted in Dulbecco's modified Eagle medium (Gibco, ThermoFisher, Waltham, USA), 10% fetal bovine serum (FBS, Gibco), 2 mM L-glutamine, 100 U ml−1 penicillin, 100 μg ml−1 streptomycin, 10 mM 4-(2-hydroxyethyl)-1-piperazineethanesulfonic acid (HEPES), 1 mM sodium pyruvate (all from Gibco). The digestion step was performed in an orbital shaker at 37°C for 3 hours at 110 rpm. The collagenase was inactivated by the addition of the same volume of CM and the solution was filtered using a 100 μm cell strainer. The cells were resuspended in fresh CM, plated at a density of 5000 cells/cm2 and cultured until passage 2 and then they were frozen and stored at -150°C. The synovial fibroblasts isolated from the four donors were thawed and plated and when confluent the same number of cells from each donor was pooled together and cultured until passage 4. When the cells reached nearly 70% of confluence, the CM was removed, the cells were washed several times with PBS to completely remove CM and cultured for further 48 days with serum-free CM. The supernatant was finally harvested, centrifuged at 380g for 5 minutes, aliquoted and harvested at -80°C.

Development of an EV separation protocol based on AF4

According to the results of the pre-treatment optimization, reported in the previous chapter, the SF was centrifuged at 3000g immediately after the arrival in the laboratory and aliquoted

before being stored at -80°C. When needed, SF aliquots were thawed at RT, digested with hyaluronidase and centrifuged, as previously described. The plasma and the culture medium were thawed at RT without any additional treatment. The separation of different size EV subpopulations was performed with asymmetric flow field-flow fractionation (AF4) using an AF2000 TM system (Postnova Analytics, Landsberg, Germany), equipped with in-line UV−vis detector at 280 nm (Shimadzu, Kyoto, Japan), a fluorescent detector (Shimadzu) and a PN3609 multiangle static light scattering (MALS) detector (Postnova Analytics, Landsberg, Germany) in the given order. The separation chamber had spacer of a 350 μm and a membrane of regenerated cellulose with a molecular weight cut off of 10 kDa as accumulation wall. The eluent used for the separation consisted in 0.1 μm filtered PBS supplemented with 0.02% of sodium azide (Sigma-Aldrich, St. Louis, USA). After an optimization phase (Supplementary Figure 1A), the following separation protocol to separate different size EV subpopulations was established: the detector flow rate was set at 0.5 mL/min and the temperature of the separation channel at 25°C; 100 μL of sample were injected over 5 minutes (injection flow rate: 0.2 mL/min). During the focusing step the initial cross-flow was set at 1.5 mL/min and the focusing flow rate at 1.8 mL/min. For the elution step the cross-flow was kept constant at 1.5 mL/min for 5 minutes and then it was exponentially (exponent

= 0.20) decreased over 30 minutes until reached 0 mL/min. To allow the elution of larger particles, the cross-flow was kept off for further 15 minutes. Finally, the purge valve was opened for a rinse step (30 seconds). Aliquots of 0.5 mL were automatically collected with the fraction collector (PN8050, Postnova Analytics). The data collected by the detectors were analyzed by using the AF2000 software (Postnova Analytics) and fitted with a Random coil model to obtain the distribution of the radius of gyration (Rg). From the software we obtained the raw data related to the light scattering intensity, the average radius of each subpopulation and the cumulative distribution of the Rg. After the development of the protocol, we assessed if the centrifugation rate we chose in the previous chapter actually did not determine the removal of larger EVs. The eluate belonging to each subpopulation was freeze-dried for the subsequent analyses, except for electron microscopy and the assessment of ζ Potential where samples were immediately analyzed after collection.

Surface evaluation markers with AF4

As proof of concept, we evaluated the possibility of assessing the presence of surface protein markers on the EVs belonging to the four subpopulations using the AF4. Briefly, after an optimization phase, 250 μL of knee arthritic SF was added with 20 μL of anti-CD63 antibody (Thermofisher), 50 μL of anti-CD81 (Thermofisher) or 1,5 μL of anti-CD44 (Abcam, Cambridge, UK).

We incubated the specimens overnight at 10°C under stirring and the following morning we performed the AF4 separation as described in the respective paragraph. Once separated, 200 μL of eluate from each subpopulation was loaded in a 96-multiwell and the specific fluorescent was read with the plate reader (Biotek, Winooski, USA). The fluorescence intensity values detected in each subpopulation were normalized against the intensity measured in the P2 peak (see Optimization of the separation protocol section in the Results), as this value corresponds to the unbound antibody. Then, the normalized intensity was expressed as ratio on the protein concentration.

Latex beads separation

To demonstrate the effective ability of the AF4 technique to isolate particles with size ranging from the nano up to the microscale, we separated standards of latex beads with different dimension. We used beads with a declared hydrodynamic radius (Rh) of 30, 62.5, 175, 250 and 500 nm (Sigma Aldrich). To be consistent with the values produced by the AF4 detectors, we reported the value of the Rg instead of the Rh, considering a ratio between Rh and Rg equal to 0.775, as reported to be for a solid sphere [24]. All beads were suspended in in Novachem (0.05% in milliQ water, Postnova) and plain eluent was injected as control. The separation of the bead suspensions was then performed with the optimized AF4 protocol described in the previous paragraph.

The intensity of the light scattering measured with the MALS was standardized used the following formula: $(x\text{-}min_{(x)})/(max_{(x)}\text{-}min_{(x)})$ and then plotted against the elution time. In the previous formula the x indicates each scattering intensity value, $min_{(x)}$ the minimum value and $max_{(x)}$ the maximum value of each separation read by the MALS detector.

Gel Permeation Chromatography (GPC)

We then compared the effectiveness of our AF4 separation protocol to gel permeation chromatography (GPC) since this technique is widely used for the EV isolation and separation according to their size and it is characterized by higher purity and removal of the contaminant proteins than differential centrifugation [11]. A 0.5 mm column was packed to a 30 cm bed height with Sepharose CL-2B (Sigma-Aldrich) and conditioned in water overnight and then in PBS for 3 hours. The GPC was performed using the same pump and detectors previously used for the AF4. PBS was used as the mobile phase, the flow was set at 0,5 mL/min and the temperature in the column compartment was set at 25°C. As for the AF4, 100 μL of both the bead suspension described in the previous paragraph and a synovial fluid sample were injected. The same SF sample was separated using the already described AF4 protocol and the data collected by the MALS detector from the two separation techniques were analyzed and compared using the AF2000 software (Postnova

Analytics) fitting the data with a Random coil model, to obtain the Rg distribution.

Transmission Electron Microscopy (TEM)

For the electron microscopy (EM) analysis, we wanted to preserve as much as possible the structural integrity of larger EVs while concentrating them. For this reason, we preferred a gentler dialysis approach instead of centrifugal-based methods. We transferred 1 mL of each EV subpopulation in floating dialysis membrane with a molecular weight cut-off of 3.5-5 kD (SpectraPor Float-A-Lyzer G2, Repligen, Waltham, USA). The membranes with the samples were immersed in a 200 gr/L solution of Poly(ethylene glycol) 100 (PEG 100, Sigma,) and concentrated overnight at RT under gently stirring. TEM imaging was performed by depositing 10 μL of concentrated EV preparation onto a carbon-coated grid and staining with a solution of uranyl acetate at 1% w/v. The samples were then dried with filter paper and incubated for 10 minutes to remove the liquid in excess. TEM pictures were acquired by means of a FEI (US) Tecnai 12 BioTWIN transmission electron microscope equipped with a Gatan Orius SC1000 CCD camera.

Immune EM

Similarly to the preparation of the samples for the TEM, 1 mL of sEV and mEV subpopulations were concentrated by dialysis as previously described. Then, the concentration of each vesicle

preparation was adjusted to approximatively 0.1 mg/mL with PBS. For the double-immunogold labeling 5 μL of samples suspension were deposited (20 minutes) on carbon film-coated 300 mesh copper grids (Electron Microscopy Sciences) after 60 seconds treatment with plasma cleaner. Specimens were washed twice with 50-μL drops of wash buffer (0.1% BSA in PBS) and incubated on 50-μL drops containing buffer A (1% BSA in PBS) for the control samples or on a solution of 50 μL of both primary antibodies: 25 μL of rabbit anti-ApoB (diluted to 0.5 mg/ml with 1% BSA in PBS) and 25 μL of mouse anti-CD81 (diluted to 0.5 mg/ml with 1% BSA in PBS) for the treated samples. Samples were incubated in a wet chamber for 30 minutes at room temperature. After thoroughly washing, all the samples (negative controls and treated samples) were incubated for 30 minutes on 50-μL drops of a mixture of secondary gold-labeled antibodies, each diluted to 1 mg/mL with buffer A, composed by 25 μL of goat anti-rabbit Ab labelled with gold NPs of 6 nm and goat anti-mouse Ab labelled with gold NPs of 15 nm. Samples were then washed with wash buffer, followed by five washes on water drops. Before TEM observation, negative staining was done on drops of 10 μL of 1% uranyl acetate in water for 60 seconds before grids drying.

ζ Potential

ζ potential was measured at a temperature of 25 °C using a Mobius instrument (Wyatt Technology, Santa Barbara, California) equipped with laser at 532 nm and a scattering angle of 163.5°. Mobility measurements were performed for 5 seconds with 3 V voltage amplitude and 20 Hz electric field frequency. Electrophoretic mobility was converted into ζ potential using the Smoluchowski model.

Protein content quantification

Due to the higher dilution of the samples eluted from the AF4, for the quantification of the protein content we used lyophilized sample obtained from 2 mL of eluate and we employed a high sensitivity BCA assay (QuantiPro BCA Assay Kit, Sigma-Aldrich). We also freeze-dried Bovine Serum Albumin (Sigma-Aldrich) for the standard curve with the same protocol used for EV lyophilization. In this assay we also included the eluate corresponding to the P2 peak of the MALS elugram to assess the concentration of the proteins removed from the EV preparation. Considering the much higher light scattering signal recorded by the MALS detector, this sample was diluted 10 times. The lyophilized samples were resuspended in water and then we added Triton X-100 (Sigma-Aldrich) at a final concentration of 0.75%. The samples were vortexed and then we followed the specifications of the manufacturer for the protein quantification. Through serial dilution of Albumin we obtained the standard

curve and the r^2 for each assay was > 0.99. The absorbance at 562 nm was read with plate reader (Biotek) after 2 hours of incubation at 37°C. Finally, from the standard curve we extrapolated the protein concentration of the samples.

Nucleic acids quantification

We used three different kits containing sensitive and specific fluorescent dyes to quantify the RNA (Quant-it™ RiboGreen RNA Assay Kit), dsDNA (Quant-iT™ PicoGreen™ dsDNA Assay Kit) and ssDNA (Quant-iT™ OliGreen™ ssDNA Assay Kit, all from ThermoFisher Scientific). We resuspended 1 mL of lyophilized sample in TE buffer provided with the kit and followed the manufacturer specifications. We obtained the standard curves by serially diluting the standards contained in the kits and the r^2 for each assay was > 0.98. After the incubation with the respective specific dye, the fluorescence of the samples was read at a 525 nm and the concentration of each nucleic acid species was then calculated using a linear equation from the standard curve.

Statistical analysis

The results presented in this work are shown as mean ± SEM (standard error of mean). Statistical analyses were performed using the software Prism Version 9 GraphPad Software. The statistical difference between the experimental groups was assessed by one-way ANOVA followed by post-hoc Tukey's

multiple tests. The correlations between the different separation were performed using the nonparametric Spearman correlation, assuming a non-Gaussian distribution of the samples and setting a confidence interval of 95%. Statistical significance was defined as p<0,05. In particular: * for p from 0,01 to 0,05; ** p from 0,001 to 0,01; *** p from 0,0001 to 0,001; **** p < 0,0001.

Results

Development and optimization of AF4 separation protocol

Optimization of the separation protocol. First of all, to assess the feasibility of this technique in separating particle within a broad size range we optimized the flows in the instrument. During the optimization phase we found that the small EVs started to elute with a cross-flow of about 0,3 mL/min and that it should be reduced to 0 to allow the elution of large EVs. In fact, with a residual flow rate of 0,1 mL/min we did not detected larger particles. In addition, to obtain a higher separation between soluble proteins and EV preparation it is more important the rate of the cross-flow (1,5 is better than 1 mL/min) than the time (5 or 10 minutes didn't change much the elugram). (data not shown). The final protocol allowed the isolation of particles within a broad size range: the gyration radius ranged from 30 to almost 700 nm (Fig. 1A). The typical results of a fractionation of a SF sample with this protocol are shown in Figure 1A. We collected

different potential EV subpopulations based on the Rg distribution that followed a sigmoidal curve (red dots, on the right Y axis), along the elution time (X axis). The particles could be separately collected by the automated fraction collector and considering the broad size range of the eluted particles, we decided to divide them in four different subpopulations, namely: small-size EVs (sEVs, with Rg < 100 nm), medium-size EVs (mEVs, with Rg comprised among 100 and 250 nm), large-size EVs (lEVs, 250 nm < Rg < 500 nm) and very large-size EVs (vlEVs, with Rg > 500 nm) (Table 2).

Subpopulation	Gyration radius
Small size EVs (sEVS)	< 100 nm
Medium size EVs (mEVS)	100 – 250 nm
Large size EVs (lEVS)	250 – 500 nm
Very large size EVs (vlEVS)	> 500 nm

Table 2. The subpopulation defined in the work and their size limits.

From the curve of the light scattering intensity (blue line in Fig. 1A, on the left Y axis), obtained in real-time from the online MALS detector, it was possible to clearly notice two peaks. The first one (P1) corresponded to the void peak of the separation chamber, while the second one (P2) represented the smallest structures, including proteins or small protein aggregates and very small particles. The light scattering signal progressively diminished and no other evident peaks were detected during the EV separation phase, probably because of the high dilution of the EVs as we used not concentrated synovial fluid. A little increased

of the signal was detected after 40 minutes, when the crossflow dropped to zero.

Polystyrene beads separation. To confirm the effectiveness of this separation protocol, we tried to separate a polystyrene bead mix with defined Rg values. As shown in Figure 1B, in which normalized light scattering values are reported, the five different beads effectively eluted at different times, especially the two smallest ones. In addition, the instrument maintained a high resolution also with larger beads, even if the difference in the elution time was smaller. In fact, it was still possible to separately collect particles with a difference of about 60 nm in their Rg, as the elution time of 135 nm and 193,75 nm differed of about 1 minute, as highlighted in the enlarged section of the graph. Almost no MALS signal was detected from the separation plain eluent separation (Supplementary Fig. 1B).

Confirmation of the SF pre-treatment. Once optimized the flow rates in the instrument, we checked that the centrifugation regimen chosen did not affect the isolation of larger EVs also with the AF4. Two 100 μL aliquots, one centrifuged at 3000g and one not centrifuged, of synovial fluid collected from the same donor were injected and separated with the developed protocol. As shown in Figure 1C, the elugrams of the two samples, reporting the Rg of the eluted particles during the time, were comparable, and after centrifugation we were able to isolate particles with a radius

higher than 700 nm in both of them. This was also confirmed by evaluating the correlation between the Rg of the two samples that showed a linear trend and a Paerson correlation coefficient (Paerson r) equal to 0,98 (Figure 1D). Similarly, also the distribution of the light scattering intensity during the elution time was comparable (Supplementary Fig. 1C). The quantification of the total protein content in each subpopulation further confirmed this result, the values were comparable in all the 4 subpopulations, including large and very large EVs (Figure 1E). All these results demonstrated that the centrifugation regimen chosen for the pre-treatment of the synovial fluid did not cause the precipitation of the largest EVs.

AF4 vs GPC

To further confirm the higher effectiveness of the AF4 over the SEC approach, we performed a separation of the same sample using a GPC column (Fig. 1F) or the AF4 separation chamber (Fig. 1G) employing the same instrumentation, pumps and detectors, used for the AF4 separation. The distribution of the Rg (red dots in both the graphs) confirmed that SEC was not able to effectively separate particles with a radius larger than 100 nm, as they eluted altogether in a very small amount of time. Instead, these large particles eluted from the AF4 for about 10 minutes, allowing their separation in different fractions. In addition, from the graph relative to the differential mass abundance in the AF4, signals

from particles with radius up to 700 nm were detectable. The same graph of the GPC separation showed basically no signal for particles with radius greater than 100 nm. These results confirmed the higher effectiveness of the AF4 approach in isolating EVs within a very broad size range, not possible with the other conventional techniques.

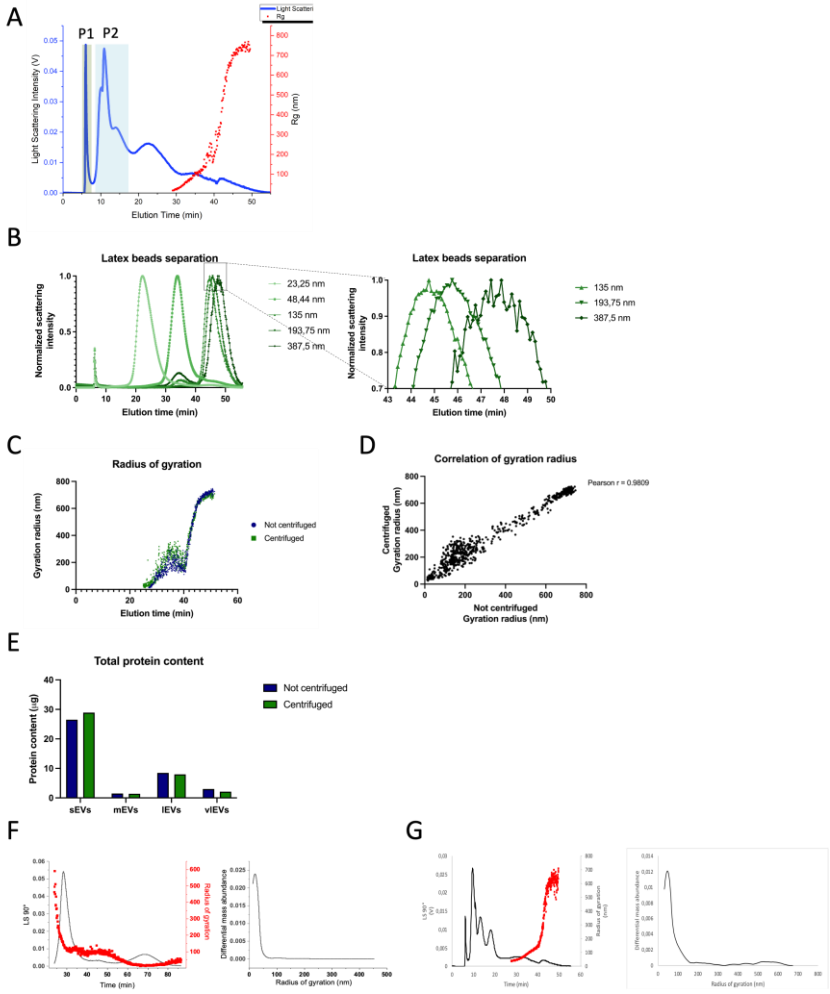

Figure 1. (A) General fractogram obtained with fractionation of synovial fluid sample reporting the light scattering intensity (blue) and the distribution of the Rg during the time (red). P1 indicates the void peak of the separation chamber, P2 the peak due soluble proteins eluted before the EVs. (B) Normalized scattering intensity of polystyrene beads with different nominal Rg and magnification of the peaks of the three largest particles. (C) Distribution of the Rg distribution in centrifuged (green) and not centrifuged (blue) synovial fluid samples. (D) The correlation of the Rg between the two distributions and (E) the total protein content in the four subpopulations demonstrated no difference between them. Comparison between the fractograms and the differential mass abundance distribution obtained by the fractionation of the same SF sample by GPC (F) and AF4 (G).

Effectiveness and reproducibility of the AF4 separation protocol

EV elugram. Thanks to this protocol based on the AF4 technique, we were able to isolate particles with a gyration radius ranging from 30 nm up to about 700 nm. Importantly, this approach proved to be highly reproducible. In fact, as shown in Figure 2A, both the distribution of the Rg and the light scattering signal were comparable in 5 different separations performed on the shoulder synovial fluid from the same donor. We quantified the correlation between the Rg distributions in these separations and reported the data in the correlation matrix in Figure 2B. The results demonstrated a great correlation between the five separations performed on the SF collected from the same donor, with values higher than 0,965. A similar trend was also found when we compared the Rg and light scattering signal distributions obtained from all the 19 separations performed on the SF of all

the three patients (Fig. 2C). The fact that the elution times of particles with similar size were similar in all the separations performed on the SF of the three different donors further demonstrated the effectiveness of this approach. The correlation between the distribution in each of the 19 separations still resulted great, with values higher than 0,94 (Supplementary Fig. 2A).

EV profile. A further strength of this technique is that from the raw data we can plot the light scattering intensity for each value of Rg within the entire size range of the isolated particles, obtaining the distribution that we called EV profile. As shown in Figure 2D, the EV profiles obtained with 5 separations from the SF of the same donors were similar. These profiles confirmed that we were able to isolate particle with a radius ranging from 30 nm to about 700 nm. We also detected two peaks of light scattering intensity, corresponding to particles with radius of about 50 and 100 nm. Particles with a radius up to 200 nm gave smaller signal, that further decreased, while remaining detectable, for the even bigger particles. Similarly to what found for the elugrams, the correlation between the different separation resulted great, with values higher than 0,957 (Fig. 2E). Calculating the average of the profile of all the separations from the three donors we obtained the EV profile of the shoulder synovial fluid (Fig. 2F). It showed the two signal peaks for radii of around 50 and 100 nm and, as

previously described, the scattering signal for particle with a radius higher than 150 nm was lower and further diminished with the progressive increase of the particle size, until reaching 700 nm. Also in this case, the correlation between all the separations performed on the SF of the three different donors was high, with a lower value of 0,9 (Supplementary Fig. 2B).

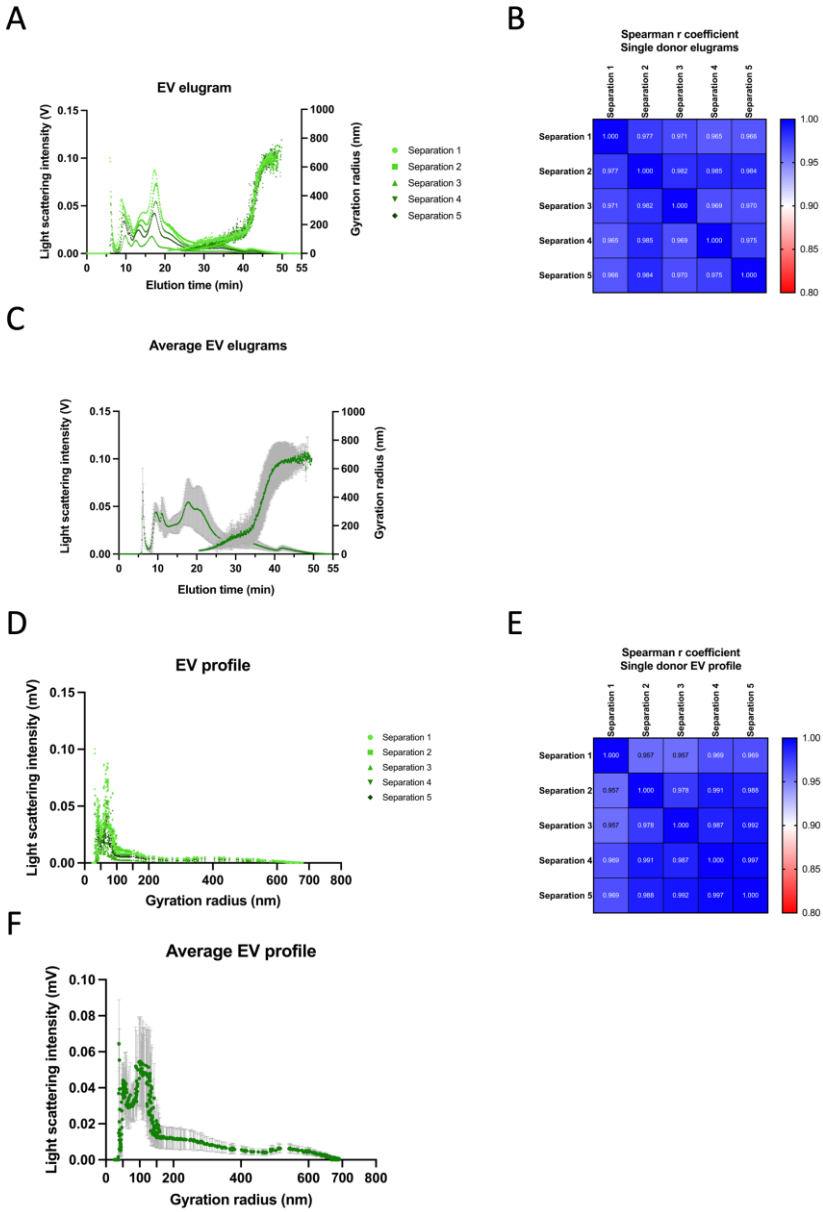

Figure 2. (A) The fractograms obtained from 5 fractionation of the SF collected from the same donor. (B) The correlation of the Rg distribution calculated among these separations. (C) The average distributions obtained from the fractionations of all the samples from the three donors. (D) The EV profile obtained from the same 5 fractionation

from the same donor, their correlation (E) and the average EV profile in the shoulder synovial fluid. Data are reported as mean ± SD.

Transmission and immune electron microscopy analysis

To evaluate the morphology of the particles, we concentrated 1 mL of eluate from each subpopulation to perform transmission electron microscopy (TEM) with negative staining.

Negative staining. Representative images of vesicles across the whole size range revealed different size for the EVs in the four different subpopulations (Fig. 3A). In the sEVs subpopulation we detected almost rounded particles with the classic cup-shape usually ascribed to EVs, with a radius below the 100 nm. We also detected amorphous material and not well-defined round, bright structures in the background that could indicate the presence of contaminants such as protein aggregates or lipoproteins. However, the effectiveness of this technique in removing most of the protein contaminants was confirmed by considering the TEM analysis performed on the P2 peak, in which the proteins were so concentrated that hindered the identification of any other biological structure (Supplementary figure 3). The EVs in the other subpopulations showed a gradually increasing size, maintaining a cup shaped morphology. Even the background resulted clearer of contaminants, indicating a very low concentration of synovial proteins or other structures.

Immune EM. As the EVs have comparable size with some classes of lipoproteins [25], we performed on small and medium EVs immune EM imaging using anti-CD81 and anti-ApoB antibodies to discriminate respectively between EVs and lipoproteins. As reported in Figure 3B, the anti-CD81 antibody (red arrows) detected high contrasted and bright structures against the background. The size of these vesicles was consistent with the previous TEM analysis. On the other hand, lipoproteins (highlighted with yellow arrows) appeared smaller than CD-81 positive EVs and less contrasted against the background. As expected, the classical cup-shaped vesicles resulted always negative for anti-ApoB.

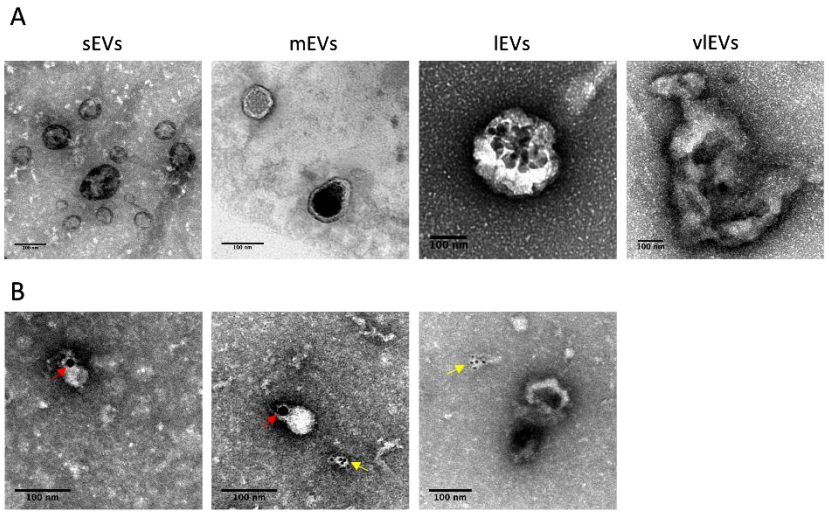

Figure 3. (A) Representative pictures of TEM with negative staining performed in the four subpopulations of EVs from shoulder synovial fluid. (B) Representative images of immune-EM performed on sEVs and mEVs of the same sample. Antibodies anti-CD81

and anti-ApoB were used to specifically detect EVs (red arrows) and lipoproteins (yellow arrows), respectively. Scale bar = 100 nm.

Characterization of the EV subpopulations

Average EV size. To characterize the isolated particles from the SF, we firstly compared the average radius of the EVs belonging to the four subpopulations for all the separations performed (Fig. 4A). The average radius resulted significantly different among each subpopulation compared to the others ($p < 0,0001$ for all the groups), while no difference was detected among the same subpopulation in the three donors. In fact, the intra- and inter-donor variability within each subpopulation was low and the values were comparable.

Relative subpopulation abundance. Another useful tool of the AF4 instrumentation is that it can give the cumulative distribution of the weight fraction. This distribution confirmed that the size of the majority of the particles belonging to each subpopulation was within the established limits (Supplementary Figure 4A). From this distribution we calculated the relative abundance of each subpopulation in the three donors (Fig. 4B, C). The sEVs, with a mean abundance of 65,9% ± 11,3%, resulted to be significantly more abundant compared to the other three subpopulations in all the donors ($p < 0,001$) (Table 3).

Tukey's multiple comparisons test	Summary	Adjusted P Value
sEVs vs. mEVs	****	<0,0001
sEVs vs. lEVs	****	<0,0001
sEVs vs. vlEVs	****	<0,0001
mEVs vs. lEVs	****	<0,0001
mEVs vs. vlEVs	**	0,0084
lEVs vs. vlEVs	*	0,0490

Table 3. Results of the statistical analysis performed on the relative abundance of each subpopulation in the three donors of synovial fluid.

The mEVs percentage (17,8% ± 7,2%) in turn resulted significantly higher than that of the lEVs (5,4% ± 2,4%; $p < 0,0001$) and vlEVS (10,9% ± 4,3%; $p = 0,0084$). The lEVs were the less represented subpopulation, and it significantly differed also from vlEVs ($p = 0,049$).

The results also showed some intra-donor variability. In fact, donor 1 showed lower percentage of sEVs (58,1% ± 8%) compared to donor 2 (74,8% ± 6,3%; $p < 0,0001$) and to donor 3 (69% ± 12,3%; $p = 0,0036$). This trend was reverted in the mEVs subpopulation, more abundant in donor 1 (22,4% ± 5,2%) than in donor 2 (14% ± 4,8; $p = 0,043$) and donor 3 (14,7% ± 8,3%; not statistical different, $p = 0,055$).

ζ *Potential.* The surface charge of particles dispersed in a solution is important to better understand the stability of the system and to have indirect information about their concentration [26]; in addition, the surface charge of EVs is important in different biological processes [27]. For these reasons, we evaluated the ζ

potential of the EVs belonging to each subpopulation isolated from the three donors. As reported in Figure 4D, the EV average values showed high variability and different trends in the four subpopulations. For instance, the ζ potential of the EVs isolated from donor 1 remained almost constant around -7,8 and -9,7 mV in the four subpopulations and no statistical difference was found among these values. In donor 3, the ζ potential decreased with the increasing size of the particles, and we found statistical difference between sEVs (-7,8 ± 1,2 mV) and both lEVs (-14,6 ± 3,5 mV, p = 0,0073) and vlEVs (-15,1 ± 1 mV, p = 0,0037). Similarly, the values of the mEVs (-7,3 ± 3,9 mV) were different when compared to lEVs (p = 0,004) and vlEVs (p = 0,002). Donor 2 showed a completely different trend of the ζ potential, that resulted more positive, showing values from -2,5 mV to -5 mV, compared to the other donors. In fact, we found statistical difference with the other two donors in the lEVs and vlEVs.

Protein concentration. Considered the high dilution of the samples, that prevented us to quantify the particles' number and concentration, we decided to normalize the further analyses on the protein concentration of the samples as suggested by the International Society for Extracellular Vesicles (ISEV) [28]. Hence, we quantified the protein concentration in each subpopulation from the three donors (Fig. 4E). Generally, the values obtained from the three donors within each subpopulation were rather

consistent among them, with the only exception of the concentration in the lEVs of donor 1 that was significantly lower than the others ($p = 0,0005$ with donor 2 and $p = 0,03$ with donor 3). Considering the mean values of the four subpopulations, the sEVs showed significantly higher protein concentration (2,32 ± 0,33 μg/mL) with respect to mEVs (1,86 ± 0,22 μg/mL, $p = 0,023$), lEVs (1,73 ± 0,84 μg/mL, $p = 0,004$) and vlEVs (1,58 ± 0,43 μg/mL, $p = 0,0007$). No significant difference emerged between mEVs, lEVs and vlEVs. Importantly, we found much higher protein concentration in the P2 peak with values between 200 and 600 μg/mL according to the donor, demonstrating the great potential of this technique to remove soluble proteins non associated with EVs (Supplementary Figure 4B).

Nucleic acid quantification. In the four subpopulations from all the three donors we quantified the concentration of three different nucleic acid species, namely single and double strand DNA (ssDNA and dsDNA) and RNA. The data presented in the graphs are normalized by the protein concentration and the specific nucleic acid/protein concentration ratio is reported. The ssDNA resulted the most concentrated nucleic acid, as reported in Figure 4F. Except for the sEVs in the donor 1 that presented a ssDNA/protein ratio higher than the other, all the other values in the 4 subpopulations were similar in all the three patients. Even if not statistical relevant, vlEVs showed a slightly higher values

in all the three patients. The dsDNA/protein ratio was generally lower than that of the ssDNA and the values in all the subpopulations were similar (Fig. 4G). In fact, no statistical difference was observed between the samples. The values of the RNA/protein ratio were instead remarkably smaller with higher variability and no clear difference between the subpopulations (Fig. 4H).

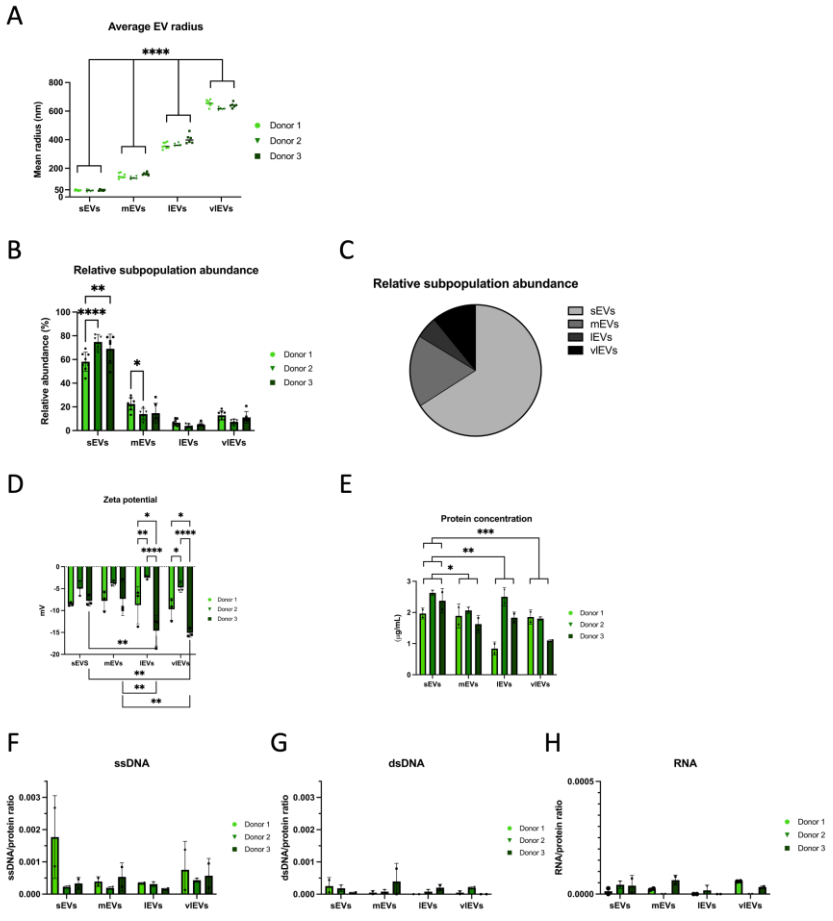

Figure 4. The average values calculated in the four subpopulations calculated in each fractionation of the synovial fluid of the three donors relative to: (A) the average radius values of the EVs; (B, C) the relative subpopulation abundance; (D) ζ potential. (E) The protein concentration evaluated in each subpopulation obtained from the three donors. The ratio between the concentration of ssDNA (F), dsDNA (G) and RNA (H) and the protein concentration. Data are reported as mean ± SD.

Effectiveness of the AF4 separation protocol with other biofluids

To demonstrate the transferability of the new developed protocol, we fractionated EVs also from other biofluids, namely knee SF, plasma and culture medium.

EV elugram. First of all, we obtained the mean elugrams of the fractionation process for all the biofluids. Figure 5A reports the elugrams obtained from these sources in comparison with the one from the shoulder SF (green). The average distribution of the Rg during the elution time obtained from the arthritic SF collected from the knee of three donors (a total of 16 fractionations) resulted exactly superimposable to that of the shoulder. In fact, also from the knee SF (red curve) we isolated particles with radius ranging from 30 nm up to little more than 700 nm, that were separately collected in the same 4 subpopulations. In addition, the particle with the same size eluted at the similar time, consistently with the operating principle of the AF4. On the other hand, the average elugram obtained from the plasma sample (6 total separations), displayed in blue, showed the same trend until minute 40, after which no larger particles were detected by the

MALS. This indicated that no greater particles are contained in the plasma or that they are too rare to be detected. Thus, the size of the eluted objects ranged from 20 nm up to about 160 nm, so they were separately collected in only sEVs and mEVs subpopulations. The same subdivision was done for the particles separated from the culture medium as they resulted the smallest ones, with a maximum size that reached only 150 nm (data collected from 5 fractionations in total).

EV profile. Also the EV profile in the arthritic knee SF was comparable with that of the shoulder (Fig. 5B). It confirmed the same size range of the eluted particle and showed also the same two intensity peaks observed in the EV from the shoulder SF, at around 50 and 100 nm. The trend of the larger vesicles was comparable and from the arthritic knee SF eluted slightly larger particles, with a radius higher than 700. Consistently with the elugram, the profile of the EV from the plasma did not show particles larger than 160 nm and it presented a first intensity peak at higher value of Rg, at about 70 nm, and a second, stronger peak after 100 nm. Differently from the others, only one peak was observed in the culture medium at around 100 nm and it was also characterized by the lowest intensity signal.

Relative subpopulation abundance. The trends observed in the elugrams and in the EV profiles were reflected also in the relative percentage of the EV subpopulations. In fact, the abundance of

the four subpopulations in the three arthritic knee SF was similar to that of the shoulder and we did not detect any statistical difference (Fig. 5C). The percentage of both sEVs and mEVs isolated from knee and shoulder SF was significantly different than that of the plasma ($p < 0,001$). In fact, the sEVs in the plasma counted for only the 4,2%, while the mEVs were almost the majority of the EVs present in the plasma (94,5% ± 7,1%). lEVs and vlEVs represented very rare subset of EVs, in fact they were not detected in all the separations performed. A similar trend was observed in the EV profile of the culture medium, in which the mEVs were more abundant than sEVs (40,5% ± 13,8% vs 59,5% ± 13,7%), even if the difference between was lower. The difference with the other biofluids was confirmed by the statistical analysis that reported difference between sEVs and mEVs from the plasma and from the culture medium ($p < 0,0001$).

Average EV size. The average size of the particles in the sEVs was similar between the four different specimens, with no difference among the biofluids (Fig. 5D). Plasma (57 nm ± 9,3 nm) and culture medium (68,8 nm ± 5,4) showed little higher average diameter than that of the synovial fluid (46,1 nm ± 4,9 in the shoulder-EVs and 46,3 nm ± 4 nm in the knee-EVs). Resembling the previous results, the average radius of the mEVs in the culture medium was lower (114,1 nm ± 3,8 nm), without statistical evidence, compared to that of the other samples, that was

between 142,3 nm of the knee SF and the 158,3 nm of the plasma. Only the SF samples have particles large enough to be included in the lEVs and vlEVs subpopulations whose average radii were similar.

ζ Potential. The ζ potential in general showed a decreasing trend with the increasing size of the particles, but it was also characterized by a high variability (Fig. 5E). In general, the EVs isolated from plasma showed more positive values of this parameter, with -3,2 mV ± 0,9 mV for sEVs and -5,4 mV ± 2,2 mV for mEVs. The values of the SF samples were comparable in all the subpopulations, whilst mEVs in the culture medium resulted slightly more negative than the others (-11,4 mV ± 1,4 mV). However, no statistical difference was detected.

Surface protein markers with AF4. As proof of concept, we assessed the presence of three surface EV protein markers in the knee SF of one single donor using the AF4. We normalized the fluorescent intensity of each subpopulation with the signal detected in the P2 peak, corresponding to the unbound antibody, and we reported the results as ratio on the protein content in each subpopulation or in the P2 peak. The expression of CD81 was detected in all the EV subpopulations, and the strongest signal emerged from the lEVs (CD81). We observed a much lower signal from the CD63, mainly in mEVs and lEVs while in the vlEVs was almost not detected (Fig. 5G). Finally, the signal from the CD44, the

transmembrane receptor of the hyaluronic acid, resulted much stronger in the two largest EV subpopulations, while the lowest ratio was observed in the mEVs (Fig. 5H). Having been obtained from a single donor, the surface marker quantifications represent only trends.

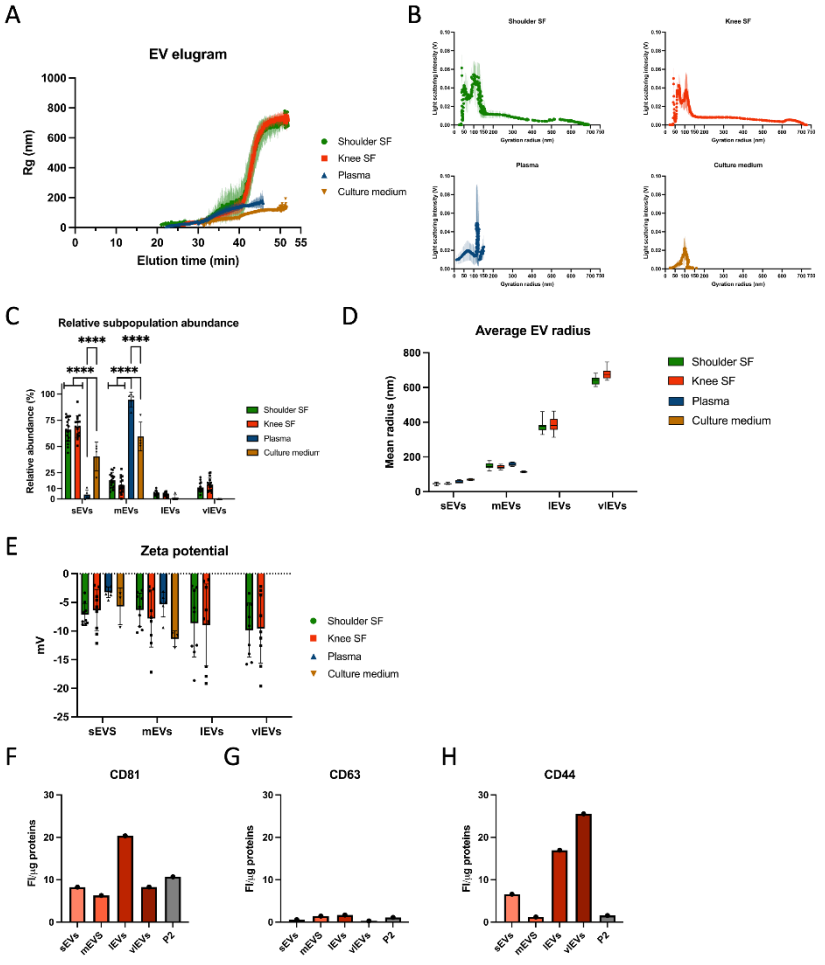

Figure 5. Comparison between different biofluids of the (A) elugrams, (B) EV profile, (C) relative subpopulation abundance, (D) average radius and (E) Zeta potential. As proof of concept, the relative amount of CD81 (F), CD63 (G) and CD44 (H) was

quantified by AF4 and normalized by the signal of the unbound antibody and the protein concentration in each subpopulation or in the P2 peak. Data are reported as mean ± SD.

Electron microscopy analyses

Negative staining. Representative images of the four different EV subpopulations isolated from knee sf, plasma and culture medium are reported in Figure 6A. Generally, the sEVs and mEVs presented the classic cup-shaped morphology in the three groups. In addition, more amorphous material was observed in the samples isolated from the plasma, probably due to the very high protein concentrations of the starting material. Larger, round and highly contrasted structures were also found in the lEVs and vlEVs isolated from the knee SF.

Immune EM. To assess the presence of lipoproteins in the plasma, we performed the same immune-EM staining previously done in the shoulder SF-derived EVs, showing similar results (Fig. 6B). In fact, we found positivity for CD81 in the bright, spherical and highly contrasted particles, while positivity for ApoB was detected in smaller and less contrasted structures. In addition, as potentially expected, we found more particles that could be ascribed to lipoproteins in the plasma than in the SF.

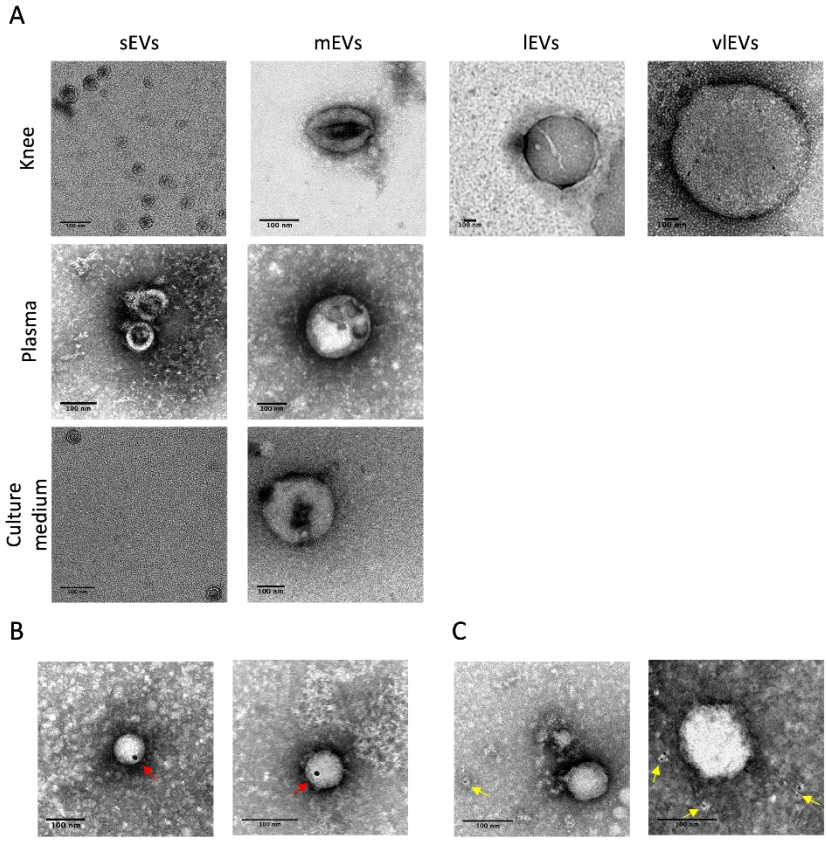

Figure 6. (A) Representative pictures of TEM with negative staining performed in the four subpopulations of EVs from knee synovial fluid and in the sEVs and mEVs of plasma and culture medium. (B, C) Representative images of immune-EM analysis performed on sEVs and mEVs of the plasma sample. Antibodies anti-CD81 (B) to detect EVs (red arrows) and anti-ApoB (C) to mark lipoproteins (yellow arrows) were used. Scale bar = 100 nm.

Discussion

In this study we developed an effective separation protocol to separate EV subpopulations with size ranging from the nanoscale to the microscale from the synovial fluid, that was applicable also

to other biofluids, namely plasma and culture medium. To the best of our knowledge, this is the first protocol capable of separate EVs with size ranging to 50 nm up to 1,4 μm, even among those that were based on the AF4. In fact, previous studies that employed AF4 in the EV field worked with vesicles with a maximum Rg of 300 nm. In some cases, AF4 was used only to evaluate the size and the concentration of the EVs isolated with other approaches, so their size depended on the specific isolation technique used [16], [22]. Other groups employed a modified AF4 approach to isolate or characterize small EVs [17], [19], [21]. This methodology, called frit inlet-AF4, was developed to avoid the focusing time by using the frit inlet. During this step the sample is accumulated on the accumulation wall, and this can cause the potential adsorption and loss of material. However, the resolution of this technique was demonstrated to be lower than the conventional AF4 [29]. Two other studies were expressly focused on the isolation of new subpopulations among the small size EVs, by taking advantage of the high resolution of the instrument. Zhang et al., identified two subpopulations of small size EVs and a new and distinct subset of even smaller EVs called exomeres, with a mean size of ~35 nm [12]. Another EV subpopulation, composed by even smaller EVs called supermere, was successively characterized [13]. Only two studies used the AF4 for the isolation of the EVs, one from plasma [20] and one

from culture medium [18]. Both of them evaluated the effect of different instrument parameters on the fractionation of EVs and demonstrated the potential of this technique in the EV isolation process. In accordance with our findings, Wu et al., reported that a prolonged focusing time can cause loss of sample [20]. On the other hand, the instrumentation setting proposed by Sitar et al. for the obtainment of an optimal EV fractionation was very similar to the flow rates and the times we used in our protocol [18]. However, there were also some differences that can explain the different outcomes of these two papers with our protocol, in terms of the size of the eluted EVs. First of all, Sitar et al. used commercial lyophilized EV preparation, while Wu and colleagues fractionated plasma samples. Another difference lays in the management of the cross-flow during the elution. In fact, in both the protocols it was linearly reduced while we exponentially reduced it. This implied in our case a lower reduction over the time of the flow rate for values below 0,3 mL/min, when the vesicles started to elute, leading to a potential increase of the resolution by enlarging the difference in the elution time of particle with similar Rg. We also found that large EVs were not eluted if the cross-flow wasn't turned off. For this reason, we allowed more time to the largest samples to elute after the cross-flow was turned off. These evidences demonstrated that, as reported also by Sitar et al. [18], the cross-flow is the very

crucial parameter to obtain the best fractionation according to the specific aim of the study. The effectiveness of our protocol was demonstrated by the separation of different beads with different Rg, especially for the lager beads. In fact, particles with radius higher than 135 nm eluted after the cross-flow was turned off with a difference of more than a minute that allowed their separate collection.

The current work is also the first that compared SEC and AF4 using the same instrumentation, changing only the separation chamber. Our results demonstrated that our AF4-based protocol is much more effective in isolating large size EVs, in fact practically all the particles detected with GPC displayed a radius below 100 nm. In addition, AF4 showed the same great capability of the SEC in removing the soluble proteins non associated with the EVs. As demonstrated by the BCA assay, the protein concentration in the P2 peak was hundreds of times greater than that detected in the EV subpopulations (Supplementary Fig. 4), confirming the effectiveness of this approach for the EV isolation from biofluids. Similar results showing a higher relevance of the AF4 in separating analytes and characterizing their size were previously published, even if in these articles AF4 was used for the separation of polymers [30], [31]. Importantly, two studies reported that the MALS detector, online connected with the AF4, is not only suitable in assessing the size of the EVs [16], but it is

also better than NTA, which can overestimate the size of the eluted particles [18]. In addition, our results demonstrated that the AF4 is also characterized by a high reproducibility, as demonstrated by the results of the fractionations performed on SF from the same patients but also from different patients and as already reported in literature [9], [20].

According to the elugram obtained with the MALS detector, we were able to collect four different subpopulations of EVs from the SF, namely sEVs, mEVS, lEVs and vlEVs. A remarkable result is the separation and the characterization of two subpopulations, mEVs and lEVs, that usually are isolated together. In fact, they constitute the so called microvesicles (or microparticle), which have been classified as vesicles with a diameter between 200 and 1000 nm [32]. In addition, an even larger subpopulation, with a diameter greater than 1000 nm, was isolated. As far as we know, this is the first protocol that allow the systematic isolation and these subpopulations of EVs in non-tumoral samples. In fact, in the oncologic research it is well known that large oncosomes, a specific subtype of EVs released by cancer cells, can reach size of ten μm, as recently reviewed [5]. However, In the non-oncologic field, evidences of micrometric vesicles are really rare [33]. Indications about the existence of large size EVs with a size up to several hundreds of nm were already reported, but these vesicles were usually isolated together as a standalone subpopulation.

The main reason is that the differential centrifugation was predominantly used in these studies. For instance, the largest vesicles secreted by neuron and glial cells after traumatic brain injury had a size of 500 nm, assessed by TEM imaging [34]. Baka and colleagues isolated vesicles with a diameter of about 600 nm from blood plasma by means of centrifugation at 16500g [35]. In another paper, vesicles up to 350-400 nm were isolated from the murine blood [36]. These results were similar to the largest size the EVs that we detected in the plasma, that had a diameter of almost 450 nm. The difference between our outcomes ant the results reported by Baka et al. was probably due to the different isolation approaches used. In fact, they used differential centrifugation that, despite a lower resolution, allows the isolation of much more concentrated EV preparations, facilitating the detection of larger EVs, rarer compared with the small ones, by electron microscopy [35]. Large EVs with a maximum dimension of about 500-600 nm were also detected from culture medium, that were all isolated with differential centrifugation [37]–[40]. In this case, the difference with our results was more pronounced as the largest EVs that we isolated from the culture medium showed a maximum size of about 300-350 nm. A possible explanation, that could explain also the difference on the size that we found between culture medium and the other biofluids, could lay in the lower number of vesicles present in the

culture supernatant. In fact, the light scattering signal came from the culture medium and quantified by the MALS detector resulted lower compared to SF and plasma, indicating a potential lower number of vesicles. The detection of larger EVs by MALS and by TEM was therefore more challenging, also because this lower number of particles were much more diluted in the AF4 eluate.

In addition to the elugrams, we also obtained the whole size profile of the EVs contained in a specific sample. For instance, in the EV profile obtained in all the samples from both the SF samples and from plasma we detected two intensity peaks, corresponding to particles with a diameter of about 120-150 and 200-250 nm. Interestingly, these results were in accordance with those of Hurwitz et al., that isolated EVs from solid brain tissue reporting two peaks for particles with a similar size, about 150 nm and 230 nm, despite the different origin tissue and the isolation method [41].

The EV profile could also allow the comparison of the whole EV spectrum in different biofluids. In fact, another interesting outcome of our approach is its transferability to different biofluids, representing a key factor for its potential use in the general diagnostic field and not only for joint disorders. The EV profile proved to be different according to the starting material and it would be interesting to investigate if it changes in the same

biofluid according to the pathological conditions. For instance, several experimental evidences reported that large EVs are involved in different pathological processes, including the inflammatory response that is a crucial factor also in the OA progression [33], [42]. Moreover, a recent paper demonstrated that during sepsis the large EVs changed not only in their content but also in their concentration [43]. If this alteration could be detected in the EV profile of the pathological samples, the investigation could be easier, faster and more reproducible than using other isolation techniques. In fact, our results demonstrated that the elugrams and the profile obtained by several fractionation of the same sample, as well as from specimens collected from different donors, resulted comparable with a low variability. With this view, we tried to develop an analytical protocol characterized by the lowest handling of the samples and without using further isolation or concentration techniques beside AF4.

However, the high dilution of the sample represents one of the major issues related to this methodology, as it makes challenging the successive characterization. In fact, due to the sample dilution, we were not able to perform NTA or similar analyses to quantify the particles in the eluate, usually used to normalize the data. Therefore, we decided to use the protein concentration for the normalization, as envisaged by the International Society for

the Extracellular Vesicles (ISEV) in their guidelines [28]. So, we freeze-dried the EV subpopulations collected from the shoulder SF to enhance their concentration allowing the quantification of the protein and nucleic acid concentration. We were able to quantify the protein concentration, that resulted higher in the sEVs compared to the other three subpopulations. We used similar freeze-dried samples to quantify three different species of nucleic acids, without using any cryoprotectant agents to avoid potential interference with the colorimetric assays. In fact, it has been demonstrated that RNA samples, the most delicate molecule among those tested, maintained their integrity after being lyophilized and stored at room temperature [44]. We found in all the subpopulation from the shoulder SF ssDNA, dsDNA and RNA. In particular, we found higher quantity of ssDNA than dsDNA. This outcome was already reported especially in the large vesicles isolated from tumoral cells and we observed the same trend, even if no statistical difference was detected, of higher ssDNA/protein ration in the vlEVs, with the exclusion of the sEVs of one donor [45], [46]. In addition, the absolute value of the ssDNA and the dsDNA concentration in the sEVs and in the mEVs were not significantly different than the values previously reported, while in the large and vlEVs it was significantly lower, probably because large oncosomes were evaluated in that paper [45]. The RNA was significantly lower than the DNA in our

samples, however the concentration detected was among the linear range of the reference curve and among the suggested detection range [47].

To maintain the structural integrity of the vesicles for the TEM analysis, we chose to concentrate the samples with dialysis because larger EVs, especially if diluted, are more delicate and susceptible to lysis [26]. Dialysis represents a milder approach, especially if compared with centrifugal filter units, that can cause structural damages to the vesicles due to impact and clogging to the filter [48]. Despite higher time for the concentration of the samples, our results showed that larger EVs were maintained almost intact at the TEM. The high dilution of the samples, also after the concentration step, prevented us to perform cryo-TEM analysis that, in our opinion, would have better maintained the size and the morphology of the EVs. The preparation process for the negative staining TEM in fact, can cause artifact and shrinkage of the vesicles up to the 12% [49], [50]. In addition, from TEM images performed on both the SF and the plasma-derived samples, we found EVs that presented a bright rounded structure high contrasted against the background and not the classic cup-shaped morphology. These were undoubtedly EVs as we found positivity for CD81, furthermore similar structures isolated from the synovial fluid were observed also in the work of Rüwald and colleagues [51]. On the contrary, these structures resulted always

negative for ApoB, marker for low- and very-low density lipoproteins (LDL and vLDL) [52], that marked smaller and less contrasted structures. We chose to use ApoB because Ashby and colleagues found higher amounts of this marker co-eluted with small size EVs in comparison with ApoA-I and ApoA-II, markers of high-density lipoproteins (HDL) [53]. These authors performed a fractionation of the serum with AF4 and then they quantified the amount of lipoproteins in different fractions by mass spectrometry. They reported that HDL eluted before the small size EVs, while the LDL and vLDL eluted at similar time than small EVs. In fact, HDL are smaller (7-10 nm) while the LDLs have a similar size than the sEVs that we isolated with our protocol [25]. In fact, we detected ApoB signal in both synovial fluid and, in a higher extent, in plasma samples, as expected. We speculated that some vesicles in our samples could appear brighter because of the presence of a protein layer on the surface of the EVs. In the case of synovial fluid EVs, this hypothesis is corroborated by the presence of CD44, the receptor of hyaluronic acid, as demonstrated by the assessment of the markers with AF4. This is in accordance with different works in literature [54], [55] and the recent evidence that a protein corona can spontaneously forms when EVs are mixed in vitro with protein suspension [56]. In addition, the higher presence of CD44 on the surface of lEVs and vlEVs could resemble a different biogenetic pathway of these

subtypes, maybe linked to the plasma membrane budding-off. These could represent interesting aspects to be elucidated in future investigations.

Conclusions

In conclusion, we developed a protocol based on the AF4 that allow the separation of several EV subpopulations from the nanoscale to the microscale from the synovial fluid, applicable also to other biofluids. With this approach we can also obtain the whole EV size profile, that resulted to be different according to the biofluid. If used as a standalone approach, this methodology represents a promising approach for the diagnostic field, since we can speculate that the whole EV size profile in specific biofluids can be different between physiologic and pathologic conditions. Future efforts need to be performed in this regard to demonstrate the applicability and the translability of this approach towards the clinical practice.

Supplementary materials

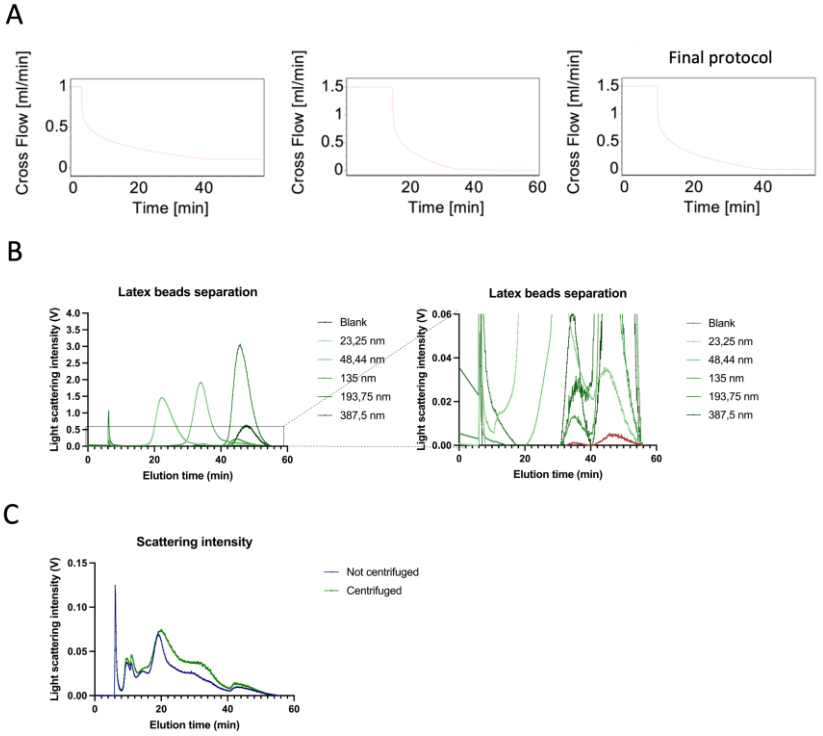

Supplementary Figure 1. (A) Graphs reporting the different cross-flow rates used during the optimization phase. In the left graph, we set a terminal cross-flow of 0,1 mL/min but the larger EVs didn't elute. The increase of the focusing time (central graph) did not improve the results. Augmenting the rate at 1,5 mL/min and the time necessary to turn it off increased the resolution and the capability of eluting large EVs. (B) Non-normalized light scattering intensity for the different polystyrene beads. In the enlarged section, the light scattering intensity of the plain eluent is showed (in red). (C) The similar distribution of the light scattering intensity in the centrifuged sample (green) and in the same sample not centrifuged (blue).

A

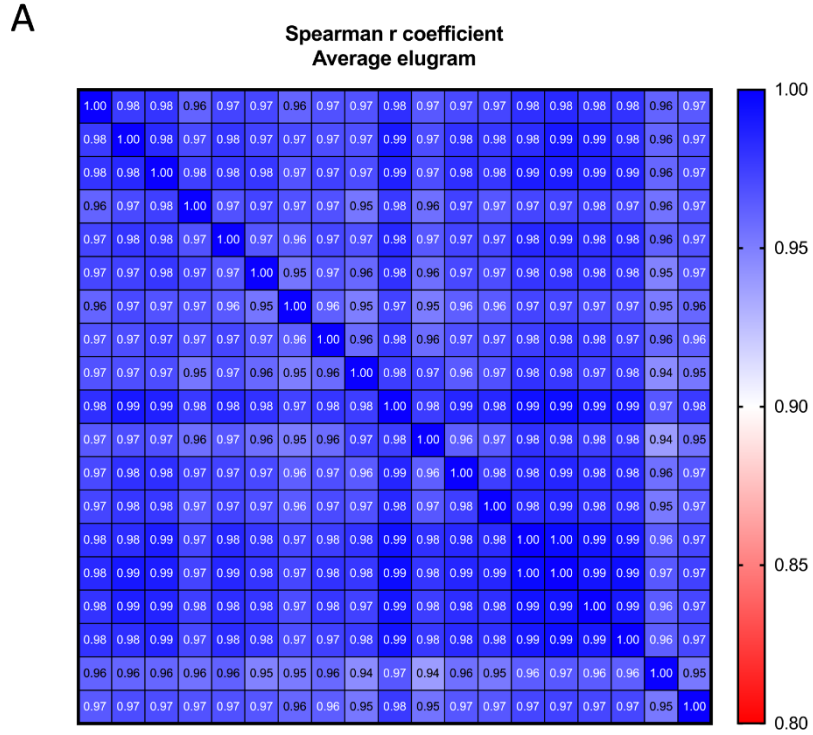
Spearman r coefficient
Average elugram
1.00
0.95
0.90
0.85
0.80

B

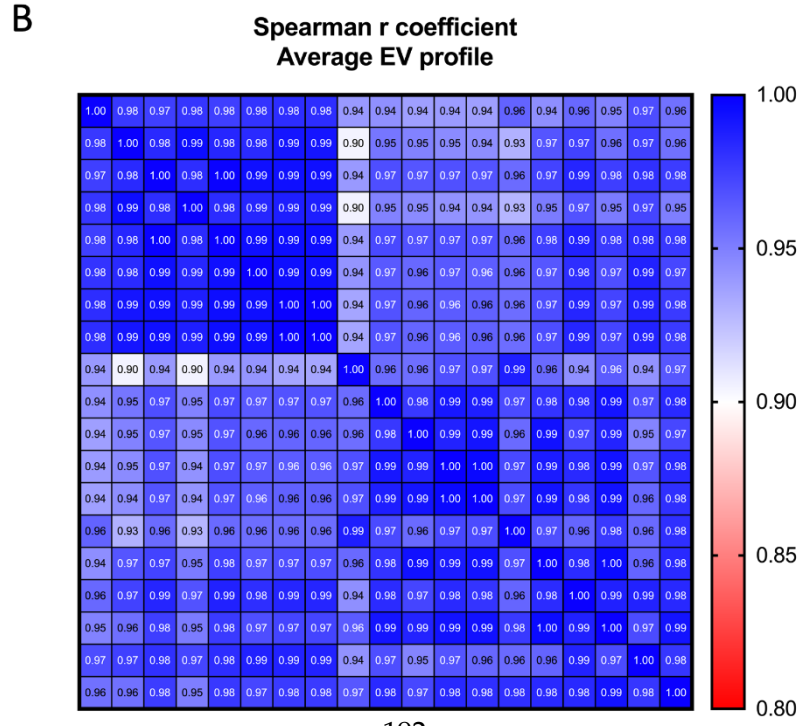
Spearman r coefficient
Average EV profile
1.00
0.95
0.90
0.85
0.80

Supplementary Figure 2. Results of the correlation of the elugrams (A) and the EV profile (B) obtianed in all the fractionation performed from the samples of shoulder synovial obtained from the three different donors.

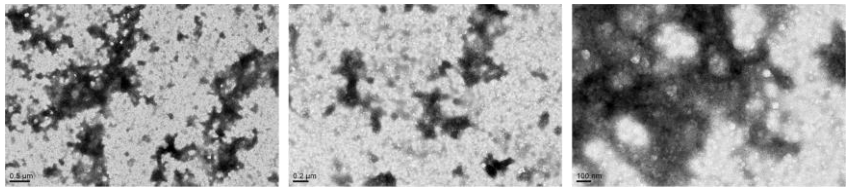

Supplementary Figure 3. Different magnifications of negative staining TEM images performed on digested synovial fluid. No biological structures attributable to EVs were detected due to the high protein concentration.

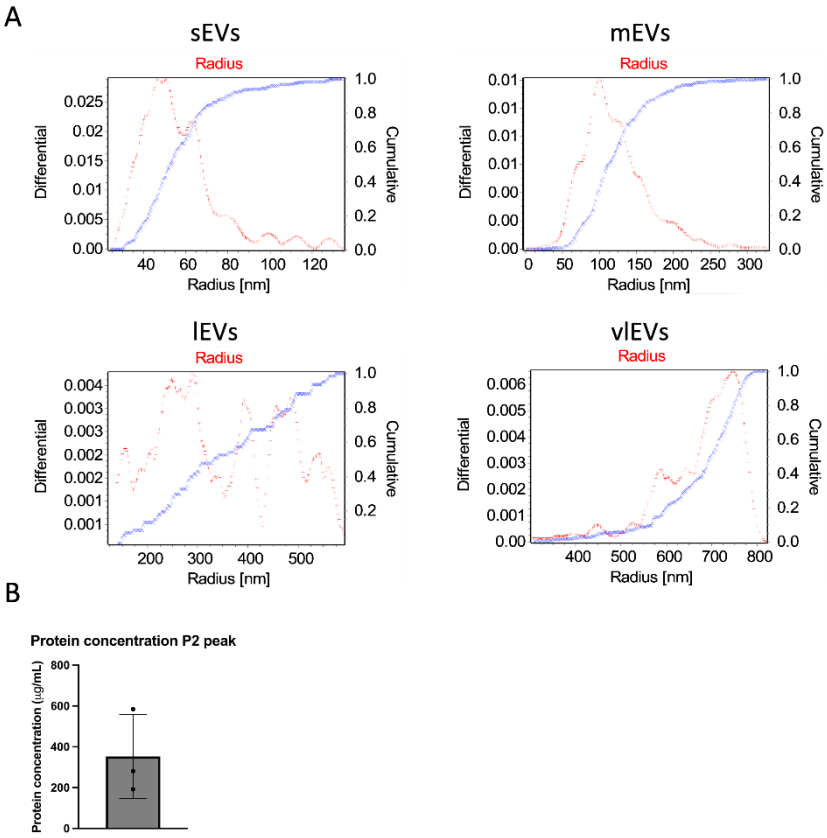

Supplementary Figure 4. (A) The differential (red) and the cumulative (blue) mass abundance distribution of the particles within each of the four subpopulations. (B) Protein concentration in the P2 peaks of the three donors.

References

[1] L. Barile and G. Vassalli, "Exosomes: Therapy delivery tools and biomarkers of diseases," Pharmacol. Ther., vol. 174, pp. 63–78, Jun. 2017.

[2] W. Yu et al., "Exosome-based liquid biopsies in cancer: opportunities and challenges.," Ann. Oncol. Off. J. Eur. Soc. Med. Oncol., vol. 32, no. 4, pp. 466–477, Apr. 2021.

[3] G. Poulet, J. Massias, and V. Taly, "Liquid Biopsy: General Concepts.," Acta Cytol., vol. 63, no. 6, pp. 449–455, 2019.

[4] C. Lässer, S. C. Jang, and J. Lötvall, “Subpopulations of extracellular vesicles and their therapeutic potential,” Mol. Aspects Med., vol. 60, pp. 1–14, 2018.
[5] C. Ciardiello, R. Migliorino, A. Leone, and A. Budillon, “Large extracellular vesicles: Size matters in tumor progression,” Cytokine Growth Factor Rev., vol. 51, pp. 69–74, 2020.
[6] V. Dolo et al., “Matrix-degrading proteinases are shed in membrane vesicles by ovarian cancer cells in vivo and in vitro.,” Clin. Exp. Metastasis, vol. 17, no. 2, pp. 131–140, Mar. 1999.
[7] G. Bodega, M. Alique, L. Puebla, J. Carracedo, and R. M. Ramírez, “Microvesicles: ROS scavengers and ROS producers.,” J. Extracell. vesicles, vol. 8, no. 1, p. 1626654, 2019.
[8] O. H. Jeon et al., “Senescence cell-associated extracellular vesicles serve as osteoarthritis disease and therapeutic markers.,” JCI insight, vol. 4, no. 7, Apr. 2019.
[9] H. Zhang and D. Lyden, “Asymmetric-flow field-flow fractionation technology for exomere and small extracellular vesicle separation and characterization,” Nat. Protoc., 2019.
[10] W. Fraunhofer and G. Winter, “The use of asymmetrical flow field-flow fractionation in pharmaceutics and biopharmaceutics,” European Journal of Pharmaceutics and Biopharmaceutics. 2004.
[11] M. Monguió-Tortajada, C. Gálvez-Montón, A. Bayes-Genis, S. Roura, and F. E. Borràs, “Extracellular vesicle isolation methods: rising impact of size-exclusion chromatography,” Cellular and Molecular Life Sciences. 2019.
[12] H. Zhang et al., “Identification of distinct nanoparticles and subsets of extracellular vesicles by asymmetric flow field-flow fractionation.,” Nat. Cell Biol., vol. 20, no. 3, pp. 332–343, Mar. 2018.
[13] Q. Zhang et al., “Supermeres are functional extracellular nanoparticles replete with disease biomarkers and therapeutic targets.,” Nat. Cell Biol., vol. 23, no. 12, pp. 1240–1254, Dec. 2021.
[14] T. J. Cho and V. A. Hackley, “Fractionation and characterization of gold nanoparticles in aqueous solution: asymmetric-flow field flow fractionation with MALS, DLS, and UV–Vis detection,” Anal. Bioanal. Chem., vol. 398, no. 5, pp. 2003–2018, 2010.
[15] D. Kang, S. Oh, S. M. Ahn, B. H. Lee, and M. H. Moon, “Proteomic analysis of exosomes from human neural stem cells by flow field-flow fractionation and nanoflow liquid chromatography-tandem mass spectrometry,” J. Proteome Res., vol. 7, no. 8, pp. 3475–3480, 2008.
[16] E. Oeyen et al., “Ultrafiltration and size exclusion chromatography combined with asymmetrical-flow field-flow fractionation for the isolation and characterisation of extracellular vesicles from urine,” J. Extracell. Vesicles, vol. 7, no. 1, 2018.

[17] S. Oh, D. Kang, S. M. Ahn, R. J. Simpson, B. H. Lee, and M. H. Moon, "Miniaturized asymmetrical flow field-flow fractionation: Application to biological vesicles," J. Sep. Sci., vol. 30, no. 7, pp. 1082–1087, 2007.
[18] S. Sitar et al., "Size Characterization and Quantification of Exosomes by Asymmetrical-Flow Field-Flow Fractionation," Anal. Chem., vol. 87, no. 18, pp. 9225–9233, 2015.
[19] R. Vogel et al., "Measuring particle concentration of multimodal synthetic reference materials and extracellular vesicles with orthogonal techniques: Who is up to the challenge?," J. Extracell. Vesicles, vol. 10, no. 3, 2021.
[20] B. Wu et al., "Separation and characterization of extracellular vesicles from human plasma by asymmetrical flow field-flow fractionation," Anal. Chim. Acta, vol. 1127, pp. 234–245, 2020.
[21] J. S. Yang, J. C. Lee, S. K. Byeon, K. H. Rha, and M. H. Moon, "Size Dependent Lipidomic Analysis of Urinary Exosomes from Patients with Prostate Cancer by Flow Field-Flow Fractionation and Nanoflow Liquid Chromatography-Tandem Mass Spectrometry," Anal. Chem., vol. 89, no. 4, pp. 2488–2496, 2017.
[22] K. Agarwal, M. Saji, S. M. Lazaroff, A. F. Palmer, M. D. Ringel, and M. E. Paulaitis, "Analysis of exosome release as a cellular response to MAPK pathway inhibition," Langmuir, 2015.
[23] R. Lacroix, C. Judicone, M. Mooberry, M. Boucekine, N. S. Key, and F. Dignat-George, "Standardization of pre-analytical variables in plasma microparticle determination: results of the International Society on Thrombosis and Haemostasis SSC Collaborative workshop.," J. Thromb. Haemost., Apr. 2013.
[24] M. Baalousha, F. V.D. Kammer, M. Motelica-Heino, H. S. Hilal, and P. Le Coustumer, "Size fractionation and characterization of natural colloids by flow-field flow fractionation coupled to multi-angle laser light scattering," J. Chromatogr. A, vol. 1104, no. 1–2, pp. 272–281, 2006.
[25] J. B. Simonsen, "What Are We Looking At? Extracellular Vesicles, Lipoproteins, or Both?," Circ. Res., vol. 121, p. 92P_922, 2017.
[26] G. Midekessa et al., "Zeta Potential of Extracellular Vesicles: Toward Understanding the Attributes that Determine Colloidal Stability.," ACS omega, vol. 5, no. 27, pp. 16701–16710, Jul. 2020.
[27] E. Fröhlich, "The role of surface charge in cellular uptake and cytotoxicity of medical nanoparticles.," Int J Nanomedicine., vol. 7, pp. 5577–5591, 2012.
[28] C. Théry et al., "Minimal information for studies of extracellular vesicles 2018 (MISEV2018): a position statement of the International Society for Extracellular Vesicles and update of the MISEV2014 guidelines," J. Extracell. Vesicles, vol. 7, no. 1, p. 1535750, 2018.
[29] C. Fuentes, J. Choi, C. Zielke, J. M. Peñarrieta, S. Lee, and L. Nilsson, "Comparison between conventional and frit-inlet channels in separation of

biopolymers by asymmetric flow field-flow fractionation," Analyst, vol. 144, no. 15, pp. 4559–4568, 2019.
[30] C. Bayart et al., "Comparison of SEC and AF4 analytical tools for size estimation of typhoid Vi polysaccharides," Anal. Methods, vol. 11, no. 37, pp. 4851–4858, 2019.
[31] Y. González-Espinosa, B. Sabagh, E. Moldenhauer, P. Clarke, and F. M. Goycoolea, "Characterisation of chitosan molecular weight distribution by multi-detection asymmetric flow-field flow fractionation (AF4) and SEC.," Int. J. Biol. Macromol., vol. 136, pp. 911–919, Sep. 2019.
[32] E. Bazzan et al., "Critical Review of the Evolution of Extracellular Vesicles' Knowledge: From 1946 to Today.," Int. J. Mol. Sci., vol. 22, no. 12, Jun. 2021.
[33] A. Słomka, S. K. Urban, V. Lukacs-Kornek, E. Żekanowska, and M. Kornek, "Large Extracellular Vesicles: Have We Found the Holy Grail of Inflammation?," Front. Immunol., vol. 9, p. 2723, 2018.
[34] Y. Tian et al., "Brain-derived microparticles induce systemic coagulation in a murine model of traumatic brain injury," Blood, vol. 125, no. 13, pp. 2151–2159, Mar. 2015.
[35] Z. Baka et al., "Increased serum concentration of immune cell derived microparticles in polymyositis/dermatomyositis," Immunol. Lett., vol. 128, no. 2, pp. 124–130, 2010.
[36] A. Kumar et al., "Microglial-derived microparticles mediate neuroinflammation after traumatic brain injury," J. Neuroinflammation, vol. 14, no. 1, p. 47, 2017.
[37] D. Povero et al., "Lipid-induced toxicity stimulates hepatocytes to release angiogenic microparticles that require Vanin-1 for uptake by endothelial cells.," Sci. Signal., vol. 6, no. 296, p. ra88, Oct. 2013.
[38] V. Combes et al., "In vitro generation of endothelial microparticles and possible prothrombotic activity in patients with lupus anticoagulant," J. Clin. Invest., vol. 104, no. 1, pp. 93–102, Jul. 1999.
[39] S. Fischer et al., "Indication of Horizontal DNA Gene Transfer by Extracellular Vesicles," PLoS One, vol. 11, no. 9, p. e0163665, Sep. 2016.
[40] T. N. Pitanga et al., "Neutrophil-derived microparticles induce myeloperoxidase-mediated damage of vascular endothelial cells," BMC Cell Biol., vol. 15, no. 1, p. 21, 2014.
[41] S. N. Hurwitz, J. M. Olcese, and D. G. J. Meckes, "Extraction of Extracellular Vesicles from Whole Tissue.," J. Vis. Exp., no. 144, Feb. 2019.
[42] M. Nawaz et al., "Extracellular Vesicles and Matrix Remodeling Enzymes: The Emerging Roles in Extracellular Matrix Remodeling, Progression of Diseases and Tissue Repair," Cells, vol. 7, no. 10, p. 167, Oct. 2018.
[43] L. Monnamorn et al., "The Concentration of Large Extracellular Vesicles Differentiates Early Septic Shock From Infection," Front. Med., vol. 8, 2021.

[44] E. L. Damsteegt, N. McHugh, and P. M. Lokman, "Storage by lyophilization - Resulting RNA quality is tissue dependent.," Anal. Biochem., vol. 511, pp. 92–96, Oct. 2016.
[45] T. Vagner et al., "Large extracellular vesicles carry most of the tumour DNA circulating in prostate cancer patient plasma.," J. Extracell. vesicles, vol. 7, no. 1, p. 1505403, 2018.
[46] L. Balaj et al., "Tumour microvesicles contain retrotransposon elements and amplified oncogene sequences," Nat. Commun., vol. 2, no. 1, p. 180, 2011.
[47] B. Mateescu et al., "Obstacles and opportunities in the functional analysis of extracellular vesicle RNA - an ISEV position paper.," J. Extracell. vesicles, vol. 6, no. 1, p. 1286095, 2017.
[48] S. J. Wallace, J. Li, R. L. Nation, and B. J. Boyd, "Drug release from nanomedicines: Selection of appropriate encapsulation and release methodology.," Drug Deliv. Transl. Res., vol. 2, no. 4, pp. 284–292, Aug. 2012.
[49] V. S. Chernyshev et al., "Size and shape characterization of hydrated and desiccated exosomes," Anal. Bioanal. Chem., vol. 407, no. 12, pp. 3285–3301, 2015.
[50] E. van der Pol et al., "Particle size distribution of exosomes and microvesicles determined by transmission electron microscopy, flow cytometry, nanoparticle tracking analysis, and resistive pulse sensing.," J. Thromb. Haemost., vol. 12, no. 7, pp. 1182–1192, Jul. 2014.
[51] J. M. Rüwald et al., "Extracellular Vesicle Isolation and Characterization from Periprosthetic Joint Synovial Fluid in Revision Total Joint Arthroplasty.," J. Clin. Med., vol. 9, no. 2, Feb. 2020.
[52] K. H. Kim, J. Y. Lee, S. Lim, and M. H. Moon, "Top-down lipidomic analysis of human lipoproteins by chip-type asymmetrical flow field-flow fractionation-electrospray ionization-tandem mass spectrometry.," J. Chromatogr. A, vol. 1280, pp. 92–97, Mar. 2013.
[53] J. Ashby et al., "Distribution Profiling of Circulating MicroRNAs in Serum," Anal. Chem., vol. 86, no. 18, pp. 9343–9349, Sep. 2014.
[54] A.-M. Mustonen et al., "Characterization of hyaluronan-coated extracellular vesicles in synovial fluid of patients with osteoarthritis and rheumatoid arthritis.," BMC Musculoskelet. Disord., vol. 22, no. 1, p. 247, Mar. 2021.
[55] U. T. Arasu et al., "Human mesenchymal stem cells secrete hyaluronan-coated extracellular vesicles.," Matrix Biol., vol. 64, pp. 54–68, Dec. 2017.
[56] E. Á. Tóth et al., "Formation of a protein corona on the surface of extracellular vesicles in blood plasma.," J. Extracell. vesicles, vol. 10, no. 11, p. e12140, Sep. 2021.

Chapter 4

Musculoskeletal tissues-on-a-chip: role of natural polymers in reproducing tissue-specific microenvironments

Musculoskeletal tissues-on-a-chip: role of natural polymers in reproducing tissue-specific microenvironments

Petta D[1], D'Amora U[2*], **D'Arrigo D[1,3]**, Tomasini M[1,4], Candrian C[5,6], Ambrosio L[2], Moretti M[1,6,7]*

[1] Regenerative Medicine Technologies Laboratory, Ente Ospedaliero Cantonale, Lugano, Switzerland.
[2] Institute of Polymers, Composites and Biomaterials, National Research Council of Italy, Naples, Italy.
[3] Department of Biotechnology and Bioscience, Università degli studi di Milano-Bicocca, Milan, Italy.
[4] Department of Chemistry, Materials and Chemical Engineering "Giulio Natta", Politecnico di Milano, Milan, Italy.
[5] Unità di Ortopedia e Traumatologia, Ospedale Regionale di Lugano, Lugano, Switzerland.
[6] Euler Institute, Faculty of Biomedical Sciences, Università della Svizzera Italiana, Lugano, Switzerland.
[7] IRCCS Istituto Ortopedico Galeazzi, Cell and Tissue Engineering Laboratory, Milan.

*Equally contributing authors

Keywords: natural biomaterials, hydrogels, microfluidic models, musculoskeletal tissues, support matrix

Paper submitted to: *Biofabrication (IF: 9,95)*

Abstract

3D in vitro models are widely employed in the regenerative medicine field. Among them, organ-on-a-chip technologies exploit multichannel microfluidic devices allowing them to establish 3D co-culture systems that offer control over the cellular, physical and biochemical microenvironments. In order to deliver the most relevant biochemical and biophysical cues to cells, it is of paramount importance to select the most appropriate matrix for mimicking the extracellular matrix of the native tissue. Therefore, natural polymers-based hydrogels are the elected candidates for reproducing tissue-specific microenvironments in musculoskeletal tissue-on-a-chip thanks to their i. high tunability of crosslinking strategies; ii. high tailoring of the mechanical properties; iii. cytocompatibility; iv. mass transport properties; v. optical transparency; vi. straightforward synthesis and material handling; vii. high large-scale reproducibility. Despite these advantages, there is still a gap between the biomaterial complexity in conventional tissue engineering and the application of these novel biomaterials in 3D in vitro microfluidic models. In this review, the aim is to discuss the main features of natural polymer-based biomaterials and suggest the translation of innovative biomaterials systems, alternative crosslinking strategies and tissue engineered-inspired approaches in

microfluidic devices in order to better mimic the complexity of the real musculoskeletal tissues.

1. Introduction

Microscale engineering has been increasingly used to mimic the three-dimensional (3D) cellular microenvironment with high spatio-temporal precision and to present cells with mechanical and biochemical signals [1]. Thanks to the employed dimensions of these devices that are comparable to the in vivo microstructures, microfluidics has gained a key role in the field of tissue engineering and regenerative medicine. This approach attempts to partially mimic human organs, such as blood vessels, muscles, airways, liver, brain, gut, kidney, and bones.

The right choice of biomaterial and the advancement in their functionalization can boost the advancement of 3D in vitro models [2]. One of the main components of the microfluidic devices is the support matrix that is employed for better mimic the cellular microenvironment. The elected support matrixes are the hydrogels, 3D crosslinked polymeric structures, which hold great potential in the development of the complex and clinically relevant 3D cellular architecture. In fact, they allow cells to retain their native tissue specific function by mimicking the in vivo 3D environment. Hydrogels can be mainly classified into two groups based on their natural or synthetic origin [3]. Gelatin, collagen, alginate, hyaluronic acid (HA) are examples of natural hydrogels,

whereas polyethylene(glycol), poly(vinyl alcohol), poly(n-isopropylacrilamide) and poly(hydroxyethyl methacrylate) are examples of synthetic ones. These polymers have emerged as pillar for biological and biomedical applications owing to their very desirable properties: biocompatibility; relevant mechanical and structural properties and their ability to deliver biological signals. Additionally, hydrogels offer a tunable porosity and stiffness that can influence the cellular fate, nutrients diffusion and help replicate the tissue functions. Among them, natural polymers are usually preferred for 3D in vitro models due to many reasons such as the intrinsic presence of bioactive groups that can improve cell recognition, adhesion, and proliferation, resulting in an improved biological response. Furthermore, they represent a suitable environment for cells because they are often components of the extracellular matrix (ECM) and therefore they closely simulate the biological properties of the ECM [4].

Usually, the 3D in vitro models employ well-established biomaterials or commercial ones as support matrix. For example, natural polymers have been employed in microfluidic devices in order to facilitate the screening of drugs and anticancer agents, to study cell-cell interaction or cell migration [5]. For example, Aizel et al. proposed a microfluidic system to study cell migration in a 3D environment made by collagen type I matrix in response to a chemokine gradient [6]. Two types of microsystems were

generated: homogenous stationary gradients with a pure diffusive mechanism and stationary gradients with a convection-diffusion mechanism. This system allowed studying cells behaviour in many different chemical conditions in a complex 3D environment. Jeong and colleagues instead developed a microfluidic assay to study sprouting and migration of endothelial cells (ECs) into a hydrogel semi-interpenetrated polymer network (semi-IPN) composed of natural polymers (HA and collagen type I) that mimic the in vivo 3D microenvironment [7].

Specifically, in the musculoskeletal field, natural polymers have been employed for developing bone-on-a-chip, joint-on-a-chip and muscle-on-a-chip devices. However, some microfluidic in vitro models do not integrate a 3D matrix to the microfluidic system, preferring material-free approaches [8,9] or they use natural polymers as coating materials. For example, Torisawa and colleagues developed a bone marrow–on–a–chip as proof of concept for the fabrication of an organ-on-chip device that reconstitutes and sustains an intact, functional, living bone marrow when cultured in vitro. Instead, in the work of Ferreira, the microfluidic device was coated with type I collagen, laminin or fibronectin and primary human myoblasts grown up in adhesion to these surfaces [10].

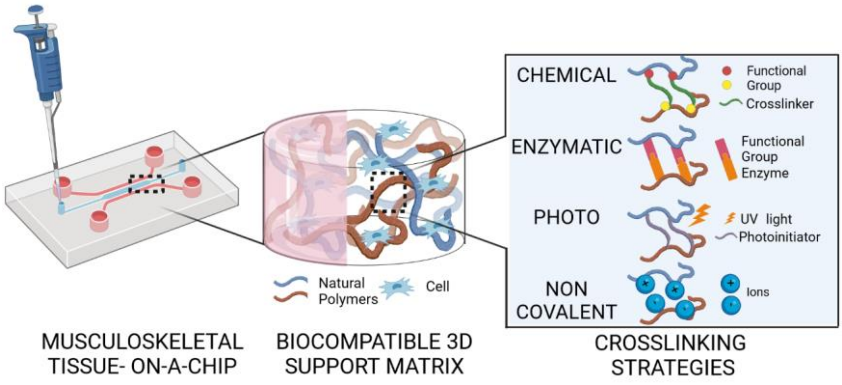

Figure 1 – Natural polymers as support matrix in in vitro microfluidic models

Despite the strong influence of biomaterials in the traditional tissue engineering approaches, there is still a gap between the biomaterial increased complexity and the application of these novel biomaterials in 3D in vitro microfluidic models. Bearing this in mind, the combination of microfluidic technology and biomaterials could be a promising route to enable the exact recapitulation of important aspects of the spatio-temporal features of complex native niches, facilitating the identification of new mechanisms of cell regulation and pathogenesis of musculoskeletal disorders (Figure 1). Therefore, in this review the main driving idea is to investigate the contribution of biomaterials, in particular natural polymers, to the microfluidic technology, looking towards alternative biomaterials systems that could be employed in this field of interest.

2. *Musculoskeletal Tissues Composition*

The complexity of the musculoskeletal system in terms of biological function is represented by the different composition of related tissues: bones, muscles, cartilage, tendons, ligaments and other connective tissues that support and bind tissues and organs together. However, in the development of arthritic joint on-a-chip models, research attention has been mainly focused on cartilage, synovial membrane and synovial fluid, as they represent the compartments more involved in the inflammatory and degenerative processes activated during different joint disorders, including osteoarthritis (OA) [11–13]. Moreover, they are characterized by a high-specialized ECM with a very different and specific composition. For this reason, in the present work the biomaterials used to mimic these tissues for in vitro models will be firstly analysed.

Table 1 - Main Musculoskeletal Tissues: Mechanical properties are expressed in terms of Young's Modulus (E), failure stress (σR), failure strain (εR). With regard to synovial fluid, G' and G'' stand for elastic and viscous moduli, respectively

Tissue	*Matrix composition*	*Main functions*	*Cell populations*	*Mechanical properties*
Cartilage	**Tangential zone:** collagen type II and IX **Transitional zone:** oblique collagen fibrils with large diameters and proteoglycans **Deep zone:** collagen fibers perpendicular to the cartilage surface, the proteoglycans at the highest content	Transmit the loads with low frictional coefficient, provide a smooth and lubricated surface between the bony heads	Chondrocytes	E: 0.23 - 0.85 MPa, in compression E: 5 - 25 MPa, in tension
Synovial Membrane	**The intima layer:** isoforms collagen (III, IV, V, VI and lower I), laminin, fibronectin and proteoglycans **The subintima layer:** fibrous, adipose and areolar connective tissues and include the vasculature	Regulate the composition of synovial fluid, maintain the functionality and the mechanical stability of the joint	Fibroblast-like synovial cells Macrophage-like synovial cells T and B cells	-
Synovial fluid	Blood plasma ultrafiltrate enriched with locally synthesized polysaccharides (high molecular weight hyaluronic acid)	Reduce friction, lubricate joints	Synoviocytes type A and B, macrophage-like cells, fibroblast-like cells that produce hyaluronic acid	G' and G'': 0.01 - 1 Pa; viscous at low frequency (G'' > G') and prevalently elastic at high frequencies (G' > G'')

2.1 Cartilage

The articular or hyaline cartilage is the specialized and resilient soft connective tissue that covers the bony heads in the diarthrodial joints. In the inferior limbs, this tissue is subjected to physiological compressive forces ranging from 1 up to and beyond 10 MPa, according to the physical activity [14]. To effectively resist to these stresses, the native hyaline cartilage is characterized by a compressive Young's modulus of 0.24-0.85 MPa and a tensile modulus of 5-25 MPa [15]. This tissue is completely deprived of blood, lymphatics and nerve tissues, and the exchange of nutrients and wastes occurs by diffusion and by the flow of the synovial fluid (SF) during the loading cycles [16]. The lack of these supporting tissues leads to a limited intrinsic ability to heal and regeneration. As reported in table 1, along the 2-4 mm of the thickness of the articular cartilage, it is possible to recognize three different zones characterized by a different organization of ECM. In the tangential zone, the matrix organization allows the tissue to contrast different mechanical stresses, such as sheer, tensile and compressive.

In the transitional zone, the collagen fibrils and the proteoglycans, mainly composed of glycosaminoglycan (GAG), such as HA and other proteins like fibronectin and laminin [17] form a sort of hydrogel. Owing to their negative charge, they attract a huge amount of water molecules, both directly and by

osmosis [18]. Therefore, the collagen fibrils give a strong resistance to tension, while the proteoglycan hydrogel supplies the swelling pressure, providing the cartilage with both stiffness and elasticity, essential for its mechanical role. The deep zone provides the maximum resistance to the compressive forces. The spherical chondrocytes display the well-known columnar arrangement parallel to the collagen fibrils. The main role of the deepest zone, the calcified cartilage, is to firmly connect the cartilage to the subchondral bone, thanks to the extension of the collagen, fibers, especially the non-fibrillar collagen type X, towards the underlaying bone [19]. In this zone, proteoglycans are not present, while the chondrocytes, in limited number, are located in the lacunae, uncalcified areas, and display the hypertrophic phenotype.

2.2 Synovial membrane and synovial fluid

The inner surface of the capsules of the synovial joints is constituted by a specialized connective tissue, the synovial membrane or synovium, which consists of two different layers: the intima and subintima layers. As mentioned in table 1, it can be possible to distinguish three different types of the subintima, according to the main component of the tissues [20]. The fibrous type is constituted by a dense collagen matrix similar to other fibrous tissues, such as fibrocartilage or ligament. In this type of

synovial tissue, the intima is made of interspersed cell layer. In the adipose synovium, a single and flattened layer of cells and a network of capillaries covers a subintimal fat tissue, with a collagen band often interposed. The areolar type can be defined as the most specialized synovial tissue. The intima is significantly thicker while the subintima is made of loose connective tissue rich in blood vessels often organized in projections or villi towards the articular space. The structure of the intima matrix is amorphous or fibrillar and it is constituted mainly by different isoforms of collagen (type III, IV, V and VI, and in a lesser extent type I). Other proteins present in this matrix are laminin, fibronectin and proteoglycan rich in chondroitin sulfate [21].

The most abundant resident cells in the synovial membrane are macrophages-like synovial cells and synovial fibroblasts. The macrophages can be found in both the subintima and in the intima layers and they are characterized by a different marker expression in the two layers [22]. These macrophages uptake and degrade extracellular proteins, cells, cell debris and microorganisms from the synovial fluid (SF) and from the intima. Similarly, the synovial fibroblasts are present in both synovial layers, and they can be distinguished from macrophages thanks to specific markers, such as CD55 [23]. These specialized fibroblasts produce and secrete several different extracellular proteins in the synovial cavity, such as HA, collagen, GAG and

mucin [24]. In the intima, macrophages and fibroblasts are usually organized in a specific pattern in which the firsts form a superficial layer under which the latter are located at various depth.

The protein secreted by fibroblasts are the main components of the SF. Its lubricating role depends on the peculiar biochemical composition and the rheological features of the SF. Indeed, the SF is a highly viscoelastic and shear-thinning fluid as it can be subjected to shear strain up to 1000 s-1 [25,26]. During small movements, such as position shifts, the SF is characterized by a high viscosity and can directly support the load [27]. Indeed, with low shear stress and frequency, the SF acts as a pseudo-Newtonian fluid with a viscosity in the range of 10-100 (Pa x s) [28,29]. In the regime of full joint movements, such as during the motion, the SF changes his behavior and forms a stable lubricating thin film on both the cartilage surfaces. In this condition, the SF is characterized by a lower viscosity, in the range of ~ 0.01 (Pa x s) [30]. These peculiar properties of the SF are mainly addressed to the high content of HA that forms a network able to withstand significant degrees of deformation [31,32]. However, also other proteins can influence the SF mechanical properties, especially its viscosity and elasticity, by interacting with HA [33,34].

3. Natural polymers as support matrix in microfluidic musculoskeletal models

Considering the tissue composition and functions, the 3D in vitro models should be able to mimic as much as possible the 3D tissue microenvironment to properly reproduce its properties (Figure 2). Different natural polymers form the ECM which provides both structural support to cells and a guide of cell migration, proliferation, differentiation, and maturation throughout development [35]. They can be exploited as support matrix in microfluidic devices thanks to their ability to generate 3D viscoelastic polymeric networks, namely hydrogels, which have similar physical properties to the natural tissue. For this reason, over the past years, hydrogels have been widely used to develop cellularized constructs in classical tissue engineering approaches [36]. Natural hydrogels can be classified into three distinct groups including: i) protein-derived polymers such as collagen, silk and elastin; ii) polysaccharide-based polymers such as GAGs or alginate among others and iii) decellularized tissue-derived biomaterials (decellularized heart valves, blood vessels, liver, tendons [37]). Their employment is favoured by their cytocompatibility, viscoelastic and mechanical properties, swelling and degradation rate. Furthermore, these hydrogels can be suitably functionalized to improve existing properties (i.e. mechanical behaviour or residence time) or to confer new

features such as the ability to respond to light, chemicals, pH, ionic concentration, temperature, and magnetic and electrical fields [38]. These materials may be engineered to be hydrolysable or degradable over time and have tunable biophysical properties through manipulation of crosslinker concentration, applied wavelength, and duration of irradiation.

Given their characteristics, these natural polymers have been employed in microfluidic devices as support matrix for cell encapsulation and for better mimicking tissue-like properties.

As explained in paragraph 2, **collagen** is the most abundant protein in mammalian tissues and the main component of natural joint ECM, in fact it is the most common polymer employed in bone-on-a-chip devices [39]. It is made up of three polypeptide chains, which self-aggregate to form a stable three-stranded rope structure. The fibrillogenesis happens with a temperature transition from 4°C to 37°C. Collagen fibers of different thickness could easily be obtained by controlling the polymerization of collagen matrix, done by varying pH and pre-incubation temperatures. A derivative of collagen is **gelatin**, obtained through the denaturation of the collagen triple helixes in acidic or alkaline conditions. Thanks to its stability at high temperature and in a wide range of pH, its functionalization is easily achievable; one of the most used derivatives is the methacrylated

gelatin (GelMA), a photo-crosslinkable natural hydrogel with tunable mechanical properties.

An alternative to collagen is **fibrin**, a protein involved in the natural repairing process of the tissues and in the coagulation cascade. The gelation process of fibrin gel mimics the last step of the coagulation cascade: thrombin-mediated cleavage of fibrinogen initiates the formation of fibrin that continues to self-assemble into a fibrin network. In addition, fibrin can be further crosslinked via the factor XIIIa [40]. Importantly for the in vitro experiments, its gel structure can be tuned: the concentration of thrombin influences the gelation time, resulting in a more densely cross-linked network with thinner fibers when employing higher concentrations or in a higher porosity network with lower concentrations [41]. Thanks to these properties, fibrin has been widely used in tissue engineering, specifically in bone and cartilage tissue engineering as bioadhesive polymer in tissue repair [42,43].

Hyaluronic acid (HA) is one of the main components of the ECM in the musculoskeletal tissues; however, it has been poorly exploited in microfluidic devices for musculoskeletal models. HA is a naturally occurring non-sulfated glycosaminoglycan that provides cellular support and hydrophilic matrix. It also regulates cell-cell adhesion, cell migration, growth, and differentiation [44]. Thanks to its unique biological and

viscoelastic properties [45–47], HA has been employed for targeting cartilage [48,49]. Furthermore, due to its amenability to chemical modification, different HA-based derivatives have been developed and characterized, overcoming the intrinsic limitations of this material such as the low mechanical features and the short residence time [47]. After functionalization, HA can be crosslinked by employing chemical, enzymatic, physical or photo-crosslinking mechanisms [50–52].

Matrigel has been used in microfluidic devices mainly for microchannel coating or in muscle-on-a-chip systems in combination with other natural polymers. It consists of natural polymers secreted by Engelbreth-Holm-Swarm mouse sarcoma cells and it contains critical growth factors and cytokines that support cell growth. In particular, it consists of about 60% laminin, 30% collagen type IV, and 8% entactin (bridging molecule that contributes to the structural organization). The 3D network formation is triggered by temperature change: its lower critical solution temperature is 6°C and it forms a stable gel at room temperature [53].

An emerging role has been given to the **decellularized ECM**, which is the closest 3D matrix to native tissues combining unique micro- and macro-architectural characteristics and an equally unique complex composition [54]. There is only one work by Marturano-Kruik and colleagues where a decellularized bone

matrix/scaffold has been integrated in a microfluidic device [55]. Usually, decellularized ECM is obtained by the decellularization of ex vivo of native tissues or from ECM proteins that are deposited by in vitro cultured cells [56]. Appropriate decellularization methods are required to deplete cells while maintaining a similar composition and structure of the original ECM. This can be achieved by chemical, physical, biological treatments and their combinations. Once decellularized, the ECM is often cross-linked to increase its stability.

In addition to those found in human ECM, there are some natural polymers that are employed in tissue engineering, but they are not found in the human body. For example, **agarose** is a linear polysaccharide prepared from seaweed consisting in repeated units of D-galactose and 3,6-anhydro-L-galactose. It undergoes thermal crosslinking after cooling the solution below 45 °C because of extensive intermolecular hydrogen-bonding between the agarose chains [57] and the agarose concentration influences the final network porosity [58].

Alginate, instead, has been used in a microfluidic device not for specific application in the musculoskeletal field but for in situ cell entrapping and anticancer drug screening. Alginate is a linear polysaccharide composed by (1,4)-linked β-D-mannuronate (M) and α-L-guluronate (G) residues that form an intermolecular cross-linking thanks to the ionic interaction of divalent cations

such as Ca2+, Ba2+, or Sr2+ with G-blocks of the polymeric chains. The composition (i.e., M/G ratio), sequence, G-block length, and molecular weight are thus critical factors affecting the physical properties of the hydrogels. Alginate is a highly hydrated polymers and is considered biocompatible, however it must be modified with adhesive peptides to facilitate cell binding [59].

Other polymers widely used in tissue engineering but not yet exploited in a microfluidic device are the **gellan-gum** and the **chitosan**. Gellan-gum (GG) has been receiving particular attention for tissue engineering applications, namely cartilage regeneration, mainly due to its good mechanical properties. GG, which has food and drug administration (FDA) approval as a food additive, is an anionic microbial polysaccharide composed of a tetrasaccharide repeating units of two b-D-glucose, one b-D-glucuronic acid and one a-L-rhamnose. Upon temperature decrease, a random coil-helix transition occurs with further aggregation of the helices leading to the formation of junction zones. The sol-gel transition of GG is ionotropic, as in alginate [60,61]. Furthermore, the functionalization of GG with methacrylate groups can lead to hydrogels with highly tunable physical and mechanical properties.

Chitosan is the second most abundant natural biopolymer currently attracting great attention for tissue engineering applications due to its intrinsic properties such as excellent

biocompatibility and controlled biodegradability with safe by-products and easy processability. It results from alkaline deacetylation of chitin, a structural element of the exoskeleton of crustaceans. It is a linear amino polysaccharide composed of glucosamine and N-acetyl glucosamine units linked by β-(1-4) glycosidic bonds. The cationic nature of this polymer, in a pH range near its pKa, is particularly important for tissue engineering applications, as it can form polyelectrolyte complexes with anionic biological macromolecules. Reactive primary amines and hydroxyl groups in chitosan remain available for the addition of side groups, peptides or amino acids, enhancing its properties in biomedical applications [62].

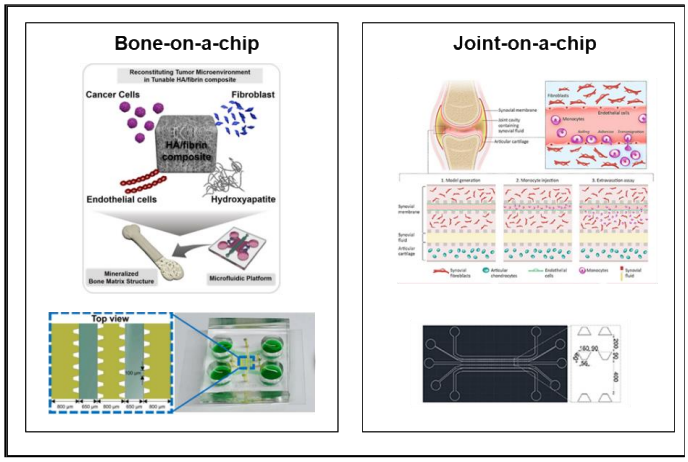

Figure 2 - Natural polymers as support matrix in miniaturized musculoskeletal models.

3.1 Joint-on-a-chip

Over the last years, great efforts have been devoted to the design of different in vitro models capable of recapitulating articular physiology to fully study joint disorders. However, there is still a lack of microfluidic models that recapitulate the joint microenvironment tacking into account all tissues and components that interact together within the joint, such as SF, synovial membrane, cartilage, adipose tissue and bone. Indeed, only three works in literature have employed so far natural polymers in a microfluidic joint-on-a-chip model. In the work of Ma and colleagues, a microfluidic model was used to perform a drug-sensitive assay based on microfluidic device [63]. In particular, this microfluidic device was used also to evaluate a drug, celastrol, which inhibits fibroblast-like synovocyte (FLS) activation and attenuates bone erosion during rheumatoid arthritis (RA). The microfluidic device consisted of one central channel where FLS cells were cultured forming a monolayer and six parallel branched microchannels jointed at cell reservoir at one end and at the central channel at the other end. Human synovium cells were cultured in pre-coated Matrigel microchannels, indirectly co-cultured with stimulated osteoclastic (RAW264.7) and osteogenic medium stimulated BMSCs. These conditions were recreated to mimic the condition of FLS cells migration and the invasion-mediated bone erosion in

RA. Thanks to this hydrogel, the authors were able to culture FLS and bone-related cells in two different microenvironments, better resembling the original tissues. Matrigel was able to recreate an environment that resembled the original organ (migration and functional activities) and allowed the cell-cell interaction with cytokines and chemokines. The authors effectively demonstrated that the FLS cells significantly passed through the Matrigel layer and migrated towards the bone compartment. The co-culture of FLSs with RAW624.7 and BMSCs, showed a migration of the FLSs more consistent with clinical observations in terms of number and distance. Furthermore, the cadherin-11 expression, which is associated with RA progression because of the secretion of IL-6, a critical inflammatory factor, was increased with the co-culture. Alkaline phosphatase (ALP), osteoblast differentiation marker, and tartrate-resistant acid phosphatase (TRAP), osteoclast differentiation marker were used to study the interaction between BMSC, RAW264.7 and FLS in the microfluidic device. After the co-culture of BMSC, RAW264.7 and FLS the number of TRAP staining-positive RAW264.7 cells increased with respect the culture of FLS without BMSC, while the number of ALP staining-positive cells decreased. It was found that 500 ng/mL of celastrol can effectively inhibit FLS migration, but also can reduce of the expression of cadherin-11 suppressing TRAP activity in RAW264.7. All these results of celastrol in vitro are consistent

with the effect of celastrol in vivo, also showing that this microfluidic device provides a rapid in vitro screening for anti-RA drugs.

In another work of Paggi et al., a microfluidic platform was developed to create gradients of mechanical compression, which reproduces the physiological range on a cartilage model, on chondrocytes cells embedded into a hydrogel [57]. This device is highly versatile, as it can allow mimicking in vivo stimulations. It can be used as a platform screening of strain levels on cells in a single experiment observing cells response in real time. The mechanical cues are very important especially in the cartilage due to their importance on ECM regulation. The microfluidic device was composed by a 3D cell-hydrogel chamber divided from the chamber medium by an array of pillars. The culture chamber was placed in contact with three actuation chambers made of a thin PDMS vertical membrane connected to a pressure controller. The hydrogel used to culture chondrocytes was agarose (4% w/w) which was not covalently attached to the PDMS membrane. Firstly, the mechanical stimulation was applied through the deflection of a thin PDMS membrane showing a direct correlation between the crosslinking degree and the material Young's Modulus. For this reason, the ratio 20:1 between prepolymer: curing agent was selected to give a large deflection to the PDMS (traditional 10:1). Contemporarily, the membrane deflection

depended on its dimension. Therefore, all the experiments were performed using 50-um thick and 200-um high membrane with a glass substrate coated with 4-mm thick PDMS layer, to maximize the membrane deflection. Chondrocytes were characterized using a homogenous compression (800 mbar and 1 Hz which corresponds to physiological strain in healthy knee cartilage) showing a decrease of the chondrocyte projected surface area. It means that cell deformation follows the same gradient as agarose displacement. Subsequently, two pressures were employed to study cell viability, one that mimics a healthy condition (800 mbar) and the other one for hyper-physiological condition (1000 mbar) and static culture as a negative control. By employing 1000 mbar, the cell membrane integrity, especially in the zone next to the membrane and not closer to the pillars, was compromised together with possible cell death. It was also demonstrated that hydrogel of agarose is suitable for chondrocytes culture creating cell deformation which mimics the in vivo situation of knee cartilage. Finally, it was tested a combination of normal and bulk shear strains on agarose with microbeads that mimic the cells, showing similar values to those observed in the knee articulation during movement. These two models, however, employed as support matrix, agarose or a Matrigel coating of the microfluidic channel. The work of Lin and colleagues is the only one that introduced a combination of more relevant natural polymers,

specifically HA- and gelatin-photo-crosslinkable derivatives, in a microfluidic-based, multichamber bioreactor for investigating osteochondral differentiation and toxicity testing [64].

An additional level of complexity was added in the work of Mondadori et al., where a 5-channels microfluidic device was designed for studying the ability of osteoarthritic SF to induce monocyte extravasation [65]. Specifically, they developed a 3D microfluidic organotypic model reproducing synovial compartments with a perfusable endothelialized channel, a channel for SF injection mimicking the articular cavity, and a cartilage compartment. Different fibrin concentrations (5, 10, 20 mg/mL) and cell densities (2.5 × 106, 5 × 106 cells/mL) were tested. The endothelial channel instead, was coated with 10 μg/ml human fibronectin and ECs (6 × 106 cells/mL) suspended in EGM-2 medium were added to the channel. The model showed a strong chemoattractant effect of the OA synovial fluid on monocytes, which most likely depends on the presence of pro-inflammatory cytokines and chemokines. The study provided direct evidence that OA synovial fluid induces monocytes to cross the endothelium and invade the synovial compartment.

There are still no studies that comprise the tendon and ligament compartments in a microfluidic joint model. To design an engineered tendon/ligament microfluidic platform, the selected polymeric support matrix should provide structures that are

suitable for tenocyte or ligamentocyte attachment, differentiation, and growth. Knowing that collagen and elastin are the main components of the ECM of tendon and ligament tissue, natural polymers, such as collagen, silk and alginate have been mainly identified as promising candidate [66–69]. These biomaterials have shown good mechanical properties, and slow degradation rate. Furthermore, their biocompatibility and hydrophilic properties could also be exploited to sustain and control the delivery of biological factors.

Table 2 – Joint-on-a-chip models

Author, year	Application	Device Structure	3D Matrix Composition	3D Matrix Gelation	Cells Embedded	Main Outcomes
Lin, 2014 [83]	Osteochondral tissue engineering; Drug screening	Chamber and 3D bioreactor insert	Chondral section: GelMA (10%), HA (1%, MW ≈ 66 kDa) Bone section: GelMA (10%), HAp (1%)	Photocrosslinking: LAP (0.15%), UV light (λ=390–395nm)	hBMSCs (2× 10^7 cells/mL)	Biphasic tissue differentiation to chondrogenic/osteogenic gradients produced by tissue-specific differentiation factors; crosstalk between different compartments in response to catabolic cues (IL-1β)
Mondadori, 2021 [124]	Monocyte extravasation in OA	Three gel compartments and two microfluidic channels	Fibrinogen (5, 10, 20 mg/mL)/Thrombin (4U/ mL), ratio 1:1, human fibronectin coating (10μg/mL)	Enzymatic crosslinking	Synovial Fibroblasts and articular chondrocytes (2.5×10^6, 5×10^6cells/mL); endothelial cells (6×10^6cells/mL); Human primary monocytes (10^6cells/mL)	Monocyte extravasation promotion by endothelial preconditioning; Inhibition of monocyte extravasation by 2 chemokine receptor antagonists
Paggi, 2020 [54]	Cartilage tissue model	Culture chamber; Perfusion channel and three actuation chambers	Agarose (2%w/w)	Thermal-mediated gelation	Chondrocytes (4×10^7cells/mL)	Generation of compressive mechanical stimulation gradients and multi-modal actuation patterns; analysis of strain levels effects on cells with real-time cell response observation
Rothbauer, 2021 [134]	Rheumatoid arthritis	Two organoid compartments and two circular medium reservoirs	Matrigel (synovial compartment) Fibrin hydrogel 50 mg/ml (cartilage compartment)	Thermal-mediated gelation (40 min, 37 °C) Enzymatic crosslinking for fibrin	Fibroblast-like synoviocytes (3×10^6cells/mL) Human primary chondrocytes ($\times10^6$cells/mL)	Formation of organoids with high reproducibility and positioning precision; co-cultivation of chondral and synovial organoids improved the phenotype of chondrocytes within chondral organoids

Methacrylated gelatin (GelMA), hyaluronic acid (HA), hydroxyapatite (HAp), human bone marrow-mesenchymal stem cells (hBMSCs), Lithium Phenyl (2,4,6-Trimethylbenzoyl) Phosphinate (LAP).

4. Common features of a 3D cell support matrix for microfluidic in vitro models

Natural polymer-based hydrogels allow tuning different parameters such as pore size, swelling ratio, crosslinking

densities, gradients, and cell seeding. Their unique ability to absorb and retain water is given by their hydrophilic nature and the amount of absorbed water depends on several factors: the hydrogel structure, the crosslink density, the composition of the solution and the technique used to synthetize the hydrogels. They can be characterized through several physical parameters, such as size, elastic modulus, swelling and degradation rate [36]. The hydrogel versatility allows their employment in multiple applications and combinations with several molecules to develop polymeric blends.

The major advantages of using hydrogels in microfluidic systems are reported below (Figure 3). Some of them will be discussed in more detail in the following paragraphs.

- High tunability of crosslinking strategies, which determines a wide range of physico-chemical properties.
- High tailoring of the mechanical properties. Most hydrogels have a comparable Young's modulus to that of cells.
- Cytocompatibility. Most hydrogels are non-toxic allowing to obtain a 3D suitable microenvironment.
- Free diffusion for small molecules. Most cell essential nutrients and growth factors are diffusible in hydrogels.
- Optically clear. This characteristic of hydrogels makes it possible to observe fluorescent molecular diffusion and cell behaviours inside the gel structures under microscopes.

- Straightforward synthesis and material handling. Most hydrogels are commercially available and their derivatives are generally easy to synthesize.
- High large-scale reproducibility. Gels can be produced in different designs and accurate size calibration.

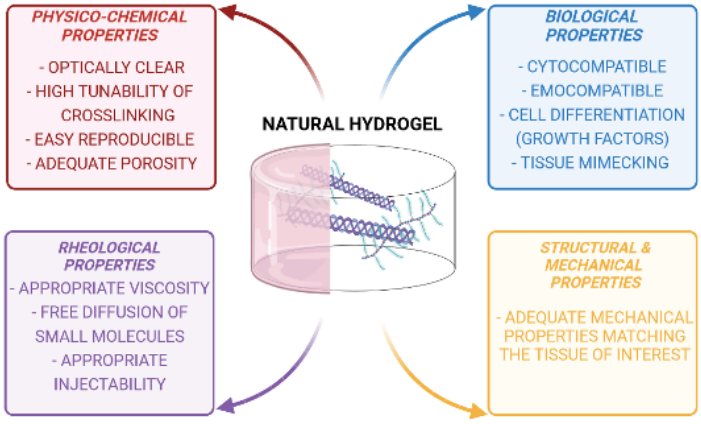

Figure 3 – Main properties of a natural hydrogel potentially used in microfluidics

4.1 Strategies for 3D networks formation

In order to obtain a 3D network, polymers undergo a crosslinking process where polymer chains are linked by covalent or non-covalent bonds [70]. The crosslinking process enhance the mechanical properties of the polymers and to extend their half-lives. Additionally, it triggers an improvement of the viscoelastic properties of the polymeric network that promotes cell encapsulation and mechanical environment required for cell differentiation. Natural polymers can be crosslinked by employing chemical, enzymatic, physical or photo-crosslinking

mechanisms. Specifically, when the gel is employed as support matrix in a microfluidic chip, the adopted crosslinking strategy has to be compliant with cell encapsulation and handling of the chip. Indeed, there should be a balance between the crosslinking kinetics and the cell encapsulation and injection of the biomaterial into the microfluidic channels. The reversible nature of non-covalent or physical interactions can trigger the formation of hydrogels responding to temperature, pH or other physical or chemical cues. These types of crosslinking mechanisms generally result in low mechanical properties and low toxicity towards the cells and tissues. Ionic interactions represent an example of non-covalent or physical reticulation. This mechanism is typical of alginate, where divalent cations, such as Ca2+, bind the glucoronate blocks leading to the crosslinking of adjacent polymers chains. However, the ionic crosslinking often results in a rapid and poorly controlled gelation, limited long-term stability and low gel uniformity. The addition of ions like Ca2+, Mg2+, Zn2+ to the precursor hydrogel can induce gelation through ionic bond formation in polymers rich in anionic groups, such as alginate. For example, in the work of Braschler et al., alginate hydrogels were employed in a microfluidic device: the polymer was reconstituted to encapsulate yeast cells and to study cell entrapping [71], showing a high cell viability of yeast cells and a degradation of the hydrogel due to the massive cell proliferation.

In the same way, Chen and colleagues employed a 2% alginate solution for embedding tumour spheroids (108 cells/mL) and screening anticancer agents [72]. Being non-adhesive, alginate allows the formation of spheroids, while at the same time protecting the cells from shear during perfusion. Furthermore, alginate can easily de-crosslinked in the presence of a calcium chelator and cells can be harvested for further analyses.

Covalent crosslinking, instead, is for example promoted by the use of chemical crosslinking agents, such as GTA, carbodiimide, epichlorohydrin, and sodium metaphosphate. For example, gelatin exhibits poor mechanical properties at 37°C and therefore it is not a suitable material for cell embedding and culture. However, it can be stabilized by chemical crosslinking with GTA: aldehyde groups on the GTA react with the free amino groups of the polymeric chains leading to stable bonds and a hydrogel. Unfortunately, the chemical crosslinker is often toxic for cells. Therefore, its use is not the best option in microfluidics, even though naturally occurring biocompatible chemical crosslinking agents, such as genipin are attracting research attention considering its multiple pharmacological properties (i.e., anti-inflammatory, anti-thrombotic, anti-angiogenic, anti-tumour, anti-diabetic, and neurotrophic properties) [73].

Nevertheless, gelatin, as other natural polymers such as HA and GG can be also modified by specific functional groups (e.g.

methacrylic groups, phenolic groups) that allow a photo-crosslinking approach, where a photoinitiator and irradiation are required to trigger the process [60,61,74–79]. Ultra-violet (UV) radiation is the light source which is the most used to improve the hydrogel mechanical properties together with the photoinitiator Irgacure 2959. However, it is well known its potential cytotoxicity effect due to the cellular damage via direct interaction with cell membranes, proteins and DNA or via indirect production of radical oxygen species (ROS). Additionally, UV has a lower penetration depth that can limit its use in deep tissue implants. Although, new photo-crosslinking systems based on visible light have been employed to overcome these limitations together with photoinitiators such as organic dyes (Eosin Y), Rose Bengal and methylene blue, aromatic hydrocarbons (quinones, porphyrins and phthalocyanines), Ruthenium(II) tris-bipyridyl dication (Ru(II)bpy32+), sodium ammonium persulfate (SPS), lithium phenyl-2, 4, 6-trimethylbenzoylphosphinate (LAP); 2,2'-Azobis[2-methyl-N-(2-hydroxyethyl)propionamide (VA-086) [78,79]. However, these systems have not been yet implemented within microfluidic devices. For example, GelMA, being the gold standard in the last 20 years in light-based biofabrication technologies, it has been employed in the work of Agrawal in which 7% of GelMA was used together with the photoinitiator LAP in a muscle-on-a-chip

model [80]. The formation of 3D muscle tissue was obtained by encapsulating myoblasts within the GelMA hydrogel that was sandwiched between two acellular polyacrylamide hydrogel layers. Similarly, in the work of Lin, a microfluidic-based multichamber bioreactor was developed for osteochondral differentiation and toxicity testing [64]. In particular, hBMSCs (2 x107 cells/mL) were resuspended in an IPN hydrogel composed by 10% GelMA and 1% HA in order to mimic the cartilage region or in 10% GelMA enriched by 1% HAp to resemble the bone compartment. GelMA was photo-crosslinked by exploiting 0.15% w/v LAP and UV irradiation (390 – 395 nm).

Another possible approach is the use of enzymatic crosslinking that occurs under mild, physiological conditions (no large temperature changes are required, no toxic chemicals and no potential harmful radiation) but there is a low control on the degree of crosslinking, and the mechanical properties. The most used enzymatic-mediated crosslinking in the microfluidic devices is employed for the formation of fibrin gels: thrombin removes fibrin peptides from fibrinogen and exposes polymerization sites that allow fibrin monomers to self-assemble into insoluble fibrin gel.

For example, in the work of Hasenberg, adipose-derived stromal cells (2 x 105 cells/mL) and HUVECs (5 x 105 cells/mL) were embedded in fibrinogen 2.5 mg/mL and thrombin 0.2 IU/mL to

emulate human microcapillaries in a multi-organ-chip platform [81]. These gels were either subjected to pulsatile flow or incubated without perfusion for 14 days. The stability of fibrin was influenced by the incapsulated cells that cause gel contraction.

Another example of enzymatic-mediated crosslinking is the use of transglutaminase such as factor XIII. In the work of Sun, microbial transglutaminase was used to enzymatically crosslink 10% (w/v) gelatin and 0.5% (w/v) Pluronic F-127 solution loaded with lung cancer cells (1.3 x 105 cells/mL) [82]. The polymeric formulation was injected before crosslinking in a microfluidic system for cancer drug screening. This method is cheaper compared to the use of collagen; however, the crosslinking mechanism can be toxic for the encapsulated cells and less efficient compared to collagen in terms of cell adhesion and differentiation.

4.2 Biological Properties: cytocompatibility, cell adhesion and biochemical stimuli responsivity

Cytocompatibility is one of the first factors that should be considered when selecting a biomaterial. Cell viability can be affected by the crosslinking methodology or by chemical byproducts. In general, hydrogels obtained from natural polymers offer a suitable 3D environment for cell encapsulation.

The selected hydrogel must not be toxic for cells and must guarantee a remodelling of the surrounding ECM to ensure cell proliferation, spreading and migration, key activities during neovascularization or tumour progression. Despite cell survival, the polymeric matrix in which the cells are embedded has to promote either cell differentiation into the desired phenotype or to maintain the specific cell phenotype. In order to ensure these biological features, often, long culture periods are required. This is one of the most challenging aims from a biological point of view in microfluidics because in some conditions the polymeric matrix can degrade very fast if the polymer concentration; the crosslinking degree and the cell number embedded in the matrix are not balanced between each other. However, the fast degradability of some natural polymers, such as fibrin and collagen, can be slow down by using polymer blends or supplements, such as aprotinin.

4.3 Mechanical Behaviour and Injectability force

The ECM plays a pivotal role as cell function mediator. Indeed, it ensures biochemical and mechanical stimuli influencing in such way the biological response at tissue and cell level. At tissue level, it is widely recognized that mechanical properties of the local microenvironment allow compression, elongation, or shear force. At cellular level, cells receive mechanical information from the

substrate to which they adhere, even without the application of external forces. This process is named mechanotransduction; it allows them to convert mechanical stimuli into a chemical response [83,84]. Among various mechanical cues, matrix elasticity influences cellular behaviour including cell adhesion through the formation of multi-protein structures, such as focal adhesion, cell spreading, as well as cell proliferation and differentiation [85–88]. These cytoskeletal modifications are crucial as they determine cell shape and morphology [89,90]. Different studies have demonstrated that stiffer substrates generally may promote cell spreading, whereas soft matrices can induce a rounded cell shape [91–93]. Furthermore, substrate stiffness also affects cell growth and viability. Indeed, the softness or stiffness of a biomaterial might influence the size of the multi-protein structures and the pressure to which cells are subjected, that in turn affects their growth and movement [94]. In fact, on a hard substrate, cells usually exert large forces, which lead to the formation of mature focal adhesions and a highly organized cytoskeleton with abundant stress fibers [91,95]. In contrast, a soft substrate is not able to ensure a good resistance to counterbalance large cell-generated forces. For this reason, cells do not develop abundant stress fibers and generate smaller forces. In other words, cells react to differences in the substrate stiffness appropriately adjusting their "musculoskeletal system". In this

scenario, it is not surprising that these changes in cell morphology led to changes also in cell phenotype and differentiation. Many studies highlighted that undifferentiated MSCs commit to specific phenotypes according to substrate stiffness. As an example, stiffer matrices that mimic muscle tissue are mostly myogenic, while rigid materials may induce an osteogenic behaviour. Substrate stiffness also influences cell migration, as well as the vascularization and angiogenesis. It was demonstrated that normal rat kidney epithelial cells and fibroblasts migrate faster on softer substrates [96], whereas vascular smooth muscle cells showed the highest migration on intermediate stiff substrates [97]. At this point, it results clear how important should be in microfluidics ensuring the appropriate mechanical cues of a biomaterial cell support to fully recapitulate complex tissues [98,99]. Collagen type I has been often used in different microfluidic platforms. However, it does not properly mimic the ECM due to the lack of good mechanical stability for long-term culture of cells. Many authors have studied cell migration under different mechanical conditions. The stiffness of the collagen mainly depends on the polymer concentration. As an example, Fraley et al. found that collagen concentrations between 1.5 and 2.5 mg/mL led to much lower elastic modulus compared to 4 mg/mL collagen type I, which was 500 Pa [100]. The influence of physical gradients on morphology, migration and other cell

behaviours were studied by Del Amo et al. [101]. The authors developed a microfluidic-based chip that allowed analysing the long-term chemoattractant effect of growth factors on 3D cell migration. The authors proved that cell migration was influenced by the substrate stiffness, which was related to collagen concentration and to change in pore size. The elastic properties of polymer matrix can be also adjusted by using UV light exposure and pyhotocrosslinkable polymers with different degree of functionalization (DOF). Chen et al. developed a microvascular microfluidic device in which GelMA was employed as biomaterial, due to the presence of natural cell binding motifs and degradability of native collagen but improved mechanical properties. Indeed, the possibility of varying the DOF as well as the crosslinking levels via UV make it easier to tune the mechanical properties [102].

With regard to musculoskeletal microfluidic devices, much more efforts should be devoted to the appropriate selection of the biomaterial for cell support, benefiting from the wide knowledge acquired in tissue engineering and biomaterial science. Babaliari et al. used gelatin solution from bovine skin, type B (2% w/v) or collagen type I, rat tail (3 mg/mL) as biomaterials for their device [86]. The results obtained from the mechanical characterization showed the typical spectra of a viscoelastic response of a soft solid with an elastic modulus, G', which exhibited a weak increase in

the frequency range investigated, and a viscous modulus, G", that was an order of magnitude lower than G". Therefore, over the entire range of applied frequencies, the materials showed a soft solid-like behaviour with no signs of a slow relaxation mode at long times. The authors assessed a good cell adhesion and growth. A significant difference in cell proliferation was observed under dynamic conditions: it increased by 2.4-fold with a flow rate of 50 μL/min compared to static conditions. Similarly, normalized ALP activity on fibrous collagen substrates significantly increased in dynamic conditions (1.6-fold with 30 μL/min) compared to the static condition. Klotz et al. used GelMA (5%wt) with different DOF. The compressive modulus slightly increased from 1.2 kPa (30 % DOF) to 1.8 kPa and 2.8 kPa for 50 % DOF and 80 % DOF, respectively. After 5 days, MSCs spread only in 30 and 50 % DOF hydrogels. Paggi et al. used a cell-laden agarose matrix (2% w/w) to develop a microfluidic platform able to generate gradients of compressive mechanical stimulation and multi-modal actuation patterns on an engineered tissue [57]. The monolithic platform was characterized by a vertical PDMS membrane with three independent and connected chambers. All the parameters were optimized to maximize the membrane deflection under uniform compression. In a such way, both healthy and hyper-physiological mechanical stimulation of the articular cartilage were simulated. Chondrocytes cultured in

the device in agarose remained viable under both static and healthy dynamic conditions, while hyper-physiological stimulation led to cell membrane rupture and possibly cell death. As such, the platform revealed to be important for screening the effect of various strain levels on cells, with real-time observation of the cell response.

However, apart from mechanical properties, there are many factors such as storage and loss moduli, viscosity and injection force, to be taken into account when evaluating biomaterials for such applications. For this reason, the knowledge of the rheological properties of the biomaterials is fundamental to proper design the product and tailor its properties for the required application. Rheology is an important tool that can be employed to quantitatively assess parameters such as viscosity and storage and loss moduli, which are important determinants of biomaterials' injectability. In particular, storage and loss moduli provide information about the elastic and viscous response behaviours of the biomaterial, respectively, in response to oscillatory shear. This information is relevant to better understand the behaviour during the injection process. Viscosity is a direct measurement of the ability of a material to resist deformation in response to stress, and to respond to changes in shear stress during injection. Biomaterials for cell support should be characterized by a shear thinning behaviour as result of their

polymer chain structure, which highlights the non-Newtonian behaviour of fluids whose viscosity decreases under shear strain. Although material properties such as storage modulus, loss modulus and viscosity, are important for determining injectability, injection force determines whether a material is relevant for injection. The term injectability refers to the needed force to expel syringe contents. Different controlled methods to measure injection force, such as a force sensor or a material testing machine, have been settled down to compare quantitatively the injectability of various biomaterials formulations [103]. However, until now these aspects are barely taken into consideration when new microfluidic platforms are developed.

5. Natural and synthetic polymers from single tissues to tissue complexity

While developing in vitro models for musculoskeletal tissues, it is essential to take into account the complexity of the tissues. Indeed, a single formulation of natural polymer cannot ensure a 3D matrix that perfectly mimics the different features of the tissues. However, the complexity can be achieved, for example, i) by embedding an inorganic component, ii) by reproducing the exact cell interactions within a tissue, including the microvascular networks, iii) by blending different polymeric materials,

synthetic or natural ones, iv) by modulating a number of biophysical and biochemical properties, to produce the so-called gradient hydrogels (Figure 4).

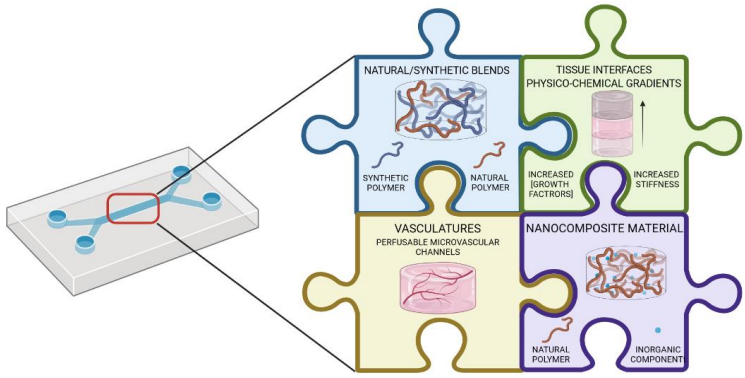

Figure 4 – Resembling tissue complexity in a musculoskeletal tissue-on-a-chip

5.1 Natural/Synthetic polymeric blends

Over the last years, synthetic hydrogels have shown several advantages over natural hydrogels, such as the tuning of the mechanical properties by controlling the crosslinking density, as well as the morphological and chemical compositions. However, they cannot provide an ideal environment to support cell adhesion and tissue formation due to their bio-inert nature. Indeed, these polymers from the biological standpoint lack much desired bioactivity and biocompatibility and may cause toxicity and immune response.

Polyethylene (glycol) remains one of the most used materials because its mechanical properties can be systematically adjusted not only by the precursor molecular weight and concentration

but also by specific chemical groups suitable grafted to the backbone [104]. Occhetta et al. employed, for their cartilage on a chip model, eight-arm PEG vinylsulfone functionalized with peptides containing either an FXIII glutamine acceptor substrate or an MMP-degradable FXIII lysine donor substrate [105]. As stated before, the native chondrocytes are subjected to a variety of mechanical stimuli, which are difficult to recapitulate in vitro. For instance, in this model, a Young's modulus of 0.1 MPa was considered. The system successfully elicited the acquisition of osteoarthritic traits by the newly formed cartilaginous tissue, through the sole imposition of a hyperphysiological mechanical stimulation. Indeed, the authors demonstrated the possibility of obtaining a stable and highly reproducible model and eliciting a biological response to mechanical overload that correlates with key traits triggered during osteoarthritis onset.

Lee et al. used a synthetic polymer, poly(D,L-lactic-co-glycolic) acid (PLGA) acid matrix, for their microfluidic 3D bone tissue model [106]. The authors used the model to evaluate the efficacy of biomaterials aimed at accelerating orthopaedic implant-related wound healing while preventing bacterial infection.

Considering the ECM as the model for the design and fabrication of bioactive hydrogels, ECM-mimetic modification of synthetic hydrogels is emerging as an important strategy to modulate specific cellular responses. In this scenario, to tether ECM-

derived bioactive molecules to synthetic hydrogels, various strategies could be developed for the incorporation of key ECM biofunctions, such as specific cell adhesion, proteolytic degradation, and signal molecule-binding.

Table 3 – Examples of synthetic polymers in musculoskeletal in vitro microfluidic models

Author, year	Tissue	Application	Device Structure	3D matrix composition	3D Matrix Gelation	Cells Embedded	Main Outcome
Occhetta, 2019 [115]	Cartilage	Drug screening	Separated top and bottom PDMS layers with 2 rows of posts delimiting culture channel	8-arm PEG vinylsulfone (40kDa) with peptides (FXIII glutamine acceptor substrate or MMP-degradable FXIII lysine donor substrate	Enzymatic crosslinking (10U/mL FXIII)	Human articular chondrocytes ($5x10^7$cells/mL)	Generation of articular cartilage constructs; Induction of osteoarthritic traits by imposition of hyperphysiological mechanical stimulation (30% confined compression)
Hosseinzadeh, 2018 [114]	Muscle	Scaffolds synthesis under multiple non-parallel steps	2 inlets connected and 1 outlet for each channel	PAA hydrogel/PANI nanofibers	Chemical Crosslinking: MBAA (0.006mol%)	Satellite cells	3D cell network formation on PAA–PANI hydrogel; stable thermal condition; reduction of mechanical stress to 0; Expression of muscle proteins by cultured satellite cells

Polydimethylsiloxane (PDMS), Poly(D,L-lactic-co-glycolic) acid (PLGA), calcium phosphate (CaP), polyethylene (glycol) (PEG), matrix metalloproteinases (MMP), polyacrylic acid (PAA), polyaniline (PANI), N,N0-methylenebisacrylamide (MBAA), Mouse calvarial preosteoblast cells (MC3T3-E1).

6. Conclusion and future perspectives

Over the past years, the interest in organ-on-a-chip technology has incredibly intensified. Through a combination of cell biology and engineering, it has the potential to elucidate cellular mechanisms and replicate tissue functions reducing the costs of in vitro tests used to study tissue models [107]. Furthermore, with this technology it is possible to predict the tissue response to an array of different stimuli including drug and environmental effects. As more sophisticated microfluidic systems will be developed, increased emphasis should also be placed on

biomaterial science, which could open new perspectives in this field. Indeed, the introduction of a polymeric matrix that helps mimicking the extracellular microenvironment must be considered a key step of paramount importance in the development of a functional in vitro model. Despite the many advantages of natural polymers employed as hydrogels for tissue engineering applications, some drawbacks for their use in microfluidic devices still exist and these are mainly associated with their biodegradability, batch to batch variability, lack of standardization. Additional technical limitations include bubble formation and inherent difficulties with injectability of cell-laden hydrogels in microfluidic channels prior to polymerization. Lastly, the length of culture time for 3D cell populations has yet to be optimized for the microfluidic devices. However, natural polymers offer the possibility to fine tune different parameters such as swelling ratio, pore size, cell seeding, crosslinking densities and mechanical properties. Introducing alternative crosslinking strategies to both the widely used enzymatic crosslinking of fibrin and the thermal gelation of collagen could be an interesting strategy. The photo-crosslinking mechanism, for example, has been introduced only in a couple of microfluidic devices, despite the fast and tunable gelation time and hydrogel stiffness. Furthermore, even though many advancements have been made in terms of cellular complexity within microfluidic in

vitro systems, there are still some unexplored possibilities in terms of 3D matrix complexity. Indeed, a higher level of complexity of the in vitro model could be achieved by combining natural and synthetic polymers in blends leading to the enhancement of hydrogel mechanical properties. Bearing these aspects in mind, a lot needs to be done as also highlighted in the last paragraphs.

The aim of this review was to investigate the state of art regarding the use of biomaterials, in particular natural polymers, as support matrix in microfluidic technology. To the best of the authors' knowledge, it is the first attempt in analysing a possible synergic combination of microfluidic and biomaterial science. The authors' hope is that this work will guide future research which will capitalize on the potential of biomaterial science looking towards alternative biomaterials systems, promising crosslinking strategies and innovative tissue engineered-inspired approaches that could be employed in this field of interest.

References

[1] S.H. Park, W.Y. Sim, B.H. Min, S.S. Yang, A. Khademhosseini, D.L. Kaplan, Chip-Based Comparison of the Osteogenesis of Human Bone Marrow- and Adipose Tissue-Derived Mesenchymal Stem Cells under Mechanical Stimulation, PLoS One. 7 (2012) 1–11. https://doi.org/10.1371/journal.pone.0046689.

[2] L.G. Griffith, M.A. Swartz, Capturing complex 3D tissue physiology in vitro, Nat. Rev. Mol. Cell Biol. 7 (2006) 211–224. https://doi.org/10.1038/nrm1858.

[3] S.R. Caliari, J.A. Burdick, A practical guide to hydrogels for cell culture, Nat. Methods 2016 135. 13 (2016) 405–414. https://doi.org/10.1038/nmeth.3839.
[4] M.G. Raucci, U. D'Amora, A. Ronca, L. Ambrosio, Injectable Functional Biomaterials for Minimally Invasive Surgery, Adv. Healthc. Mater. 9 (2020) 2000349. https://doi.org/10.1002/adhm.202000349.
[5] P. Ertl, Recent Advances of Biologically Inspired 3D Microfluidic Hydrogel Cell Culture Systems, Cell Biol. Cell Metab. 2 (2015) 1–14. https://doi.org/10.24966/cbcm-1943/100005.
[6] K. Aizel, A.G. Clark, A. Simon, S. Geraldo, A. Funfak, P. Vargas, J. Bibette, D.M. Vignjevic, N. Bremond, A tuneable microfluidic system for long duration chemotaxis experiments in a 3D collagen matrix, Lab Chip. 17 (2017) 3851–3861. https://doi.org/10.1039/c7lc00649g.
[7] G.S. Jeong, G.H. Kwon, A.R. Kang, B.Y. Jung, Y. Park, S. Chung, S.H. Lee, Microfluidic assay of endothelial cell migration in 3D interpenetrating polymer semi-network HA-Collagen hydrogel, Biomed. Microdevices. 13 (2011) 717–723. https://doi.org/10.1007/s10544-011-9541-7.
[8] Y.S. Torisawa, C.S. Spina, T. Mammoto, A. Mammoto, J.C. Weaver, T. Tat, J.J. Collins, D.E. Ingber, Bone marrow-on-a-chip replicates hematopoietic niche physiology in vitro, Nat. Methods. 11 (2014) 663–669. https://doi.org/10.1038/nmeth.2938.
[9] D.I. Silva, B.P. dos Santos, J. Leng, H. Oliveira, J. Amédée, Dorsal root ganglion neurons regulate the transcriptional and translational programs of osteoblast differentiation in a microfluidic platform, Cell Death Dis. 8 (2017). https://doi.org/10.1038/S41419-017-0034-3.
[10] F. MM, D. RE, H. SC, Microfluidic analysis of extracellular matrix-bFGF crosstalk on primary human myoblast chemoproliferation, chemokinesis, and chemotaxis, Integr. Biol. (Camb). 7 (2015) 569–579. https://doi.org/10.1039/C5IB00060B.
[11] S. Bersini, C. Arrigoni, S. Lopa, M. Bongio, I. Martin, M. Moretti, Engineered miniaturized models of musculoskeletal diseases, Drug Discov. Today. 21 (2016) 1429–1436. https://doi.org/10.1016/j.drudis.2016.04.015.
[12] C. Arrigoni, S. Lopa, C. Candrian, M. Moretti, Organs-on-a-chip as model systems for multifactorial musculoskeletal diseases, Curr. Opin. Biotechnol. 63 (2020) 79–88. https://doi.org/10.1016/j.copbio.2019.12.006.
[13] K.H. Benam, S. Dauth, B. Hassell, A. Herland, A. Jain, K.-J. Jang, K. Karalis, H.J. Kim, L. MacQueen, R. Mahmoodian, S. Musah, Y. Torisawa, A.D. van der Meer, R. Villenave, M. Yadid, K.K. Parker, D.E. Ingber, Engineered in vitro disease models., Annu. Rev. Pathol. 10 (2015) 195–262. https://doi.org/10.1146/annurev-pathol-012414-040418.
[14] D.K. Temple, A.A. Cederlund, B.M. Lawless, R.M. Aspden, D.M. Espino, Viscoelastic properties of human and bovine articular cartilage: a comparison of frequency-dependent trends, BMC Musculoskelet. Disord. 17 (2016) 1–8. https://doi.org/10.1186/s12891-016-1279-1.

[15] Z. Izadifar, X. Chen, W. Kulyk, Strategic Design and Fabrication of Engineered Scaffolds for Articular Cartilage Repair, J. Funct. Biomater. 3 (2012) 799–838. https://doi.org/10.3390/jfb3040799.
[16] T.M. Tamer, Hyaluronan and synovial joint: Function, distribution and healing, Interdiscip. Toxicol. 6 (2013) 111–125. https://doi.org/10.2478/intox-2013-0019.
[17] Y. Gao, S. Liu, J. Huang, W. Guo, J. Chen, L. Zhang, B. Zhao, J. Peng, A. Wang, Y. Wang, W. Xu, S. Lu, M. Yuan, Q. Guo, The ECM-cell interaction of cartilage extracellular matrix on chondrocytes, Biomed Res. Int. 2014 (2014). https://doi.org/10.1155/2014/648459.
[18] C. Gentili/snm, >, R. Cancedda, Cartilage and Bone Extracellular Matrix, Curr. Pharm. Des. 15 (2009) 1334–1348. https://doi.org/10.2174/138161209787846739.
[19] A.J. Sophia Fox, A. Bedi, S.A. Rodeo, The basic science of articular cartilage: Structure, composition, and function, Sports Health. 1 (2009) 461–468. https://doi.org/10.1177/1941738109350438.
[20] T. Iwanaga, M. Shikichi, H. Kitamura, H. Yanase, K. Nozawa-Inoue, Morphology and functional roles of synoviocytes in the joint, Arch. Histol. Cytol. 63 (2000) 17–31. https://doi.org/10.1679/aohc.63.17.
[21] P.A. Revell, N. Al-Saffar, S. Fish, D. Osei, Extracellular matrix of the synovial intimal cell layer, in: Ann. Rheum. Dis., BMJ Publishing Group, 1995: pp. 404–407. https://doi.org/10.1136/ard.54.5.404.
[22] A. Bhatia, S. Blades, G. Cambridge, J.C.W. Edwards, Differential distribution of FcγRIIIa in normal human tissues and co- localization with DAF and fibrillin-1: Implications for immunological microenvironments, Immunology. 94 (1998) 56–63. https://doi.org/10.1046/j.1365-2567.1998.00491.x.
[23] M.D. Smith, E. Barg, H. Weedon, V. Papengelis, T. Smeets, P.P. Tak, M. Kraan, M. Coleman, M.J. Ahern, Microarchitecture and protective mechanisms in synovial tissue from clinically and arthroscopically normal knee joints, Ann. Rheum. Dis. 62 (2003) 303–307. https://doi.org/10.1136/ard.62.4.303.
[24] L.S. Wilkinson, A.A. Pitsillides, J.G. Worrall, J.C.W. Edwards, Light microscopic characterization of the fibroblast-like synovial intimal cell (synoviocyte), Arthritis Rheum. 35 (1992) 1179–1184. https://doi.org/10.1002/art.1780351010.
[25] P.C. Seller, D. Dowson, V. Wright, The rheology of synovial fluid, Rheol. Acta. 10 (1971) 2–7. https://doi.org/10.1007/BF01972469.
[26] T.F. Novacheck, The biomechanics of running, Gait Posture. 7 (1998) 77–95. https://doi.org/10.1016/S0966-6362(97)00038-6.
[27] L. Martin-Alarcon, T.A. Schmidt, Rheological effects of macromolecular interactions in synovial fluid, Biorheology. 53 (2016) 49–67. https://doi.org/10.3233/BIR-15104.
[28] S. Al-Assaf, J. Meadows, G.O. Phillips, P.A. Williams, The application of shear and extensional viscosity measurements to assess the potential of hylan

in viscosupplementation, Biorheology. 33 (1996) 319–332. https://doi.org/10.1016/0006-355X(96)00025-X.
[29] J. Schurz, V. Ribitsch, Rheology of synovial fluid, Biorheology. 24 (1987) 385–399. https://doi.org/10.3233/bir-1987-24404.
[30] A.Ö. Bingöl, D. Lohmann, K. Püschel, W.M. Kulicke, Characterization and comparison of shear and extensional flow of sodium hyaluronate and human synovial fluid, Biorheology. 47 (2010) 205–224. https://doi.org/10.3233/BIR-2010-0572.
[31] M.K. Cowman, T.A. Schmidt, P. Raghavan, A. Stecco, Viscoelastic Properties of Hyaluronan in Physiological Conditions, F1000Research. 4 (2015). https://doi.org/10.12688/f1000research.6885.1.
[32] M.K. Cowman, S. Matsuoka, Experimental approaches to hyaluronan structure, Carbohydr. Res. 340 (2005) 791–809. https://doi.org/10.1016/j.carres.2005.01.022.
[33] V. Tirtaatmadja, D. V Boger, J.R.E. Fraser, The dynamic and steady shear properties of synovial fluid and of the components making up synovial fluid, Rheol. Acta. 23 (1984) 311–321. https://doi.org/10.1007/BF01332196.
[34] G.D. Jay, J.R. Torres, M.L. Warman, M.C. Laderer, K.S. Breuer, The role of lubricin in the mechanical behavior of synovial fluid, Proc. Natl. Acad. Sci. U. S. A. 104 (2007) 6194–6199. https://doi.org/10.1073/pnas.0608558104.
[35] T. Le Bao Ha, T. Minh, D. Nguyen, D. Minh, Naturally Derived Biomaterials: Preparation and Application, in: Regen. Med. Tissue Eng., InTech, 2013. https://doi.org/10.5772/55668.
[36] M.C. Catoira, L. Fusaro, D. Di Francesco, M. Ramella, F. Boccafoschi, Overview of natural hydrogels for regenerative medicine applications, J. Mater. Sci. Mater. Med. 30 (2019) 1–10. https://doi.org/10.1007/s10856-019-6318-7.
[37] G. Talò, D. D'Arrigo, S. Lorenzi, M. Moretti, A.B. Lovati, Independent, Controllable Stretch-Perfusion Bioreactor Chambers to Functionalize Cell-Seeded Decellularized Tendons, Ann. Biomed. Eng. 2019 483. 48 (2019) 1112–1126. https://doi.org/10.1007/S10439-019-02257-6.
[38] Lh. Yahia, N. Chirani, L. Gritsch, F.L. Motta, SoumiaChirani, S. Fare, History and Applications of Hydrogels, J. Biomed. Sci. 4 (2015). https://doi.org/10.4172/2254-609X.100013.
[39] N.K. Karamanos, A.D. Theocharis, Z. Piperigkou, D. Manou, A. Passi, S.S. Skandalis, D.H. Vynios, V. Orian-Rousseau, S. Ricard-Blum, C.E.H. Schmelzer, L. Duca, M. Durbeej, N.A. Afratis, L. Troeberg, M. Franchi, V. Masola, M. Onisto, A guide to the composition and functions of the extracellular matrix, FEBS J. (2021). https://doi.org/10.1111/FEBS.15776.
[40] E. Tous, B. Purcell, J.L. Ifkovits, J.A. Burdick, Injectable acellular hydrogels for cardiac repair, J. Cardiovasc. Transl. Res. 4 (2011) 528–542. https://doi.org/10.1007/s12265-011-9291-1.
[41] Y. Li, H. Meng, Y. Liu, B.P. Lee, Fibrin gel as an injectable biodegradable scaffold and cell carrier for tissue engineering, Sci. World J. 2015 (2015). https://doi.org/10.1155/2015/685690.

[42] A. Noori, S.J. Ashrafi, R. Vaez-Ghaemi, A. Hatamian-Zaremi, T.J. Webster, A review of fibrin and fibrin composites for bone tissue engineering, Int. J. Nanomedicine. 12 (2017) 4937. https://doi.org/10.2147/IJN.S124671.
[43] D. D, D.G. A, M. L, P. A, F. G, S. C, D. C, P. GM, Fibrin-based model for cartilage regeneration: tissue maturation from in vitro to in vivo, Tissue Eng. Part A. 18 (2012) 1109–1122. https://doi.org/10.1089/TEN.TEA.2011.0272.
[44] T.C. Laurent, J.R.E. Fraser, Hyaluronan 1, FASEB J. 6 (1992) 2397–2404. https://doi.org/10.1096/fasebj.6.7.1563592.
[45] Biomaterials from Chemically-Modified Hyaluronan, (n.d.). https://www.glycoforum.gr.jp/article/05A4.html (accessed April 26, 2021).
[46] J.A. Burdick, G.D. Prestwich, Hyaluronic acid hydrogels for biomedical applications, Adv. Mater. 23 (2011) H41. https://doi.org/10.1002/adma.201003963.
[47] C.E. Schanté, G. Zuber, C. Herlin, T.F. Vandamme, Chemical modifications of hyaluronic acid for the synthesis of derivatives for a broad range of biomedical applications, Carbohydr. Polym. 85 (2011) 469–489. https://doi.org/10.1016/j.carbpol.2011.03.019.
[48] C. Chung, J. Mesa, M.A. Randolph, M. Yaremchuk, J.A. Burdick, Influence of gel properties on neocartilage formation by auricular chondrocytes photoencapsulated in hyaluronic acid networks, J. Biomed. Mater. Res. - Part A. 77 (2006) 518–525. https://doi.org/10.1002/jbm.a.30660.
[49] H. Tan, C.R. Chu, K.A. Payne, K.G. Marra, Injectable in situ forming biodegradable chitosan-hyaluronic acid based hydrogels for cartilage tissue engineering, Biomaterials. 30 (2009) 2499–2506. https://doi.org/10.1016/j.biomaterials.2008.12.080.
[50] L. Kenne, S. Gohil, E.M. Nilsson, A. Karlsson, D. Ericsson, A. Helander Kenne, L.I. Nord, Modification and cross-linking parameters in hyaluronic acid hydrogels - Definitions and analytical methods, Carbohydr. Polym. 91 (2013) 410–418. https://doi.org/10.1016/j.carbpol.2012.08.066.
[51] S. Khunmanee, Y. Jeong, H. Park, Crosslinking method of hyaluronic-based hydrogel for biomedical applications, J. Tissue Eng. 8 (2017). https://doi.org/10.1177/2041731417726464.
[52] T. Segura, B.C. Anderson, P.H. Chung, R.E. Webber, K.R. Shull, L.D. Shea, Crosslinked hyaluronic acid hydrogels: A strategy to functionalize and pattern, Biomaterials. 26 (2005) 359–371. https://doi.org/10.1016/j.biomaterials.2004.02.067.
[53] K.I.W. Kane, E. Lucumi Moreno, C.M. Lehr, S. Hachi, R. Dannert, R. Sanctuary, C. Wagner, R.M.T. Fleming, J. Baller, Determination of the rheological properties of Matrigel for optimum seeding conditions in microfluidic cell cultures, AIP Adv. 8 (2018) 125332. https://doi.org/10.1063/1.5067382.
[54] T. DA, S. LC, F. Z, G. AS, T. LJ, Decellularized matrices in regenerative medicine, Acta Biomater. 74 (2018) 74–89. https://doi.org/10.1016/J.ACTBIO.2018.04.044.

[55] A. Marturano-Kruik, M.M. Nava, K. Yeager, A. Chramiec, L. Hao, S. Robinson, E. Guo, M.T. Raimondi, G. Vunjak-Novakovic, Human bone perivascular niche-on-a-chip for studying metastatic colonization, Proc. Natl. Acad. Sci. U. S. A. 115 (2018) 1256–1261. https://doi.org/10.1073/pnas.1714282115.
[56] T. Hoshiba, G. Chen, C. Endo, H. Maruyama, M. Wakui, E. Nemoto, N. Kawazoe, M. Tanaka, Decellularized Extracellular Matrix as an In Vitro Model to Study the Comprehensive Roles of the ECM in Stem Cell Differentiation, Stem Cells Int. 2016 (2016). https://doi.org/10.1155/2016/6397820.
[57] C. Paggi, B. Venzac, J. Leijten, L.M.T. Leijten, S. Le Gac, M. Karperien, Cartilage-on-chip: a multi-modal platform to study human chondrocyte's response to mechanical stimuli, Osteoarthr. Cartil. 28 (2020) S176--S177. https://doi.org/10.1016/J.JOCA.2020.02.287.
[58] M.A. Salati, J. Khazai, A.M. Tahmuri, A. Samadi, A. Taghizadeh, M. Taghizadeh, P. Zarrintaj, J.D. Ramsey, S. Habibzadeh, F. Seidi, M.R. Saeb, M. Mozafari, Agarose-Based biomaterials: Opportunities and challenges in cartilage tissue engineering, Polymers (Basel). 12 (2020). https://doi.org/10.3390/POLYM12051150.
[59] K.Y. Lee, D.J. Mooney, Alginate: Properties and biomedical applications, Prog. Polym. Sci. 37 (2012) 106–126. https://doi.org/10.1016/j.progpolymsci.2011.06.003.
[60] L.E. Agibayeva, D.B. Kaldybekov, N.N. Porfiryeva, V.R. Garipova, R.A. Mangazbayeva, R.I. Moustafine, I.I. Semina, G.A. Mun, S.E. Kudaibergenov, V. V Khutoryanskiy, Gellan gum and its methacrylated derivatives as in situ gelling mucoadhesive formulations of pilocarpine: In vitro and in vivo studies, Int. J. Pharm. 577 (2020) 119093. https://doi.org/10.1016/j.ijpharm.2020.119093.
[61] D.F. Coutinho, S. V Sant, H. Shin, J.T. Oliveira, M.E. Gomes, N.M. Neves, A. Khademhosseini, R.L. Reis, Modified Gellan Gum hydrogels with tunable physical and mechanical properties, Biomaterials. 31 (2010) 7494–7502. https://doi.org/10.1016/j.biomaterials.2010.06.035.
[62] S. Scialla, A. Barca, B. Palazzo, U. D'Amora, T. Russo, A. Gloria, R. De Santis, T. Verri, A. Sannino, L. Ambrosio, F. Gervaso, Bioactive chitosan-based scaffolds with improved properties induced by dextran-grafted nano-maghemite and l-arginine amino acid, J. Biomed. Mater. Res. Part A. 107 (2019) 1244–1252. https://doi.org/10.1002/JBM.A.36633.
[63] H.-P. Ma, X. Deng, D.-Y. Chen, D. Zhu, J.-L. Tong, T. Zhao, J.-H. Ma, Y.-Q. Liu, A microfluidic chip-based co-culture of fibroblast-like synoviocytes with osteoblasts and osteoclasts to test bone erosion and drug evaluation, R. Soc. Open Sci. 5 (2018). https://doi.org/10.1098/RSOS.180528.
[64] H. Lin, T.P. Lozito, P.G. Alexander, R. Gottardi, R.S. Tuan, Stem cell-based microphysiological osteochondral system to model tissue response to interleukin-1beta., Mol. Pharm. 11 (2014) 2203–2212. https://doi.org/10.1021/mp500136b.

[65] C. Mondadori, S. Palombella, S. Salehi, R. Visone, M. Rasponi, A. Redaelli, V. Sansone, M. Moretti, S. Lopa, Recapitulating monocyte extravasation to the synovium in an organotypic microfluidic model of the articular joint Biofabrication OPEN ACCESS RECEIVED Recapitulating monocyte extravasation to the synovium in an organotypic microfluidic model of the articul, (2021). https://doi.org/10.1088/1758-5090/ac0c5e.
[66] G. UA, C. X, K. V, U. JA, A. O, Comparison of morphology, orientation, and migration of tendon derived fibroblasts and bone marrow stromal cells on electrochemically aligned collagen constructs, J. Biomed. Mater. Res. A. 94 (2010) 1070–1079. https://doi.org/10.1002/JBM.A.32783.
[67] F.T. S, B. W, B. ER, F. P, M. A, M. C, van G. M, * Fabrication and Characterization of Biphasic Silk Fibroin Scaffolds for Tendon/Ligament-to-Bone Tissue Engineering, Tissue Eng. Part A. 23 (2017) 859–872. https://doi.org/10.1089/TEN.TEA.2016.0460.
[68] Y. JP, L. CH, J. JW, L. HJ, L. YS, K. JY, P. GY, C. JH, C. SW, Sustained Delivery of Transforming Growth Factor β1 by Use of Absorbable Alginate Scaffold Enhances Rotator Cuff Healing in a Rabbit Model, Am. J. Sports Med. 46 (2018) 1441–1450. https://doi.org/10.1177/0363546518757759.
[69] L. Ambrosio, A. Gloria, F. Causa, Composite materials for replacement of ligaments and tendons, Biomed. Compos. (2010) 234–254. https://doi.org/10.1533/9781845697372.2.234.
[70] R. N, R. R, J. Q, Crosslinking biopolymers for biomedical applications, Trends Biotechnol. 33 (2015) 362–369. https://doi.org/10.1016/J.TIBTECH.2015.03.008.
[71] T. Braschler, R. Johann, M. Heule, L. Metref, P. Renaud, Gentle cell trapping and release on a microfluidic chip by in situ alginate hydrogel formation, Lab Chip. 5 (2005) 553–559. https://doi.org/10.1039/b417604a.
[72] M.C.W. Chen, M. Gupta, K.C. Cheung, Alginate-based microfluidic system for tumor spheroid formation and anticancer agent screening, Biomed. Microdevices. 12 (2010) 647–654. https://doi.org/10.1007/s10544-010-9417-2.
[73] M. G, B. G, C. G, L. C, B.-N. F, J. D, S. S, F. S, M.-B. M, C. G, V.-B. C, Collagen Hybrid Formulations for the 3D Printing of Nanostructured Bone Scaffolds: An Optimized Genipin-Crosslinking Strategy, Nanomater. (Basel, Switzerland). 10 (2020) 1–23. https://doi.org/10.3390/NANO10091681.
[74] L. Zhang, U. D'Amora, A. Ronca, Y. Li, X. Mo, F. Zhou, M. Yuan, L. Ambrosio, J. Wu, M.G. Raucci, In vitro and in vivo biocompatibility and inflammation response of methacrylated and maleated hyaluronic acid for wound healing, RSC Adv. 10 (2020) 32183–32192. https://doi.org/10.1039/d0ra06025a.
[75] A. Ronca, U. D'Amora, M. Raucci, H. Lin, Y. Fan, X. Zhang, L. Ambrosio, A Combined Approach of Double Network Hydrogel and Nanocomposites Based on Hyaluronic Acid and Poly(ethylene glycol) Diacrylate Blend, Materials (Basel). 11 (2018) 2454. https://doi.org/10.3390/ma11122454.

[76] U. D'Amora, A. Ronca, M.G. Raucci, S.M. Dozio, H. Lin, Y. Fan, X. Zhang, L. Ambrosio, In situ sol-gel synthesis of hyaluronan derivatives bio-nanocomposite hydrogels, Regen. Biomater. 6 (2019) 249–258. https://doi.org/10.1093/rb/rbz029.
[77] U. D'Amora, A. Ronca, M.G. Raucci, H. Lin, A. Soriente, Y. Fan, X. Zhang, L. Ambrosio, Bioactive composites based on double network approach with tailored mechanical, physico-chemical, and biological features, J. Biomed. Mater. Res. - Part A. 106 (2018) 3079–3089. https://doi.org/10.1002/jbm.a.36498.
[78] D. Petta, D.W. Grijpma, M. Alini, D. Eglin, M. D'Este, Three-Dimensional Printing of a Tyramine Hyaluronan Derivative with Double Gelation Mechanism for Independent Tuning of Shear Thinning and Postprinting Curing, ACS Biomater. Sci. Eng. 4 (2018). https://doi.org/10.1021/acsbiomaterials.8b00416.
[79] D. Petta, A.R. Armiento, D. Grijpma, M. Alini, D. Eglin, M. D'Este, 3D bioprinting of a hyaluronan bioink through enzymatic-and visible light-crosslinking, Biofabrication. 10 (2018). https://doi.org/10.1088/1758-5090/aadf58.
[80] G. Agrawal, A. Aung, S. Varghese, Skeletal muscle-on-a-chip: An in vitro model to evaluate tissue formation and injury, Lab Chip. 17 (2017) 3447–3461. https://doi.org/10.1039/c7lc00512a.
[81] T. Hasenberg, S. Mühleder, A. Dotzler, S. Bauer, K. Labuda, W. Holnthoner, H. Redl, R. Lauster, U. Marx, Emulating human microcapillaries in a multi-organ-chip platform, J. Biotechnol. 216 (2015) 1–10. https://doi.org/10.1016/j.jbiotec.2015.09.038.
[82] S. YJ, H. CH, L. TY, L. L, L. TC, J. S, Y. IC, L. FH, The preparation of cell-containing microbubble scaffolds to mimic alveoli structure as a 3D drug-screening system for lung cancer, Biofabrication. 12 (2020). https://doi.org/10.1088/1758-5090/AB78EE.
[83] S. Ahadian, R. Civitarese, D. Bannerman, M.H. Mohammadi, R. Lu, E. Wang, L. Davenport-Huyer, B. Lai, B. Zhang, Y. Zhao, S. Mandla, A. Korolj, M. Radisic, Organ-On-A-Chip Platforms: A Convergence of Advanced Materials, Cells, and Microscale Technologies, Adv. Healthc. Mater. 7 (2018). https://doi.org/10.1002/adhm.201700506.
[84] M.W. Laschke, M.D. Menger, Prevascularization in tissue engineering: Current concepts and future directions, Biotechnol. Adv. 34 (2016) 112–121. https://doi.org/10.1016/j.biotechadv.2015.12.004.
[85] G.J. Meijer, J.D. de Bruijn, R. Koole, C.A. van Blitterswijk, Cell-Based Bone Tissue Engineering, PLoS Med. 4 (2007) e9. https://doi.org/10.1371/journal.pmed.0040009.
[86] E. Babaliari, G. Petekidis, M. Chatzinikolaidou, A precisely flow-controlled microfluidic system for enhanced pre-osteoblastic cell response for bone tissue engineering, Bioengineering. 5 (2018). https://doi.org/10.3390/bioengineering5030066.

[87] R.G.M. Breuls, T.U. Jiya, T.H. Smit, Scaffold Stiffness Influences Cell Behavior: Opportunities for Skeletal Tissue Engineering, Open Orthop. J. 2 (2008) 103–109. https://doi.org/10.2174/1874325000802010103.
[88] S.F. Badylak, The extracellular matrix as a scaffold for tissue reconstruction, Semin. Cell Dev. Biol. 13 (2002) 377–383. https://doi.org/10.1016/S1084952102000940.
[89] P.A. Janmey, The cytoskeleton and cell signaling: Component localization and mechanical coupling, Physiol. Rev. 78 (1998) 763–781. https://doi.org/10.1152/physrev.1998.78.3.763.
[90] E. Cukierman, R. Pankov, K.M. Yamada, Cell interactions with three-dimensional matrices, Curr. Opin. Cell Biol. 14 (2002) 633–640. https://doi.org/10.1016/S0955-0674(02)00364-2.
[91] T. Yeung, P.C. Georges, L.A. Flanagan, B. Marg, M. Ortiz, M. Funaki, N. Zahir, W. Ming, V. Weaver, P.A. Janmey, Effects of substrate stiffness on cell morphology, cytoskeletal structure, and adhesion, Cell Motil. Cytoskeleton. 60 (2005) 24–34. https://doi.org/10.1002/cm.20041.
[92] G. C, M. WA, K. S, B. CT, G. V, D. M, W. JY, Influence of type I collagen surface density on fibroblast spreading, motility, and contractility, Biophys. J. 85 (2003) 3329–3335. https://doi.org/10.1016/S0006-3495(03)74752-3.
[93] A. Engler, L. Bacakova, C. Newman, A. Hategan, M. Griffin, D. Discher, Substrate Compliance versus Ligand Density in Cell on Gel Responses, Biophys. J. 86 (2004) 617. https://doi.org/10.1016/S0006-3495(04)74140-5.
[94] X. Zhang, L. Li, C. Luo, Gel integration for microfluidic applications, Lab Chip. 16 (2016) 1757–1776. https://doi.org/10.1039/c6lc00247a.
[95] D.E. Discher, P. Janmey, Y.L. Wang, Tissue cells feel and respond to the stiffness of their substrate, Science (80-.). 310 (2005) 1139–1143. https://doi.org/10.1126/science.1116995.
[96] R.J. Pelham, Y.L. Wang, Cell locomotion and focal adhesions are regulated by substrate flexibility, Proc. Natl. Acad. Sci. U. S. A. 94 (1997) 13661–13665. https://doi.org/10.1073/pnas.94.25.13661.
[97] S.R. Peyton, A.J. Putnam, Extracellular matrix rigidity governs smooth muscle cell motility in a biphasic fashion, J. Cell. Physiol. 204 (2005) 198–209. https://doi.org/10.1002/jcp.20274.
[98] A. Khademhosseini, R. Langer, Microengineered hydrogels for tissue engineering, Biomaterials. 28 (2007) 5087–5092. https://doi.org/10.1016/j.biomaterials.2007.07.021.
[99] H. Geckil, F. Xu, X. Zhang, S. Moon, U. Demirci, Engineering hydrogels as extracellular matrix mimics, Nanomedicine. 5 (2010) 469–484. https://doi.org/10.2217/nnm.10.12.
[100] S.I. Fraley, P.H. Wu, L. He, Y. Feng, R. Krisnamurthy, G.D. Longmore, D. Wirtz, Three-dimensional matrix fiber alignment modulates cell migration and MT1-MMP utility by spatially and temporally directing protrusions, Sci. Rep. 5 (2015) 14580. https://doi.org/10.1038/srep14580.

[101] D.A. C, B. C, M. N, A. J, G.-A. JM, Quantifying 3D chemotaxis in microfluidic-based chips with step gradients of collagen hydrogel concentrations, Integr. Biol. (Camb). 9 (2017) 339–349. https://doi.org/10.1039/C7IB00022G.
[102] M.B. Chen, S. Srigunapalan, A.R. Wheeler, C.A. Simmons, A 3D microfluidic platform incorporating methacrylated gelatin hydrogels to study physiological cardiovascular cell–cell interactions, Lab Chip. 13 (2013) 2591–2598. https://doi.org/10.1039/C3LC00051F.
[103] M.H. Chen, L.L. Wang, J.J. Chung, Y.H. Kim, P. Atluri, J.A. Burdick, Methods to Assess Shear-Thinning Hydrogels for Application As Injectable Biomaterials, ACS Biomater. Sci. Eng. 3 (2017) 3146–3160. https://doi.org/10.1021/acsbiomaterials.7b00734.
[104] †,‡ Jason A. Burdick, ‡,§ and Ali Khademhosseini, †,§ Robert Langer*, Fabrication of Gradient Hydrogels Using a Microfluidics/Photopolymerization Process, Langmuir. 20 (2004) 5153–5156. https://doi.org/10.1021/LA049298N.
[105] P. Occhetta, A. Mainardi, E. Votta, Q. Vallmajo-Martin, M. Ehrbar, I. Martin, A. Barbero, M. Rasponi, Hyperphysiological compression of articular cartilage induces an osteoarthritic phenotype in a cartilage-on-a-chip model., Nat. Biomed. Eng. 3 (2019) 545–557. https://doi.org/10.1038/s41551-019-0406-3.
[106] L. AG, A. CP, B. DJ, P. SP, Development of macroporous poly(ethylene glycol) hydrogel arrays within microfluidic channels, Biomacromolecules. 11 (2010) 3316–3324. https://doi.org/10.1021/BM100792Y.
[107] K. Fetah, P. Tebon, M.J. Goudie, J. Eichenbaum, L. Ren, N. Barros, R. Nasiri, S. Ahadian, N. Ashammakhi, M.R. Dokmeci, A. Khademhosseini, The emergence of 3D bioprinting in organ-on-chip systems, Prog. Biomed. Eng. 1 (2019) 12001. https://doi.org/10.1088/2516-1091/ab23df.

Chapter 5

Development of a microfluidic OA-joint model as a screening platform for biological treatments

Development of a microfluidic OA-joint model as a screening platform for biological treatments

D'Arrigo D[1,2*], Petta D[1*], Arrigoni C[1], Talò G[1,3], Bonetti L[4], Salehi S[3], Vanoni M[2,5], Deabate L[6], De Nardo L[4], Candrian C[6,7], Lopa S[3], Moretti M[1,3,7]

1 - Regenerative Medicine Technologies Lab, Service of Orthopaedics and Traumatology, Department of Surgery, EOC, via Federico Chiesa 5, 6500 Bellinzona, Switzerland (CH)

2 - Department of Biotechnology and Bioscience, Università degli studi di Milano-Bicocca, 20126 Milan (IT)

3 - Cell and Tissue Engineering Laboratory, IRCCS Istituto Ortopedico Galeazzi, Via Riccardo Galeazzi 4, 20161 Milan, Italy (IT)

4 - Department of Chemistry, Materials and Chemical Engineering, '' G.Natta'', Politecnico di Milano, Milan, IT

5 - ISBE/SYSBIO Centre of Systems Biology, Milan, Italy (IT)

6 - Service of Orthopaedics and Traumatology, Department of Surgery, EOC, Via Tesserete 46, 6900 Lugano, Switzerland (CH)

7 - Euler Institute, Biomedical Sciences Faculty, Università della Svizzera Italiana (USI), via Buffi 13, 6900 Lugano, Switzerland (CH)

Keywords: Joint-on-a-chip, Osteoarthritis, Microfluidics, Chondrogenic matrix, Drug screening platform

Status: finalizing experimental section and preparation of the manuscript for submission

Abstract

The osteoarthritis (OA) represents the most prevalent form of arthritis and one of the leading causes of disability in the aged population. Despite its increasing incidence, the treatment of OA is still hampered by the lack of effective therapeutic approaches and preclinical models whereby new candidate therapies can be evaluated. In fact, the currently available in vitro models oversimplified the cartilaginous compartment with potential repercussion on the cell phenotype. For this reason, the first aim of this work is the development of a relevant donor-specific microfluidic model of an arthritic joint. In addition, we will also assess the potential use of this model as drug screening platform for biological treatments of OA.

To obtain a more relevant hydrogel for the chondrocytes, we tested different formulations based on hyaluronic acid and/or collagen type I and crosslinked enzymatically or via UV light, evaluating the biocompatibility and the phenotype of embedded cells. We then optimized the OA microenvironment by evaluating the effect of healthy or OA synovial fluid within the

device, and finally the anti-inflammatory capabilities of adipose and bone-marrow MSCs were assessed.

Our results showed that the enzymatically crosslinked hyaluronic acid-based hydrogel ensured a high chondrocyte viability, associated to a stronger chondrogenic phenotype. We also effectively reproduced an inflammatory microenvironment within the model upon the addition of OA synovial fluid. The donor-matched device allowed the addition, mimicking an intra-articular injection, of different MSCs and the assessment of their effect on cartilage-like and synovium-like environments.

In conclusion, we developed a relevant and donor-specific model of an arthritic joint that allows the evaluation and the comparison of different innovative biological OA treatments. This platform could be used in future as a drug screening platform for OA treatments in the context of precision medicine.

Introduction

As the most prevalent form of arthritis and the leading cause of disability in aged adults, osteoarthritis (OA) imposes a high socioeconomic burden on the healthcare system [1]. Despite various research endeavours to understand the cause and pathogenesis of OA, our insight about all aspects of the disease initiation and progression is limited. Although the most evident clinical outcome of OA is progressive articular cartilage

degeneration, other evidences such as synovial tissue inflammation and alteration in subchondral bone imply the fact that OA is a disorder of the whole joint complex [2]. Therefore, as a multifactorial disease whose exact mechanism of action is not thoroughly understood yet, the current treatments concentrate predominately on symptom suppression and pain alleviation by prescribing anti-inflammatory drugs [3]. The most recent approaches which have been put into practice attempting to recover cartilage regeneration are intraarticular injection of biologic agents such as growth factors, platelet rich plasma (PRP) [4], bone marrow aspirate concentrate, adipose-derived and bone-marrow mesenchymal stromal cells or their secretome [5]. Although the application of orthobiologics has demonstrated promising outcomes in functional improvement and symptom relief, further research is needed to determine more precisely their method of action and efficacy. Another shortcoming related to the use of biologics might also be attributed to the inconsistent and unreproducible results due to its donor dependency characteristics, culminating in lack of standard preparation and administration protocols. In this scenario, developing relevant models to study OA pathogenesis and to compare innovative therapeutics which actually counteract the disease progression is crucially needed. In this regard, animal models might sound more appealing as they provide more clinically translatable

results. However, considering the ethical issues, high cost and inherent differences with human physiology, the development of complex in vitro models which can mimic as closely as possible the in vivo microenvironment represents a reliable solution to accelerate the development of new OA treatments [6]. The currently available in vitro models have failed to recapitulate the complexity of articular joints when studying OA. This stems largely from the fact that they are often over simplified models including only one element involved in OA such as cartilage, neglecting the important role of other joint elements and the crosstalk between different cell types. Another important factor to consider when developing a reliable model of such heterogenous organs is including relevant extracellular matrix component related to each tissue present in the system. In fact, the cell behaviour can be influenced by the physical and biochemical cues that the extra cellular environment imposes [7]. This is even of greater significance when it comes to modelling the articular cartilage as it is a complex tissue with hierarchical structure made of mainly collagen, proteoglycan and hyaluronic acid [8]. Microfluidic, due to the numerous advantages it can offer, is a great means in the context of OA 3D in vitro modelling and assessing candidate therapeutics. To name a few, it allows recapitulating cell-matrix and cell-cell interactions within compartmentalized 3D microenvironment requiring minimal

number of cells and biochemical reagents [9]. Although a plethora of in vitro models of articular joints from monolayer culture to 3D multi-tissue microfluidic ones have been developed [10], few of them are organotypic models exploited to study the pathogenesis of OA and to test potential therapeutic targets. Recently, a joint-on-chip model including synovium and cartilage was developed to study the excessive monocyte extravasation in osteoarthritic conditions and potential inhibitors of the process was examined [11]. In another microfluidic model which was used as a drug screening tool, the osteochondral interface was incorporated to also include the role of subchondral bone in the pathogenesis of OA [12]. Occhetta and colleagues also offered a screening platform to examine the effect of candidate drugs currently under-investigation through a mechanically actuated cartilage-on-chip model [13].

However, within the previously developed models, the chondrocytes were cultured in hydrogels made of non-cartilaginous polymers. The adequacy of ECM surrounding cells is a crucial point especially for chondrocytes, terminally differentiated cells prone to hypertrophy and to phenotypic change [14] when cultured in standard culture systems [15]. For this reason, the development of more physiologic hydrogels would be of great importance in this field. In addition, in these

devices only chemical drugs were tested, while no platforms evaluated innovative biological approaches.

In the present study we designed a microfluid chip incorporating three main channels resembling synovial membrane, articular cartilage and the joint cavity, filled with synovial fluid. To better mimic the cartilage extracellular matrix, we compared the chondrogenic properties of hydrogels made of collagen and hyaluronic acid and their combination for the culture of chondrocytes in the model. After characterizing the hydrogels as well as the whole model, it was used to assess its potential in drug screening application. As an example, we evaluated the biological effect of two different types of mesenchymal stromal cells (MSCs), added in the model resembling an intra-articular injection, as one of the currently used treatment methods of OA [16].

Materials and methods

OA joint on chip model design and fabrication

Chip design. To reproduce the three different articular compartments, the final configuration of the chip, designed with the of CAD software (AutoCAD, AutoDesk Inc.), comprised five channels. We designed the chip to inject the syn flu the central channel, the two articular cell types in the two different flanking compartments while the culture medium in two externals (Figure

1A, C). The length of all channels was 6 mm, the height was 150 μm and the width of the two channels for the cell seeding was 1000 μm, while for the central one was 600 μm. Trapezoidal and regularly distributed posts with a width of 400 μm delimited the two cell compartments and prevented the hydrogels from leakage during the injection.

Production of the PDMS device. Firstly, we drew the master mold by CAD software that was then printed with a digital light processing (DLP) 3D printer (Asiga, Sydney, Australia) using the FREEPRINT® 385 grey liquid photopolymer (Detax), cured under light exposure following the manufacturer's instructions. Then, the microfluidic chips were fabricated by replica molding using polydimethylsiloxane (PDMS) mixed with the curing agent at a ratio of 10:1, poured on the printed molds and cured at 65°C for 2 hours. Once solidified, we used biopsy punch to form the inlets and outlets of the channels. In particular, we used a 1,4 mm punch for the three inner channels and a 4 mm puncher for the two externals. The chips were then autoclaved and allowed to dry at 65°C for at least 12 hours. Finally, the devices were bonded to glass slides (35 mm in diameter, Menzel-Gläser Braunschweig, Germany) using plasma (Harrick plasma, Ithaca, USA) and incubated overnight at 65°C (Fig 1B).

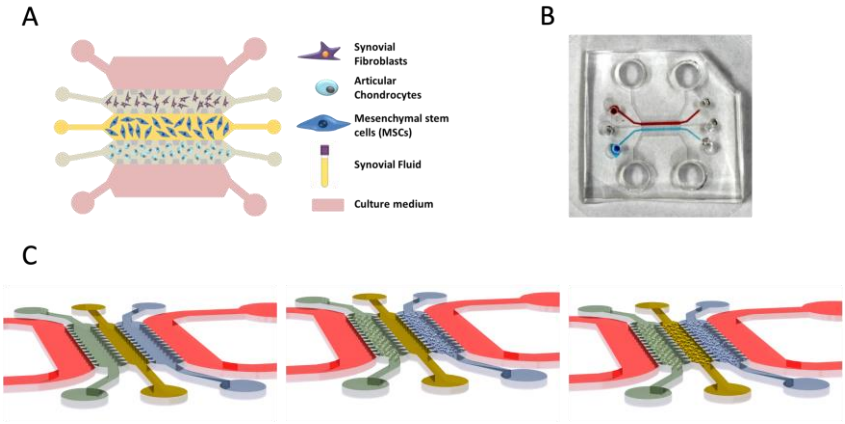

Figure 1. (A) Schematic representation of the configuration of the final device. (B) Picture of the bonded device with highlighted the compartment for the hydrogels. (C) CAD reconstruction of the three configurations of the chip: the device alone (left), with articular cells (central) and with MSCs in the central channel.

Biological samples

All the human-derived biological specimens used in this study as well as the sampling techniques were in accordance with the respective guidelines, regulations and procedures of the Ente Ospedaliero Cantonale (Bellinzona, Switzerland) and the Galeazzi Orthopaedic Institute (Milan, Italy) and were approved by the ethical committee (approval n. 2020-00029). All the biological samples were collected upon the acceptance of the informed consent from the donors.

Model development and optimization. Arthritic synovial fluid (syn flu) was collected from the knee of arthritic patients underwent total knee arthroplasty at the Regional Hospital of Lugano (Switzerland). Healthy synovial fluid was collected from an

organ donor without any previous history of OA at the Lugano hospital (male, 52 years). It was pooled with commercial healthy syn flu collected from a female donor (Articular Engineering, Northbrook, USA). Cartilage and synovial membrane samples were collected from the same four end-stage arthritic patients (2 males, 66 ± 9,9 years; 2 females, 57,5 ± 0,7 years) underwent total knee arthroplasty at the Regional Hospital of Lugano.

Patient-specific OA model. From the same donor we collected syn flu, synovial membrane and cartilage. Four arthritic patients underwent total knee arthroplasty at the Lugano Hospital were recruited: 2 males (70 ± 14,1 years) and two females (65,5 ± 13,4 years). For this model we also collected bone marrow and infrapatellar fat pad from the same four donors: 2 males (average age: 58 ± 8,5 years) and two females (average age: 59 ± 8,5 years). These donors underwent total knee arthroplasty at the Galeazzi Orthopedic Institute.

Primary cell isolation and culture

All the biological tissues, except for the bone marrow, were first mechanically digested into small pieces (~ 2 x 2 x 1 mm). Subsequently, the synovial membrane was digested with Collagenase type I (Worthington Biochemical Corporation, Lakewood, USA) at a concentration of 2.5 mg/mL in complete culture medium (chondro-CM) for 3 hours in an orbital shaker (110 rpm) at 37°C. Cartilage was treated with Collagenase type II

at a final concentration of 0,15% in chondro-CM for 22 hours, at 37°C in an orbital shaker at 110 rpm. Adipose tissue was digested at 37°C for 30 minutes with Collagenase type I diluted in MSC-CM at a final concentration of 0,075%.

The chondro-CM consisted in Dulbecco's modified Eagle medium (Gibco, ThermoFisher Scientific, Waltham, USA), 10% fetal bovine serum (FBS, Gibco, ThermoFisher Scientific), 2 mM L-glutamine, 100 U/ml penicillin, 100 μg ml−1 streptomycin, 10 mM 4-(2-hydroxyethyl)-1-piperazineethanesulfonic acid (HEPES), 1 mM sodium pyruvate (all from Gibco). Only for chondrocytes, we added TGF-β and basic-FGF at a final concentration of 1 and 5 ng/mL, respectively. The MSC-CM was made with Minimum Essential Medium Eagle - Alpha Modification (α-MEM) with the addition of the same factors used for the articular cells CM but without glutamine and sodium pyruvate. To both the MSC cell types we added basic-FGF at a final concentration of 5 ng/mL.

After the enzymatic digestion, the collagenase was inactivated in all the tissues by the addition of the same volume of the respective CM and the solution was filtered using a 100 μm cell strainer. The cells were resuspended in the respective fresh CM, plated at a density of 5000 cells/cm2 and cultured for one passage (chondrocytes) or until passage 2 (fibroblast-like synoviocytes (FLS) and ASCs) and then they were frozen and stored at -150°C.

For the pools, the chondrocytes, FLS and ASCs from the respective donors were thawed, plated and when confluent the same number of cells from each donor was pooled together and cultured until passage 3 (chondrocytes and ASCs) or 4 (FLS).
The bone marrow was centrifuged at 510g for 10 minutes at RT, washed with PBS (Gibco) and then the cells were resuspended in MSC-CM and plated. After one week, the cells were washed with PBS to remove red blood cells and we continued the culture until passage 2. The cells were then treated and pooled as previously described for ASCs.

Hydrogel selection

Synovial membrane compartment. Fibrin hydrogel is widely used in other musculoskeletal microfluidic models. Therefore, we employed this gel as the matrix for the synovial membrane compartment. 40 mg/mL of human fibrinogen (Sigma-Aldrich, St. Louis, USA) were mixed with 4 U/mL thrombin diluted in calcium chloride (40 mM, pH 7,5). at a 1:1 ratio and the gelation was achieved by incubating for 5 minutes at 37°C.

Cartilage compartment

Natural polymers that are structural components of the extracellular matrix (ECM) of native cartilage were selected as support matrix for mimicking cartilage tissue. In particular, the photocrosslinkable hyaluronic acid (HA) and collagen (Col) derivatives, namely methacrylate Hyaluronic Acid (HA-MA,

degree of methacrylation of 45-65%) and methacrylate Collagen type I (Col-MA, degree of methacrylation of 20%) were purchased from Advanced BioMatrix and were selected as 3D hydrogel network for chondrocytes encapsulation. The lyophilized Col-MA was reconstituted, as suggested by the supplier, at a concentration of 8 mg/mL by adding 20 mM acetic acid and by incubating overnight under stirring at 4°C. Instead, the HA-MA was reconstituted at 30 mg/ml and afterwards was diluted to reach a final concentration of 15 mg/mL. HA-MA was employed both as self-standing material and for generating polymeric network with Col-MA. In particular, Col-MA/HA-MA (MIX) hydrogels were obtained by mixing the two polymers at selected ratios (1:2, HA-MA 6 mg/mL and the Coll-MA 3 mg/mL, and 1:6, 2 mg/mL HA-MA and 12 mg/mL Col-MA) and by triggering the triple helix formation of Col-MA by pH neutralization and temperature (37°C) before light exposure. The final photo-crosslinking was triggered by light exposure (UV light, 365 nm, 30 mW/cm^2) and by using Lithium phenyl-2,4,6-trimethylbenzoylphosphinate (LAP) (Sigma) as photoinitiator.

Additionally, a Thiol-Modified Hyaluronan hydrogel, the Hyaluronic acid with Polyethylene (glycol) Diacrylate (PEGDA) crosslinker (HA-PEGDA) (Advanced BioMatrix) was employed. The gelation of HAPEGDA was obtained as suggested by the supplier by mixing the two components with a ratio 1:4.

Fibrin gel was selected as control matrix for the cartilage compartment. The concentration of both fibrinogen and thrombin was kept the same as the one in the synovial membrane compartment. The final concentration of cells used for each hydrogel was 1.5 M of cells/mL. These hydrogels were first tested as bulk materials outside the microfluidic device, and subsequently the more promising ones were employed in the microfluidic devices. The culture conditions and the fibrin and cell seeding density were previously optimized (Supplementary Figure 1 and 2).

Rheology

The rheological properties of the hydrogel specimens were assessed with a rotational rheometer (MCR 302, Anton Paar) equipped with a parallel plate geometry (Ø = 25 mm, working gap = 0.2 mm). Silicone oil (Sigma Aldrich, 10836) was applied to seal the plate-plate during each measurement. Table 1 resumes the tests carried out and the parameter set for each test. Shear rate sweep tests in the 0.1 – 1000 s-1 shear rate ($\dot{\gamma}$) range were carried out at 25 °C on each pre-gel formulation (i.e., prior to physical or chemical crosslinking) to assess their injectability. Then, strain sweep tests were performed on each hydrogel formulation by applying an oscillatory strain (γ) in the 0.01–100% strain range at 1 Hz frequency (ν). Strain sweep tests were carried out i) at 25 °C, ii) 37 °C, and (iii) at 37 °C after UV curing for photo-crosslinkable

gels. Such analyses allowed for the identification of the linear viscoelastic region (LVR) of each hydrogel formulation and, were applicable, the effects of physical (i.e., temperature-mediated) and chemical (i.e., UV-mediated) crosslinking.

Then, time sweep tests were performed on selected hydrogel formulations to determine the kinetics of crosslinking. Each specimen was first pre-conditioned at 25 °C for 1 min (γ = 0.5 %, ν = 1 Hz), then the temperature was raised at 37 °C (γ = 0.5 %, ν = 1 Hz) and the viscoelastic parameters (G', G'') measured, as a function of time, for 30 min.

Sample	**Shear rate sweep**	**Strain sweep**	**Time sweep**
HA-PEGDA	$\dot{\gamma}$ = 0.01 - 1000 s^{-1} T = 25 °C	(Pre-conditioning: 30 min, T= 37°C) γ = 0.01 - 100 %, ν = 1 Hz T = 37 °C	(Pre-conditioning: t = 60 s, T = 25 °C, ν = 1 Hz, γ = 0.5 %) t = 0 – 30 min, T = 37 °C, γ = 0.5 %, ν = 1 Hz
HA-MA		γ = 0.01 - 100 %, ν = 1 Hz T = 37°C, 37 °C + UV	-
MIX 1:2		γ = 0.01 - 100 %, ν = 1 Hz T = 25°C , 37 °C, 37 °C + UV	(Pre-conditioning: t = 60 s, T = 25 °C, ν = 1 Hz, γ = 0.5 %) t = 0 – 30 min, T = 37 °C, γ = 0.5 %, ν = 1 Hz
MIX 1:6			
Fibrin		γ = 0.01 - 100 %, ν = 1 Hz T = 37 °C	

Table 1 – Rheological characterization: hydrogel formulations and tests type

Evaluation of chondrocyte phenotype outside the model

To select the most promising hydrogel for the 3D culture of the chondrocytes within our model, we evaluated and compared the phenotype of the chondrocytes cultured in the previously described hydrogels. Passage 3 chondrocytes were detached and

resuspended in a HA-MA of HA-PEGDA solution. For the HA-MA hydrogels, the chips were immediately exposed to UV light for 30 seconds. For HA-PEGDA, the cells were resuspended in a solution of Glycosyl and PEGDA (at a fixed ratio of 1:4), aliquoted and added in the respective wells of a 96-well plate. The hydrogel polymerization took 30 minutes after cell seeding at 37°C. The cell seeding procedure for the Col-MA/HA-MA hydrogels was the same. The cells (1,5 M/mL) are added to the pre-polymers, the hydrogel was incubated at 37°C and then exposed to UV light for 30 seconds.

Live and Dead assay. The viability of the cells was assessed at day 1 and 10 using live/dead assay (ThermoFisher Scientific). At each time point, the fluorescent dyes, diluted in the same medium used in the culture, were added and the sample were incubated for 60 minutes in a humidified incubator (37°C, 5% CO2) protected from light to allow the diffusion of the dyes within the hydrogels. After the incubation, pictures were taken with microscope (Eclipse Ti, Nikon, Japan) equipped with a CCD camera (Nikon DS-QiMc) at magnification 4X and 10X.

Metabolic activity. The metabolic activity of the cells embedded in the hydrogels previously described was quantified after 1, 4 and 10 days of culture using the AlamarBlue assay (Invitrogen, Waltham, USA). A 10% v/v solution of AlamarBlue diluted in Chondro-CM was directly added to each well. The samples were

kept for further 4 hours in the humidified incubator (37°C, 5% CO2), protected from direct light. Finally, 100 μL of supernatant from each well were put in a 96 well-plate (Corning, Corning, USA) and the fluorescence (excitation wavelength: 560 nm, emission: 590 nm) was read using a plate reader (Infinite M Plex, Tecan, Männedorf, Switzerland).

Optimization of the hydrogels within the chip

Cell seeding. Chondrocyte and fibroblast-like synoviocytes pools were seeded within the microfluidic chip at a final density of 1,5 x 106 cells/mL. The cell density was previously optimized to prevent hydrogel degradation and the sprouting of the cells from the gel (Figure S1 and S2).

Passage 3 chondrocytes were detached and resuspended in a HA-MA of HA-PEGDA solution. For the HA-MA hydrogels, the chips were immediately exposed to UV light for 30 seconds. For HA-PEGDA, the cells were resuspended in a solution of Glycosyl and PEGDA (at a fixed ratio of 1:4), aliquoted and injected in the respective channel. Approximately, 7-8 μL of cell suspension, containing around 10.000 cells, were injected to fill the channel. The hydrogel polymerization took 30 minutes after cell seeding at 37°C.

FLS at passage 4 were resuspended in thrombin (final concentration of 2 U/mL, in CaCl2 (40 mM, pH 7.5), aliquoted, mixed with the same volume of fibrinogen (final concentration of

20 mg/mL) and the solution was injected in the respective channel of the chip. The volume of the hydrogel and the number of the injected cells was the same as for the chondrocytes. After the cell injection the chips were kept in a humidified chamber in the incubator (37°C, 5% CO2) for 5 minutes to allow the fibrin gel gelation.

When the hydrogels were polymerized, we injected 5 μL of pooled arthritic or healthy syn flu or serum-free chondrogenic medium in the central channel. Finally, we added 100 μL of the serum-free chondrogenic medium in each external channel. This medium was made of Dulbecco's modified Eagle medium (Gibco, ThermoFisher) with the addition of, 2 mM L-glutamine, 100 U/ml penicillin, 100 μg ml−1 streptomycin, 10 mM 4-(2-hydroxyethyl)-1-piperazineethanesulfonic acid (HEPES), 1% ITS+ (ThermoFisher Scientific; containing insulin, human transferrin and sodium selenite at a final concentration of 10 μg/mL, 5,5 μg/mL and 6,7 ng/mL respectively) and 1,25 mg/mL of HAS. We then moved the chips in each of a 6-well plate (Corning, Glendale, USA) and we filled with PBS the space between the wells to create a humidified chamber. The devices were cultured in incubator for 1, 4 or 10 days, changing the medium or the syn flu only at day 4, accordingly to the experimental group. For the devices in which we wanted to assess the expression of metalloproteinases (MMPs), we impeded the protein secretion by using brefeldin

(Sigma-Aldrich). Briefly, we aspirate the medium in the chips, and we injected the brefeldin, diluted at a final concentration of 1:1000 in serum-free chondrogenic medium, and we incubated for 5 hours in incubator at 37°C. After the incubation the devices were further processed for immunostaining as described below.

Cell viability. To check the viability of the cells, after 1, 4 and 10 days we performed Live and Dead assay (ThermoFisher). Briefly, we aspirated the medium from the channels and washed with PBS before adding the Live/Dead solution and incubating at RT for 10 minutes in the dark.

Cell phenotype. To check the phenotype and the expression of specific proteins, we performed immunofluorescence analysis. We fixed the chips with 4% paraformaldehyde for 10 min at RT and we blocked aspecific binding site by incubation with 1% bovine serum albumin (Sigma-Aldrich) in PBS. Then we added the following primary antibodies diluted in PBS: Anti-Collagen type 1 (1:200, ThermoFisher Scientific), Anti-Collagen type 2 (2 μg/mL, ThermoFisher Scientific), Anti-Lubricin (1:200; Invitrogen), Anti-Aggrecan (2 μg/mL, ThermoFisher Scientific), Anti-MMP-1 (1:100, Abcam, Cambridge, UK) and Anti-MMP-13 (1:200, Santa Cruz Biotechnology, Dallas, USA). After incubation of 1 hour at 37°C, the primary antibodies were washed away and the respective secondary antibody was added and incubated 1 hour at 37°C. We used anti-mouse and anti-rabbit secondary

antibodies (both at 2 μg/mL, Thermofisher). Finally, the nuclei were stained with NUCBLUE-DAPI (ThermoFisher Scientific, 8 drops/mL) for 20 minutes at room temperature and pictures were taken at the microscope (Nikon).

Patient specific OA joint on chip model

The primary chondrocytes and FLS, at passage 2 and 3 respectively, isolated from the same arthritic patient were seeded as previously described. For chondrocytes, based on the results of the optimization phase, we injected the cells only in the HA-PEGDA hydrogel. After the cell seeding, we added the patient specific syn flu in the central channel and the serum-free chondrogenic medium in the two external ones. The devices were cultured in incubator at 37°C and 5% CO2 in the humidified chambers previously described for 4 and 10 days. At day 4, we collected the medium from the two external channels of the chip for cytokine quantification. Then, fresh medium was added and the ASCs or BMSCs were injected in the central channel. Briefly, pooled BMSCs and ASCs at passage 3 were detached from the culture flasks and resuspended in the donor matched syn flu at a concentration of 1 million cells/mL and, simulating an intra-articular injection of heterologous MSCs, were injected in the central channel of the device, accordingly to the experimental groups. In the control group we injected only donor matched syn flu with no MSCs. We cultured the chips for further 6 days. On

these donor-matched models, we quantified the cytokines in the syn flu and culture medium collected on day 4 and day 10, as previously described in the “Optimization of the hydrogels within the chip” section. The samples used for this analysis were: the culture medium of the articular cells of all the donors before the seeding, culture medium of the ASCs and BMSCs, the synovial fluid of each donor and the medium collected from the chips at day 4 and 10.

Fluorescence signal quantification. The immunostaining images acquired using a Leica SP8 confocal microscope were analysed using ImageJ software where a custom macro was developed to perform different passages as described below. First of all, the images were split in the 4 channels and then for each channel, a "Z project" with max intensity projection was performed and a representative merged channels image was saved. For each projected channel a custom regulated threshold was performed, and the result was analysed with “Analyze Particles" excluding the particles smaller than 10 um^2, to count all the signal spots. The spots were then converted to a mask, that was applied to the original non-thresholded channel to evaluate the signal intensity only in the ROIs previously extracted. The nuclei were separated with the function “Whatershed” and then were automatically counted by the “Analyze Particles”. All the data were then saved in an .xls file for subsequent statistical analysis.

Cytokine quantification. To assess our device as potential screening platform for biological treatments of OA, we evaluated the secretion of inflammatory and anti-inflammatory cytokines in control conditions and in presence of BMSCs and ASCs in our donor specific OA joint on chip model. We used the Q1 Quantibody array (Ray Biotech, Peachtree Corners, USA) for the quantification of 10 human cytokines in the following samples: the culture medium of the articular cells of all the donors before the seeding, culture medium of the ASCs and BMSCs, the synovial fluid of each donor and in the medium collected from the chips at day 10. In addition, we also included in the analysis the healthy and OA syn flu and the medium collected at day 10 from the three experimental groups described in the previous section ("Optimization of the hydrogels within the chip"). Following the manufacturer's instructions, we first prepared the standard curve by serially diluting the standard provided in the kit. Then we blocked the slides for 30 minutes at RT before adding 100 µL of sample or standard in the respective wells and incubating overnight at 4°C. The slides were then washed and 80 µL of the biotinylated detection antibody cocktail was added for 2 hours at RT. Finally, the slides were incubated with 80 µL of the Cy3 equivalent dye-streptavidin for 1 hour at RT, washed and left to dry. Slides reading and data extraction were outsourced to TebuBio (France). To better visualize and compare the whole

data, they were normalized keeping as 100% the highest concentration value for each cytokine. Normalized data were then reported in a heatmap, while raw data are displayed in Figure S4 on the Supplementary material.

Statistical analysis

The results reported in this study are shown as mean ± the standard deviation (SD). We used the software Prism GraphPad Software Version 9 to perform the statistical analyses. In particular, the statistical difference was quantified by one-way ANOVA, followed by the post-hoc Tukey's multiple tests and statistical significance was defined as $p<0,05$.

Results

Characterization of the hydrogels for the chondrocyte culture

Rheological properties

Aiming at characterizing mechanical properties of the selected hydrogel formulations, we assessed the flow, strain sweep, and time sweep curves of their formations. For all the formulation tested, the viscosity decreased with the increasing of the shear rate, evidencing a shear-thinning behaviour, thus demonstrating a good injectability for all the hydrogels (Fig. 2A). Among the different samples, fibrin gel showed the highest viscosity in the

first part of the curve, while the viscosity of the HA-PEGDA was slightly lower than that of the other specimens.

Strain sweep measurements were then carried out at, according to the hydrogel formulation (Table 1), 25 °C, 37 °C, and at 37 °C after UV irradiation, with the purpose of studying the effect of physical (i.e., temperature-mediated) and chemical (i.e., UV-mediated) crosslinking on the viscoelastic behaviour of the specimens. Figure 2B reports the strain sweep curves for all the tested formulations in their functioning conditions (i.e., after crosslinking in the microfluidic device), to explore the mechanical milieu experienced by the cells. For all the samples, G' resulted almost constant at low shear strains while for higher strain values, in all the specimens (except for HA-PEGDA) the G' decreased until reaching similar of lower values than G''. On the contrary, the values of the G' and the G'' in the HA-PEGDA hydrogel were constant, with the former always higher than the latter. For the subsequent characterization, the limit of the LVR was set at γ = 0.5 % for all the specimens. As it is possible to observe from Figure 2B, the two MIX hydrogels showed similar values of G' in the VLR range and they were the highest compared to the other hydrogels. The G' of the fibrin gel, with values of about 300 Pa in the VLR, was in turn higher than that of the hydrogels made of hyaluronic acid (HA-PEGDA and HA-MA) which showed similar values of ~100 Pa.

Lastly, we performed also time sweep measurements (Fig. 2C) to follow the crosslinking kinetics in all the formulations. It was not possible to test UV-mediated crosslinking, in our experimental setup for measuring time sweep, thus HA-MA specimen was not tested, since not subjected to any crosslinking (e.g., temperature-mediated) unless UV irradiated. MIX 1:2 and MIX 1:6 displayed a fast increase in the viscoelastic parameters within 1 min, after which a plateau is reached and preserved until the end of the test. Observing the conservative moduli, MIX 1:2 presented higher values compared with MIX 1:6. Fibrin formulation showed a significative increase of the G' within the first 10 min of test. After such a rapid increase, G' displayed only a slight increase in time until the end of the test. A different behaviour was observed for the HAPEGDA formulation: initially ($t < 6$ min) the G' and G'' had similar values, while later G' significantly increased approaching a plateau by the end of the test. The significantly different time taken by HAPEGDA to reach a plateau in rheological properties during crosslinking evidence its longer crosslinking process, as compared to the other hydrogel formulations.

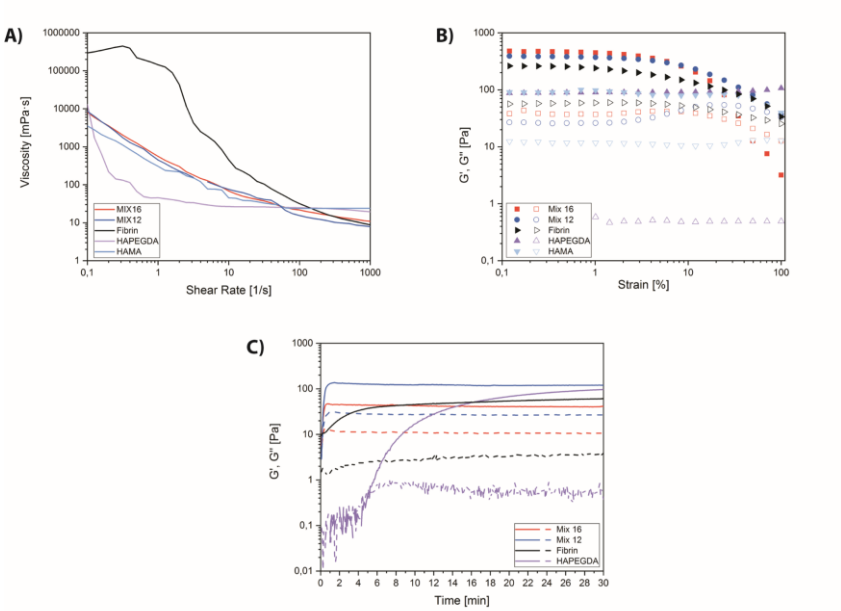

Figure 2. (A) Representative shear rate sweep tests for the pre-gel formulations. (B) Representative strain sweep tests performed on all the tested hydrogel formulations in their functioning conditions (i.e., after crosslinking in the microfluidic device). Filled symbol = G', empty symbol = G''. (C) Representative time sweep tests on selected hydrogel formulations.

Hydrogel cytocompatibility. Firstly, we assessed and compared the viability and the metabolic activity of the chondrocytes embedded within the different hydrogels at day 1, 4 and 10. As shown in Figure 3A the Live/Dead viability assay showed that the fibrin gel, assumed as control, maintained a high viability of the chondrocytes during the entire culture period. The cells cultured in the HA-PEGDA showed slightly lower values at all the time points compared to the fibrin preparation but at the end of the culture period the viability was the highest among the new

formulations (around 70%). In fact, the cell viability in the other hydrogels dropped after 10 days to value of about 60% or even lower in the MIX 1:6, while in the 1:2 Col-MA/HA-MA hydrogel this decrease was already evident after 4 days after the seeding.

The metabolic activity (Fig. 3B) of the chondrocytes cultured in the fibrin gel, assessed with Alamar blue assay, showed an alternating trend during the culture period. In fact, when compared with day 1, it increased after 4 days but then decreased at day 10 to a value that was lower than initial one. On the contrary, the metabolic activity of chondrocytes cultured in the HA-PEGDA hydrogel depicted an increasing trend during the time. It started from a lower level than that of the fibrin at day 1 but then it augmented and reached the maximum at day 10 that was similar to the day 4 of the fibrin gel. The HA-MA behaviour was similar to the HA-PEGDA: it increased over the time but with lower values than those measured with the HA-PEGDA. Finally, both the Col-MA/HA-MA mix 1:2 and 1:6 showed the same tendency over the time of the fibrin gel, but the metabolic activity of the chondrocytes resulted much lower than the all the other hydrogels, especially for the mix 1:6.

Maintenance of the correct chondrogenic phenotype. We performed an immunostaining to target the presence of Collagen type 2 (Fig 3C) and Aggrecan (Fig. 3D) at day 4, 10 and 21 to compare the chondrogenic properties of the new hydrogels. In the fibrin

hydrogel, the chondrocytes resulted negative for both the markers during time, also after 21 days from the seeding. On the contrary, cells cultured in the HA-PEGDA hydrogel showed the strongest expression of the two markers, presenting a good expression already at day 4, that further increased at day 10 and 21. The same increasing trend was observed in the other three hydrogels, though with differences. In fact, at day 10, the end of the culture period in our chip, a high number of cells resulted still negative for collagen 2, whose expression was substantially promoted only 21 days after the cell seeding. Regarding the aggrecan, the HA-PEGDA still stimulated the strongest expression, that was already detectable at day 4 and then increased over the time. The results of the HA-MA hydrogels were similar, and a good signal was observed also at day 10. On the other hand, the two mix hydrogels still allowed a lower expression of also aggrecan, even if it was higher than that of the collagen 2. Given the significantly lower viability, metabolic activity and chondrogenic capability of the HA-MA and the 1:2 and 1:6 Col-MA/HA-MA hydrogels, we decided to not include them in the following part of the optimization within the device.

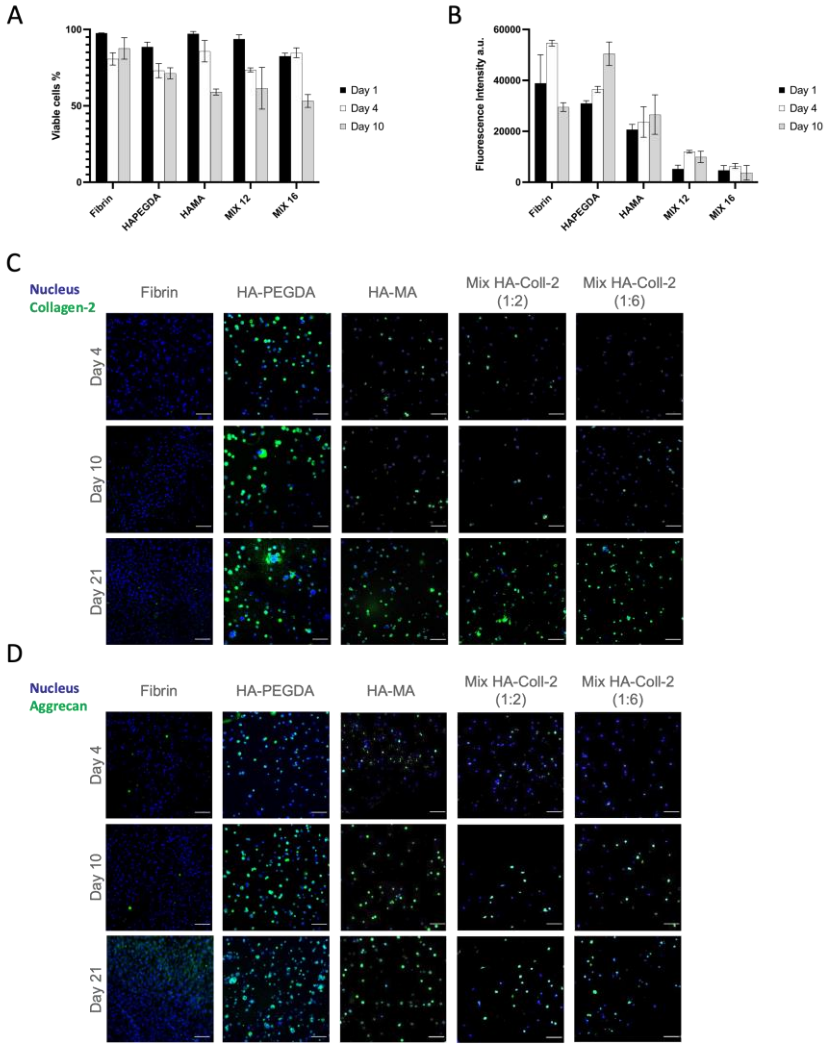

Figure 3. (A) Quantification of the number of live chondrocytes and their metabolic activity (B) upon being cultured in the different hydrogels outside the chip. Data are reported as average ± standard deviation. Expression of Collagen type II (C) and Aggrecan (D) at different time points by chondrocytes cultured in the different hydrogels. Scale bar = 100 μm

Hydrogel behaviour within the chip

The selected HA-PEGDA hydrogel for the chondrocytes, together with the fibrin gel used as standard, were then characterized within the microfluidic devices in association with FLS embedded in a fibrin gel in the other channel and synovial fluid in the central channel. We assessed the cell viability at day 1, 4 and 10 and the expression of specific markers at day 4 and 10. Regarding the FLS, the culture period did not have an effect on the viability, that resulted always higher than 80% at all the three time points and exceeded 90% at day 10 (Fig. 4A). We also found positivity for the expression of collagen type I already after 4 days from the seeding, that was maintained until the end of the culture period. Similarly, we detected also the expression of lubricin, an FLS specific marker that differentiate FLS from other fibroblast lineages [17] (Fig. 4B). In fact, already at day 4 a good percentage of the cells expressed the marker, whose expression resulted strengthened at day 10. Regarding the chondrocyte compartment, we found a decreasing trend of their viability during the time within the chip (Fig. 4C). The values in fibrin compared to those in HA-PEGDA were slightly higher at day 1 (92,6% vs 88,6%) and day 4 (79,8% vs 73,1%), whilst the difference was significant at day 10 (81,6% vs 67,1%), however being not very far from the values shown in both gels outside the chip. We performed immunostaining to confirm the phenotype of the chondrocytes cultured in the HA-PEGDA also within the device

microenvironment. Similarly to what we've seen in the culture outside the chip, the cells showed a strong and time-dependent expression of both collagen II and aggrecan, visible already after 4 days from the injection (Fig. 4D).

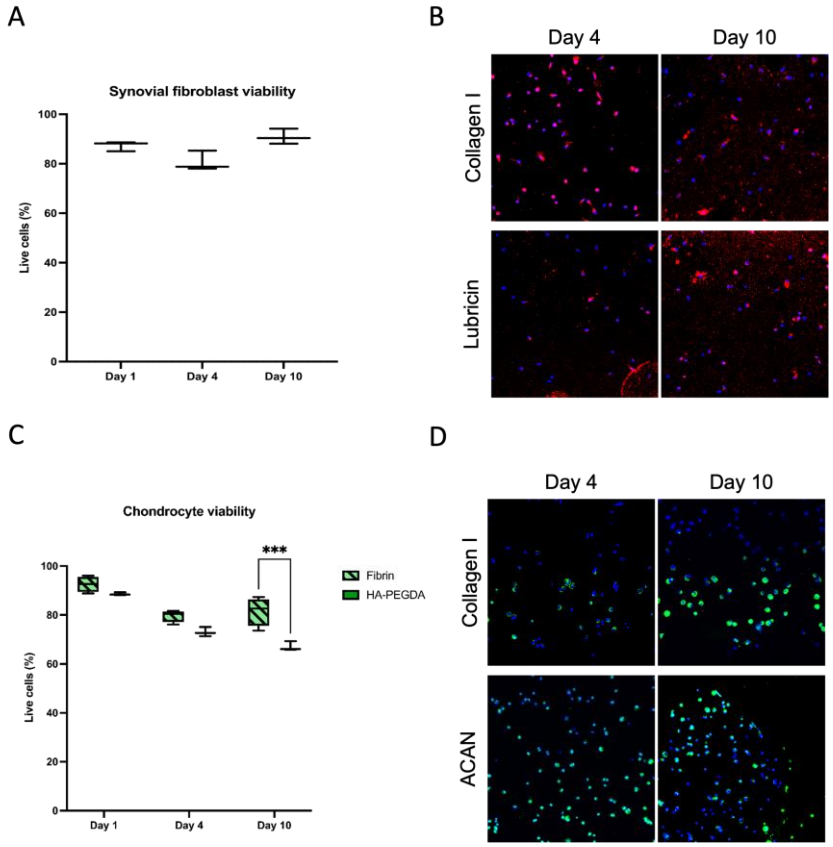

Figure 4. (A) Viability at different time points of FLS cultured in the fibrin gel within the device for up to 10 days. (B) The phenotype of the same FLS after 10 days of culture. Antibody for Collagen I was used in the upper panels, while for Lubricin in the lower ones. Nuclei are stained in blue, targets in green. (C) Viability of chondrocytes cultured in fibrin or in HA-PEGDA hydrogel within the device. Data are reported as mean ± standard deviation. Confirmation of the expression of Collagen II (upper panels) and

Aggrecan (lower panels) of the chondrocyte embedded in the HA-PEGDA within the chip. Nuclei are stained in blue, targets in green.

Optimization of the joint environment – effect of the synovial fluid

We then evaluated the effect of the synovial fluid on the articular cells in the joint on chip microenvironment. We cultured both FLS and chondrocytes in their respective hydrogels with the addition of serum-free medium, pooled healthy or arthritic Syn Flu in the central channel. We then compared among the three groups the cell viability, the cell morphology and the expression of different markers and cytokines.

Cell viability. The data reported in Figure 5A and quantified in Figure 5B, showed that the synovial fluid had in general a positive effect on the FLS viability. In fact, the number of live cells in presence of syn flu was significantly higher at day 4 as compared to control conditions with culture medium (82,6% with culture medium vs 92 and 95,9% for healthy and OA syn flu respectively). However, OA synovial fluid had a detrimental effect on FLS viability with the continuation of the culture period. In fact, 10 days after the injection viability dropped below 75%, being significantly lower than the healthy syn flu at the end of the culture, that was stable at 92,6%. With the culture medium, the cell viability remained constant at day 10 (83,2%). On the other hand, the effect of synovial fluid on chondrocytes was positive at

both time points (Fig. 5 C, D). In fact, with the addition of healthy or arthritic synovial fluid, the cell viability was significantly higher than that calculated upon the addition of the culture medium. This effect was evident at day 4 (81,6% with the medium vs. over 90% with the syn flu samples) and was even increased at day 10, when the viability with the culture medium was only 65,6% compared to the 85% and 87% in presence of healthy and OA syn flu respectively. No difference was found between the two syn flu samples, with the arthritic one that resulted slightly higher.

Cytokine quantification. To evaluate the effective establishment of an arthritic environment within our model, we quantified the concentration of 10 different cytokines at the end of the culture period. For a better comparison, we quantified the same cytokines in the healthy and arthritic syn flu used for these experiments before the injection. The normalized data, reported in Figure 5E, showed that the OA syn flu increased the secretion of all the 10 cytokines by the articular cells compared with the healthy syn flu and the medium. The MCP-1 concentration in the microfluidic model cultured in presence of OA syn flu was too high and exceeded the detection limit of the assay. On the contrary, the healthy syn flu led to cytokine secretion levels comparable to the medium, in fact only 3 cytokines (MCP-1, TNF-α, IL-10) were substantially more concentrated in the chips with

healthy syn flu. Interestingly, the differences between the arthritic and the healthy groups were not so clearly visible in the respective original syn flu samples. The raw concentration data are reported in Supplementary Figure 4.

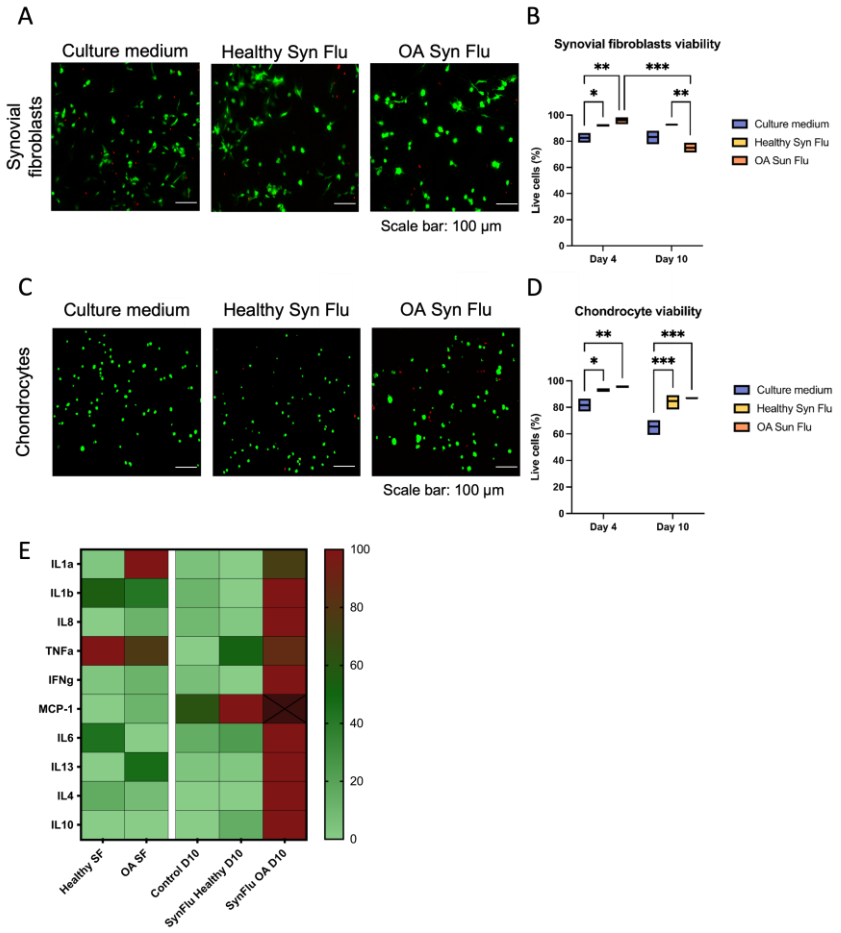

Figure 5. (A) Representative picture of the Live and Dead assay performed during the optimization of the arthritic microenvironment of the FLS and (B) the quantification of the percentage of live cells. Same analyses performed on the chondrocytes cultured in HA-PEGDA hydrogel (C, D). Heatmap reporting the normalized cytokine

concentration data. The value of MCP-1 in the syn flu sample at day 10 exceeded the detection limit of the assay.

Protein expression. To further assess the biological effects of the syn flu in our model, we also performed immunostaining for cell type-specific markers and metalloproteinases, after the inhibition of protein secretion trough brefeldin treatment, at 10 days of culture. The FLS expressed collagen type I at similar level in all three conditions, even if in the OA syn flu group, it was qualitatively lower than in the others (Fig. 6A, top row). On the contrary, we detected differences in the expression of Lubricin and MMPs. In fact, Lubricin was almost not expressed by FLS cultured with medium. Similarly to the collagen-I, the strongest expression was observed in the healthy syn flu, while with the arthritic one, a smaller number of cells expressed it (Fig. 6A, middle row). Regarding the MMPs, the worst scenario was noticed in the culture medium group: several cells resulted positive for MMP-13, while fewer cells expressed MMP-1. In addition, we also found the contemporary expression of both MMPs in some cells. In healthy syn flu group, we found a clear prevalence of the signal from MMP-1, while MMP-13 was poorly detected. In the OA syn flu, we did not observe a clear preponderance of one signal over the other (Fig. 6A, bottom row). In both the syn flu groups we detected both the signals from MMP-1 and -13 only in few cells.

Regarding the chondrocytes, the collagen type II resembled what we found in the optimization phase: a widespread and strong expression in most of the cells in all the three conditions (Fig. 6B, top row). The aggrecan seemed to be qualitatively more widely produced in the two syn flu groups, especially in the OA group (Fig. 5B, middle row). Similarly to what seen for the FLS, the culture medium determined the strongest expression of both the MMPs. However, together with the high number of cells that expressed the MMP-13, there were more cells positive for the MMP-1 than the FLS and more double positive cells. In the syn flu groups, the strongest production of MMPs was found in the OA group, with a prevalence of the MMP-13 and few cells with double positivity. On the contrary, in the healthy syn flu the expression of both the MMPs was very low and most of the cells were positive for the MMP-13 (Fig. 6B, bottom row).

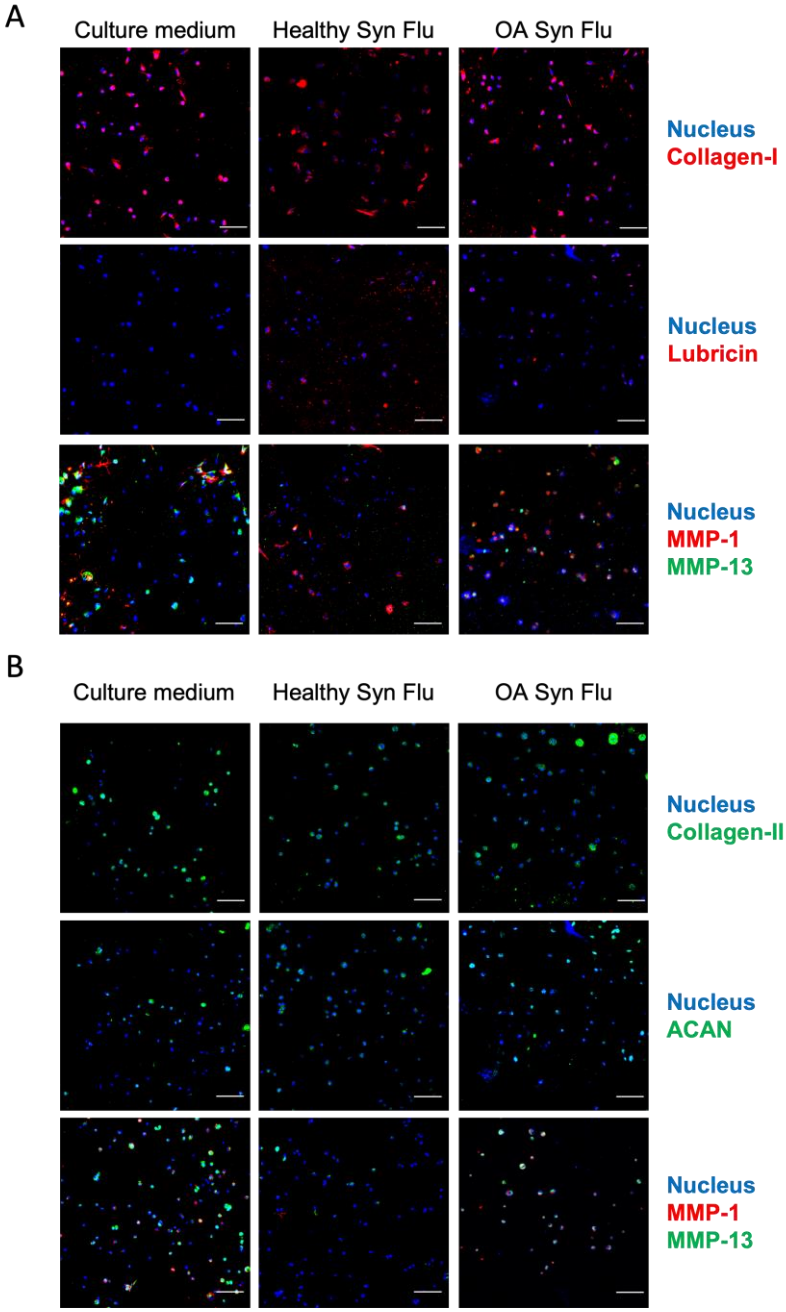

Figure 6. (A) Representative images of FLS assessing the expression of Collagen I (red, top row), Lubricin (red, central row) and MMP-1 (red) or MMP-13 (green, bottom row)

in presence of culture medium (left column), healthy (central column) or arthritic synovial fluid (right column) in the central channel. (B) Immunofluorescence analysis performed on chondrocytes to detect Collagen II (green, top row), Aggrecan (green, central row) and MMP-1 (red) or MMP-13 (green, bottom row). Nuclei are stained in blue; scale bar = 100 nm.

Donor-matched model and MSCs effect

Protein expression. As previously performed for the optimization of the arthritic microenvironment, we assessed the articular cell phenotype and their secretion of degradative enzymes in three donor-matched models. The hydrogels in the fourth donor resulted more degraded and we did not perform this analysis on these samples. For each marker, the positive area was quantified and then normalized on the number of the nuclei quantified in each picture. The FLS expressed collagen type I at similar levels, in fact we found a statistically significant increase only in the ASC group of donor 1 and in the control group of donor 2, as shown in Figure 7A. As expected, the secretion of collagen I by the chondrocytes was lower (Figure S5 A). The expression of lubricin resulted more homogeneous among all the fibroblast samples, while chondrocytes displayed more variability.

The inter-individual variability emerged also from the chondrocytes, as showed in Figure 7B. In general, they showed similar values of positive area for collagen type II and aggrecan, except for some samples, for instance the ASC group of donor 1 and the BMSC group of donor 3. As expected, the expression of

collagen type II by fibroblasts, reported in Figure S5 B, was close to zero, while that of the aggrecan was slightly higher, even if not at the chondrocyte level.

Regarding the expression of the two metalloproteinases, different trends emerged from the donors, as reported in Figure 7C-D. In fact, in donor 3 both ASCs and BMSC decreased the expression of both MMP-13 and MMP-1. On the contrary, in donor 2 we detected more positivity in the MSC groups (except for MMP1 in the chondrocytes). The values in donor 1 was almost comparable between the different samples and markers, with exception for the ASC group, that showed lower signal of MMP-13 in the chondrocytes and MMP-1 in the fibroblasts. Also in the case of MMPs, no statistical differences were found.

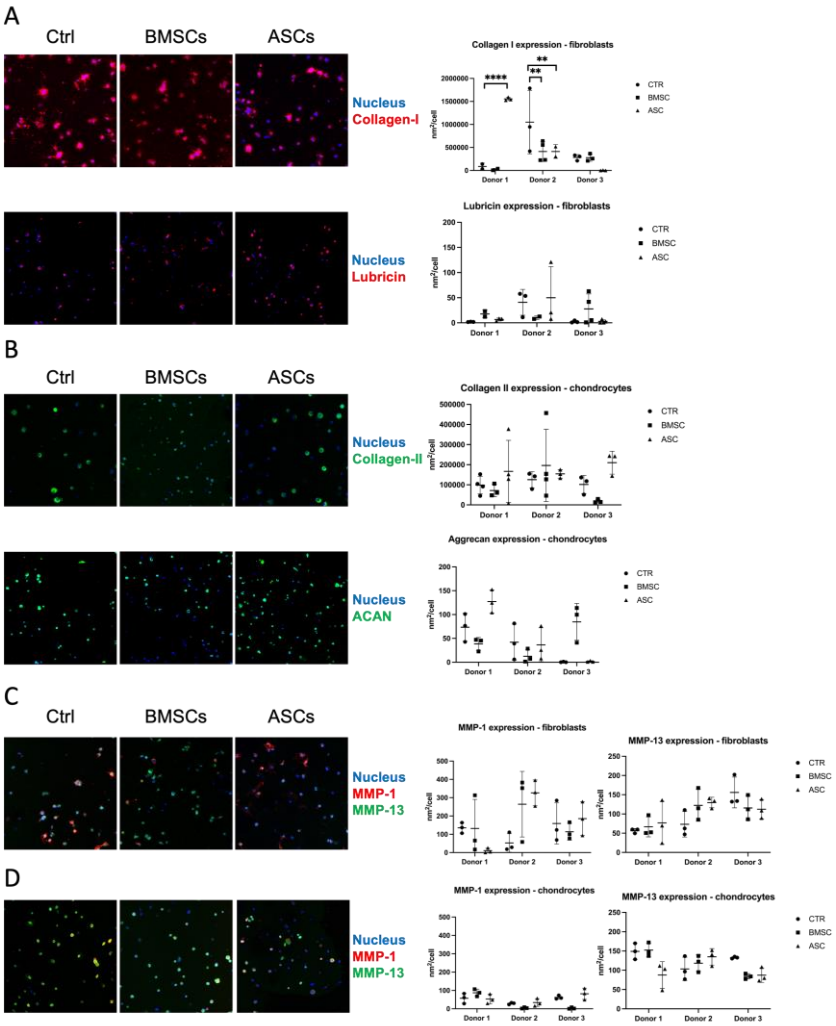

Figure 7. Representative images of immunofluorescence analysis assessing the expression of (A) Collagen I (red) and Lubricin (red) in the FLS; (B) Collagen II (green) and Aggrecan (green) in the chondrocytes; MMP-1 (red) an MMP-13 (green) in FLS (C) and in the chondrocytes (D). Alongside the pictures the quantification of the positive signal, normalized by the number of the nuclei, are reported for each marker.

Cytokine quantification. To collect quantitative data from a relatively high number of targets and considered the low volume available from the microfluidic devices, we used a multiplexed array for the quantification of the concentration of ten cytokines. In Figure 8 and 9 we reported the results related to 7 cytokines in which it was possible to outline a trend among the different donors. In general, the concentration of the pro-inflammatory cytokines (Fig. 8) in the syn flu resulted lower or comparable than that quantified in the devices. In all the four donors the concentration of IL8 resulted lower in the ASC compared to the BMSC group and the value of the ASC group were similar or slightly lower to the values of the control group and to that at day 4. The concentration of IL1ß and TNFα were instead mostly comparable among the 4 different groups from the chips and the syn flu, with few exceptions. On the contrary, MCP-1 increased between day 4 and day 10 in most of the samples. The values in both the MSCs groups were greater than the control group and the BMSC group resulted higher than ASC in donors 3 and 4 (the samples were more concentrated than the assay's detection limit).

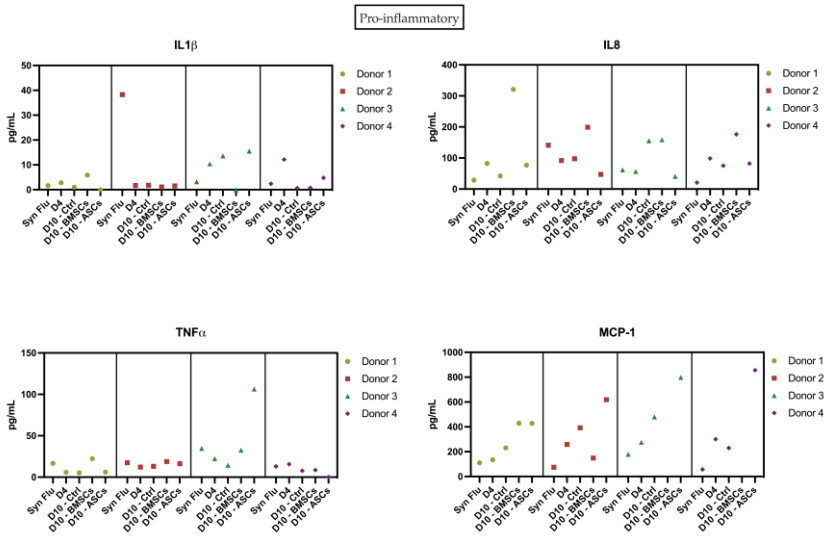

Figure 8. Quantification of 5 different pro-inflammatory cytokines (IL1ß, IL8, TNFα and MCP-1) in the synovial fluid and in the donor-matched microfluidic model at day 4 (D4) and day 10 (D10) with or without (Ctrl) the addition of BMSCs or ASCs. Data are reported as pg/mL.

Regarding the cytokines for which bot anti- and pro-inflammatory activity have been described, the concentration of IL6 in the syn flu was always smaller than that evaluated in the device, while IL13 was lower or comparable (Figure 9). Interestingly, the level of IL6 in general decreased from day 4 to day 10 in all the samples, with a greater reduction in the ASC group that showed similar values than the control group, while the concentration in the BMSC group was higher in 3 donors out of 4. The data of IL13 were more variable between day 4 and day 10 and in donors 1, 2 and 4 the ASC were lower than the BMSC. IL10, an anti-inflammatory cytokine, showed low concentration

in most of the samples. Only donor 3 had detectable amount of this cytokine and in control conditions its concentration decreased during the time compared to the syn flu. On the contrary, following the addition of mesenchymal stromal cells, it increased with the addition of BMSCs and even more with ASCs.

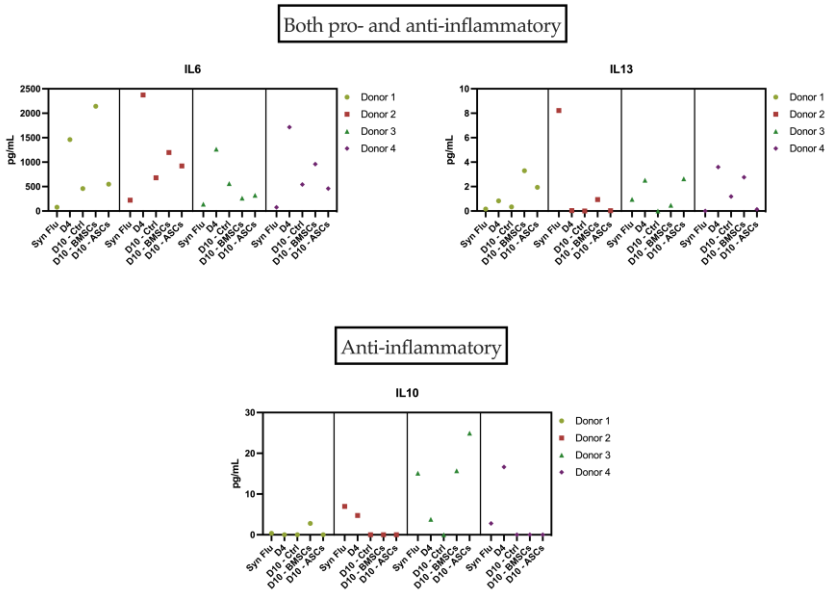

Figure 9. Quantification of cytokines with both pro- and anti-inflammatory effect (IL6 and IL13) and IL10, an anti-inflammatory cytokine. The data were assessed in the synovial fluid and in the different samples from the donor-matched device. Data are reported as pg/mL.

Since the concentration of IL1α and IFN-γ resulted highly variable while that of IL4 was not detectable in many samples, we couldn't find any trend to comment. The results of these samples are reported in Supplementary Figure 6.

Discussion

In this work we aimed at optimizing an arthritic joint on chip microfluidic model that could serve as innovative drug screening platform, with the focus to evaluate the anti-inflammatory potential of biological treatments for OA, such as MSCs. To assess the immunomodulatory capability of biological treatments, we used a five-channel microfluidic model to resemble the cartilaginous and the synovial compartment, biochemically connected by the synovial fluid. In fact, these three tissues are the most involved in the establishment and the maintenance of the positive pro-inflammatory feedback that cause the tissue degeneration during the OA progression [18], [19]. Previous experimental evidence demonstrated the key role of the cross-talk between the synovial and the cartilage compartments in the inflammation and in the degradative processes in in vitro or ex vivo settings [20], [21]. Within our device, the two external channels served as reservoir of serum-free culture medium, as we found that the combination of syn flu and serum-free medium preserved the hydrogel structure better than the complete medium (Figure S2). We derived the composition of the serum-free medium from previous studies that cultured cartilage explants [22] and synovial fibroblasts in a 3D alginate hydrogel [23]. Another advantage in using serum-free consists in avoiding the detrimental effects of FBS on the phenotype and the

chondrogenic potential of chondrocytes [24]–[26]. In addition, the absence of the serum can also assure more standardized and reproducible culture conditions and reduce the interference of analytical assays [27], [28]. This is due to the complex and not completely defined serum supplement composition, that can also vary between different lots of the same manufacturer [29].

The maintenance of the proper phenotype of the chondrocytes, that are fully differentiated cells characterized by a delicate phenotype balance, is fundamental to obtain reliable results. The articular cartilage presents an unique combination of biochemical and mechanical cues that finely regulate the stability of the chondrocyte phenotype, through several mechanotransduction pathways [30], [31]. However, despite the importance of the surrounding ECM, in the previously developed OA models used as drug screening platform, the hydrogels were relatively different from the physiologic cartilaginous environment [11]–[13]. For this reason, we tested new hydrogels made of hyaluronic acid and collagen type I as they were already used for the chondrocytes culture, as discussed below. The methacrylate group is important in the polymerization reaction, as the degree of photocrosslinking of this group allows to finely tune the features of the formulation in terms of mechanical and swelling characteristics and enzymatic degradability [32]. In addition, we also tested Thiol-Modified Hyaluronan hydrogel, in which the

crosslinking was realized with the addition of the PEGDA crosslinker (HA-PEGDA). Despite HA is one of the main components of the cartilaginous ECM, it has been poorly exploited in microfluidic devices for musculoskeletal models. For instance, Lin et al. combined HA- and gelatin-photo-crosslinkable derivatives to investigate osteochondral differentiation in a microfluidic, multichamber bioreactor [33]. In another studies, the injectability of the HA was demonstrated with computational simulations [34]. Toh et al. demonstrated that the crosslinking degree of a modified HA, and the consequent stiffness of the matrix, can influence the MSC chondrogenic process, demonstrating the fundamental role of the microenvironment [35]. Beside HA, we chose to evaluate collagen type I, primarily because chemically modified derivatives are available, whilst there are no photocrosslinkable hydrogels based on collagen type II. Despite it is present in higher concentrations in other musculoskeletal tissues, type I collagen is found also in the cartilage, for instance during the spontaneous healing of osteochondral defects. In this process, it represents the first matrix secreted by the spindle-shaped cells in the repairing tissue [36]. In addition, collagen type I was already used in a microfluidic device to culture chondrocytes and the results showed a good viability and the maintenance of the proper phenotype, demonstrating a good compatibility with

chondrocytes [37]. In the present study, HA-MA was employed both as self-standing material and for generating polymeric network (MIX 1:2 and 1:6) with Col-MA, that was used only associated with HA, given its higher degradability and stiffness of the matrix obtained. Together with the HA-PEGDA formulation, these relevant hydrogels were compared with the fibrin gel, taken as a standard, since it represents the most used hydrogel in cartilage microfluidic models [11], [38].

Firstly, to better understand the behaviour and to evaluate the injectability of all the preparations, we evaluated their rheological properties. Rheology plays a crucial role in the design and the fine tuning of hydrogels according to the final application, so we collected the flow, the strain sweep, and the time sweep curves. Shear rate sweep tests were carried out to study the flow properties of the pre-gel formulations. For all the tested formulations, the flow curves obtained displayed a shear-thinning behaviour characterized by a decrease of the viscosity as a function of the shear rate. Typically, this is observed for hydrogels, since the increase in the shear rate causes the disentanglement of the polymer chains, lastly resulting in a reduction of the solution viscosity [39]. Shear-thinning behaviour has been extensively investigated in various biomedical fields, including drug/cell delivery [40]–[42], tissue engineering [43], [44], and bioprinting [45], [46], with the aim of obtaining

hydrogels that can be delivered by applying a defined shear stress (e.g., by passing through a syringe/needle) [47]. For the purpose of this study, the assessment of the shear thinning behaviour of all the pre-gels was essential to ensure their facile injection into the microfluidic device. From the strain sweep measurements performed after the crosslinking within the microfluidic chip, G′ was almost constant at low shear strains, indicating a linear viscoelastic region. Furthermore, since in this strain range G′ > G′′, the specimens were in a gel-like state, behaving as solid viscoelastic materials [48]. For higher strain values, all the specimens (except for HA-PEGDA) entered a yielding region, undergoing a decrease in their structural resistance (G′ decrease), but still behaving as gel-like materials. Once reached the flow point (i.e., G′ = G′′), the G′′ dominates and the samples start to flow. Conversely, HA-PEGDA specimen does not experience any yielding, displaying constant G′ and G′′ values, thus indicating that yielding is not reached within the strain range tested [49]. From these curves, a trend for G′ was clearly visible: MIX 1:2 ≅ MIX 1:6 > Fibrin > HA-PEGDA ≅ HA-MA, that reflect an increase in the gel strength [50], [51]. As expected, MIX 1:2 and MIX 1:6 displayed the highest G′ values among all the tested formulation, due to the double nature of their crosslinking, i.e., physical (temperature) and chemical (UV-mediated). Interestingly, both G′ and G′′ were nearly equivalent

in the two formulations after UV irradiation, indicating a predominant effect of the chemical crosslinking on the viscoelastic properties of these gels. Differently, given the higher amount of Col-MA in MIX 1:2 compared to MIX 1:6, and due to the thermo-responsive nature of collagen [52], MIX 1:2 displayed higher mechanical performance compared to MIX 1:6 after the sole physical crosslinking (Figure S3, Supporting Information). Moving to fibrin, it displayed slight lower viscoelastic properties compared to MIX 1:2 and MIX 1:6 formulations, with G' values in accordance with the literature [53]. HA-PEGDA and HA-MA formulations owned the lowest viscoelastic moduli among the analysed formulations at low strain values.

Lastly, time sweep measurements were carried out to follow the kinetics of the crosslinking for the selected hydrogel formulations with exception of the HA-MA hydrogel since it wasn't subjected to any crosslinking (e.g., temperature-mediated) unless UV irradiated. The viscoelastic parameter rapidly increased in the both the MIX hydrogels and MIX 1:2 showed higher conservative modulus, thus reflecting the higher amount of collagen which undergoes physical crosslinking upon temperature increase, lastly resulting in a more compact gel [54], [55]. Fibrin formulation displayed a gel-like behaviour (G' > G'') from the beginning of the test, with a significative increase in G' within 10 min of test, compatible with the formation of protofibrils and

subsequent lateral aggregation between adjacent protofibrils to form fibrin fibres [56]. After this phase, G' was almost constant, a behaviour that finds support in the literature, where it has been reported that the time for the complete polymerization of fibrin gels varies in the 10 - 30 min range [56]–[58]. A different trend was instead observable for the HA-PEGDA formulation, initially characterized by a liquid-like behaviour where viscous properties dominate. Once reached the gel point, the HA-PEGDA displayed an increase in both G' and G'', reaching a plateau. Such trend find support in the literature, where the gelation time for HA-PEGDA solutions has been found to change, as a function of PEGDA concentration, from few seconds to 20 min [59], [60]. For the purposes of this investigation, time sweep curves were also useful, as a positive feedback loop, to find the gelation time of all the tested formulations and set an appropriate preconditioning time for the strain sweep tests.

Once injectability has been demonstrated and mechanical properties have been assessed for all the different hydrogels, we evaluated their biologic effects on the embedded chondrocytes. First of all, we optimized the culture conditions in terms of cell seeding and fibrin gel density (Figure S1). We found that the structural stability of the constructs was ensured with the lower cell density (1,5 million cells/mL) in the densest gel tested (20 mg/mL). The density to which chondrocyte are cultured is

fundamental, as the expression of chondrocyte-specific genes is higher if cells are cultured at low density [61]. For this reason, together with the results reported in Figure S1 and S2, we chose a seeding density of 1,5 millions of cells per ml. The viability and the metabolic activity of the chondrocytes cultured in the new formulations resulted lower than those in the fibrin gel, both outside and within the chip. In addition, among the optimized relevant hydrogels, the cells in HA-PEGDA resulted more viable and more active than in the photocrosslinked preparations. A possible explanation could rely in the presence of PEGDA and LAP as photoinitiator for relatively long time in a confined environment, as multi-well and the channels in the microfluidic device. In fact, contrarily to the fibrinogen and the thrombin, used for the polymerization of the fibrin gel the PEGDA and the LAP are not physiologically present in the body. For instance, the PEGDA resulted cytotoxic at high concentrations [62], while LAP is cytotoxic as itself and even more under light exposure [63]. Although we used the suggested concentrations, it is plausible that also lower concentrations can affect the cell viability for prolonged culture time in a relatively confined environment. A potential improvement of the polymerization process of these hydrogels within microfluidic devices could be the addition of an early medium change to remove the excess of the polymerization agent thus increasing the cell viability and the metabolic activity.

The effect of a more relevant microenvironment was clearly beneficial for the chondrocytes, as the expression of lineage specific collagen type II and aggrecan was much stronger within these hydrogels. Among the newly developed matrices, the HA-PEGDA resulted the most effective in supporting the expression of chondrocyte specific markers. This could be due to the lower cytotoxicity of the PEGDA compared to the LAP that we saw in the viability assay. In fact, in HA-PEGDA hydrogel cells could experiment a more favourable environment that, given the facility whit which these cells lose their phenotype and the importance of the surrounding cues, ensured an earlier expression of the specific markers. In addition, we also visually noticed a non-uniform distribution of the Col and HA polymers in the MIX hydrogels, that could have affected the proper panel of the biochemical signals perceived by the cells. Interestingly, the expression of these markers was detected also if the chondrocyte were cultured in a HA-PEGDA within the microfluidic device. As a confirmation of a better maintenance of the proper phenotype, the morphology of the chondrocytes in this hydrogel was visually more spherical, while the same cells appeared with a fibroblast-like morphology in the fibrin gel. This was not due to a stiffer gel, as the rheology analyses demonstrated a higher G', and a consequent great stiffness, for the fibrin gel. For instance, Tan and colleagues reported that the chondrogenic differentiation

increases with the matrix stiffness [64]. Therefore, since fibrin showed a superior gel strength, this implies that it lacks in essential biochemical cues that lead to the activation of intracellular chondrogenic pathways. These processes can be triggered by the membrane receptors connected to the cytoskeleton, explaining the predominance of the matrix composition over the stiffness in guaranteeing the cell phenotype [65].

Moving to the synovial fibroblasts, they are less specialized than the chondrocytes and are characterized by a relatively more stable phenotype. For instance, the phenotype of primary fibroblasts isolated from patients affected by rheumatoid arthritis resulted stable until passage 7 in classic in vitro culture [66], [67]. Similarly, the composition of the synovial membrane ECM is not highly specialized as the cartilaginous one. For this reason, we decided to culture the fibroblasts in a classic fibrin hydrogel, a major component of the clot, frequently used in microfluidics as an alternative to collagen. The results here presented are in accordance with this observation, as the cells resulted positive for lubricin. This protein, also called proteoglycan 4, is expressed by the FLS [68] and differentiate these cell subtype from other fibroblasts lineages [17]. Fibroblasts resulted also mostly alive after 10 days of culture, without showing any decrease during the culture time.

Within our device, we were able to recreate different microenvironments according to the syn flu employed. This is the first example in which the healthy or the OA syn flu are used in a microfluidic joint model and in which their effect has been evaluated and compared. The addition of syn flu, both healthy and OA, had a general beneficial effect on the viability of the chondrocytes compared to the control device in which we injected only serum free medium. This outcome was in line with recent works in which the authors reported a significant increase in the viability of chondrocytes cultured with OA syn flu compared to those grew with culture medium, even if they were cultured in a classic 2D system [69], [70]. The beneficial effect of OA syn flu on chondrocytes was also demonstrated in a 3D culture system in which they were encapsulated in alginate beads and cultured in culture medium or in increasing concentrations of OA syn flu. The authors demonstrated that the expression of the apoptosis-associated Caspase 3 mRNA decreased with the increase of the syn flu concentrations [71]. On the contrary, Hoff et al. reported a decrease in the viability of the chondrocytes in presence of OA syn flu [72]. This difference could be since, in addition to the use of a 2D culture system, the authors used medium with serum in the control group, while we used serum-free medium. The presence of the serum could have provided the

surplus of nutrients that in our system is supplied only with the synovial fluid.

To the best of our knowledge, the effect of arthritic syn flu on the viability of the fibroblasts has never been evaluated before. Our data suggested that initially, it had beneficial effects for the cells. However, after 10 days of culture the viability significantly decreased with OA syn flu but not with the healthy one. Being also lower than the viability of the cells cultured with medium, this suggests the presence of some components in the OA syn flu more harmful than the potential lack of surplus nutrients, acting specifically on the FLS.

The difference of the three microenvironments reproduced in the different chip configurations, strongly emerged from the quantification of the cytokine concentration in the model. In fact, the OA model displayed the highest concentration of both pro- and anti-inflammatory mediators as compared to the healthy syn flu, the control group and the initial syn flu, indicating the active secretion of cytokines by the articular cells. Our outcomes are in accordance with two previous studies in which the chondrocytes exposed to OA syn flu displayed an increased expression of IL1, IL6, IL8, IFNγ and MCP-1 [72], [73]. In addition to the cytokines, we also detected a different expression of both MMP-1 and -13, assessed by immunofluorescence. In particular, both the chondrocytes and the fibroblasts expressed more MMPs in

absence of syn flu. We speculate that in this configuration the cells are somehow suffering the lower concentration of certain elements, and this led to a decrease of the viability and to the attempt of digesting the surrounding matrix. As proof of this, the addition of only serum-free medium led the cells to completely digest the hydrogels already after 5 days of culture (Fig. S2). Among the syn flu groups, the chondrocytes in the OA were more positive than the healthy ones. Similar results were already reported, even if in these studies the authors found a lower expression of MMPs in chondrocytes cultured with medium, but, as already discussed, they used serum supplementation [69], [71]. In the final part of this work, we exploit our model to create a donor-matched OA joint on chip by collecting the articular cells and the synovial fluid from the same arthritic patient. To evaluate the possibility of using it as drug screening platform, as proof of concept, we recreated 4 different donor specific models and we injected the ASCs and the BMSCs, evaluating and comparing their effect. The creation of donor-matched model can represent one of the most promising results of this project, even if it still requires a deeper biological validation, as from the results it emerged a relatively high inter-individual variability. This variability reflects the need to develop personalized models to better predict treatment outcome on one hand, but it also limits the reliability of the results on the other. In fact, as previously

reported, the anti-inflammatory capabilities of MSCs depend on the degree of inflammation of the cells used in the specific experiment [74]. In this paper the authors demonstrated that ASCs were effectively immunomodulatory when cocultured with chondrocytes or FLS that secrete high levels of pro-inflammatory mediators, while no effect was found with low levels. Therefore, the results of this work could be affected by the specific inflammation of each donor, possibly hindering the global effect of the MSCs. For this reason, a high number of donors will probably be needed to validate the chip. To overcome the intrinsic inter-individual variability when working with primary cells, a high number of donors is usually necessary [75]. The relatively low number of donors represents one limitation of this work.

The inter-donor variability emerged from the quantification of the fluorescent signal in the immunofluorescence analyses. In fact, in general we did not detect clear differences between the MSC and the control groups. The three experimental groups seemed to have a comparable effect in supporting the expression of both chondrocyte and fibroblast lineage specific markers. However, the MMPs expression seemed to tend to lower values in the MSC compared to the control group in two out of the three donors assessed, as expected and widely demonstrated [76]. However, to represent an effective drug screening platform, the

model have to ensure high-throughput screening analyses to guarantee the robustness of the assay and the pharmacologic relevance [77]. For this reason, we employed a 10-cytokine array that is compatible with the low reagent volume collected from the microfluidic devices, that represent one of the usual limitations of this approach [78]. In addition, arrays with dozens of targets are already commercially available, making this approach feasible for the high-throughput needs. The intra-donor variability appeared also from the cytokine quantification. In fact, only for IL8 we detected a common trend in all the four donors, in which emerged a decrease of concentration upon the addition of ASCs. The ASCs isolated from three different anatomical sources were able to downregulate the expression, at both the mRNA and the protein level, of IL-8 when cocultured with chondrocytes or fibroblasts [74]. On the other hand, the concentration of MCP-1 increased in the device during the culture time compared with the synovial fluid, and even more with the MSCs. This chemokine resulted highly secreted by both BMSCs and ASCs in response to inflammatory environment, in accordance with previous literature [76], [79]. The function MCP-1 is not only to recruit specific immune cells, but it can induce the anti-inflammatory polarization and the expression of anti-inflammatory cytokines in macrophages [80], [81]. This process is fundamental for the resolution of the inflammation process and

the consequent tissue restoration [82]. Therefore, as previously demonstrated, the MSCs can recruit and stimulate the monocytes towards an anti-inflammatory phenotype, representing an indirect and potent immunomodulatory capability of these cells [83]. Regarding the other pro-inflammatory cytokines, we did not detect a clear trend between the different group in the donors. The array we used also included two cytokines that have been indicated as both pro- and anti-inflammatory cytokines. Among these, IL6 resulted in all the donors higher at day 4 while decreased at the end of the culture period, when the control and the ASCs showed lower levels than BMSC. In the OA progression, the pro-inflammatory role of this molecule prevails on the immunomodulatory one and IL6 can ultimately affect the cartilage degradation by affecting the activity of MMPs [84], [85]. On the other hand, IL13 showed an alternating trend, being more concentrated in the BMSCs group in two donors and in the ASC in the remaining two. However, the effects of this cytokine in OA are not fully elucidated and could be plausible that its effect is due to concomitant and not easily addressable factors. In fact, based on the specific aspect under investigation, IL13 proved to downregulate the inflammatory mediators [86] but also to stimulate the activity of matrix-degrading enzymes [87], [88]. Unfortunately, the anti-inflammatory cytokines that could better elucidate the immunomodulatory aspects of the MSCs resulted

mostly under the detection limit of the assay. The only detectable values showed a decreasing trend of IL10 concentration moving from the syn flu to the device at day 4 and even more at day 10. Interestingly, upon the addition of BMSCs and even more of the ASCs, the levels of this cytokine increased at higher concentration than the starting one. IL10 is well recognized as anti-inflammatory mediator during the OA and its overexpression reduced the inflammatory mediators in a 3D model of synovitis [89]. From the trend we found in our models, and considered the limitations of our results, it seems that the ASCs emerged more often as the BMSCs as immunomodulatory actors. In literature different evidence supported a better anti-inflammatory potential for adipose-derived MSCs over the bone marrow derived ones. For instance, the BMSCs appeared to be more prone to environmental factors that can decrease their anti-inflammatory capability, that was instead maintained in the ASCs [90]. In addition, ASCs can induce the macrophages more towards an anti-inflammatory phenotype [91]. Considering their use for the cell-therapy, from a comparative study emerged a preponderance of the immunomodulatory effect of the ASCs over the BMSCs [92].

Conclusions

In this work we first optimized a relevant hydrogel able to maintain the correct chondrocyte phenotype in a microfluidic device. We then developed a microfluidic model of an arthritic joint in which we were effectively able to resemble a pro-inflammatory and degradative microenvironment. In addition, as proof of concept we resembled donor-matched models that supported the injection of mesenchymal stromal cells and allowed the quantification of their effect on the inflamed articular cells. Therefore, after future validation, this OA joint on chip model could be used as drug screening platform for the evaluation and the comparison of innovative and biological treatments for the OA. However, to represent an effective precision medicine tool, it would need a further validation to detect the biological effect of the tested treatments.

Supplementary materials

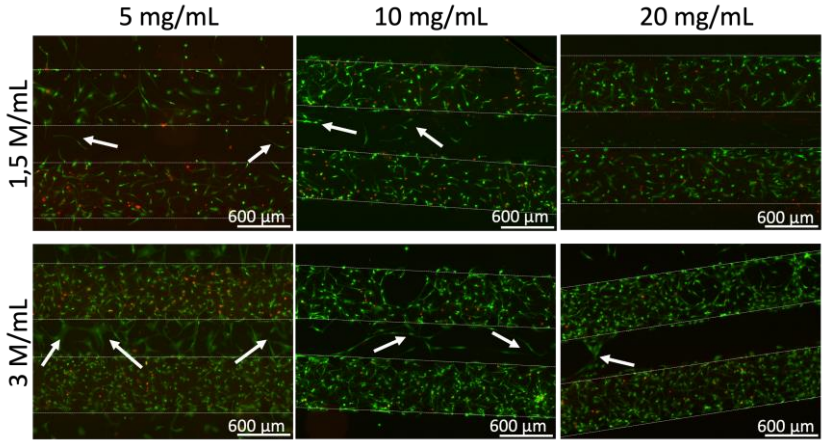

Supplementary Figure 1: Optimization of the culture conditions of FLS (upper channel) and chondrocytes (lower channel) in fibrin hydrogels. Three different fibrinogen concentrations (5, 10 and 20 mg/mL) and two cell density (1,5 or 3 M/mL) were tested. In green are stained live cells, in red the dead ones. White arrow indicates cells sprouted from the gel. Parameters chose: 1,5 M/mL for cell density and 20 mg/mL for the fibrin hydrogel. Scale bar = 600 µm.

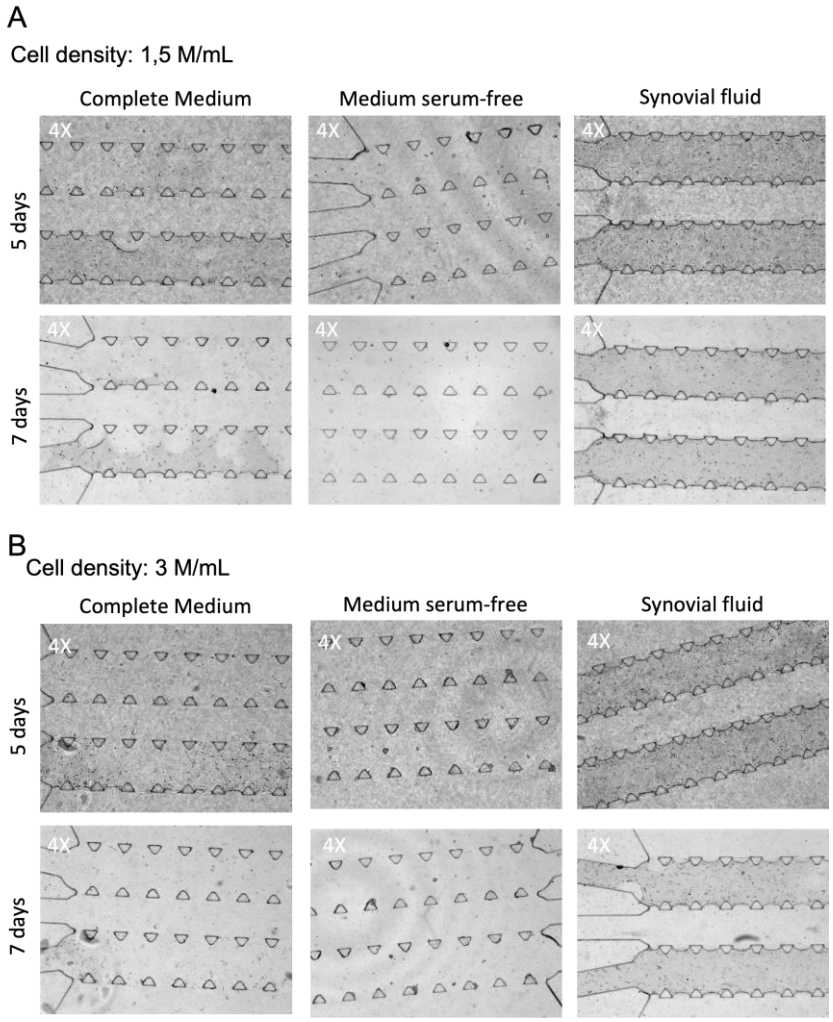

Supplementary Figure 2: Optimization of the culture conditions of FLS (upper channel) and chondrocytes (lower channel) in fibrin hydrogel during the time. Two different cell seeding density of 1,5 or 3 M/mL were tested with complete medium, serum-free medium or synovial fluid. In the two external channels serum-free medium was added. The synovial fluid was beneficial for the microenvironment in the device as it allowed the maintenance of the hydrogel structural integrity after 7 days of culture. Magnification: 4X.

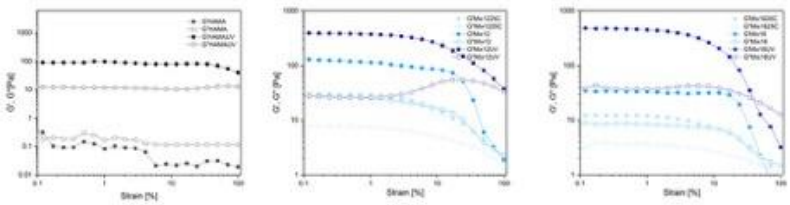

Supplementary Figure 3: Strain Sweep for the HA-MA (A), MIX 12 (B), MIX 16 (C) before and after UV photocrosslinking. Filled symbol = G', empty symbol = G''.

	IL1a	IL1b	IL8	TNFa	IFNg	MCP-1	IL6	IL13	IL4	IL10
Healthy Syn Flu	5,09	19,62	21,84	31,19	120,80	43,23	347,41	0	3,34	0
OA Syn Flu	62,10	15,35	39,46	25,83	319,36	117,37	29,84	19,5	1,70	0
Control D10	6,39	5,4	35,44	7,98	194,65	439,06	135,17	1,65	0	0
Healthy Syn Flu D10	3,31	1,65	25,32	19,97	44,74	690,47	198,62	1,16	0	16,3
OA Syn Flu D10	47,04	34,34	168	27,91	2300,62	n.a.	743,53	41,66	21,35	107,92

Supplementary Figure 4: Concentration of 10 cytokines quantified in the healthy and OA Syn Flu samples and in the three different microfluidic models after 10 days of culture. Values are reported as pg/mL. The value of MCP-1 quantified in the microfluidic with the OA Syn Flu was too high and out of scale. n.a. = not available.

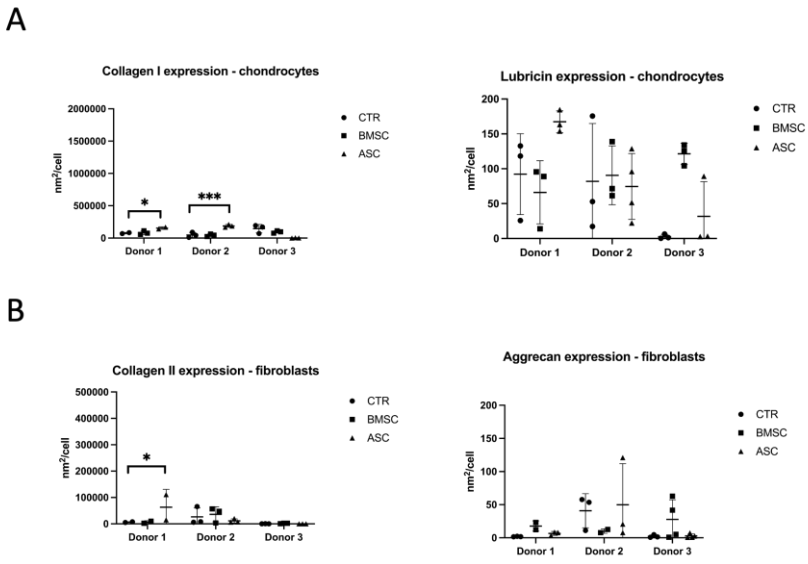

Supplementary Figure 5. Quantification of the signal from the immunofluorescence analysis relative to the (A) Collagen I and Lubricin expression in chondrocytes and (B)

the expression of Collagen II and aggrecan in FLS. Data are normalized on the number of the nuclei for each picture.

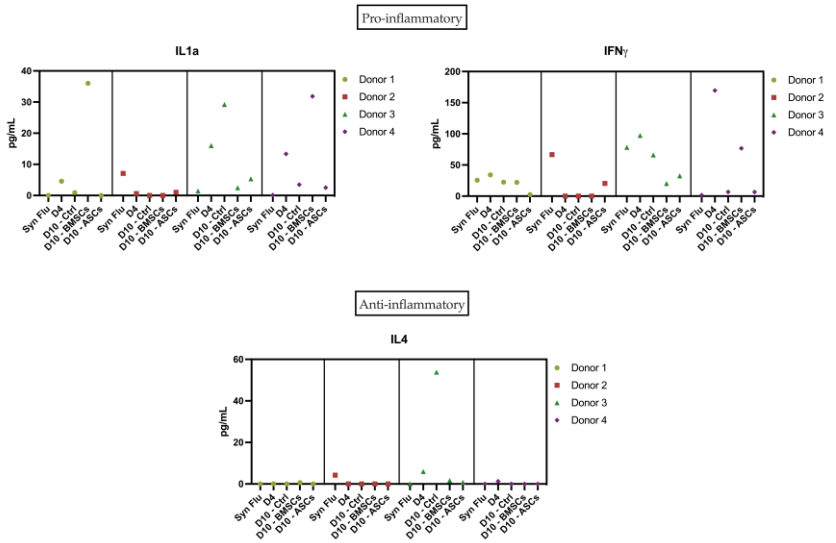

Supplementary Figure 6: Concentration of IL1α, IFN-γ and IL4 quantified in the synovial fluid and at the two time points in the different experimental group in the four donor-matched models. Values are expressed as pg/mL.

References

[1] D. J. Hunter and S. Bierma-Zeinstra, "Osteoarthritis," Lancet, vol. 393, no. 10182, pp. 1745–1759, 2019.

[2] A. R. Poole, "Osteoarthritis as a whole joint disease.," HSS J., vol. 8, no. 1, pp. 4–6, Feb. 2012.

[3] J.-R. Kim, J. J. Yoo, and H. A. Kim, "Therapeutics in Osteoarthritis Based on an Understanding of Its Molecular Pathogenesis.," Int. J. Mol. Sci., vol. 19, no. 3, Feb. 2018.

[4] G. Moatshe et al., "Biological treatment of the knee with platelet-rich plasma or bone marrow aspirate concentrates.," Acta Orthop., vol. 88, no. 6, pp. 670–674, Dec. 2017.

[5] A. E. Weber, I. K. Bolia, and N. A. Trasolini, "Biological strategies for osteoarthritis: from early diagnosis to treatment.," Int. Orthop., vol. 45, no. 2, pp. 335–344, Feb. 2021.

[6] N. G. Sommer, "Animal Models in Orthopedic Research: The Proper Animal Model to Answer Fundamental Questions on Bone Healing Depending

on Pathology and Implant Material," D. Hahn, Ed. Rijeka: IntechOpen, 2020, p. Ch. 2.
[7] T. Wang, S. S. Nanda, G. C. Papaefthymiou, and D. K. Yi, "Mechanophysical Cues in Extracellular Matrix Regulation of Cell Behavior.," Chembiochem, vol. 21, no. 9, pp. 1254–1264, May 2020.
[8] C. Gentili and R. Cancedda, "Cartilage and bone extracellular matrix.," Curr. Pharm. Des., vol. 15, no. 12, pp. 1334–1348, 2009.
[9] I. I. Lungu and A. M. Grumezescu, "Microfluidics – Organ-on-chip," Biomed Eng Int, vol. 1, pp. 2–8, 2019.
[10] S. Piluso et al., "Mimicking the Articular Joint with In Vitro Models.," Trends Biotechnol., vol. 37, no. 10, pp. 1063–1077, Oct. 2019.
[11] C. Mondadori et al., "Recapitulating monocyte extravasation to the synovium in an organotypic microfluidic model of the articular joint.," Biofabrication, vol. 13, no. 4, Jul. 2021.
[12] Z. Lin et al., "Osteochondral Tissue Chip Derived From iPSCs: Modeling OA Pathologies and Testing Drugs.," Front. Bioeng. Biotechnol., vol. 7, p. 411, 2019.
[13] P. Occhetta et al., "Hyperphysiological compression of articular cartilage induces an osteoarthritic phenotype in a cartilage-on-a-chip model.," Nat. Biomed. Eng., vol. 3, no. 7, pp. 545–557, Jul. 2019.
[14] M. B. Goldring, M. B. Goldring, E. D. Harris, R. C. Budd, and M. C. Genovese, "Kelley's Textbook of Rheumatology," Harris, ED, pp. 203–234, 2008.
[15] R. Okubo et al., "Proliferation medium in three-dimensional culture of auricular chondrocytes promotes effective cartilage regeneration in vivo," Regen. Ther., vol. 11, pp. 306–315, 2019.
[16] S. Lopa, A. Colombini, M. Moretti, and L. de Girolamo, "Injective mesenchymal stem cell-based treatments for knee osteoarthritis: from mechanisms of action to current clinical evidences.," Knee Surg. Sports Traumatol. Arthrosc., vol. 27, no. 6, pp. 2003–2020, 2019.
[17] M. Asif Amin, D. A. Fox, and J. H. Ruth, "Synovial cellular and molecular markers in rheumatoid arthritis.," Semin. Immunopathol., vol. 39, no. 4, pp. 385–393, Jun. 2017.
[18] R. Rainbow, W. Ren, and L. Zeng, "Inflammation and Joint Tissue Interactions in OA: Implications for Potential herapeutic Approaches.," Arthritis, vol. 2012, p. 741582, 2012.
[19] J. Sokolove and C. M. Lepus, "Role of inflammation in the pathogenesis of osteoarthritis: latest findings and interpretations.," Ther. Adv. Musculoskelet. Dis., vol. 5, no. 2, pp. 77–94, Apr. 2013.
[20] M. J. Pearson et al., "IL-6 secretion in osteoarthritis patients is mediated by chondrocyte-synovial fibroblast cross-talk and is enhanced by obesity.," Sci. Rep., vol. 7, no. 1, p. 3451, Jun. 2017.
[21] D. Pretzel, D. Pohlers, S. Weinert, and R. W. Kinne, "In vitro model for the analysis of synovial fibroblast-mediated degradation of intact cartilage.," Arthritis Res. Ther., vol. 11, no. 1, p. R25, 2009.

[22] L. Bian et al., “Mechanical and biochemical characterization of cartilage explants in serum-free culture.,” J. Biomech., vol. 41, no. 6, pp. 1153–1159, 2008.
[23] Y. Park, M. Sugimoto, A. Watrin, M. Chiquet, and E. B. Hunziker, “BMP-2 induces the expression of chondrocyte-specific genes in bovine synovium-derived progenitor cells cultured in three-dimensional alginate hydrogel.,” Osteoarthr. Cartil., vol. 13, no. 6, pp. 527–536, Jun. 2005.
[24] E. W. Mandl et al., “Fibroblast growth factor-2 in serum-free medium is a potent mitogen and reduces dedifferentiation of human ear chondrocytes in monolayer culture.,” Matrix Biol., vol. 23, no. 4, pp. 231–241, Jul. 2004.
[25] M. Malpeli, N. Randazzo, R. Cancedda, and B. Dozin, “Serum-Free Growth Medium Sustains Commitment of Human Articular Chondrocyte through Maintenance of Sox9 Expression,” Tissue Eng., vol. 10, no. 1–2, pp. 145–155, Jan. 2004.
[26] A. M. Garcia and M. L. Gray, “Dimensional growth and extracellular matrix accumulation by neonatal rat mandibular condyles in long-term culture.,” J. Orthop. Res. Off. Publ. Orthop. Res. Soc., vol. 13, no. 2, pp. 208–219, Mar. 1995.
[27] M. Colzani, P. Waridel, J. Laurent, E. Faes, C. Rüegg, and M. Quadroni, “Metabolic Labeling and Protein Linearization Technology Allow the Study of Proteins Secreted by Cultured Cells in Serum-Containing Media,” J. Proteome Res., vol. 8, no. 10, pp. 4779–4788, Oct. 2009.
[28] F. Mbeunkui, O. Fodstad, and L. K. Pannell, “Secretory protein enrichment and analysis: an optimized approach applied on cancer cell lines using 2D LC-MS/MS.,” J. Proteome Res., vol. 5, no. 4, pp. 899–906, Apr. 2006.
[29] X. Zheng, H. Baker, W. S. Hancock, F. Fawaz, M. McCaman, and E. J. Pungor, “Proteomic analysis for the assessment of different lots of fetal bovine serum as a raw material for cell culture. Part IV. Application of proteomics to the manufacture of biological drugs.,” Biotechnol. Prog., vol. 22, no. 5, pp. 1294–1300, 2006.
[30] K. E. Kuettner, M. B. Aydelotte, and E. J. Thonar, “Articular cartilage matrix and structure: a minireview.,” J. Rheumatol. Suppl., vol. 27, pp. 46–48, Feb. 1991.
[31] S. J. Gilbert, C. S. Bonnet, and E. J. Blain, “Mechanical Cues: Bidirectional Reciprocity in the Extracellular Matrix Drives Mechano-Signalling in Articular Cartilage.,” Int. J. Mol. Sci., vol. 22, no. 24, Dec. 2021.
[32] C. C. L. Schuurmans, M. Mihajlovic, C. Hiemstra, K. Ito, W. E. Hennink, and T. Vermonden, “Hyaluronic acid and chondroitin sulfate (meth)acrylate-based hydrogels for tissue engineering: Synthesis, characteristics and pre-clinical evaluation,” Biomaterials, vol. 268, p. 120602, 2021.
[33] H. Lin, T. P. Lozito, P. G. Alexander, R. Gottardi, and R. S. Tuan, “Stem cell-based microphysiological osteochondral system to model tissue response to interleukin-1beta.,” Mol. Pharm., vol. 11, no. 7, pp. 2203–2212, Jul. 2014.
[34] S. Han et al., “Hydrophobic Patterning-Based 3D Microfluidic Cell Culture Assay.,” Adv. Healthc. Mater., vol. 7, no. 12, p. e1800122, Jun. 2018.

[35] W. S. Toh, T. C. Lim, M. Kurisawa, and M. Spector, "Modulation of mesenchymal stem cell chondrogenesis in a tunable hyaluronic acid hydrogel microenvironment," Biomaterials, vol. 33, no. 15, pp. 3835–3845, 2012.
[36] H. Madry, C. N. van Dijk, and M. Mueller-Gerbl, "The basic science of the subchondral bone.," Knee Surg. Sports Traumatol. Arthrosc., vol. 18, no. 4, pp. 419–433, Apr. 2010.
[37] Y. Li, J. Qin, B. Lin, and W. Zhang, "The Effects of Insulin-Like Growth Factor-1 and Basic Fibroblast Growth Factor on the Proliferation of Chondrocytes Embedded in the Collagen Gel Using an Integrated Microfluidic Device," Tissue Eng. Part C Methods, vol. 16, no. 6, pp. 1267–1275, 2010.
[38] E. Kahraman, R. Ribeiro, M. Lamghari, and E. Neto, "Cutting-Edge Technologies for Inflamed Joints on Chip: How Close Are We?," Front. Immunol., vol. 13, 2022.
[39] M. Guvendiren, H. D. Lu, and J. A. Burdick, "Shear-thinning hydrogels for biomedical applications," Soft Matter, vol. 8, no. 2, pp. 260–272, 2012.
[40] S. Samimi Gharaie, S. M. H. Dabiri, and M. Akbari, "Smart Shear-Thinning Hydrogels as Injectable Drug Delivery Systems.," Polymers (Basel)., vol. 10, no. 12, Nov. 2018.
[41] A. Thakur et al., "Injectable shear-thinning nanoengineered hydrogels for stem cell delivery," Nanoscale, vol. 8, no. 24, pp. 12362–12372, 2016.
[42] A. C. Gaffey et al., "Injectable shear-thinning hydrogels used to deliver endothelial progenitor cells, enhance cell engraftment, and improve ischemic myocardium.," J. Thorac. Cardiovasc. Surg., vol. 150, no. 5, pp. 1268–1276, Nov. 2015.
[43] J. A. Burdick and G. D. Prestwich, "Hyaluronic acid hydrogels for biomedical applications," Adv. Mater., vol. 23, no. 12, p. H41, Mar. 2011.
[44] E. Tous, B. Purcell, J. L. Ifkovits, and J. A. Burdick, "Injectable acellular hydrogels for cardiac repair," Journal of Cardiovascular Translational Research, vol. 4, no. 5. J Cardiovasc Transl Res, pp. 528–542, Oct-2011.
[45] W. Liu et al., "Extrusion Bioprinting of Shear-Thinning Gelatin Methacryloyl Bioinks," Adv. Healthc. Mater., vol. 6, no. 12, p. 10.1002/adhm.201601451, Jun. 2017.
[46] L. Ouyang, C. B. Highley, C. B. Rodell, W. Sun, and J. A. Burdick, "3D Printing of Shear-Thinning Hyaluronic Acid Hydrogels with Secondary Cross-Linking," ACS Biomater. Sci. Eng., vol. 2, no. 10, pp. 1743–1751, Oct. 2016.
[47] M. H. Chen, L. L. Wang, J. J. Chung, Y. H. Kim, P. Atluri, and J. A. Burdick, "Methods to Assess Shear-Thinning Hydrogels for Application As Injectable Biomaterials," ACS Biomater. Sci. Eng., vol. 3, no. 12, pp. 3146–3160, Dec. 2017.
[48] M. C. Tanzi and S. Farè, Eds., Characterization of Polymeric Biomaterials. 2017.
[49] L. Mendoza, W. Batchelor, R. F. Tabor, and G. Garnier, "Gelation mechanism of cellulose nanofibre gels: A colloids and interfacial perspective.," J. Colloid Interface Sci., vol. 509, pp. 39–46, Jan. 2018.

[50] F. Cuomo, M. Cofelice, and F. Lopez, “Rheological Characterization of Hydrogels from Alginate-Based Nanodispersion,” Polymers , vol. 11, no. 2. 2019.
[51] G. Stojkov, Z. Niyazov, F. Picchioni, and R. K. Bose, “Relationship between Structure and Rheology of Hydrogels for Various Applications,” Gels , vol. 7, no. 4. 2021.
[52] L. Altomare et al., “Biopolymer-based strategies in the design of smart medical devices and artificial organs,” Int. J. Artif. Organs, vol. 41, no. 6, pp. 337–359, Apr. 2018.
[53] N. Salam, S. Toumpaniari, P. Gentile, A. Marina Ferreira, K. Dalgarno, and S. Partridge, “Assessment of Migration of Human MSCs through Fibrin Hydrogels as a Tool for Formulation Optimisation,” Materials , vol. 11, no. 9. 2018.
[54] M. Shayegan and N. R. Forde, “Microrheological Characterization of Collagen Systems: From Molecular Solutions to Fibrillar Gels,” PLoS One, vol. 8, no. 8, p. e70590, Aug. 2013.
[55] G. Lai, Y. Li, and G. Li, “Effect of concentration and temperature on the rheological behavior of collagen solution.,” Int. J. Biol. Macromol., vol. 42, no. 3, pp. 285–291, Apr. 2008.
[56] N. Okumura, O. V Gorkun, F. Terasawa, and S. T. Lord, “Substitution of the γ-chain Asn308 disturbs the D:D interface affecting fibrin polymerization, fibrinopeptide B release, and FXIIIa-catalyzed cross-linking,” Blood, vol. 103, no. 11, pp. 4157–4163, Jun. 2004.
[57] H. J. Ridgway, S. O. Brennan, J. M. Faed, and P. M. George, “Fibrinogen Otago: a major alpha chain truncation associated with severe hypofibrinogenaemia and recurrent miscarriage.,” Br. J. Haematol., vol. 98, no. 3, pp. 632–639, Sep. 1997.
[58] H. J. Ridgway, S. O. Brennan, R. M. Loreth, and P. M. George, “Fibrinogen Kaiserslautern (gamma 380 Lys to Asn): a new glycosylated fibrinogen variant with delayed polymerization.,” Br. J. Haematol., vol. 99, no. 3, pp. 562–569, Dec. 1997.
[59] K. Ghosh et al., “Rheological characterization of in situ cross-linkable hyaluronan hydrogels.,” Biomacromolecules, vol. 6, no. 5, pp. 2857–2865, 2005.
[60] X. Zheng Shu, Y. Liu, F. S. Palumbo, Y. Luo, and G. D. Prestwich, “In situ crosslinkable hyaluronan hydrogels for tissue engineering.,” Biomaterials, vol. 25, no. 7–8, pp. 1339–1348, 2004.
[61] E. Kolettas, H. I. Muir, J. C. Barrett, and T. E. Hardingham, “Chondrocyte phenotype and cell survival are regulated by culture conditions and by specific cytokines through the expression of Sox-9 transcription factor,” Rheumatology, vol. 40, no. 10, pp. 1146–1156, Oct. 2001.
[62] J. P. Mazzoccoli, D. L. Feke, H. Baskaran, and P. N. Pintauro, “Mechanical and cell viability properties of crosslinked low- and high-molecular weight poly(ethylene glycol) diacrylate blends,” J. Biomed. Mater. Res. A, vol. 93, no. 2, pp. 558–566, May 2010.

[63] A. K. Nguyen, P. L. Goering, R. K. Elespuru, S. Sarkar Das, and R. J. Narayan, "The Photoinitiator Lithium Phenyl (2,4,6-Trimethylbenzoyl) Phosphinate with Exposure to 405 nm Light Is Cytotoxic to Mammalian Cells but Not Mutagenic in Bacterial Reverse Mutation Assays.," Polymers (Basel)., vol. 12, no. 7, Jul. 2020.
[64] S. Tan, W. Fang, C. T. Vangsness, and B. Han, "Influence of Cellular Microenvironment on Human Articular Chondrocyte Cell Signaling," Cartilage, vol. 13, no. 2_suppl, pp. 935S-946S, Jul. 2020.
[65] J. C. Lauer, M. Selig, M. L. Hart, B. Kurz, and B. Rolauffs, "Articular Chondrocyte Phenotype Regulation through the Cytoskeleton and the Signaling Processes That Originate from or Converge on the Cytoskeleton: Towards a Novel Understanding of the Intersection between Actin Dynamics and Chondrogenic Function.," Int. J. Mol. Sci., vol. 22, no. 6, Mar. 2021.
[66] J. W. Whitaker et al., "An imprinted rheumatoid arthritis methylome signature reflects pathogenic phenotype," Genome Med., vol. 5, no. 4, p. 40, 2013.
[67] E. Neumann et al., "Cell culture and passaging alters gene expression pattern and proliferation rate in rheumatoid arthritis synovial fibroblasts," Arthritis Res. Ther., vol. 12, no. 3, p. R83, 2010.
[68] G. D. Jay, D. E. Britt, and C. J. Cha, "Lubricin is a product of megakaryocyte stimulating factor gene expression by human synovial fibroblasts.," J. Rheumatol., vol. 27, no. 3, pp. 594–600, Mar. 2000.
[69] C. B. Carballo et al., "Osteoarthritic Synovial Fluid and TGF-β1 Induce Interleukin-18 in Articular Chondrocytes," Cartilage, vol. 11, no. 3, pp. 385–394, Jul. 2020.
[70] B. A. C. Housmans et al., "Synovial fluid from end-stage osteoarthritis induces proliferation and fibrosis of articular chondrocytes via MAPK and RhoGTPase signaling," Osteoarthr. Cartil., 2022.
[71] J. A. Brand, T. E. McAlindon, and L. Zeng, "A 3D system for culturing human articular chondrocytes in synovial fluid.," J. Vis. Exp., no. 59, p. e3587, Jan. 2012.
[72] P. Hoff et al., "Osteoarthritis synovial fluid activates pro-inflammatory cytokines in primary human chondrocytes," Int. Orthop., vol. 37, no. 1, pp. 145–151, Jan. 2013.
[73] G. R. Webb, C. I. Westacott, and C. J. Elson, "Osteoarthritic synovial fluid and synovium supernatants up-regulate tumor necrosis factor receptors on human articular chondrocytes.," Osteoarthr. Cartil., vol. 6, no. 3, pp. 167–176, May 1998.
[74] C. Manferdini et al., "Adipose-derived mesenchymal stem cells exert antiinflammatory effects on chondrocytes and synoviocytes from osteoarthritis patients through prostaglandin E2.," Arthritis Rheum., vol. 65, no. 5, pp. 1271–1281, May 2013.

[75] M. Laganà et al., "Characterization of articular chondrocytes isolated from 211 osteoarthritic patients.," Cell Tissue Bank., vol. 15, no. 1, pp. 59–66, Mar. 2014.
[76] Y.-M. Pers, M. Ruiz, D. Noël, and C. Jorgensen, "Mesenchymal stem cells for the management of inflammation in osteoarthritis: state of the art and perspectives," Osteoarthr. Cartil., vol. 23, no. 11, pp. 2027–2035, 2015.
[77] K. Boehnke et al., "Assay Establishment and Validation of a High-Throughput Screening Platform for Three-Dimensional Patient-Derived Colon Cancer Organoid Cultures," J. Biomol. Screen., vol. 21, no. 9, pp. 931–941, May 2016.
[78] A. E. Danku, E.-H. Dulf, C. Braicu, A. Jurj, and I. Berindan-Neagoe, "Organ-On-A-Chip: A Survey of Technical Results and Problems," Front. Bioeng. Biotechnol., vol. 10, 2022.
[79] R. A. Boomsma and D. L. Geenen, "Mesenchymal stem cells secrete multiple cytokines that promote angiogenesis and have contrasting effects on chemotaxis and apoptosis," PLoS One, vol. 7, no. 4, pp. e35685–e35685, 2012.
[80] H. Roca, Z. S. Varsos, S. Sud, M. J. Craig, C. Ying, and K. J. Pienta, "CCL2 and interleukin-6 promote survival of human CD11b+ peripheral blood mononuclear cells and induce M2-type macrophage polarization.," J. Biol. Chem., vol. 284, no. 49, pp. 34342–34354, Dec. 2009.
[81] E. Sierra-Filardi et al., "CCL2 Shapes Macrophage Polarization by GM-CSF and M-CSF: Identification of CCL2/CCR2-Dependent Gene Expression Profile," J. Immunol., vol. 192, no. 8, pp. 3858 LP – 3867, Apr. 2014.
[82] S. C. Funes, M. Rios, J. Escobar-Vera, and A. M. Kalergis, "Implications of macrophage polarization in autoimmunity," Immunology, vol. 154, no. 2, pp. 186–195, Jun. 2018.
[83] C. Cao, S. Tarlé, and D. Kaigler, "Characterization of the immunomodulatory properties of alveolar bone-derived mesenchymal stem cells," Stem Cell Res. Ther., vol. 11, no. 1, p. 102, 2020.
[84] R. Wiegertjes, F. A. J. van de Loo, and E. N. Blaney Davidson, "A roadmap to target interleukin-6 in osteoarthritis," Rheumatology, vol. 59, no. 10, pp. 2681–2694, Oct. 2020.
[85] G. Akeson and C. J. Malemud, "A Role for Soluble IL-6 Receptor in Osteoarthritis.," J. Funct. Morphol. Kinesiol., vol. 2, no. 3, 2017.
[86] D. Jovanovic et al., "Effect of IL-13 on cytokines, cytokine receptors and inhibitors on human osteoarthritis synovium and synovial fibroblasts.," Osteoarthr. Cartil., vol. 6, no. 1, pp. 40–49, Jan. 1998.
[87] T. Moue et al., "Influence of IL13 on Periostin Secretion by Synoviocytes in Osteoarthritis," In Vivo, vol. 31, no. 1, pp. 79–85, Jan. 2017.
[88] C. Y. Yang et al., "Interleukin 13 (IL-13)-regulated expression of the chondroprotective metalloproteinase ADAM15 is reduced in aging cartilage," Osteoarthr. Cartil. Open, vol. 2, no. 4, p. 100128, 2020.
[89] M. G. A. Broeren et al., "Suppression of the inflammatory response by disease-inducible interleukin-10 gene therapy in a three-dimensional

micromass model of the human synovial membrane," Arthritis Res. Ther., vol. 18, no. 1, p. 186, 2016.
[90] C.-X. Zheng et al., "Adipose mesenchymal stem cells from osteoporotic donors preserve functionality and modulate systemic inflammatory microenvironment in osteoporotic cytotherapy.," Sci. Rep., vol. 8, no. 1, p. 5215, Mar. 2018.
[91] P. Sukho, J. W. Hesselink, N. Kops, J. Kirpensteijn, F. Verseijden, and Y. M. Bastiaansen-Jenniskens, "Human Mesenchymal Stromal Cell Sheets Induce Macrophages Predominantly to an Anti-Inflammatory Phenotype.," Stem Cells Dev., vol. 27, no. 13, pp. 922–934, Jul. 2018.
[92] C. Li et al., "Comparative analysis of human mesenchymal stem cells from bone marrow and adipose tissue under xeno-free conditions for cell therapy," Stem Cell Res. Ther., vol. 6, no. 1, p. 55, 2015.

Chapter 6

Secretome and extracellular vesicles as new biological therapies for knee osteoarthritis. A systematic review

Review

Secretome and extracellular vesicles as new biological therapies for knee osteoarthritis. A systematic review

Daniele D'Arrigo[1,2], Alice Roffi[3], Magali Cucchiarini[4], Matteo Moretti[1,5], Christian Candrian[6], Giuseppe Filardo[3,6]

1 - Regenerative Medicine Technologies Lab, Ente Ospedaliero Cantonale (EOC), Via Tesserete 46, 6900 Lugano, Switzerland.
2 - Department of Biotechnology and Biosciences, University of Milano-Bicocca, Piazza dell'Ateneo Nuovo 1, 20126, Milano, Italy.
3 - ATRC, IRCCS Istituto Ortopedico Rizzoli, Via di Barbiano 1/10, 40136, Bologna, Italy.
4 - Center of Experimental Orthopaedics, Saarland University Medical Center, 66421 Homburg/Saar, Germany.
5 - Cell and Tissue Engineering Laboratory, IRCCS Istituto Ortopedico Galeazzi, via Galeazzi, 4, 20161, Milan, Italy
6 - Orthopaedic and Traumatology Unit, Ospedale Regionale di Lugano, Ente Ospedaliero Cantonale, Via Tesserete 46, 6900 Lugano, Switzerland.

J. Clin. Med. 2019, 8(11), 1867; https://doi.org/10.3390/jcm8111867

(*IF: 4,24*)

Received: 13 September 2019 / Revised: 16 October 2019 / Accepted: 23 October 2019 / Published: 4 November 2019

Abstract

Secretome and extracellular vesicles (EVs) are considered a promising option to exploit MSCs properties to address knee OA. Aim of this systematic review was to analyze both in vitro and in vivo literature, in order to understand the potential of secretome and EVs as minimally invasive injective biological approach. A systematic review of the literature was performed on PubMed, Embase, and Web of Science databases up to the 31st of August 2019: 20 studies were analyzed: 9 in vitro, 9 in vitro and in vivo, and 2 in vivo. The analysis showed an increasing interest towards this emerging field, with overall positive findings. Promising in vitro results were documented in terms of enhanced cell proliferation, reduction of inflammation, down regulation of catabolic pathways while promoting anabolic processes. The positive in vitro findings were confirmed in vivo, with studies showing positive effects on cartilage, subchondral bone, and synovial tissues in both OA and osteochondral models. However, several aspects remain to be clarified, such as the different effects induced by EVs and secretome, which is the most suitable cell source and production protocol, and the identification of patients who may benefit more from this new biological approach for knee OA treatment.

Keywords: Exosome; extracellular vesicles; mesenchymal stem cell; knee osteoarthritis; injection

Introduction

Osteoarthritis (OA) is a degenerative disease with progressive degradation of articular cartilage and subchondral bone leading to loss of joint function and pain, which significantly impair patient quality of life [1,2]. Worldwide estimates indicate that 9.6% of men and 18.0% of women over 60 years old suffer from symptoms of OA, with knee OA representing one of the most disabling conditions, with a huge social impact [3–5]. This high prevalence of OA is further increasing due to the augmented risk of OA due both to non-modifiable risk factors, such as the aging population and the gender, and to local risk factors, such as physical activity [6]. The classic clinical approaches in the treatment of OA offer mainly temporary symptoms relief without disease modifying effects [7]. The limitations of available treatments fostered the development of new strategies, with cell-based procedures being proposed, such as minimally invasive injective approaches with the aim of modulating the inflammation process as well as stimulating and supporting the regeneration of articular tissues, thus re-establishing joint homeostasis. Mesenchymal stem cells (MSCs) represent the most promising cell population [8,9] showing, in several clinical studies, the possibility to increase joint function and reduce pain in knee OA patients [10–12]. However, the efficacy of this cell

injection approach may be impaired by cell manipulation, and its wide application is strongly limited by regulatory issues [13,14]. To overcome these limitations, in the past 15 years researchers focused on the secretome of MSCs. In fact, it has been demonstrated that the therapeutic ability of MSCs is mainly related to their secretion of biologically active factors, rather than their differentiation properties [15]. These soluble factors belong to different biochemical classes and include growth factors, cytokines, chemokines, lipids, and other molecules with immunomodulatory effects [15]. All these paracrine factors, with the addition of a broad variety of acid nucleic and different lipids, can also be found within cell-secreted vesicles (extracellular vesicles - EVs), a key part of the secretome which is gaining increasing attention by the scientific community. EVs (either microvesicles – MVs - or Exosomes - Exo) represent important mediators between articular cell types [16]. Once secreted in the extracellular space, they can interact and be internalized by target cells, ultimately influencing and modifying their phenotype. Preclinical in vitro studies suggested a wide range of potential benefits with immunomodulatory, regenerative, anti-catabolic, and chondro-protective properties of secretome and EVs, which could overcome the limits of cell therapies while offering comparable biological effects. However, while secretome and EVs appear to be very promising, it is important to confirm their

role and effects in the complex in vivo environment of knee OA joints [17].

Therefore, aim of this systematic review was to analyze the available literature on both in vitro and in vivo settings, in order to understand the potential of secretome and EVs as minimally invasive injective biological approach for the treatment of knee OA.

Materials and methods

Data source

A systematic review of the literature was performed on the use of secretome and EVs in both in vitro and in vivo studies for the treatment of OA affecting the knee joint. This search was performed on PubMed, Embase, and Web of Science databases up to the 31st of August 2019 using the following string: (exosom* OR microvesicle* OR vesicle* OR ectosom* OR secretome) AND (mesenchymal stem cell* OR MSC* OR mesenchymal stromal cell* OR ASC* OR ADSC* OR BMC OR BMSC* OR stem cell*) AND (cartilage OR synovi* OR menisc* OR chondrocyte OR chondral OR osteoarthritis OR OA).

Study selection process

Two independent reviewers (AR and DD) conducted the screening process and the analysis of the papers according to PRISMA guidelines. First, the reviewers screened the resulting

records by title and abstract, then the full text of selected manuscripts was screened entirely according to the following inclusion criteria: in vitro and in vivo studies of any level of evidence, written in English language, on the use of secretome and EVs for the treatment of cartilage lesions and OA with focus on the knee joint. Exclusion criteria were articles written in other languages, reviews, studies not analyzing the effect of secretome and EVs or exploiting their potential effect not in the knee. The reviewers also screened the reference lists of the selected papers. The flowchart reported in Figure 1 graphically describes the systematic review process.

Data extraction and synthesis

From the included studies relevant data were extracted, summarized and analyzed according to the purpose of the present work. In particular, the following data were evaluated: cell source of secretome and EVs, target cell types, type of the secreted products (divided in secretome, Exo, and MVs, Figure 2), production method, storage and study design; for the in vivo studies the animal model was also considered together with the method of OA induction. In vitro effects were evaluated in terms of: EVs internalization, effect on viability, proliferation and migration, effect on chondrocyte phenotype, production of cartilaginous ECM, anti-catabolic effect, anti-inflammatory and immunomodulatory effect, effect on apoptosis, autophagy and

senescence. The in vivo effects were evaluated in terms of: effect on cartilage tissue and ECM deposition, effect on synovial inflammation and cytokines, effect on bone tissue, effect on pain and gait.

Results

According to the search strategy, 154 papers were found from PubMed, 148 from Embase, 206 from Web of science. After duplicates removal, 20 papers were analyzed: 9 of those were in vitro studies, 9 in vitro and in vivo, and 2 in vivo studies. In vitro studies have been described in detail in Table 1 while Table 2 pools together studies performed both in vitro and in vivo and those in vivo only. All these studies have been summarized in the following paragraphs.

References	Cell types	Secretome/vesicle types	Isolation method and storage	Study design	Results
Niada *et al.* 2019 Stem Cell Res	Source: Human ASCs (2 males; 6 females; 46 ± 16y) Target: Human chondrocytes (11 m and 7 f; 62 ± 11 y)	Secretome	Cell Passage: NA Secretome collected after 72h of ASCs starvation (ca 10^6 ASCs)	CH+TNFa vs CH+TNFa+ASCs-secretome	No alteration on chondrocytes viability. Secretome addiction reduce osteocalcin, collagen X (anti-hypertrophic effect) MMP3, 13 activity reduction correlated to the abundance of TIMPs in secretome (anticatabolic effect)
Sun *et al.* 2019 J Cell Biochem	Source: BMSCs (3 males; 27,3 y) Target: Human chondrocytes (3 males; mean age, 68.2 ± 7.1 y)	Exo (50 – 200 nm)	Cell passage: 3 Isolation method: Precipitation Storage at – 80 °C	hBMSC-320c-Exos vs hBMSC-Exo vs PBS	Increase of chondrocyte proliferation in hBMSC-320c-Exo group than other Exo, with down-regulated MMP 13 and up-regulated Sox 9 expression during hBMSC chondrogenic differentiation.
Ragni *et al.* 2019 Stem Cell Res & Ther	Source: Human ASCs (mean age 54 ± 8y ;3 female) Target: Human fibroblast-like synoviocytes (mean age 72 ± 7y; 3 female)	EVs (40-400 nm)	Cell passage: range 3-5 Isolation method: Centrifugation Storage: at 4°C for use within 2 days or at – 80 °C	EVs vs EVs+HA	HA is involved in EV internalization EVs reduced the expression of pro-inflammatory cytokines and chemokines in a chronic model of FLS inflammation
Qi *et al.* 2019 In vitro cell & develop biology	Source: rabbit BMSCs Target: Rabbit chondrocytes	Exo (50 – 150 nm)	Cell passage: 3 Isolation method: Ultracentrifugation Storage: NA	BMSCs Exo vs control	All changes induced by Il1b, as decreased cell viability, increased apoptosis was abolished by the addition of BMSCs-Exo.
Liu *et al.* 2018 Cell Cycle	Source: commercial MSCs Target: mouse chondrocytes	Exo (NA)	Cell passage: 3 Isolation method: Exosome isolation reagent Storage: NA	MSCs vs MSCs - Exo	MSC-Exo increased chondrogenic genes Col2a1 and aggrecan, decreased MMP-13 and Runx2. Moreover, MSC-Exo induced cells proliferation and cells apoptosis inhibition
Mao *et al.* 2018 J Cell Mol Med	Source: miR-95-5p-chondrocytes (3M+3F; mean age 35y)	Exo (90-200 nm)	Cell passage: 3 Isolation method: Centrifugation Storage NA	AC-miR-95-5p-Exo vs AC Exo (10 ug vs 50 ug)	50 µg Exo/mL. AC-miR-95-5p-Exo showed greater proliferation than those incubated with other doses. Up-regulated the expression levels
Vonk *et al.* 2018 Theranostic	Source: human BMSCs (1 M+1F; mean age NA) Target: Human chondrocytes (5F+3M; mean age: NA)	EVs (40 -150 nm)	Cell passage: BMSCs 4-7 Chondrocytes 2 Isolation method: Ultracentrifugation + sucrose density Storage NA	EVs vs CM vs CM-EVs	BMMSC-EVs down-regulated COX-2, pro-inflammatory interleukins and inhibited TNF-alpha-induced collagenase activity. Increase proteoglycans production and type II collagen
Tofino-Vian *et al.* 2018 Cell Physiol Biochem	Source: human ASCs (4M and 7F; mean age 53,8 y) Target: Human chondrocytes (27F, 14M)	MVs (279 nm) and Exo (104 nm)	Cell passage: 0 Isolation method: Filtration + Ultracentrifugation Storage: −80°C	MVs vs Exo vs CM vs control	MVs and Exo reduced the production of inflammatory mediators (TNFα, IL-6, PGE_2, NO) Anti-inflammatory and chondroprotective effect mediated by upregulation of annexin1, especially in MVs group
Tofino-Vian *et al.* 2017 Oxid Med Cell Longev	Source: hASC (2M+2F, mean age 54,4 y) Target: human osteoblasts (21F, 9M)	MVs (mean 316 nm) and Exo (115 nm)	Cell passage: 0 Isolation method: Filtration + Ultracentrifugation Storage: −80°C	MVs vs Exo vs CM vs control	CM, MVs and Exo downregulate senescence activity and reduced the production of inflammatory mediators

Table 1: Details of papers with in vitro experiments. Abbreviations: hBMSCs, human bone marrow-derived mesenchymal stem cells; Exo, exosome; EV, extracellular vesicles; HA, hyaluronic acid; ASC, adipose-derived mesenchymal stem cells; MVs, microvesicles; CM, conditioned medium; FLS, fibroblast-like synoviocytes.

References	Animal model	Sources	Secretome/vesicle types	Isolation method and storage	Study design	Results
Only *in vivo* studies						
Khatab S *et al.* 2018 ECM Journal	Mouse OA model	Human BMSCs (mean age 55.3 ± 10 y; female:male ratio 1:2)	Secretome	Cell Passage: 3 Storage: -80°C	MSCs secretome vs MSCs vs medium	Pain reduction at day 7 and better cartilage repair for MSCs secretome and MSC-groups compared to the control. No effects on synovial inflammation, subchondral bone volume or presence of different macrophage subtypes
Zhang *et al.* 2016 Osteoarthritis and Cartilage	Rat Osteochondral defect model	Human embryonic stem cell-derived MSCs	Exo (100 nm)	Cell passage: NA Isolation method: Filtration Storage at -20°C	Exosomes (100 mg) vs PBS	In Exo group, complete restoration of hyaline-like cartilage and subchondral bone with good surface regularity, complete bonding to adjacent cartilage, and ECM deposition
***In vitro* and *in vivo* studies**						
Wu J *et al.* 2019 Biomaterials	Mouse OA model	Source: Human IPFP MSCs Target: human chondrocytes	Exo (mean 121.9 nm)	Cell Passage: 1 Isolation method: Ultrafiltration Storage: -80°C	*In vitro* study IPFP-MSCs vs Exo *In vivo* study 1 sham vs PBS vs Exo-IPFP *In vivo* study 2 PBS + antagomir-NC vs PBS-ExoIPFP + antogomir-NC vs Exo-IPFP+ antagomir-100-5p	*In vitro*: Cell apoptosis inhibition, matrix synthesis promotion, reduction of catabolic markers expression, enhance autophagy level via mTOR inhibition *In vivo*: Exosome significantly prevent cartilage destruction and partially improve gait abnormality. I.A. of antagomir demolishes the remedial effect of MSCs Exo
Liu *et al.* 2018 Biochem J	Rat OA model	Source: commercial MSCs Target: mouse chondrocytes	Exo (NA)	Cell passage: NA Isolation method: isolation reagent kit Storage: NA	*In vitro* study Exo vs Exo- KLF3-AS1 *In vivo* study Normal vs OA vs PBS vs MSCs-Exo Vs MSCsi-KLF3-AS1-Exo	*In vitro*: Exo KLF3-AS1 suppressed IL-1β-induced apoptosis of chondrocytes and promote chondrocytes proliferation. *In vivo*: Exo-KLF3-AS1 promoted cartilage repair in a OA rat model.
Mao G *et al.* 2018 Stem Cell Res & Ther	Mouse OA model	Human BMSCs (mean age: 35; male: 3, female: 3) OA Primary human chondrocytes (mean age: 60.24 y; male: 3, female: 3) Normal cartilage (mean age: 54.46 y; male: 3, female: 3)	Exo (50-150 nm)	Cell passage: BMSCs 3; primary chondrocytes 0 Isolation method: Differential Centrifugation Storage: NA	*In vitro* study Exo (50, 100 and 200 ug) vs miR-92a-3p-Exo (50, 100 and 200 ug) vs PBS for proliferation For other tests 200 ug *In vivo*: MSC-exosome (500 μg/mL) vs MSC-miR-92a-3p-exosome (500 μg/mL) vs OA and normal groups	*In vitro*: miR-92a-3p- exosome promoted higher cells proliferation, matrix genes expression in MSCs and chondrocytes, respectively at 200 ug concentration *In vivo*: *In vivo*: MSC-miR-92a-3p-Exo inhibit cartilage degradation in OA model
Xiang *et al.* 2018 Transl Res	Rabbit Osteochondral defect model	Source: human BMSCs (commercial) Target: human chondrocytes (commercial)	MVs (200 nm)	Cell passage: NA Isolation method: Ultrafiltration+sucrose cushion Storage: NA	*In vitro* MVs 5ul vs MVs 10ul vs MVs 20ul vs PBS *In vivo* 3 weekly I.A. injection PBS vs BMSCs vs MVs	*In vitro* MVs induced chondrocytes proliferation in a dose dependent manner and protected chondrocytes from apoptosis via bioactive lipid, S1P *In vivo* MVs significantly accelerated cartilage recovery as BMSCs. Blocking S1P *in vivo* reduced the therapeutic effect of MVs
Zhang *et al.* 2018 Biomaterials	Rat Osteochondral defect model	Source: human embryonic stem cell-derived MSCs Target: Rat chondrocytes	Exo (100 nm)	Cell passage: 2 Isolation method: Filtration Storage at -20°C	*In vitro* Control vs Exosome 1ug/ml vs 5 ug/ml vs 10ug/ml *In vivo* Exo (100mg) vs PBS (100 ml)	*In vitro* Exosome groups induced cells proliferation and migration increase, with dose-dependent effect; matrix synthesis increase; apoptosis decrease *In vivo* In Exosome group, initial repair at 2 w with neotissue formation and ECM deposition. Improved surface regularity and integration at 6w and complete integration at 12w. MSC exosomes increase M2 macrophage infiltration with a concomitant decrease in M1 macrophages and inflammatory cytokines

Cosenza *et al.* 2017 Scientific Report	Mouse OA model	Source: BMSCs Target: Murine Chondrocytes	Exo (112 ± 6.6 nm) vs MVs (223 ± 15.6 nm)	Cell passage: BMSCs 10-20; Isolation method: Centrifugation No storage, freshly use	*In vitro* MVs or Exosome (12.5 ng; 125 ng or 1.25 μg) vs BM-MSC-CM (1 mL) vs BM-MSCs (10^5 cells). *In vivo* a single I.A. injection BM-MSCs (2.5×10^5 cells/5 μL saline) vs MVs (500 ng/5 μL) vs Exosome (250 ng/5 μL)	*In vitro* MVs and exosome exerted similar chondroprotective and anti-inflammatory function *In vivo* MVs and exosome protected from developing OA
Tao *et al.* 2017 Theranostic	Rat OA model	Source: SMSC from pts aged 30-35 Target: Human Chondorcytes from pts aged 45-55	Exo (30 -150 nm)	Cell passage: SMSC 5 Isolation method: Centrifugation No storage, freshly use	*In vitro* SMSC-exosome vs SMSC-140-exosome *In vivo* 4 weekly I.A injection sham vs saline vs SMSC-140-Exosome vs SMSC-exosome	*In vitro* SMSC-140-exosome enhanced the proliferation and migration of ACs without damaging ECM secretion *In vivo* SMSC-140-Exosome slowed the progression of early OA and prevent severe damage to knee articular cartilage.
Wang *et al.* 2017 Stem Cell Research & Therapy	Mouse OA model	Source: Human ES embryonic stem cells Target: mouse chondrocytes	Exo (38 nm to 169 nm)	Cell passage: ES 4 - 7; chondrocytes 3 Isolation method: Centrifugation Storage at -80 °C	*In vitro* CM+exosome vs CM vs exosome *In vivo* 2 I.A. inj/week Exo (1×10^9) vs PBS	*In vitro* Chondrocyte phenotype maintainance in Exosome group by increasing collagen type II synthesis and decreasing ADAMTS5 expression *In vivo* Exo alleviated cartilage destruction and matrix degradation
Zhu *et al.* 2017 Stem Cell Research & Therapy	Mouse OA model	Source: human SMSC from synovium of aged 22-28 and iMSC	Exo (50–150 nm)	Cell passage: NA Isolation method: Ultrafiltration Storage at -80 °C	*In vitro* iMSC-Exosome vs SMSC - Exosome *In vivo* 3 weekly I.A. injection normal vs iMSC-Exosome (1.0×10^{10}/ml) vs SMSC - Exosome (1.0×10^{10}/ml) vs untreated	*In vitro* Chondrocyte migration and proliferation were stimulated by both iMSC-Exosome and SMMSC-Exosome, with iMSC-Exosome exerting a stronger effect. *In vivo* iMSC-Exosome and SMMSC-Exosome both attenuated OA in the mouse OA model, but iMSC-Exosome had a superior therapeutic effect compared with SMMSC-Exosome.

Table 2. Details of studies with in vitro and in vivo experiments. Abbreviations: IPFP, infrapatellar fat pad MSCs; I.A., intra-articular; Exo, Exosome; BMSCs, bone marrow-derived MSCs; MVs, microvesicles/microparticles; synovial MSCs (SMSC); ACs, articular chondrocytes; ES, embryonic stem cells; CM, conditioned medium; iMSC, induced pluripotent stem cell-derived MSCs; ECM, extracellular matrix.

In vitro studies

In vitro studies were published from 2017 with a rapidly increasing trend of publications (Figure 3). Among the 18 in vitro studies, 6 articles used bone marrow-derived MSCs (BMSCs), 4 adipose-derived stem cells (ASCs), 2 embryonic stem cell-derived MSCs (EMSCs), 2 commercial (not otherwise specified) MSCs, 1

synovial-derived MSCs (SMSCs), 1 chondrocytes, 1 infra patellar fat pad (IPFP)-derived MSCs, and 1 compared SMSCs with induced pluripotent stem cell line (iPSC)-derived MSCs; furthermore, 1 study compared the effects of secretome, MVs, and Exo compared to BMSCs. Twelve articles investigated the effect of Exo, 4 evaluated Exo with MVs, 1 EVs (without other details), and 1 secretome. The most selected method to isolate EVs was differential centrifugation (5), followed by precipitation-based commercial kits (4), differential centrifugation coupled with a filtration step (3), filtration (3), differential centrifugation with sucrose density centrifugation (1), filtration and sucrose density centrifugation (1), while one paper did not report the detailed isolation protocol (1). Results of in vitro studies were summarized according to:

- *EVs internalization*: EVs [18–23] can be internalized very quickly, already after 30 min from their administration [20]. Moreover, the kinetic of their uptake reached a maximum after 12-18 h [19,21] when cells appeared to be saturated, and continued up to the last evaluation performed at 24 h after EVs addition [19,21]. The intracytoplasmic localization of internalized Exo was identified in the perinuclear region [18,19,23].

- *Effect on viability, proliferation, and migration*: A total of 14 papers investigated the effect of EVs or secretome on cell proliferation, viability, and migration (Table 1) [18,20,29–32,21–28]. Twelve

papers reported that EVs derived from MSCs increased the proliferation and/or the viability of OA chondrocytes or chondrocyte progenitor cells [18,20,31,32,21–23,25,26,28–30], with a dose dependent effect [18,21,22,26], while two papers [24,27] reported no significant effects on chondrocytes viability. One study compared the effect on chondrocyte proliferation of Exo derived from two different MSCs sources [31], iPS-derived MSCs and SMSCs, finding that Exo from iPS-MSCs had superior effects than SMSC-Exo. While high proliferation mediated by SMSCs-Exo was correlated with a concomitant decrease of the extracellular matrix (ECM) components: this was not observed with Exo enriched with a particular micro RNA (miR-140-5p), as shown by Tao et al. [23]. Finally, 7 articles [21,23,25,26,28,30,31] documented that cell migration increased after Exo administration, showing also dose dependency [21,26,28].

- *Effect on chondrocyte phenotype*: Thirteen papers assessed phenotype maintenance and chondrocyte hypertrophy after the treatment with EVs or secretome [20,21,32–34,23–30]. Regarding the maintenance or the induction of chondrocyte phenotype, 3 studies described the increase of the expression of SOX9 [20,25,30], mediated by EVs. Six works analyzed chondrocyte hypertrophy status after EVs addition [20,24,28–30,32], and 4 of them showed that the expression of the transcription factor RUNX2 diminished with EVs [20,28,30,32]. Liu et al. [28] reported

that this reduction was dose dependent. At protein level, 4 papers observed the decreased expression of type-X collagen mediated by EVs, either normal [20,24] or overexpressing miR-92a-3p [30] or miR-95-5p [29]. Similarly, the level of other two hypertrophy markers (alkaline phosphatase and osteocalcin) were lowered [20,24].

- *Production of cartilaginous ECM*: ECM protein expression was investigated in 13 studies [19,20,32–34,21,23,25–30]. Among these papers, 11 quantified the expression of ECM components, in particular type-II collagen and aggrecan, in chondrocytes treated with EVs or secretome [20,23,34,25–30,32,33]. Nine papers reported induction of type-II collagen and aggrecan expression by EVs, with a dose dependent effect [28,33,34] and showed a tendency towards better effects exerted by MVs over Exo [27,33]. Only one study by Tao et al. [23] reported that SMSCs-Exo diminished the expression of COL2A1 and aggrecan in a dose-dependent manner, but this effect was reverted with the use of Exo overexpressing miR-140-5p. In general, all papers investigating the effects of EVs enriched with specific miRNA [25,26,29,30] reported a significant improvement of ECM protein level. Finally, Exo had positive effects also on Cartilage Oligomeric Matrix Protein (COMP) [21] and on HAS-1,2,3 levels [19] increase. In particular, Ragni et al. [19] showed that 2 days after Exo addition HAS-1 was upregulated while HAS-3 was

downregulated and the isoform 2 did not show any significant variation.

- *Anti-catabolic effect*: Twelve of the included papers evaluated the anti-catabolic effect of EVs on chondrocytes or synovial fibroblasts [19,20,33,34,24–30,32], showing a general positive effect with a dual action on catabolic proteins decrease or increase of their inhibitors. The expression of matrix metalloproteinase 13 (MMP-13) resulted lower in 8 studies [19,26–30,32,33], with a dose-dependent effect [28]; while two papers did not observe any variation [24,25]. In particular, Sun et al. [25] demonstrated the superiority of Exo-miR-320c in decreasing MMP-13 levels with respect to normal Exo. Two works reported a tendency of superior effects exerted by MVs over Exo and secretome [27,33] in reducing MMP-13 expression [33] and MMP activity in a dose-dependent manner [27]. Ragni et al. [19] showed a reduction of MMP-1 levels at an early time point (2 days). On the other hand, Niada et al. [24] reported that secretome increased tissue inhibitors of MMPs (TIMP) -1, -2, -3, and -4, supporting that the minor MMP activity might be ascribed to the production of TIMPs. Three papers [26,33,35], investigated the expression of ADAMTS5, describing a comparable reduction in Exo and MVs groups, but greater than the one induced by the secretome [33]. Finally, Vonk et al. [20] showed that collagenase activity was significantly reduced by EVs administration, with a concomitant

increase of Wnt-7a expression, which could contribute to the prevention of cartilage damage and to the regeneration process.

- *Anti-inflammatory and Immunomodulatory effect*: Positive effects have also been reported for the anti-inflammatory and immunomodulatory action mediated by secretome or EVs, and described in 6 studies [19,20,27,30,33,36], showing the reduction of inflammatory mediators and the increase of anti-inflammatory molecules. In particular, it was demonstrated that the expression of Cyclooxygenase 2 (COX-2), Interleukin 1 alpha (IL-1α), -1 beta (-1β), -6, -8, and -17 [20], Tumor necrosis Factor alpha (TNF-α), IL-6, Microsomal Prostaglandin E Synthase-1 (mPGES-1), inducible Nitric Oxide Synthase (iNOS), and Prostaglandin E2 (PGE-2) [27] decreases following secretome or EVs administration, while anti-inflammatory factors like IL-10 increases [27]. Concerning the effects exerted by different EVs types, secretome was shown to be significantly more effective than Exo in decreasing COX-2 and mPGES-1 expression [27], as well as TNF-α quantity [33]. Conversely, the expression of iNOS showed a dose-dependent reduction following the administration of Exo and MVs, which both exerted significantly better results than the secretome [33]. Finally, the study of the polarization of macrophages phenotype showed that both Exo and MVs diminished their activation [33].

- Effect on apoptosis: As increased chondrocyte apoptosis represents another feature of OA cartilage, 6 papers investigated the impact of EVs on this cell process [18,22,26,28,32,33], all reporting a significant decrease in apoptosis rate. Among these, 3 also demonstrated a dose dependent reduction of OA chondrocyte apoptosis [22,28,33], with superior results for Exo versus MVs [33]. One paper studied the effect of Exo overexpressing a long non-coding RNA (KLF3-AS1) [32], showing that not transfected MSC-Exo significantly reversed IL-1β-mediated chondrocyte apoptosis, and that KLF3-AS1-Exo consolidated this inhibition.
- Autophagy and senescence: Another cell process important for cartilage biology during OA progression is autophagy, assessed by Wu et al. [26], showing that Exo significantly increased autophagy in IL-1β-treated chondrocytes. Finally, Tofiño-Viann et al. [36] demonstrated that Exo, MVs, and secretome significantly reverted mitochondrial membrane increase and oxidative stress induced by IL-1β, thus causing a reduction in DNA damage and resulting in inhibition of the senescence process.

In vivo studies

In vivo studies were published from 2016 with a rapidly increasing trend of publications (Figure 3). Among 11 in vivo

studies, 9 included both an in vitro investigation and an animal model study. Six studies have been performed in mouse, 4 in rat, and 1 in rabbit. Three studies created an osteochondral defect model and 8 an OA model. Eight articles investigated the effect of Exo, 1 of secretome, 1 of MVs, and 1 compared Exo with MVs. Regarding the cell source, 4 used EVs or secretome from BMSCs, 3 from EMSCs, 2 from SMSCs, 1 from IPFP, and 1 commercial not better specified MSCs. The most selected method to isolate EVs was differential centrifugation (4), followed by ultrafiltration (2), filtration (2), precipitation-based commercial kits (1), and sucrose density centrifugation (1). All studies showed positive effects after the administration of secretome, Exo, or MVs in both osteochondral [21,22,35] and OA defect models [23,26,28,30,31,33,34,37]. The results of in vivo studies have been summarized according to:

- *Effect on cartilage tissue and ECM deposition*: Animal studies showed that Exo was effective in cartilage surface restoration and ECM deposition [21,26,31,34,35], regenerating a hyaline-like cartilage completely integrated with the adjacent tissues [31,35]. Zhang et al. [21] demonstrated that this repair and the deposition of ECM started 2 weeks post-injection and increased over time for up to 12 weeks. Similar results after Exo and MVs injections were reported, both providing protection from OA development [33] and showing that both vesicles are equally effective in

counteracting tissues degeneration and promoting cartilage regeneration. Positive effects on cartilage repair and ECM deposition have also been described for Exo derived from cells over-expressing microRNA [23,30] or engineered to silence specific genes [28]. These results were superior to those induced by normal Exo. Finally, Khatab et al. [37] and Xiang et al. [22] demonstrated that the effect of secretome and MVs injections on cartilage and ECM were the same as those exerted by MSC injection.

- *Effect on synovial inflammation and cytokines*: Two studies addressed this issue, one showing that Exo increased M2 macrophage infiltration while decreased M1 and inflammatory cytokines [21], while the other study was unable to demonstrate any effect on synovial inflammation for both secretome and MSCs [37].

- *Effect on bone tissue*: Regarding subchondral bone, both Exo and MVs were effective in terms of regeneration: Zhang et al. [21,35] showed complete subchondral bone restoration; Cosenza et al. [33] described higher bone volume and lower bone degradation at epiphyseal and subchondral level following MVs or MSCs injections with respect to controls. Conversely, no effect on bone remodeling was reported by Khatab et al. for both secretome and MSCs [37].

- *Effect on pain and gait*: Another interesting aspect is that Exo injections were able to partially ameliorate gait abnormality patterns in the OA mouse model [26]. Moreover, Khatab et al. [37] demonstrated that both secretome and MSCs provided early (day 7) pain reduction in the treated animals.

Discussion

The main finding of this systematic review is that the use of secretome and EVs for the treatment of cartilage pathology and knee OA had pleiotropic effects and overall positive results. In vitro, both secretome and EVs showed anticatabolic, immunomodulatory, and regenerative properties, and in vivo studies confirmed the effectiveness as minimally invasive treatment, with positive effects on the whole joint.

The literature analysis supports the use of secretome and EVs with an increasing number of preclinical studies. The overall successful results, coupled with the same low immunogenicity of MSCs, and potentially fewer legal issues compared to therapies based on cell transplantation [38], make this biological approach a good candidate for human translatability. The use of secretome and EVs as a minimally invasive treatment for OA in an in vivo preclinical model showed that it was equally effective as MSCs in terms of pain improvement and morphological changes [37], and even proved the superiority of MVs and Exo over BMSCs in terms

of joint protection from OA [33]. On the other hand, the literature analysis also underlined that, despite the increasing interest with many recent publications, this field is still in its infancy, with several approaches proposed but lacking the underlying understanding of biological roles and functions. In addition, standardizations and indications on the most suitable strategies for exploiting the potential of this biological approach are also still lacking.

With the aim to evaluate the potential of secretome and EVs as new cell derived approaches for the treatment of knee OA, the available literature was screened for both in vitro and in vivo studies assessing the role of these biological products in the different physiologic processes involved in cartilage lesions and OA progression and treatment. Three different cell derived products were considered: secretome, Exo, and MVs. For this analysis, the secretome group included all studies that specifically referred to the secretome. Regarding the EVs, they are a heterogeneous population which has been classified into three classes according to their biogenesis and size: apoptotic bodies, MVs and Exo [39]. The apoptotic bodies, the largest EVs population, range from 200 nm to 5000 nm, and they are secreted by the shedding of the plasma membrane of apoptotic dying cells. The MVs, also called ectosomes or microparticles, are 200-800 nm sized EVs that are shedded from the plasma membrane of viable

cells. Exo, which are 30-200 nm in size, are formed intracellularly and then released within the multivesicular bodies pathway. However, this classic EVs nomenclature results overburdened and sometimes confusing [40]. For the purpose of this systematic review EVs have been subdivided in two different population as small (below 200 nm) and medium-sized EVs (larger vesicles), following the statement of the of the International Society for Extracellular Vesicles [41], but maintaining the nomenclature used in all the papers analyzed, Exo and MVs respectively.

The literature analysis showed a great heterogeneity among studies in terms of EVs used, size, and isolation procedures. The most investigated EVs type is Exo, with a different size range (from 50 to 200 nm), making it difficult to compare among studies or correlate EVs characteristics and in vitro and in vivo results. Only one study [33] investigated the effect of different EVs types, comparing MVs and Exo on a chondrocytes culture and an in vivo OA model. The study showed that both EVs exert similar chondroprotective and anti-inflammatory effects, delaying OA development, leaving the question on the most suitable approach still open. The isolation procedures represent a critical aspect, since there is no standardized method to isolate EVs, resulting in different protocols and therefore different products to be used. The main methods used are differential centrifugation, filtration and precipitation-based reagent, but there is a lack of

standardized methods to obtain them, possibly contributing to EVs variability. Moreover, secretome and EVs can be obtained from different cell sources.

This systematic review showed that the most used cell source are currently BMSCs, followed by ASCs, EMSCs, SMSCs, but there is lack of information available about the difference between vesicles derived from different cells and thus the optimal cell source to address OA remains elusive. Only one study [31] compared the effects of Exo secreted by iPS-derived MSCs and SMSCs in vitro. This showed that they both stimulated chondrocyte proliferation in a dose-dependent manner, but results depended on the cell source, with superior effect of Exo from iPS-derived MSCs on cell proliferation, at high concentration, and superior therapeutic effect in attenuating OA in a mouse model.

The proper selection of EVs cell source and also the stage of cell differentiation are actually critical aspects, since they can determine the characteristics and properties of EVs to fit specific applications (such as reducing inflammation, promoting cartilage regeneration and protection from OA features) [38]. Furthermore, the surrounding microenvironment seems to play an active role in determining the composition of both secretome and EVs cargo, ultimately affecting their action on target cells [42]. Analogously, the type of media and substrate used for cell culture, as well as

the use of primary or immortalized cells can also independently affect secretome and EVs composition [38]. For the translational potential of secretome and EVs into a clinically available therapeutic option, another key factor to be considered is the proper dosage [21,22,29,30,33]. In this regard, the literature presents concordant findings, with all papers that compared different amounts reporting a dose dependent effect and superior results at the higher quantities. However, no effects of different dosages were described in the analyzed animal models. In addition, the lack of standardization, also in terms of unit of measurement employed to express the used amount of EVs and thus the presence of heterogeneous products, prevents the possibility to identify the best EVs concentration for an optimal effect in terms of OA treatment. Further efforts should investigate the protocols to optimize secretome and EVs production toward OA treatment.

While studies focusing on the most suitable cell source and dosage could foster the clinical translatability of this biological approach, research efforts are already invested into the investigation on how to further develop this field by optimizing secretome and EVS potential. In this light, among the beneficial effects mediated by EVs, one aspect remains critical: Tao et al. [23] reported that chondrocytes treated with normal Exo decreased ECM proteins expression. On the contrary, the treatment with

miR-140-5p-Exo, expressed during the development and homeostasis of cartilage and lowered in OA [43], did not affect ECM protein secretion. miRNAs are important Exo components, and their role has been demonstrated in repressing chondrocytes inflammation, promoting chondrogenesis, and inhibiting cartilage degeneration. Considering these effects on chondrocytes, 5 studies [23,25,26,29,30] investigated the overexpression of different miRNAs in Exo, describing in general better results compared to the normal Exo in terms of cell proliferation, gene expression, ECM components' production in vitro and inhibition of cartilage degradation in vivo. Furthermore, Liu et al. [32] described the effect of over expressing a long non-coding RNA KLF3-AS1, a competitive endogenous RNA which was able to inhibit miR-206, a miRNA that resulted overexpressed in OA.

Another feature of OA is synovial inflammation, notably characterized by activation of monocytes and macrophages. One major immunosuppressive effect of BM-MSCs is to inhibit macrophage activation and to induce a shift from M1 pro-inflammatory to M2 anti-inflammatory phenotype [44]. In this light, Cosenza et al. [33] demonstrated that both MVs, Exo, and BM-MSCs inhibited in vitro macrophage activation to a similar extent. On the contrary, Khatab et al. [37] did not report any significant change on synovial thickness or synovial

macrophages phenotypes using secretome injection in an OA mouse model, although several significant moderate correlations between macrophage phenotypes and OA characteristics were found. Another aspect was investigated: different types of stress can lead to a premature cellular senescence. Among these, chronic inflammation can increases oxidative stress driving to cellular senescence, a process that can contribute to the development and progression of OA [45]. In this context, Exo was able to revert the oxidative stress induced by IL-1β, thus causing a reduction in DNA damage and resulting in inhibition of the senescence process [36].

All these investigated targets confirmed the pleiotropic effects of secretome and EVs, which led to positive effects also in vivo. Exo injections were able to partially ameliorate the gait abnormality patterns in the OA mouse model [26], and secretome injections provided early (day 7) pain reduction in treated animals, similar to MSCs [37], further supporting the translational potential of this biological approach. On the other hand, this systematic review also underlined several critical aspects needing additional investigation to further develop and optimize this biological treatment strategy. The promising in vitro and in vivo results support the potential of this new treatment approach, opening new perspectives for cell-based therapies. Secretome and EVs could require less complex regulation procedures than

treatments based on cell transplantation, while providing similar results of MSCs. The standardization of protocols could further facilitate clinical translatability. In this light, research efforts are required for the identification of the proper cell source, the best preparation protocol and the most suitable target and, in the end, for the translation of the preclinical promising findings into clinical trials to confirm the potential of secretome and EVs as minimally invasive biological treatment to address knee OA.

Conclusion

This systematic review of the literature underlined an increasing interest towards this emerging field, with overall positive findings. Promising in vitro results have been documented in terms of enhanced cell proliferation, reduction of inflammation, down regulation of catabolic pathways while promoting anabolic processes. The positive in vitro findings were confirmed in vivo, with studies showing positive effects on cartilage, subchondral bone, and synovial tissues in both OA and osteochondral models. However, several aspects remain to be clarified, like the different effects induced by EVs and secretome, the most suitable cell source and production protocol, as well as the identification of patients that may benefit more from this new biological approach for the treatment of knee OA.

Acknowledgments: This work was partially supported by ABREOC project (Grant n° 17-019).

Authors contribution: DD Systematic research and writing; AR Systematic research and writing; MC Review and editing; MM Methodology, review and editing; CC Review and editing; GF Conceptualization, methodology, senior editing.

Conflicts of Interest: The authors declare no conflict of interest

Legend

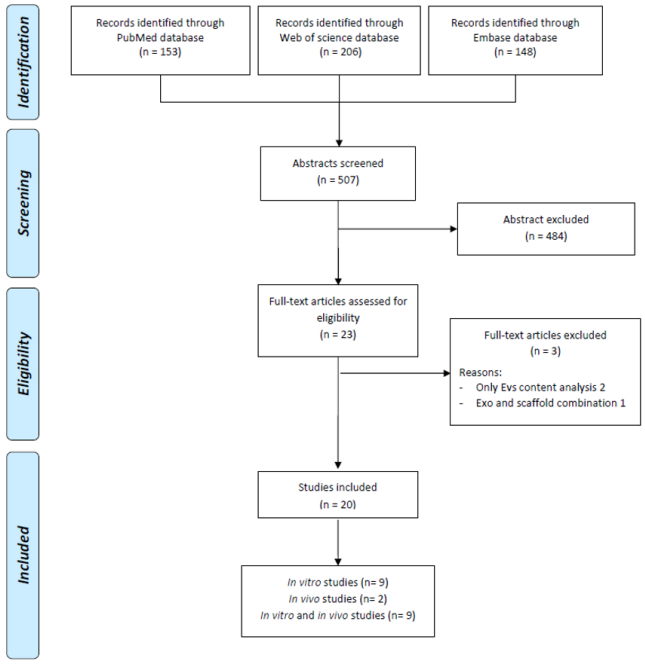

Figure 1. PRISMA (Preferred Reporting Items for Systematic Reviews and Meta-Analysis) flowchart of the systematic literature review.

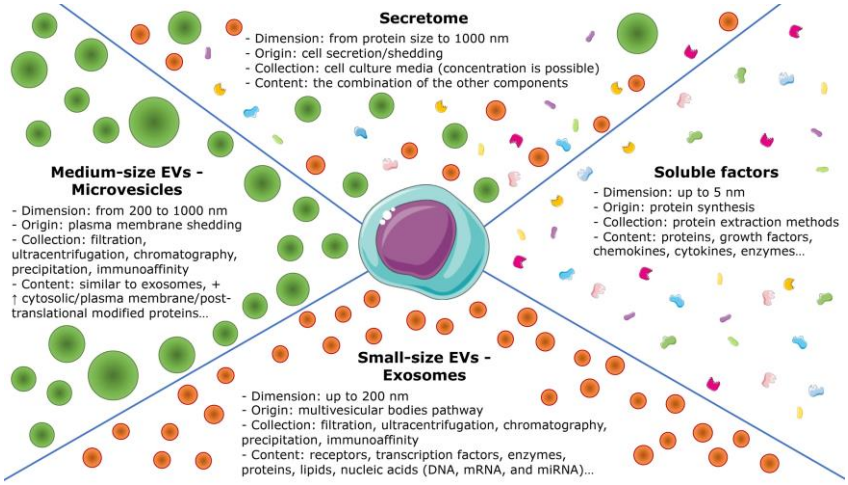

Figure 2. Schematic representation of secretome components.

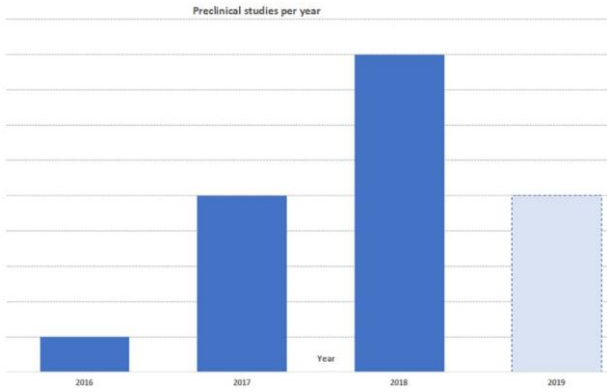

Figure 3. Published preclinical articles per year.

References

1. van der Kraan, P.M.; van den Berg, W.B. Osteoarthritis in the context of ageing and evolution. Loss of chondrocyte differentiation block during ageing. Ageing Res. Rev. 2008, 7, 106–113.
2. Aigner, T.; Rose, J.; Martin, J.; Buckwalter, J. Aging theories of primary osteoarthritis: from epidemiology to molecular biology. Rejuvenation Res. 2004, 7, 134–145.

3. Jafarzadeh, S.R.; Felson, D.T. Updated Estimates Suggest a Much Higher Prevalence of Arthritis in United States Adults Than Previous Ones. Arthritis Rheumatol. 2018.
4. Farr Ii, J.; Miller, L.E.; Block, J.E. Quality of life in patients with knee osteoarthritis: a commentary on nonsurgical and surgical treatments. Open Orthop. J. 2013, 7, 619–623.
5. Deshpande, B.R.; Katz, J.N.; Solomon, D.H.; Yelin, E.H.; Hunter, D.J.; Messier, S.P.; Suter, L.G.; Losina, E. Number of Persons With Symptomatic Knee Osteoarthritis in the US: Impact of Race and Ethnicity, Age, Sex, and Obesity. Arthritis Care Res. (Hoboken). 2016, 68, 1743–1750.
6. Musumeci, G.; Aiello, F.C.; Szychlinska, M.A.; Di Rosa, M.; Castrogiovanni, P.; Mobasheri, A. Osteoarthritis in the XXIst century: Risk factors and behaviours that influence disease onset and progression. Int. J. Mol. Sci. 2015, 16, 6093–6112.
7. Bijlsma, J.W.J.; Berenbaum, F.; Lafeber, F.P.J.G. Osteoarthritis: An update with relevance for clinical practice. Lancet 2011.
8. Caplan, A.I.; Correa, D. The MSC: An injury drugstore. Cell Stem Cell 2011.
9. Prockop, D.J.; Youn Oh, J. Mesenchymal stem/stromal cells (MSCs): Role as guardians of inflammation. Mol. Ther. 2012.
10. Filardo, G.; Perdisa, F.; Roffi, A.; Marcacci, M.; Kon, E. Stem cells in articular cartilage regeneration. J. Orthop. Surg. Res. 2016, 11, 42.
11. Roffi, A.; Nakamura, N.; Sanchez, M.; Cucchiarini, M.; Filardo, G. Injectable Systems for Intra-Articular Delivery of Mesenchymal Stromal Cells for Cartilage Treatment: A Systematic Review of Preclinical and Clinical Evidence. Int. J. Mol. Sci. 2018, 19.
12. Lopa, S.; Colombini, A.; Moretti, M.; de Girolamo, L. Injective mesenchymal stem cell-based treatments for knee osteoarthritis: from mechanisms of action to current clinical evidences. Knee Surg. Sports Traumatol. Arthrosc. 2019, 27, 2003–2020.
13. Deasy, B.M.; Anderson, J.E.; Zelina, S. Regulatory Issues in the Therapeutic Use of Stem Cells. In Regenerative Medicine and Tissue Engineering; Andrades, J.A., Ed.; IntechOpen: Rijeka, 2013.
14. Turner, L.; Knoepfler, P. Selling Stem Cells in the USA: Assessing the Direct-to-Consumer Industry. Cell Stem Cell 2016.
15. Madrigal, M.; Rao, K.S.; Riordan, N.H. A review of therapeutic effects of mesenchymal stem cell secretions and induction of secretory modification by different culture methods. J. Transl. Med. 2014.
16. Malda, J.; Boere, J.; Van De Lest, C.H.A.; Van Weeren, P.R.; Wauben, M.H.M. Extracellular vesicles - New tool for joint repair and regeneration. Nat. Rev. Rheumatol. 2016.
17. Mancuso, P.; Raman, S.; Glynn, A.; Barry, F.; Murphy, J.M. Mesenchymal Stem Cell Therapy for Osteoarthritis: The Critical Role of the Cell Secretome. Front. Bioeng. Biotechnol. 2019, 7, 9.

18. Qi, H.; Liu, D.; Xiao, D.; Tian, D.; Su, Y.; Jin, S. Exosomes derived from mesenchymal stem cells inhibit mitochondrial dysfunction-induced apoptosis of chondrocytes via p38 , ERK , and Akt pathways. Vitr. Cell. Dev. Biol. - Anim. 2019, 55, 203–210.
19. Ragni, E.; Perucca Orfei, C.; De Luca, P.; Lugano, G.; Viganò, M.; Colombini, A.; Valli, F.; Zacchetti, D.; Bollati, V.; De Girolamo, L. Interaction with hyaluronan matrix and miRNA cargo as contributors for in vitro potential of mesenchymal stem cell-derived extracellular vesicles in a model of human osteoarthritic synoviocytes. Stem Cell Res. Ther. 2019, 10, 1–17.
20. Vonk, L.A.; van Dooremalen, S.F.J.; Liv, N.; Klumperman, J.; Coffer, P.J.; Saris, D.B.F.; Lorenowicz, M.J. Mesenchymal stromal/stem cell-derived extracellular vesicles promote human cartilage regeneration in vitro. Theranostics 2018, 8, 906–920.
21. Zhang, S.; Chuah, S.J.; Lai, R.C.; Hui, J.H.P.; Lim, S.K.; Toh, W.S. MSC exosomes mediate cartilage repair by enhancing proliferation, attenuating apoptosis and modulating immune reactivity. Biomaterials 2018, 156, 16–27.
22. Xiang, C.; Yang, K.; Liang, Z.; Wan, Y.; Cheng, Y.; Ma, D.; Zhang, H.; Hou, W.; Fu, P. Sphingosine-1-phosphate mediates the therapeutic effects of bone marrow mesenchymal stem cell-derived microvesicles on articular cartilage defect. Transl. Res. 2018, 193, 42–53.
23. Tao, S.C.; Yuan, T.; Zhang, Y.L.; Yin, W.J.; Guo, S.C.; Zhang, C.Q. Exosomes derived from miR-140-5p-overexpressing human synovial mesenchymal stem cells enhance cartilage tissue regeneration and prevent osteoarthritis of the knee in a rat model. Theranostics 2017, 7, 180–195.
24. Niada, S.; Giannasi, C.; Gomarasca, M.; Stanco, D.; Casati, S.; Brini, A.T. Adipose-derived stromal cell secretome reduces TNFα-induced hypertrophy and catabolic markers in primary human articular chondrocytes. Stem Cell Res. 2019, 38, 101463.
25. Sun, H.; Hu, S.; Zhang, Z.; Lun, J.; Liao, W.; Zhang, Z. Expression of exosomal microRNAs during chondrogenic differentiation of human bone mesenchymal stem cells. J. Cell. Biochem. 2019, 120, 171–181.
26. Wu, J.; Kuang, L.; Chen, C.; Yang, J.; Zeng, W.N.; Li, T.; Chen, H.; Huang, S.; Fu, Z.; Li, J.; et al. miR-100-5p-abundant exosomes derived from infrapatellar fat pad MSCs protect articular cartilage and ameliorate gait abnormalities via inhibition of mTOR in osteoarthritis. Biomaterials 2019, 206, 87–100.
27. Tofiño-Vian, M.; Guillén, M.I.; Pérez Del Caz, M.D.; Silvestre, A.; Alcaraz, M.J. Microvesicles from Human Adipose Tissue-Derived Mesenchymal Stem Cells as a New Protective Strategy in Osteoarthritic Chondrocytes. Cell. Physiol. Biochem. 2018, 47, 11–25.
28. Liu, Y.; Zou, R.; Wang, Z.; Wen, C.; Zhang, F.; Lin, F. Exosomal KLF3-AS1 from hMSCs promoted cartilage repair and chondrocyte proliferation in osteoarthritis. Biochem. J. 2018, 475, 3629–3638.

29. Mao, G.; Hu, S.; Zhang, Z.; Wu, P.; Zhao, X.; Lin, R.; Liao, W.; Kang, Y. Exosomal miR-95-5p regulates chondrogenesis and cartilage degradation via histone deacetylase 2/8. J. Cell. Mol. Med. 2018, 22, 5354–5366.
30. Mao, G.; Zhang, Z.; Hu, S.; Zhang, Z.; Chang, Z.; Huang, Z.; Liao, W.; Kang, Y. Exosomes derived from miR-92a-3poverexpressing human mesenchymal stem cells enhance chondrogenesis and suppress cartilage degradation via targeting WNT5A. Stem Cell Res. Ther. 2018, 9, 1–13.
31. Zhu, Y.; Wang, Y.; Zhao, B.; Niu, X.; Hu, B.; Li, Q.; Zhang, J.; Ding, J.; Chen, Y.; Wang, Y. Comparison of exosomes secreted by induced pluripotent stem cell-derived mesenchymal stem cells and synovial membrane-derived mesenchymal stem cells for the treatment of osteoarthritis. Stem Cell Res. Ther. 2017, 8, 1–11.
32. Liu, Y.; Lin, L.; Zou, R.; Wen, C.; Wang, Z.; Lin, F. MSC-derived exosomes promote proliferation and inhibit apoptosis of chondrocytes via lncRNA-KLF3-AS1/miR-206/GIT1 axis in osteoarthritis. Cell Cycle 2018, 17, 2411–2422.
33. Cosenza, S.; Ruiz, M.; Toupet, K.; Jorgensen, C.; Noël, D. Mesenchymal stem cells derived exosomes and microparticles protect cartilage and bone from degradation in osteoarthritis. Sci. Rep. 2017, 7, 1–12.
34. Wang, Y.; Yu, D.; Liu, Z.; Zhou, F.; Dai, J.; Wu, B.; Zhou, J.; Heng, B.C.; Zou, X.H.; Ouyang, H.; et al. Exosomes from embryonic mesenchymal stem cells alleviate osteoarthritis through balancing synthesis and degradation of cartilage extracellular matrix. Stem Cell Res. Ther. 2017, 8, 1–13.
35. Zhang, S.; Chu, W.C.; Lai, R.C.; Lim, S.K.; Hui, J.H.P.; Toh, W.S. Exosomes derived from human embryonic mesenchymal stem cells promote osteochondral regeneration. Osteoarthr. Cartil. 2016, 24, 2135–2140.
36. Tofiño-Vian, M.; Guillén, M.I.; Pérez Del Caz, M.D.; Castejón, M.A.; Alcaraz, M.J. Extracellular vesicles from adipose-derived mesenchymal stem cells downregulate senescence features in osteoarthritic osteoblasts. Oxid. Med. Cell. Longev. 2017, 2017.

37. Khatab, S.; van Osch, G.; Kops, N.; Bastiaansen-Jenniskens, Y.; Bos, P.; Verhaar, J.; Bernsen, M.; van Buul, G. Mesenchymal stem cell secretome reduces pain and prevents cartilage damage in a murine osteoarthritis model. Eur. Cells Mater. 2018, 36, 218–230.
38. Li, J.J.; Hosseini-Beheshti, E.; Grau, G.E.; Zreiqat, H.; Little, C.B. Stem Cell-Derived Extracellular Vesicles for Treating Joint Injury and Osteoarthritis. Nanomater. (Basel, Switzerland) 2019, 9.
39. Barile, L.; Vassalli, G. Exosomes: Therapy delivery tools and biomarkers of diseases. Pharmacol. Ther. 2017, 174, 63–78.
40. Lässer, C.; Jang, S.C.; Lötvall, J. Subpopulations of extracellular vesicles and their therapeutic potential. Mol. Aspects Med. 2018.
41. Théry, C.; Witwer, K.W.; Aikawa, E.; Alcaraz, M.J.; Anderson, J.D.; Andriantsitohaina, R.; Antoniou, A.; Arab, T.; Archer, F.; Atkin-Smith, G.K.; et

al. Minimal information for studies of extracellular vesicles 2018 (MISEV2018): a position statement of the International Society for Extracellular Vesicles and update of the MISEV2014 guidelines. J. Extracell. Vesicles 2018, 7, 1535750.
42. Baraniak, P.R.; McDevitt, T.C. Stem cell paracrine actions and tissue regeneration. Regen. Med. 2010.
43. Endisha, H.; Rockel, J.; Jurisica, I.; Kapoor, M. The complex landscape of microRNAs in articular cartilage: biology, pathology, and therapeutic targets. JCI insight 2018, 3, e121630.
44. Nemeth, K.; Leelahavanichkul, A.; Yuen, P.S.T.; Mayer, B.; Parmelee, A.; Doi, K.; Robey, P.G.; Leelahavanichkul, K.; Koller, B.H.; Brown, J.M.; et al. Bone marrow stromal cells attenuate sepsis via prostaglandin E(2)-dependent reprogramming of host macrophages to increase their interleukin-10 production. Nat. Med. 2009, 15, 42–49.
45. Loeser, R.F. Aging processes and the development of osteoarthritis. Curr. Opin. Rheumatol. 2013, 25, 108–113.

Chapter 7

Discussion

Osteoarthritis represents a relevant global burden, and it is characterized by an increasing incidence and a rising socio-economic impact. Despite its relatively high morbidity, the diagnosis of OA is still hampered by the lack of effective biomarkers able to signal the precocious biological and structural alterations that occur during the disease development. In addition, the clinical treatments currently available are limited to the management of the symptoms and can't reverse the degenerative processes activated during the OA progression. Therefore, in this thesis I aimed to address both these shortcomings.

EVs as diagnostic tool

The EVs have gained increasing importance thanks to their fundamental role in the cell communication process, and recently, we are witnessing a transition toward their use in the diagnostic field. In fact, EVs have been proposed as promising diagnostic candidates for an increasing number of pathological conditions.

However, this project demonstrated that the basic knowledge of the EV biology, especially regarding different subpopulations, is still far from being complete. In fact, even within the small size EVs, that are by far the most characterized, recent evidence suggested the existence of different subpopulations, according to

the biogenesis, the density, the surface markers and other parameters. In addition, large EVs do exist and have important pathophysiological roles in many processes, such as the inflammation, a key response in the OA progression. For these reasons, a deeper basic knowledge of the EVs is, in my opinion, essential for their transition from the bench to the bedside.

In my project, I developed a new experimental approach to isolate different size EV subpopulations from the synovial fluid that could serve in future as innovative OA diagnostic tool. The classic isolation protocols are optimized for the isolation of EVs with a maximum diameter of few hundred nanometres, so they don't allow the separation of the whole spectrum size of EVs, that can measure up to few micrometres. Unfortunately, making minor changes to these techniques is not enough to isolate large size EVs. In fact, they resulted to be by far rarer and more fragile than the small ones, exposing all the limitations of the classic approaches. In this perspective, after a systematic comparison of size-based isolation techniques, the asymmetrical flow field-flow fractionation (AF4) resulted to be the most effective approach. The optimization of the AF4 protocol that I developed allowed the isolation and the separation of the EVs in a very broad size range, from about 20 up to 1400 nm. In addition, it effectively removed the soluble proteins not associated with the EVs, which represents a fundamental aspect in the research of EV-associated

biomarkers. Thanks to the optimization work performed during its development, it would be advisable if the future works with similar aim will start from this protocol, optimizing it. This will allow to obtain a more standardized set of experimental procedures based on the AF4, avoiding the proliferation of a multitude of variants of the same technique. It is increasingly clear that the lack of standardization of the classic isolation approaches can hamper the direct comparison of the results obtained in different studies. So, as the use of AF4 is still in its infancy in the EV field, it would be favourable to develop and abide by a limited number of protocols.

Leaving aside the several variants that have been developed, the availability of different size-based isolation techniques represents an advantage if properly chosen, according to the aim of the specific study and the starting material. For instance, the use of AF4, also thank to its great capability of removing soluble proteins, can be employed to effectively separate EV subpopulations in a broad size range from complex samples such as the biofluids, in which the EV concentration is higher than culture medium. The size exclusion chromatography can also be employed with biological fluids, but only if the aim of the project is not focused on the isolation of large EVs or, given its lower resolution, of rare subpopulations. On the other hand, ultracentrifugation should not be used with biofluids to avoid the

enrichment of protein contaminants. To exploit its main feature, the concentration the final sample as needed, the use of ultracentrifugation can be scaled with large-scale systems for the massive EV production.

The issue of the sample concentration represents, together with the need of specific and expensive instrumentation and specifically trained personnel, a limitation that can hamper the widespread adoption of the AF4. From a technical point of view, the eluted EVs are extremely diluted, especially the largest ones that are rarer. So, the EV subpopulations isolated by the AF4 without further processing, could serve as a diagnostic tool in those pathologies in which the pathological signatures are evident already in the EV profile or in the relative subpopulation abundance, without the need for a deep characterization of the EV cargo. In addition, this approach would faster, simplify and make cheaper the diagnostic process, all important aspects for the potential validation of new diagnostic protocols. In the case of OA diagnosis, an interesting continuation of this project would be the comparison of the EV profile in the arthritic and in the healthy synovial fluid, even if the difficulty of the retrieval of fresh non-arthritic synovial fluid should be considered. To further improve the AF4 technique for the in-depth characterization of the eluted EVs, the coupling with a suitable method for the concentration of the EVs will be very useful. In

this regard, two different approaches can be followed: the concentration of the starting material or the concentration of the eluate. In my opinion, the former could represent a better option for two different reasons. The first one is related to the increased signal that could be detected by the instrument. The second lies in the higher concentration of the solution in which EVs are eluted, possibly increasing their stability and limiting their degeneration.

Microfluidic OA joint on chip model as drug screening platform

With the aim to facilitate the future development of innovative treatments for the OA, in the second project of my PhD, I developed a microfluidic model of an arthritic joint to be used as drug screening platform for innovative and biological treatments for the OA. To establish a relevant precision medicine platform, the model allows the 3D culture of primary chondrocytes and synovial fibroblasts in presence of synovial fluid, all collected from the same arthritic donor. This device permits the injection of biological therapeutics resuspended in synovial fluid, mimicking an intra-articular injection. I was able to quantify and compare the anti-inflammatory effects of two different types of mesenchymal stromal cells. The possibility to create a donor-matched OA knee model is one of the most promising results of

this project, even if it still needs a deeper biological validation. In fact, the results showed a relatively high inter-individual variability, reflecting the need to develop personalized models to better predict treatment outcome on one hand, but also limiting the reliability of the results on the other. For this reason, a high number of donors will be probably needed to validate the chip that, once validated, could represent an effective drug screening platform. In the future, in addition to the mesenchymal stromal cells, it would be interesting to use it to evaluate the effects of other cell-derived products and possibly compare them with the effect obtained by the parent cells. As the literature on these biologics is fragmentary and considered the difficulties to compare them in in vivo models, the device here developed could help to shed light on which treatment owns the highest anti-inflammatory capabilities. For instance, it would be interesting to evaluate the effect of the EVs, platelet rich plasma, bone marrow concentrate, fragmented adipose tissue, and other cell-derived products. This will better elucidate the potential role of the innovative biologics that have been proposed in the recent years for the treatment of OA.

The lack of basic knowledge that affect some of the aspects in the EV field, emerged to some extent also from the development of in vitro models of an osteoarthritic joint. In particular, the biological implications of the microenvironment composition

surrounding the chondrocytes, characterized by a delicate phenotype balance, was not completely considered in the previous studies. In these models the hydrogels employed were made of classic polymers already used in microfluidics, such as fibrin. However, their composition is relatively different compared to native tissues and this can affect the phenotype of the embedded cells, especially for the highly specialized ones that populate the thoroughly organized matrices, such as chondrocytes. This is the reason why in the first part of this project, different hydrogel preparations were tested and compared. The results demonstrated that different hydrogels (hyaluronic acid, collagen, their mix and fibrin) have a different capability in ensuring the maintenance of the proper cell phenotype. In addition, also the rheological properties of different hydrogels can vary, and this should be taken into account in their development, especially if used within these miniaturized models. The hydrogels employed in the microfluidic models can not reflect the exact composition of the in vivo tissue, but they have to provide the sufficient biochemical and mechanical cues to sustain the correct cell phenotype. In fact, the maintenance of the proper functional properties of the cells included in these platforms has to be considered as a mandatory aspect. Only in this way the biological system will actually resemble the in vivo environment and will give the most reliable

results as possible, especially if used for the assessment of innovative treatments.

Chapter 8

Conclusions and perspective

In conclusion, during my PhD project I tried to lay the foundations for relevant advancements in the approach to OA, both in the diagnosis and in the clinical treatment. In this thesis I emphasized the importance, in the translational research, of an in-depth knowledge of the biological systems to facilitate their shift towards the clinics, especially for the more recent and less studied ones, as the EVs. For this reason, in the future it would be relevant to combine the two fields addressed in this thesis, namely the EVs and the microfluidics. In fact, I developed a protocol that allow the isolation of different size EV subpopulations and parallelly a model that resemble a relevant articular 3D microenvironment. Therefore, the biological effect of the EV subgroups could be assessed in this device, giving the essential indication about their potential pathological role in the OA. In addition, other key biological processes related to the EVs, such as their secretion, their cargo, their upload and in general their effect on the recipient cells, could be studied in a different 3D microfluidic model. This will allow a better understanding of how the microenvironment influence the biology of the EVs, that is still missing in the literature. The implementation of a similar project could be relatively easily thanks to the use of fluorescent EVs obtained, for instance, from engineered cells. Precisely the increasing ability of cell engineering, that has been finely optimized in the last years, would allow the obtainment of EV

with desired features that, together with a larger knowledge of the EV behaviour in a 3D microenvironment, could help the translation of the EVs towards the clinical setting.

Chapter 9

Other publications

Umbilical Cord MSCs and Their Secretome in the Therapy of Arthritic Diseases: A Research and Industrial Perspective

Chiara Arrigoni[1], **Daniele D'Arrigo[1]**, Valeria Rossella[2], Christian Candrian[3,4], Veronica Albertini[2] and Matteo Moretti[1,5]

1 - Regenerative Medicine Technologies Laboratory, Ente Ospedaliero Cantonale (EOC), via Tesserete 46, 6900 Lugano, Switzerland.

2 - Swiss Stem Cells Biotech, Via Pizzamiglio 12, 6833 Vacallo, Switzerland.

3 - Unità di Ortopedia e Traumatologia, Ospedale Regionale di Lugano, Ente Ospedaliero Cantonale (EOC), via Tesserete 46, 6900 Lugano, Switzerland.

4 - Faculty of Biomedical Sciences, Università della Svizzera Italiana, Via Buffi 13, 6900 Lugano, Switzerland.

5 - Cell and Tissue Engineering Laboratory, IRCCS Istituto Ortopedico Galeazzi, via R. Galeazzi 4, 20161 Milano, Italy.

Cells 2020 May 28;9(6):1343. doi: 10.3390/cells9061343 (*IF: 6,6*)

Received: 30 April 2020; Accepted: 26 May 2020; Published: 28 May 2020

Abstract

The prevalence of arthritic diseases is increasing in developed countries, but effective treatments are currently lacking. The injection of mesenchymal stem cells (MSCs) represents a promising approach to counteract the degenerative and inflammatory environment characterizing those pathologies, such as osteoarthritis (OA). However, the majority of clinical approaches based on MSCs are used within an autologous paradigm, with important limitations. For this reason, allogeneic MSCs isolated from cord blood (cbMSCs) and Wharton's jelly (wjMSCs) gained increasing interest, demonstrating promising results in this field. Moreover, recent evidences shows that MSCs beneficial effects can be related to their secretome rather than to the presence of cells themselves. Among the trophic factors secreted by MSCs, extracellular vesicles (EVs) are emerging as a promising candidate for the treatment of arthritic joints. In the present review, the application of umbilical cord MSCs and their secretome as innovative therapeutic approaches in the treatment of arthritic joints will be examined. With the prospective of routine clinical applications, umbilical cord MSCs and EVs will be discussed also within an industrial and regulatory perspective.
Keywords: umbilical cord MSC; secretome; osteoarthritis; extracellular vesicles; cell therapies

Contribution: writing and original draft preparation.

Independent, Controllable Stretch-Perfusion Bioreactor Chambers to Functionalize Cell-Seeded Decellularized Tendons

Giuseppe Talò,[1] **Daniele D'Arrigo**,[1] Sergio Lorenzi,[2] Matteo Moretti,[1,3,4] and Arianna B. Lovati[1]

1 - Cell and Tissue Engineering Laboratory, IRCCS Istituto Ortopedico Galeazzi, Via Riccardo Galeazzi 4, 20161 Milan, Italy;

2 - Department of Engineering and Applied Sciences (DISA), University of Bergamo, Dalmine, Italy;

3 - Regenerative Medicine Technologies Lab, Ente Ospedaliero Cantonale, Lugano, Switzerland;

4 - Cardiocentro Ticino, Lugano, Switzerland

Annals of Biomedical Engineering, Vol. 48, No. 3, March 2020 (Ó 2019) pp. 1112–1126 https://doi.org/10.1007/s10439-019-02257-6 (*IF: 3,74*)

Received 23 January 2019; accepted 27 March 2019; published online 8 April 2019

Abstract

Tissue-engineered decellularized matrices can progress clinical replacement of full-thickness ruptures or tendon defects. This study develops and validates a custom-made automated bioreactor, called oscillating stretch-perfusion bioreactor (OSPB), consisting of multiple, independent culture chambers able to combine a bidirectional perfusion with a programmable, uniaxial strain to functionalize cell-seeded decellularized tendons. Decellularized tendon matrices were seeded on their surfaces and within the tendon fibers with mesenchymal stem cells. Then, they were subjected to a bidirectional perfusion and programmed stretching cycles of 15–30–60 min on–off two times per day for 7 days of culture. In vitro analyses showed viable cells, homogenously dis- tributed on the surface of the constructs. More importantly, cell-seeded decellularized tendon grafts undergoing cyclic load in our bioreactor had a superior production and organization of newly formed collagen matrix compared to static cultured constructs. The coherency and local alignment of the new collagen deposition within the inner injected channels quantitatively supported histological findings. The designed OSPB could be considered a unique, cost-effective system able to involve multiple independently controlled chambers in terms of biological and mechanical protocols. This system allows parallel processing of several customized tendon

constructs to be used as grafts to enhance the surgical repair of large tendon defects.

Contribution: bioreactor development; performing in vitro studies; writing and original draft preparation.

Achilles Tendon Repair by Decellularized and Engineered Xenografts in a Rabbit Model

Marta Bottagisio,[1*] **Daniele D'Arrigo,[2*]** Giuseppe Talò,[2] Matilde Bongio,[2] Marco Ferroni,[3] Federica Boschetti,[3] Matteo Moretti,[2,4,5] and Arianna B. Lovati[2]

[1] Laboratory of Clinical Chemistry and Microbiology, IRCCS Istituto Ortopedico Galeazzi, Milan 20161, Italy

[2] Cell and Tissue Engineering Laboratory, IRCCS Istituto Ortopedico Galeazzi, Milan 20161, Italy

[3] Department of Chemistry, Materials and Chemical Engineering Giulio Natta, Politecnico di Milano, Milan 20133, Italy [4] Regenerative Medicine Technologies Lab, Ente Ospedaliero Cantonale, Lugano 6900, Switzerland

[5] Cardiocentro Ticino, Lugano 6900, Switzerland

Stem Cells Int. 2019 Aug 29;2019:5267479. doi: 10.1155/2019/5267479. eCollection 2019 (*IF: 3,87*)

Received 30 April 2019; Revised 1 July 2019; Accepted 10 July 2019; Published 29 August 2019

Abstract

Tendon tissue ruptures often require the replacement of damaged tissues. The use of auto- or allografts is notoriously limited due to the scarce supply and the high risks of immune adverse reactions. To overcome these limitations, tissue engineering (TE) has been considered a promising approach. Among several biomaterials, decellularized xenografts are available in large quantity and could represent a possible solution for tendon reconstruction. The present study is aimed at evaluating TE xenografts in Achilles tendon defects. Specifically, the ability to enhance the biomechanical functionality, while improving the graft interaction with the host, was tested. The combination of decellularized equine-derived tendon xenografts with or without the matrix repopulation with autologous bone marrow mesenchymal stem cells (BMSCs) under stretch-perfusion dynamic conditions might improve the side-to-side tendon reconstruction. Thirty-six New Zealand rabbits were used to create 2cm long segmental defects of the Achilles tendon. Then, animals were implanted with autograft (AG) as the gold standard control, decellularized graft (DG), or in vitro tissue-engineered graft (TEG) and evaluated postoperatively at 12 weeks. After sacrifice, histological, immunohistochemical, biochemical, and biomechanical analyses were performed along with the matrix

metalloproteinases. The results demonstrated the beneficial role of undifferentiated BMSCs loaded within decellularized xenografts undergoing a stretch-perfusion culture as an immunomodulatory weapon reducing the inflammatory process. Interestingly, AG and TEG groups exhibited similar results, behaved similarly, and showed a significant superior tissue healing compared to DG in terms of newly formed collagen fibres and biomechanical parameters. Whereas, DG demonstrated a massive inflammatory and giant cell response associated with graft destruction and necrosis, absence of type I and III collagen, and a higher amount of proteoglycans and MMP-2, thus unfavourably affecting the biomechanical response. In conclusion, this in vivo study suggests a potential use of the proposed tissue-engineered constructs for tendon reconstruction.

Contribution: performing in vitro studies; histological, histochemistry and histomorphometric analyses; writing and original draft preparation.

Pulsed electromagnetic fields improve the healing process of Achilles tendinopathy

C. Perucca Orfei[1], A. B. Lovati[1], G. Lugano[1], M. Viganò[1], M. Bottagisio[1], **D. D'Arrigo[1,2]**, V. Sansone[1,3], S. Setti[4], L. de Girolamo[1]

1 - IRCCS Orthopedic Institute Galeazzi, Milan, Italy

2 - Regenerative Medicine Technologies Laboratory, Ente Ospedaliero Cantonale (EOC), Lugano, Switzerland.

3 - Faculty of Medicine and Surgery, University of Milan, Milan, Italy.

4 - IGEA SpA Clinical Biophysics, Carpi, Italy.

Bone Joint Res 2020;9(9):613–622; doi: 10.1302/2046-3758.99.BJR-2020-0113.R1 (*IF: 5,09*)

Abstract

Aims

In the context of tendon degenerative disorders, the need for innovative conservative treatments that can improve the intrinsic healing potential of tendon tissue is progressively increasing. In this study, the role of pulsed electromagnetic fields (PEMFs) in improving the tendon healing process was evaluated in a rat model of collagenase-induced Achilles tendinopathy.

Methods

A total of 68 Sprague Dawley rats received a single injection of type I collagenase in Achilles tendons to induce the tendinopathy and then were daily exposed to PEMFs (1.5 mT and 75 Hz) for up to 14 days - starting 1, 7, or 15 days after the injection - to identify the best treatment option with respect to the phase of the disease. Then, 7 and 14 days of PEMF exposure were compared to identify the most effective protocol.

Results

The daily exposure to PEMFs generally provided an improvement in the fibre organization, a decrease in cell density, vascularity, and fat deposition, and a restoration of the physiological cell morphology compared to untreated tendons. These improvements were more evident when the tendons were

exposed to PEMFs during the mid-acute phase of the pathology (7 days after induction) rather than during the early (1 day after induction) or the late acute phase (15 days after induction). Moreover, the exposure to PEMFs for 14 days during the mid-acute phase was more effective than for 7 days.

Conclusion

PEMFs exerted a positive role in the tendon healing process, thus representing a promising conservative treatment for tendinopathy, although further investigations regarding the clinical evaluation are needed.

Contribution: performing the in vivo study, histomorphometric analyses, manuscript reviewing